Human Brain Project
Education Programme

5th HBP STUDENT CONFERENCE

On Interdisciplinary Brain Research

Virtual Event - February 1–4, 2021

BOOK OF ABSTRACTS

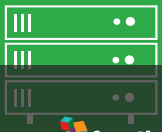

frontiers Event Abstracts

5th HBP STUDENT CONFERENCE ON INTERDISCIPLINARY BRAIN RESEARCH

ISBN: 978-2-88966-541-9
DOI: 10.3389/978-2-88966-541-9
Citation: Petruţ Bogdan, Sandra Díaz, Alice Geminiani, Carmen Lupascu, Jens Egholm Pedersen, Ingrid Reiten, Alper Yegenoglu, HBP Education Programme. (2020). 5th HBP Student Conference on Interdisciplinary Brain Research.

February 1–4, 2021, Virtual Event

The abstracts in this collection have not been subject to any Frontiers peer review or checks, and are not endorsed by Frontiers. They are made available through the Frontiers publishing platform as a service to conference organizers and presenters. The copyright in the individual abstracts is owned by the author of each abstract or his/her employer unless otherwise stated. Each abstract, as well as the collection of abstracts, are published under a Creative Commons CC-BY 4.0 (attribution) licence (https://creativecommons.org/licenses/by/4.0/) and may thus be reproduced, translated, adapted and be the subject of derivative works provided the authors and Frontiers are attributed.

For Frontiers' terms and conditions please see https://www.frontiersin.org/legal/terms-and-conditions.

Table of Contents

IV Cognitive and behavioral neuroscience

Welcome to the 5th HBP Student Conference on Interdisciplinary Brain Research

It is our pleasure to present the proceedings of the 5th Human Brain Project Student Conference on Interdisciplinary Brain Research, a conference for and by young researchers which provides an open forum for exchange of knowledge within and across the various research fields addressed by the Human Brain Project (HBP). Going virtual for the first time, from the 1st to the 4th of February 2021, the 5th edition proved that also as a virtual meeting, the HBP Student Conference offers invaluable opportunities for extensive scientific discussions among fellow early career researchers and faculty. The abstracts hereby presented cover a wide range of topics, spanning from brain disease modelling, the organisation, structure and function of neural systems, simulation, brain-inspired architectures as well as cognitive and behavioral neuroscience. Together, these abstracts reflect the world-wide multidisciplinary ongoing scientific efforts of young researchers towards understanding the brain.

LIST OF ORGANIZERS

Conference program committee
Petruţ Bogdan (The University of Manchester)
Sandra Díaz (Forschungszentrum Jülich)
Alice Geminiani (The University of Pavia)
Carmen Lupascu (Italian National Research Council)
Jens Egholm Pedersen (KTH Royal Institute of Technology)
Ingrid Reiten (The University of Oslo)
Alper Yegenoglu (Forschungszentrum Jülich)
HBP Education Programme (Medical University Innsbruck)

Conference organisers
HBP Education Programme | Medical University Innsbruck

Proceedings editors
Johanna Fusseis, Medical University Innsbruck
Alice Geminiani, The University of Pavia
Manuel Gran, Medical University Innsbruck
Ingrid Reiten, The University of Oslo

PREFACE

It is our pleasure to present the proceedings of the 5th Human Brain Project Student Conference on Interdisciplinary Brain Research. The conference provides an open forum for exchange of new ideas among young researchers working in the various research fields addressed by the Human Brain Project (HBP). Going virtual for the first time, from the 1st to the 4th of February 2021, the 5th edition proved that also as a virtual meeting, the HBP Student Conference offers invaluable opportunities for extensive scientific discussions among fellow early career researchers and faculty. Through a variety of lectures, workshops, discussion sessions and social events, participants could learn about recent developments and tools in brain research, as well as interact with world-leading researchers and experts on career development, neuroethics and dual use.

At the heart of the conference was the engaging contributions of all participants through talks and posters. It is our honour to present all related abstracts in this book. Particularly encouraged were high-quality submissions introducing new and relevant problems, concepts and ideas, with the potential to inspire collaboration across research disciplines. The accepted abstracts cover a wide range of topics, spanning from brain disease modelling, the organisation, structure and function of neural systems, simulation, brain-inspired architectures as well as cognitive and behavioral neuroscience. Together, these abstracts reflect the multidisciplinary ongoing scientific efforts of young researchers towards understanding the brain.

We would like to express our utmost appreciation to all authors for submitting their work to the 5th HBP Student Conference. We hope this selected set of abstracts can be of inspiration for new discussions, interactions and research opportunities for the whole scientific community.

Ingrid Reiten & Alice Geminiani
Program Committee Chairs of the 5th HBP Student Conference

I Brain dynamics and disease modelling

Withdrawal of antiepileptic drugs after resective epilepsy surgery

Tünde Benedek[1]*, Dániel Fabó[2], Anna Kelemen[2]

[1]University of Medicine and Pharmacy, Târgu Mureș, Romania
[2]Department of Neurology, National Institute of Clinical Neurosciences, Budapest, Hungary
**tundikebenedek@gmail.com*

INTRODUCTION/MOTIVATION

Epilepsy is one of the most common serious neurological disorders affecting approximately 50–70 million people globally [1] and about 30 percent of the patients have inadequate control of seizure with pharmacotherapy [2]. Resective surgery as a treatment option for drug-resistant epilepsies is presently well accepted and performed worldwide [3]. The ideal outcome is seizure freedom without the need for antiepileptic drug (AED) therapy but the management of postoperative withdrawal remains an unsolved therapeutic challenge and the optimum timing is still unclear. The overall aim of the present study, therefore, was to determine the rate of successful AED discontinuation and to summarize the current methods of tapering. Moreover, this study aimed to explore the potential prognostic factors that influence the outcome of AED withdrawal.

METHODS

We performed a retrospective analysis of the postoperative AED profile of 128 patients with epilepsy who underwent resective surgery performed between 2006 and 2017 in the National Institute of Clinical Neurosciences and were followed up for at least two years. Data regarding postoperative treatment strategies (medications, time interval from surgery to AED tapering, rate of withdrawal, preferred discontinuation order of AEDs) was extracted systematically. To identify the factors contributing to the decision to discontinue antiepileptic medication we compared the potential predictors of withdrawal outcome in patients with successful AED discontinuation versus seizure recurrence during tapering. The collected data included duration of epilepsy, age at surgery and histopathological diagnosis.

RESULTS AND DISCUSSION

Of the 128 followed up patients, pharmacotherapy was discontinued successfully in 20 patients (15.63%) and polytherapy was reduced to monotherapy in 28 patients (21.88%) without complications. 58 patients (45.31%) did not achieve seizure freedom after surgery (n=35, 27.34%) or had seizure recurrence while tapering (n=23, 17.97%). Antiepileptic therapy withdrawal was started in 22 patients (17.19%) on the last follow-up appointments. (Figure 1)

Our analysis showed that the prescribed presurgical AEDs in patients who remained seizure free after tapering were carbamazepine (n=23), levetiracetam (n=22), lamotrigine (n=16), clobazam (n=14), oxcarbamazepine (n=10), topiramate (n=6), lacosamide (n=5), phenytoin (n=4), valproate (n=2), brivaracetam (n=1), clonazepam (n=1), felbamate (n=1), sultiame (n=1), zonisamide (n=1). The mean interval from surgery to starting withdrawal was 20.21 months, and 34.92 months from surgery to complete AED discontinuation. After a successful resection the tapering was started with topiramate (mean=16.80 months) in 83.33%, clobazam (mean=19.91 months) in 64.29% and oxcarbamazepine (mean=22.00 months) in 60.00% of patients receiving the medication in combined therapy. We found that carbamazepine (n=8, 28.57%), lamotrigine (n=7, 25.00%) and levetiracetam (n=8, 28.57%) were commonly used as monotherapy for patients with former polytherapy.

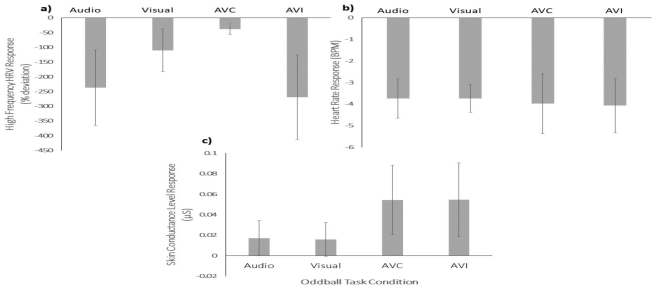

FIGURE 1: Postoperactive antiepileptic theraphy management .

Table 1: Predictares of seizure recurrence on attempted AED withdrawal by univariate analysis

Variables	Seizure freedom after complete withdrawal (n=20) mean ± SD or n (%)	Seizure recurrence during tapering (n=23) mean ± SD or n (%)	*p* Value
Nr. of AEDs prior to surgery	5,350 ± 2,907	7,889 ± 3,530	0,0330
Age at surgery, y	29,132 ± 11,302	36,743 ± 12,865	0,0472
Epilepsy duration, y	11,667 ± 8,547	20,500 ± 16,750	0,0387
Well-defined focal lesions (Low grade neoplasms + vascular malformations)	9 (45%)	3 (13,043%)	0,0390

The successfully discontinued group was more likely to have a shorter duration of epilepsy and lower number of antiepileptic drugs prior to surgery compared to the group who continued to receive medication. We found that younger age at surgery also predicted a positive outcome of AED tapering. Histopathological evaluation of patients with favorable withdrawal showed higher percentage of low-grade neoplasms and vascular malformations (Table 1).

Tapering AEDs after resective epilepsy surgery is common practice though no specific guideline or recommendations are found in the literature. The most difficult decision facing a clinician is when or how to stop antiepileptic treatment. Neurologists and patients would benefit greatly from future research into safe tapering strategies for discontinuing AED therapy. Seizure recurrence risk could be minimized by considering the possible risk factors that influence the outcome of withdrawal.

Keywords: epilepsy, epilepsy surgery, antiepileptic drugs, discontinuation

REFERENCES

[1] Ngugi, A. K., Bottomley, C., Kleinschmidt, I., Sander, J. W., & Newton, C. R. (2010). Estimation of the burden of active and life-time epilepsy: A meta-analytic approach. Epilepsia, 51(5), 883–890.

[2] Picot, M. C., Baldy-Moulinier, M., Daurès, J. P., Dujols, P., & Crespel, A. (2008). The prevalence of epilepsy and pharmacoresistant epilepsy in adults: A population-based study in a Western European country. Epilepsia, 49(7), 1230–1238.

[3] Sheng, J., Liu, S., Qin, H., Li, B., & Zhang, X. (2017). Drug-Resistant Epilepsy and Surgery. Current Neuropharmacology, 16(1), 17–28.

Deep brain stimulation's effect on hippocampal High Frequency Oscillations in the pilocarpine model of epilepsy

Réka-Barbara Bod*, Ádám-József Berki*, István Mihály*, Károly Orbán-Kis* , Tibor Szilágyi*

Department of Physiology, Faculty of Medicine, George Emil Palade University of Medicine, Pharmacy, Science, and Technology of Târgu Mureș, Târgu Mureș, Romania
**bod.reka-barbara@stud16.umftgm.ro; berki.adam-jozsef@stud15.umftgm.ro; istvan.mihaly@umfst.ro; karoly.orban-kis@umfst.ro; tibor.szilagyi@umfst.ro*

INTRODUCTION/MOTIVATION

Temporal lobe epilepsy (TLE) is a serious condition, responsible for recurrent epileptic seizures [1]. As TLE is frequently pharmacoresistant, deep brain stimulation (DBS) has been proposed to treat epileptic patients [2], [3]. Despite its invasiveness [4], DBS has proven to be a safe and potentially effective treatment in several neurological disorders, although its mechanism of action is not fully clarified. DBS seems to reduce the severity and overall rate of both seizures and interictal epileptiform discharges (IEDs), the classical electrophysiological markers of epilepsy [5]. High frequency oscillations (HFOs) are a type of IED that have lately been anticipated as a promising biomarker of seizure onset zone. HFOs constitute gamma (60-150 Hz), ripple (150-250 Hz) and fast ripple (250-600 Hz) frequency bands [6], thus HFO detection may require elaborate data acquisition tools, such as local field potential (LFP) recordings with a high sampling rate [7]. HFOs are prevailingly detected in the hippocampal formation, which is greatly involved in TLE [8]. Amygdala, with a function to pre-process information before that reaches the hippocampus, likewise plays a crucial role in epileptogenesis [9]. Nevertheless, its wide-ranging input and output connections make it an ideal site for deep brain stimulation [10]. Therefore, our aim was to detect HFOs present in the hippocampal recordings in TLE rats and to outline the possible effects of amygdala low-frequency stimulation on HFOs.

METHODS

For modeling TLE, the pilocarpine model of epilepsy was selected (Fig. 1). The design of this study respected the 2010/63/EU directive of the European

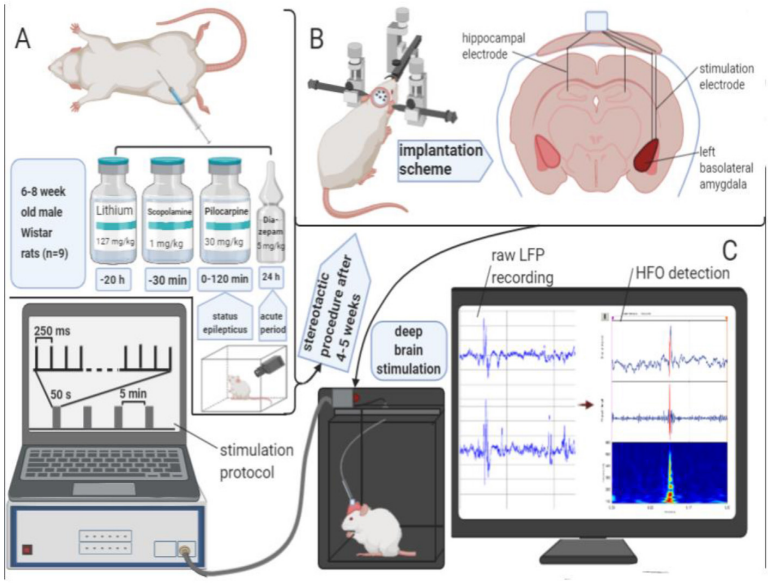

FIGURE 1: Visual representation of the Methods section. (**A**) Administration of the substances for evoking status epilepticus. (**B**) Implantation of the amygdala stimulation electrodes and hippocampal LFP recording electrodes. (**C**) Stimulation protocol, DBS treatment and a simultaneous recording. After processing, note the detection of an HFO (LFP = local field potential, DBS = deep brain stimulation, HFO = high frequency oscillation).

Parliament and the local regulations approved by the Ethics Committee for Scientific Research of the George Emil Palade University of Medicine, Pharmacy, Science, and Technology of Târgu Mures, (ethical committee license no: 340/17 November 2017, extended by no. 54/2 April 2019). 6-8-week-old male Wistar rats (n=9) received lithium chloride, and 20 hours later pilocarpine was administered intraperitoneally to trigger status epilepticus (SE). SE was suspended by administration of diazepam after 2 hours. After 2-3 weeks, spontaneous recurrent seizures appeared. The animals were continuously video monitored for seizure detection. 7-8 weeks after SE, rats underwent stereotactic implantation of two hippocampal electrodes on both sides. A stimulation electrode in the left basolateral amygdala was also implanted. Following a 10-day recovery period, simultaneous DBS protocol

and hippocampal LFP recordings began. During DBS 0.1 ms-long biphasic stimuli of 500 μA intensity were used, with 250 ms inter-pulse interval. This sequence was repeated for 50 seconds, regarded as a stimulus pack. A daily DBS treatment consisted of four stimulus trains, with each of the trains followed by a 5-minute pause, for a total number of ten days. The LFP recording was started 5 minutes before the first train and stopped 5 minutes after the last one. LFP recordings were analyzed with RIPPLELAB, a MATLAB open-source application. RIPPLELAB, a semi-automated tool, allows opting for various methods and parameters of HFO detection [11]. For this work, the Montreal Neurological Institute (MNI) detection method was selected, which detects HFOs with a sensitivity of 91%. As described by Zelmann et al., MNI detector applies a bandpass filter between 80 and 600 Hz, then calculates the activity baseline if at least 5 s/min of baseline segment is present, otherwise root mean square amplitude of the signal is used to find possible HFOs. If a 99.9999 percentile of the empirical cumulative distribution function of each 10 s baseline segment is reached, the event is declared an HFO [12]. Event length was set to a minimum of 10 ms, events less than 10 ms apart were accepted as a single event. HFOs recognized by the MNI algorithm were validated visually as well, rejecting false positive events. Finally, a database of 1001 HFOs was created, with information regarding the time, duration, frequency band power of every HFO respectively.

RESULTS

All animals' recordings displayed hippocampal HFOs, the average HFO rate being 0.41 $\pm$ 0.14 HFO/min (mean $\pm$ SEM). The rate of HFOs during DBS stimulus trains was significantly smaller than the HFO rate during the intervals without stimulus trains (0.07$\pm$0.03 vs 0.45$\pm$0.15 HFO/min, p=0.017, paired t-test). During the 10 days stimulation protocol, there was no significant HFO rate difference between the first and the last day (0.31$\pm$ 0.12 vs. 0.16$\pm$ 0.06 HFO/min, p=0.12). There was no significant difference in the average duration of HFOs between the first and the last days (13.89 $\pm$ 0.56 ms vs. 13.71 $\pm$ 0.69 ms, p=0.57). The left hippocampus had an average ripple power spectrum of 44.1$\pm$0.73% of the total HFO power spectrum, in contrast, right hippocampus values were significantly lower, with an average of 37.7$\pm$1.11%, (p <0.001). Differences between the two hippocampi were not significant on the first day (p=0.36). When the fast ripple power spectrum was measured, the left hippocampus had an average of 35.9$\pm$0.64%, while the right hippocampus had 41.2%$\pm$1.64%, p=0.008.

DISCUSSION

DBS instantaneously reduced HFO rate, a phenomenon that could justify DBS's therapeutic effect in a very short time window. Nevertheless, changes that encompass longer intervals were not observed regarding the HFO rate, as the difference did not last between different days. For observing DBS's long-term effect on HFOs, duration of the single sessions, as well as number of DBS days should be increased. The fact that ripple power was higher on the side of the stimulation while the fast ripple power was lower could be attributed to the asymmetric involvement of the two hemispheres in TLE. Based on literature findings, bilateral amygdala DBS brings about better results compared to unilateral stimulation protocols in terms of seizure suppression [10]. Yet, bilateral DBS could similarly help us to understand whether uneven HFO spectra in the right and left hippocampi are exclusively due to functional hemispheric asymmetricity. The difference in the inter-hippocampal distribution of different HFO subtypes highlights the need of analysing them separately, but further investigations are needed to elucidate the effect of DBS on them. There is evidence that irregular inter-pulse intervals (i.e. irregularly distributed stimuli) are superior to the regularly applied DBS [13], however, there are no remarks on how HFOs are impacted by them.

Keywords: temporal lobe epilepsy, high frequency oscillations, deep brain stimulation, epilepsy biomarkers, local field potentials

REFERENCES

[1] M. Rosa and Q. Pascual, "Temporal Lobe Epilepsy : Clinical Semiology and Neurophysiological Studies," pp. 416–423, 2007.

[2] N. Zangiabadi, L. D. Ladino, and F. Sina, "Deep Brain Stimulation and Drug-Resistant Epilepsy : A Review of the Literature," vol. 10, no. June, pp. 1–18, 2019.

[3] N. Klinger and S. Mittal, "Deep brain stimulation for seizure control in drug-resistant epilepsy," vol. 45, no. August, pp. 1–8, 2018.

[4] M. Sprengers et al., "Deep brain and cortical stimulation for epilepsy (Review)," 2017.

[5] R. J. Staba, M. Stead, and G. A. Worrell, "Electrophysiological Biomarkers of Epilepsy," 2014.

[6] I. Naggar, M. Stewart, and R. Orman, "High Frequency Oscillations in Rat Hippocampal Slices : Origin , Frequency Characteristics , and Spread," vol. 11, no. April, pp. 1–14, 2020.

[7] M. Zijlmans, P. Jiruska, R. Zelmann, F. S. S. Leijten, J. G. R. Jefferys, and J. Gotman, "High-frequency oscillations as a new biomarker in epilepsy," Ann. Neurol., 2012.

[8] L. Li, M. Patel, J. Almajano, J. Engel, and A. Bragin, "Extrahippocampal high-frequency oscillations during epileptogenesis," no. February, pp. 1–5, 2018.

[9] J. C. De Oliveira, R. M. Maciel, M. Flavio, D. Moraes, and V. R. Cota, "Asynchronous, bilateral, and biphasic temporally unstructured electrical stimulation of amygdalae enhances the suppression of pentylenetetrazole-induced seizures in rats," Epilepsy Res., vol. 146, pp. 1–8, 2018.

[10] R. Tyrand et al., "Effects of amygdala — hippocampal stimulation on interictal epileptic discharges," Epilepsy Res., vol. 99, no. 1–2, pp. 87–93, 2012.

[11] M. Navarrete, C. Alvarado-rojas, and M. L. Van Quyen, "RIPPLELAB : A Comprehensive Application for the Detection , Analysis and Classification of High Frequency Oscillations in Electroencephalographic Signals," 2016.

[12] R. Zelmann, F. Mari, J. Jacobs, M. Zijlmans, F. Dubeau, and J. Gotman, "Clinical Neurophysiology A comparison between detectors of high frequency oscillations," Clin. Neurophysiol., vol. 123, no. 1, pp. 106–116, 2012.

[13] T. Wyckhuys, P. Boon, R. Raedt, B. Van Nieuwenhuyse, and K. Vonck, "Suppression of hippocampal epileptic seizures in the kainate rat by Poisson distributed stimulation," vol. 51, no. 11, pp. 2297–2304, 2010.

Characterization of HCN2 in the medial septo-hippocampal system on regard of electrophysiological properties, theta rhythm, REM-sleep, learning and memory

Manuela Brümmer[1], Marc Sebastian Stieglitz[1], Verena Mehlfeld[1]*, Christian Wahl-Schott[2], Martin Biel[1]

[1]Department of Pharmacy, Center of Drug Research, Center of Integrated Protein Science Munich, Ludwig-Maximilians-Universität München, Munich, Germany
[2]Insitut für Neurophysiologie, Medizinische Hochschule Hannover, Germany
**Verena.Mehlfeld@cup.uni-muenchen.de*

INTRODUCTION/MOTIVATION

The theta rhythm is one of the most prominent synchronous neuronal brain oscillation found in the mammalian brain and plays an important role for information processing and for the organization of learning and memory (Winson 1978). It is characterized by an oscillation-frequency of 4 to 12 Hz, is prominent in the hippocampus and strongly influenced by the activity of the medial septum (MS). Both are interconnected via GABAergic, cholinergic and glutamatergic projecting neurons (Stewart and Fox 1990). Consequently, different oscillations where activated and inhibited in the hippocampus, leading to long-term potentiation (LTP) or depression (LTD) respectively (Kemp 2004). Physiological functions arise, like REM-sleep (rapid eye movement), cognitive processes such as learning and memory, which are strongly influenced by the hippocampus and in turn by the MS (Hasselmo and Stern 2014). The MS contains hyperpolarization-activated cyclic-nucleotide-gated cation (HCN) channels, in this work most importantly the HCN2 subunit, which is highly expressed in the brain (Notomi and Shigemoto 2004). Their characteristics include activation by hyperpolarization and the regulation by cyclic nucleotides like cAMP. The resulting current of HCN channels is termed I_h, which is essential in a variety of physiological processes, such as the generation of the theta oscillation (Biel, Wahl-Schott et al. 2009).

The influence of HCN channels on hippocampal oscillations is already known (Matt, Michalakis et al. 2011). Still unknown is the influence of the interconnecting neurons like GABAergic, cholinergic and glutamatergic neurons in this oscillations forming connection. What particular role does the HCN2

subunit play in the formation of the theta rhythm? Can physiological processes as learning, REM-sleep and memory be pinpointed down to a neuron type? Are there any abnormal behaviors resulting from a deletion of HCN2 in specific neurons?

METHODS

To investigate the role of HCN2 in different neuron types in the MS, a selective knock out the HCN2 channel in all neurons or in a subset of medial septal neurons like GABAergic or cholinergic neurons will be needed. Therefore, a lentiviral approach will be used to drive CRE expression in subpopulations of medial septal neurons in the floxed HCN2 mouse (HCN2 L2). For specific targeting of these subpopulations selective promotors (hSyn, GAD67, CaMKIIalpha) will be used. Successfully transduced cells are visible by the expression of a red fluorescent dye (mCherry). The lentiviral particles will be stereotactically injected bilaterally into the MS. After 2-3 weeks expression time, electrophysiological measurements (whole-cell patch-clamp measurements), EEG recordings or behavioral experiments will be performed.

RESULTS AND DISCUSSION

The success of the viral transduction was proved using immunohistochemistry (data not shown). Electrophysiological experiments (whole-cell patch-clamp) were performed to investigate the changes in firing patterns in the MS caused by the loss of HCN2 in neurons. As expected, electrophysiological recordings revealed that the I_h current was significantly reduced in hSyn-Cre-injected animals compared to control-injected animals, while other electrophysiological parameters like resting membrane potential, mean firing rate or the spike threshold seemed not to be altered by the deletion (see Figure 1). The I_h activation time was significantly increased, because the slow opening HCN4 mainly determine the activation time in absence of HCN2. Future experiments will reveal the influence of GABAergic and glutamatergic neurons on I_h and the theta rhythm.

Additionally, injected animals were characterized using EEG telemetry and behavioral experiments to investigate the physiological outcome regarding Rapid Eye Movement-sleep (REM) and learning behavior. The EEG measurements were analyzed for the three different vigilance states wakefulness,

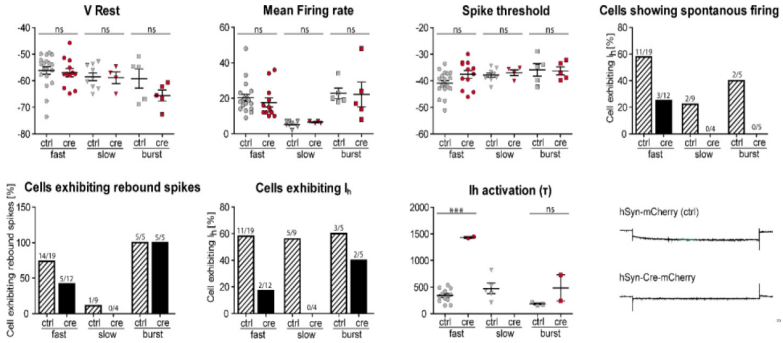

FIGURE 1: Whole-cell patch-clamp results in hSyn-Cre-mCherry and hSyn-mCherry injected animals. Electrophysiological parameters were investigated: Resting membrane potential (V Rest), mean firing rate (Mean Firing rate), spike threshold, number of cells showing spontaneous firing, number of cells exhibiting rebound spikes, number of cells exhibiting Ih, Ih activation time (τ), sample traces of Ih for Cre- and control injected neurons. Statistics: t-test.

NREM- and REM-sleep. There was no significant difference in wake state, NREM- or REM-sleep-properties (data not shown). A focus of a more detailed analysis will be the transition between vigilance stages.

Finally, the correlation of neuronal activity - generated in the MS - with hippocampus dependent learning using a Water Cross Maze (WCM) approach was investigated.

In Figure 2 the differences between control group and Cre-injected animals is not significant in the first week (day 1-5, learning week, LTP dependent). However, in the second week (day 1r-5r), which shows the ability of reversal learning (LTD dependent), Cre-injected animals show significant differences in the parameter's latency, accuracy, wrong platform visits and accurate learners. Cre-injected animals do not show a constant improve of reversal learning, more a deficit in re-learning. This might be explainable with a lack of LTD. In further experiments, LTP/LTD measurements will be performed to support this hypothesis.

The results confirm an important influence of HCN2 on the septo-hippocampal neurons and therefore on the hippocampus and the generation of theta

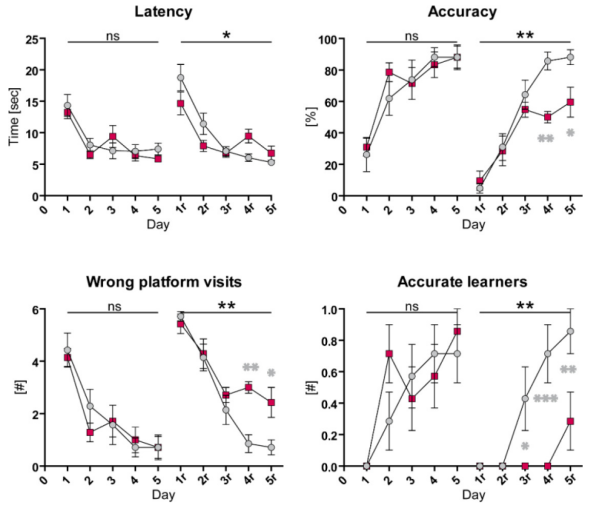

FIGURE 2: Water Cross Maze experiment. Analyzed parameters during first week (learning week, LTP) and second week (reversal learning, LTD). Statistics: Black stars: Two-way ANOVA, grey stars: Bonferroni Posttest.

oscillations. Especially LTD seems to be impaired by the HCN2 deletion in the MS. If HCN2-deletion in the MS does on the other hand lead to a kind of focal seizures, it could be helpful for epileptic patients to specify medication in case of an existing HCN2 mutation.

Keywords: HCN channel, medial septum, mouse brain, firing-properties, cholinergic, GABAergic and glutamatergic neurons, theta oscillations, EEG, Water Cross Maze

REFERENCES

[1] Biel, M., C. Wahl-Schott, S. Michalakis and X. Zong (2009). "Hyperpolarization-activated cation channels: from genes to function." Physiol Rev **89**(3): 847-885.

[2] Hasselmo, M. E. and C. E. Stern (2014). "Theta rhythm and the encoding and retrieval of space and time." Neuroimage **85 Pt 2**: 656-666.

[3] Kemp, M.-V. (2004). "Hippocampal long-term depression and long-term potentiation encode different aspects of novelty acquisition." PNAS **101**: 8192-8197.

[4] Matt, L., S. Michalakis, F. Hofmann, V. Hammelmann, A. Ludwig, M. Biel and T. Kleppisch (2011). "HCN2 channels in local inhibitory interneurons constrain LTP in the hippocampal direct perforant path." Cell Mol Life Sci **68**(1): 125-137.

[5] Notomi, T. and R. Shigemoto (2004). "Immunohistochemical localization of Ih channel subunits, HCN1-4, in the rat brain." J Comp Neurol **471**(3): 241-276.

[6] Stewart, M. and S. E. Fox (1990). "Do Septal Neurons Pace the Hippocampal Theta Rhythm?" TINS **13**(5).

[7] Winson, J. (1978). "Loss of hippocampal theta rhythm results in spatial memory deficit in the rat." Science **201**: 160-163.

Designing and validating the functional assessment of motor and process skills scale (FUMPS) among clients with acquired brain injury

Reetha Janet Sureka S.,Stuti Chakraborty*, Samuel Kamalesh Kumar S., Judy Ann John

Occupational Therapy Unit, Department of Physical Medicine and Rehabilitation, Christian Medical College and Hospital, Vellore, Tamil Nadu, India
**stuti.chakraborty@cmcvellore.ac.in*

INTRODUCTION/MOTIVATION

Occupational Therapy intervention aims to improve the client's occupational performance, hence there is a need for occupational therapists to assess the client's deficits in areas such as cognitive, motor or psychosocial ability. Current tools available for assessing such deficits are not performance based or specific to skills required for occupational performance.

AIM

To develop and validate a function-based assessment tool – the Functional Assessment of Motor and Process Skills Scale (FUMPS) in order to determine the specific deficits in motor and processing skills required for occupational performance, among clients with Acquired Brain Injury.

METHODS

The study consisted of 2 phases. The first phase involved tool development. This phase consisted of categorizing Basic and Instrumental Activities of Daily Living tasks that are expected to be impacted in a client's life due to brain injury. These tasks were collated using the ICF core set for Brain Injury (1). Specific performance skills i.e. both motor and process were identified for each task using the Occupational Therapy Practice Framework (OTPF) (2) which is a globally used and widely accepted clinical practice framework. The finalized tasks and corresponding skills were forwarded for further obtaining an expert panel's opinion consisting of senior (having >10 years of experience)

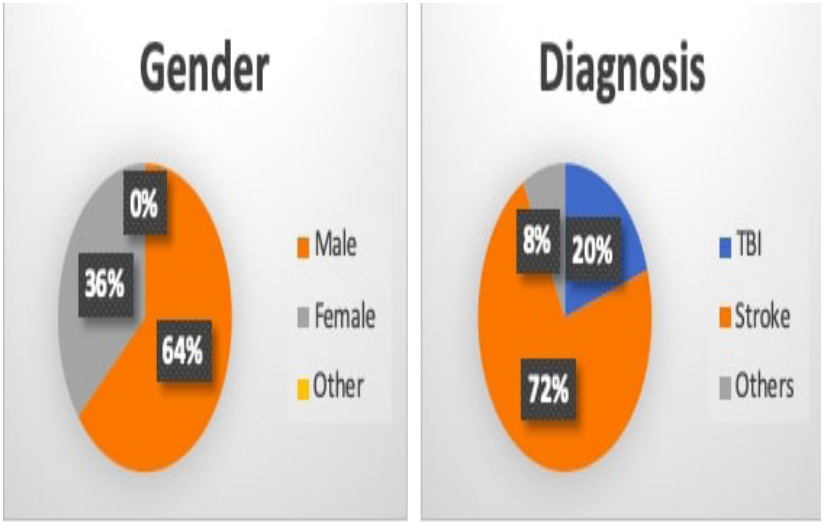

FIGURE 1: Pie-chart representation of gender and diagnosis representation.

rehabilitation professionals in order to measure the face validity of the tool. The second phase consisted of standardization of the tool. For standardization, psychometric properties i.e. convergent validity and reliability of the tool were assessed. It was administered on 25 participants (Demographic and Diagnosis details of participants in Figure 1) with acquired brain injury by two different raters and at two different points of time for finding the inter rater and test retest reliability. For finding the concurrent validity, motor skills component of tool was compared with COVS (3), (4) (Clinical Outcome Variable Scale and the process skills component of the tool with MoCA (5), (6) (Montreal Cognitive Assessment) scores of the participants. These tools were chosen as a the standard for comparison as they were being utilized for routine rehabilitation in the clinical setting where the study was carried out.

RESULTS

FUMPS was found to have good correlation for inter rater reliability for both the motor and process skill components (motor skill - Cronbach's alpha 0.98 , process skill – Cronbach's alpha = 0.99) between two raters and was also statistically significant (P = 0.0 for both motor and process skill).

Table 1: Results of Inter-rater, test re-test reliability and concurrent validity with COVS and MoCA. COVS - Clinical Outcome Variables Scale, MoCA - Montreal Cognitive Assessment

Rater	Cronbach 's alpha and Intra- class correlation (ICC)
Motor Rater 1 and Rater 2	09.8, 0.981
Process Rater 1 and Rater 2	0.99, 0.99
Motor Test Rater 1 and Rater 2	0.99, 0.99
Process Test rater 1 and Rater 2	0.97, 0.97
MOCA and Process Score	0.83, 0.83
COVS and Motor Score	0.78, 0.78

It was also found to have good correlation for test retest reliability (motor skill – Cronbach's alpha = 0.99, process skill – Cronbach's alpha = 0.97) and was also statistically significant (P = 0.00 for both motor and process skill). While assessing concurrent validity, the tool was found to have good correlation with MOCA (Cronbach's alpha = 0.83), moderate correlation with COVS (Cronbach's alpha = 0.78) and was statistically significant (P = 0.00 for both) (Table 1).

DISCUSSION AND CONCLUSION

From this study it can be concluded that the FUMPS is a reliable and valid measure for finding the specific motor and process skill deficits while performing functional tasks among persons with acquired brain injury. Clinicians that used the tool also shared qualitative feedback highlighting the feasibility and ease of use of this tool in comparison other regular standardized assessment tools being utilized as a part of routine neurological rehabilitation protocols. This tool can aid rehabilitation professionals to set realistic, accurate and more function-based goals that can enable the client's optimal level of performance skills to be achieved. In addition, once standardized, the tool can be utilized within multiple contexts, as it is feasible for use and does not require additional training apart from the rehabilitation clinician's existing knowledge. It can further, in the future be used to performance skills deficits in clients with chronic mental illnesses such as Schizophrenia or Bipolar Affective Disorder, but will require further standardization.

ACKNOWLEDGEMENTS

The author would like to thank their guide Ms. Reetha Janet as well as all the co-investigators of this study for their inputs and contributions.

Keywords: occupational therapy, acquired brain injury, traumatic brain injury, activities of daily living, ICF

REFERENCES

[1] Comprehensive_ICF_Core_Set_for_TBI.pdf [Internet]. [cited 2020 Dec 15]. Available from: https://www.icf-research-branch.org/images/ICF%20Core%20Sets%20Download/Comprehensive_ICF_Core_Set_for_TBI.pdf

[2] Occupational Therapy Practice Framework: Domain and Process (3rd Edition). Am J Occup Ther. 2017 Sep 11;68(Supplement_1):S1.

[3] Low Choy, Nancy, Kuys, Suzanne, Richards Megan, Isles Rosemary. Measurement of functional ability following traumatic brain injury using the Clinical Outcomes Variable Scale: A reliability study. AJPT. 2002;48:35–9.

[4] SEABY L. Reliability of a physiotherapy functional assessment used a rehabilitation setting. Physiotherapy Canada. 1989;41:264–71.

[5] The Montreal Cognitive Assessment, MoCA: A Brief Screening Tool For Mild Cognitive Impairment - Nasreddine - 2005 - Journal of the American Geriatrics Society - Wiley Online Library [Internet]. [cited 2019 Apr 29]. Available from: https://onlinelibrary.wiley.com/doi/full/10.1111/j.1532-5415.2005.53221.x

[6] Trzepacz PT, Hochstetler H, Wang S, Walker B, Saykin AJ. Relationship between the Montreal Cognitive Assessment and Mini-mental State Examination for assessment of mild cognitive impairment in older adults. BMC Geriatrics; London [Internet]. 2015 [cited 2019 Apr 29];15. Available from: https://search.proquest.com/docview/1779996706/abstract/F17BF091F3374779PQ/1

Attention and memory encoding in healthy aging and implications for cognitive impairment

Nicholas Cicero*, Elizabeth Riley, Adam Anderson, Eve De Rosa

Department of Human Development, Cornell University, Ithaca, United States
**ngc26@cornell.edu*

INTRODUCTION/MOTIVATION

With lifespan development, various changes occur in the brain that make aging a vulnerable period for cognition. The locus coeruleus (LC), a small area of the brainstem important for attention, plays an important role in neurocognitive aging.[1] The LC-hippocampal pathway supports memory formation as phasic LC activity and LC release of norepinephrine in several hippocampal subfields promotes memory encoding.[2,3] With mild cognitive impairment (MCI) and Alzheimer's Disease (AD), the LC and hippocampus undergo several structural and functional changes.[4,5] In healthy aging, the LC appears to become more important to attention and memory processing, suggesting that LC and hippocampal changes may partly determine neurocognitive outcomes with aging.[6-9] The lifespan trajectory of the LC-hippocampal pathway remain to be fully understood. Additionally, previous research lacks direct and robust neuroimaging of LC activity and functional connectivity. Neuromelanin-sensitive turbo-spin echo (TSE) anatomical MRI and multi-echo functional MRI localize the small LC at a high resolution and will allow us to more robustly obtain LC activity when administering an attention task that has been shown to induce LC activity.[10-12] A better understanding of the LC and hippocampus' role in attention and memory processing with aging will characterize this dynamic brain pathway related to cognition, as well as suggest neural deficits that may occur with MCI or AD.

METHODS

With the use of neuromelanin-sensitive MRI scans to localize the LC and multi-echo fMRI scans, we measured LC and hippocampal activity in young (n = 16) and old (n = 16) healthy adults during the attentional boost effect paradigm. Young adults were between 18 and 65 years old (M = 23) and old adults were those over 65 years old (M = 69). The attentional boost effect is the observed phenomenon that attention to relevant stimuli during a task

may enhance, rather than impair, the ability to process concurrently presented stimuli.[10,11] In this paradigm, participants pressed a button whenever a pre-specified target stimulus (e.g., a high-pitched tone) appears amongst several distractor stimuli (e.g., a low-pitched tone). At the same time participants were instructed to memorize a series of briefly presented images that were paired with the tones. As this task has shown to induce phasic LC activity, which is important for promoting memory encoding, we used this specific task to probe LC and hippocampal activity during attention and memory processing.[12] Following the scan, participants performed a subsequent memory test where they were asked to recall images shown to them in the scanner. Percent accuracy and confidence (rated 0-100) were measured on the subsequent memory test. We additionally administered several neuropsychological assessments to assess cognitive abilities. LC and hippocampal activity during different attention trial types were compared between age groups. Task-related functional connectivity for the LC and hippocampus between target and distractor trials were also compared between age groups. Functional connectivity was computed by correlating LC and hippocampal BOLD during target and distractor trials separately and then subtracting distractor trial correlation coefficients from target trial correlation coefficients. From this we obtain LC-hippocampal functional connectivity during target compared to distractor trials. Whole-brain functional connectivity maps using the LC and hippocampus as separate seeds in relation to attention, memory, and age were also computed using a multivariate model. Currently in progress is a multivoxel pattern analysis (MVPA) using a support vector machine with a searchlight approach to classify whole-brain functional connectivity maps by age group.

RESULTS AND DISCUSSION

An attentional boost effect was defined as more accurate recall or confidence for target trials than distractor trials during the subsequent memory task. There was no significant attentional boost effect for accuracy for young (target: M = 62%, distractor: M = 63%; $t(15)$ = -0.37, p = 0.72) or old adults (target: M = 70%, distractor: M = 71%; $t(15)$ = -0.66, p = 0.52). However, old adults exhibited an attentional boost effect for confidence (target: M = 75, distractor: M = 72; $t(15)$ = 2.18, p = 0.05), which was not observed in young adults (target: M = 62, distractor: M = 60; $t(15)$ = 1.13, p = 0.28). Differences in LC and hippocampal activity during target and distractor trials between young and old adults were present. Task-related LC-hippocampal functional con-

nectivity during target compared to distractor trials was marginally stronger in older adults, suggesting a stronger and positive correlation between LC and hippocampal activity in older adults during attention (young: M = -0.12, SD = 0.41; old: M = 0.20, SD = 0.56; $t(15)$ = -1.90, p = 0.07) (Figure 1). Whole-brain functional connectivity maps indicate large-scale network differences between the LC, hippocampus and several regions, in relation to differences in attention and memory with aging. Preliminary results for MVPA have identified several areas which have functional connectivity with the LC and hippocampus that classify age group greater than chance (Figure 2). Our results indicate differential LC and hippocampal activity between young and old adults in relation to attention processes. Additionally, there appears to be a greater role of the LC-hippocampal pathway in distinguishing task-relevant from distracting information during attention processing in older adults. Whole-brain functional connectivity maps suggest large-scale functional connectivity changes in the LC and hippocampus with neurocognitive aging. Preliminary MVPA results suggest that these large-scale functional changes may be of use in classifying individuals by age group. Future research should explore the mechanisms behind these neurological changes and assess this

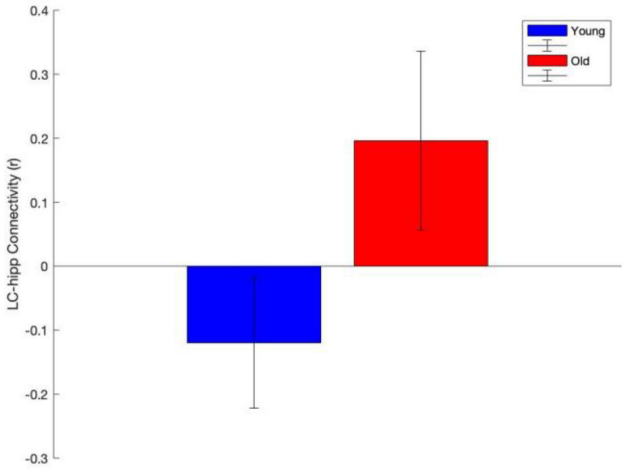

FIGURE 1: LC-hippocampal functional connectivity across age groups. Correlation coefficients displayed are BOLD time series correlations between LC and hippocampal target trials subtracted from correlation coefficients in LC and hippocampal distractor trials.

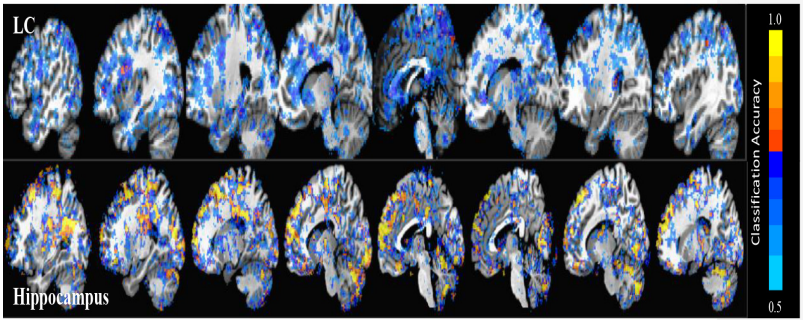

FIGURE 2: Multivoxel pattern analysis of whole-brain functional connectivity maps with LC and hippocampus as separate seed regions using searchlight technique. Classification of age group (chance = 0.5).

relationship in individuals with MCI or AD to understand the role of the LC and hippocampus in pathological aging.

Keywords: locus coeruleus, hippocampus, aging, attention, memory

REFERENCES

[1] Clewett, D.V., et al., *Neuromelanin marks the spot: identifying a locus coeruleus biomarker of cognitive reserve in healthy aging.* 2016. **37**: p. 117-126.

[2] Mello-Carpes et al. *Neurobiology of Learning and Memory* 2013 100:56-63.

[3] Khapour-Taleghani et al. *Behavioral Brain Research* 2008 189:257-262.

[4] Kraak, H. and K. Del Tredici, *The pathological process underlying Alzheimer's disease in individuals under thirty.* Acta Neuropathologica, 2011. **121**(2): p. 171-181.

[5] Braak, H., et al., *Stages of the Pathologic Process in Alzheimer Disease: Age Categories From 1 to 100 Years.* Journal of Neuropathology & Experimental Neurology, 2011. **70**(11): p. 960-969.

[6] Kim, S.Y. and K.S. Giovanello, *The effects of attention on age-related relational memory deficits: evidence from a novel attentional manipulation.* Psychol Aging, 2011. **26**(3): p. 678-88.

[7] Theofilas, P., et al., *Locus coeruleus volume and cell population changes during Alzheimer's disease progression: A stereological study in human postmortem brains with potential implication for early-stage biomarker discovery.* Alzheimers Dement, 2017. **13**(3): p. 236-246.

[8] Mather, M. and C.W. Harley, *The Locus Coeruleus: Essential for Maintaining Cognitive Function and the Aging Brain.* Trends Cogn Sci, 2016. **20**(3): p. 214-226.

[9] Hämmerer, D., et al., *Locus coeruleus integrity in old age is selectively related to memories linked with salient negative events.* Proc Natl Acad Sci U S A, 2018. **115**(9): p. 2228-2233.

[10] Swallow, K.M. and Y.V. Jiang, *The attentional boost effect really is a boost: Evidence from a new baseline.* Attention, Perception, & Psychophysics, 2014. **76**(5): p. 1298-1307.

[11] Swallow, K.M. and Y.V. Jiang, *Attentional load and attentional boost: a review of data and theory.* Front Psychol, 2013. **4**: p. 274.

[12] Turker, H.B., et al., *Estimates of locus coeruleus function with functional magnetic resonance imaging are influenced by localization approaches and the use of multi-echo data*. 2019, bioRxiv.

Glial cells are affected by mitochondrial defect in the Harlequin mouse

Miguel Fernández de la Torre[1]*, Sara Laine Menéndez[1], María Jesús Morán Bermejo[1,2]

[1]Mitochondrial and Neuromuscular Diseases Laboratory, Hospital Universitario de Octubre Research Institute (imas12), Madrid, Spain

[2]Spanish Network for Biomedical Research in Rare Diseases (CIBERER), Spain

**miguel.fnandezt.imas12@h12o.es; mmoran@h12o.es*

INTRODUCTION/MOTIVATION

Mitochondrial diseases (MD) are rare genetic disorders caused by failures in the oxidative phosphorylation system (OXPHOS) function. MD are often multisystemic disorders, in which high-energy demanding cells and tissues, such as the nervous tissue, are the most affected by the mitochondrial failure. Neurons heavily rely on a correct mitochondrial function for many diverse processes and they modulate surrounding glia, through paracrine signals, to assure neuronal metabolism and synaptic activity. Due to their high energy requirements and the limited activity of antioxidant systems, neurons are more susceptible than other cells to OXPHOS defects, that can lead to neurodegeneration [1]. Although glial cells, with a predominant glycolytic metabolism, are more resistant to mitochondrial failure [2], OXPHOS defect in astrocytes has previously shown negative effects on neuronal survival [3]. However, to date, little is known about the role of glia in the progression of MD, and if glial cells are also vulnerable to OXPHOS dysfunction. The `Harlequin´ (Hq) mouse is a representative model of MD with a partial dysfunction of the respiratory chain complex I, caused by a pro-viral insertion in the Apoptosis Inducing Factor gene (AIF) leading to AIF deficiency, that shows cerebellar ataxia among other symptoms [4]. Neurodegeneration in the Hq cerebellum starts with the progressive loss of granular neurons and subsequent Purkinje cell death, and is reportedly accompanied by local neuroinflammation [5], a phenomenon also described in other models of MD [6]. However, the molecular mechanisms underlying glial activation in this and other MD models are unknown. The aim of the present work was to assess if in the Hq mouse model of MD, cerebellum-derived astrocytes and microglial cells show OXPHOS dysfunction, and whether it can trigger neuroinflammation.

METHODS

Primary cell culture of mixed glial cells (astrocytes and microglia) was obtained from P3-P5 postnatal mice cerebella, from hemizygous `Harlequin´ (Hq/Y, B6CBACa Aw-J/A-Aifm1Hq/J) and 'wild-type' (WT, B6CBACa) male mice. Astrocytes and microglia were isolated of mixed culture by MACS magnetic isolation system (Miltenyi Biotec, Bergisch, Gladbach, Germany), and were cultured in DMEM/F12 culture medium, supplemented with 10% fetal bovine serum,100 IU/ml penicillin and 100 IU/ml streptomycin, in poly-L-lysine-coated plates.

For Western blot, cell lysate samples were loaded onto SDS-PAGE gels. Resolved proteins were transferred to PVDF membranes, subsequently blocked, incubated with primary and HRP-conjugated secondary antibodies, and developed with ECL Prime Western Blotting Detection Reagent (Amersham GE Healthcare, Little Chalfont, UK). Cellular oxygen consumption rate was determined in intact cells with the XFp Extracellular Flux Analyzer (Agilent, Billerica, Masachussets, USA). Hydrogen peroxide (H_2O_2) levels were measured in cultured astrocytes by confocal microscopy with the redox-sensitive fluorescent probe 2´,7´-dichlorodihydrofluorescein diacetate (DCFH-DA). Quantitative immunoassay technique, based on Luminex xMAP technology (EMD Millipore Corporation, Billerica, Massachusetts, USA), was performed to assess the levels of IL-1β and TNFα (pg/ml) in the cell culture medium. All study variables are presented as mean $\pm$ SEM. Non-parametric Mann-Whitney U test was used for comparisons between the two groups. Statistical significance was set at p value $p < 0.05$. Tukey test was used as *post hoc* test for multiple comparisons between experimental groups.

RESULTS AND DISCUSSION

Lower levels of complex I subunits were observed in cultured astrocytes from Hq mice in comparison to WT cells, as well as lower levels of mitochondrial protein MIA40, which is involved in the import of cysteine-rich subunits from OXPHOS complexes I and IV [7] (Figure 1A). Respirometry analysis demonstrated lower oxygen consumption rate in Hq-derived astrocytes (Fig.1B). These cells also presented with higher levels of antioxidant enzymes catalase and peroxiredoxin 6 (Fig.1C), as well as higher endogenous H_2O_2 levels and lower H_2O_2 decomposition capacity (Fig.1D). Altogether, these data demonstrate that Hq-derived astrocytes present an intrinsic OXPHOS defect and evidences of oxidative stress.

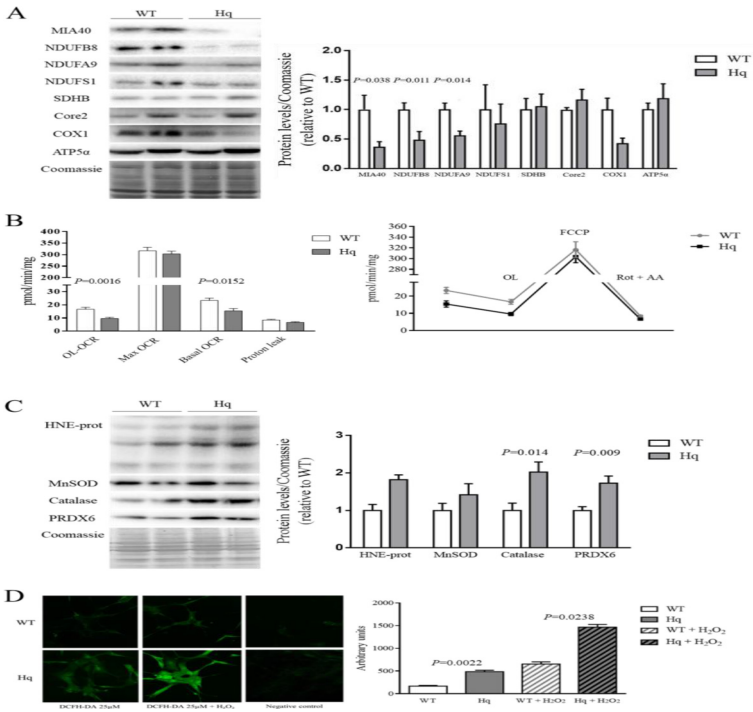

FIGURE 1: WT and Hq-derived astrocytes. (**A**) OXPHOS subunits. Representative Western Blot and densitometry analysis of mitochondrial protein MIA40 and OXPHOS subunits NDUFB8, NDUFA9, NDUFS1, SDHB, Core2, COX1 and ATP5α in WT and Hq-derived astrocytes. Coomassie staining was used as loading control. (**B**) Respirometry analysis. Oligomycin-sensitive (OL-OCR), basal (Basal OCR), maximum (Max OCR) oxygen consumption and proton leak in WT and Hq-derived astrocytes. (**C**) Oxidative stress markers. Representative Western Blot and densitometry analysis of proteins modified by lipid peroxide marker HNE-prot and antioxidant enzymes superoxide dismutase MnSOD, catalase and PRDX6 in WT and Hq-derived astrocytes. Coomassie staining was used as loading control. (**D**) Basal H_2O_2 levels and ability for H_2O_2 removal. Images from confocal fluorescence microscopy of WT and Hq-derived astrocytes, marked with DCFH-DA probe. Mean fluorescence intensity of each cell (15-20 cells) was quantified and expressed as fluorescence arbitrary units compared to control.

In isolated microglia, we observed lower levels of OXPHOS complexes I and IV subunits and MIA40 (Fig.2A), and higher levels of mitochondrial content markers citrate synthase (CS) and heat-shock protein 60 (HSP60) in Hq-derived microglia in comparison to WT cells (Fig.2B). Higher levels of both TNFα and IL-1β were also detected in the culture medium after

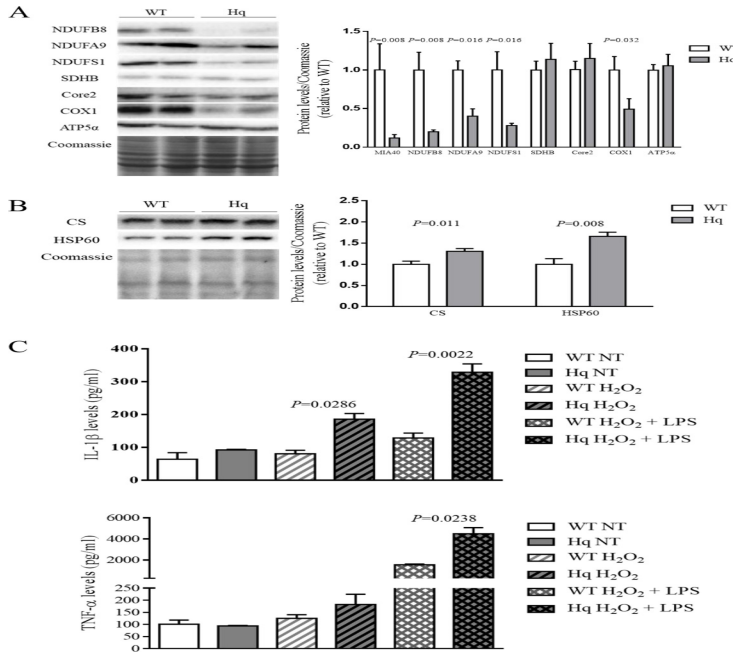

FIGURE 2: WT and Hq-derived microglia. (**A**) OXPHOS subunits. Representative Western Blot and densitometry analysis of OXPHOS subunits NDUFB8, NDUFA9, NDUFS1, SDHB, Core2, COX1 and ATP5α in WT and Hq-derived microglia. Coomassie staining was used as loading control. (**B**) Mitochondrial content markers. Representative Western Blot and densitometry analysis of mitochondrial markers CS and HSP60 in WT and Hq-derived microglia. Coomassie staining was used as loading control. (**C**) IL-1β and TNFα levels. Graphs of IL-1β and TNFα levels in cell culture medium in WT and Hq-derived microglia.

H_2O_2 + lipopolysaccharide (LPS) exposure in Hq-derived microglia (Fig.2C). These results indicate that microglial cells are also affected by the OXPHOS defect, and that it promotes microglia proinflammatory polarization in conditions of exogenous oxidative stress. Combined complex I and IV deficiency suggest that OXPHOS defect is more pronounced in microglia and higher mitochondrial content evidences mitochondrial proliferation, a phenomenon not present in astrocytes.

Although neuroinflammation has been previously reported in the Hq cerebellum by our group and others [5we first revealed that mitofusion 1 (Mfn1,8], it has been

considered an adaptive response of glia to neuronal death. However, our data suggest that AIF deficiency induces, not only a mitochondrial defect in neurons, but also in glial cells, which might trigger their activation and neuroinflammation, independently of the neuronal damage observed in this model. The modulation of astrocyte activation and microglial polarization could be a promising therapeutic target to limit neuroinflammation and neuronal death in MD.

ACKNOWLEDGEMENTS

This work was supported by Fondo de Investigaciones Sanitarias (FIS, ISCIII-MICINN) grants: PI14/01085, PI17/00093 and co-financed by the Regional Development Fund (ERDF/FEDER). MM is supported by Miguel Servet contracts (CPII16/00023). "Ayudas cofinanciadas por el Fondo Europeo de Desarrollo Regional (FEDER). Una manera de hacer Europa".

Keywords: Mitochondrial diseases, neurodegeneration, neuroinflammation, OXPHOS system, Harlequin mouse, ataxia

REFERENCES

[1] Cobley, J. N., Fiorello, M. L. & Bailey, D. M. 13 reasons why the brain is susceptible to oxidative stress. *Redox Biol.* **15**, 490–503 (2018).

[2] Rose, J. *et al.* Mitochondrial dysfunction in glial cells: Implications for neuronal homeostasis and survival. *Toxicology* **391**, 109–115 (2017).

[3] Fiebig, C. *et al.* Mitochondrial dysfunction in astrocytes impairs the generation of reactive astrocytes and enhances neuronal cell death in the cortex upon photothrombotic lesion. *Front. Mol. Neurosci.* **12**, 40 (2019).

[4] Klein, J. A. *et al.* The harlequin mouse mutation downregulates apoptosis-inducing factor. *Nature* **419**, 367–374 (2002).

[5] Chung, S. H., Calafiore, M., Plane, J. M., Pleasure, D. E. & Deng, W. Apoptosis inducing factor deficiency causes reduced mitofusion 1 expression and patterned Purkinje cell degeneration. *Neurobiol. Dis.* **41**, 445–457 (2011).

[6] Quintana, A., Kruse, S. E., Kapur, R. P., Sanz, E. & Palmiter, R. D. Complex I deficiency due to loss of Ndufs4 in the brain results in progressive encephalopathy resembling Leigh syndrome. *PNAS* **107**, 10996–11001 (2010).

[7] Hangen, E. *et al.* Interaction between AIF and CHCHD4 regulates respiratory chain biogenesis. *Mol. Cell* **58**, 1001–1014 (2015).

[8] Fernández-de la Torre, M. *et al*. Exercise training and neurodegeneration in mitochondrial disorders: insights from the Harlequin mouse. *Front. Physiol*. Accepted in press. (2020).

Characterization and correlation of neurodegeneration and biological markers of model mice with traumatic brain injury and Alzheimer's disease

Jason DeBoard*, Rose Dietrich*, James Hughes*, Kyrah Yurko*, Gregory Harms*

Departments of Biology, Bioengineering, and Neuroscience, Wilkes University, Wilkes-Barre, PA., United States of America

**jason.deboard@wilkes.edu, rose.dietrich@wilkes.edu, james.hughes2@wilkes.edu, kyrah.yurko@wilkes.edu, gregory.harms@wilkes.edu*

INTRODUCTION/MOTIVATION

Alzheimer's disease (AD) is the most predominant type of dementia, continues to be a major cause of neural network impairment, and is the 6th leading cause of death in the United States for adults. When compared to the top ten leading causes of death, AD is increasing in mortality more rapidly than other leading causes. Recent findings now indicate that due to either misdiagnosis of AD or due to comorbidity, AD might even need to be corrected to the third (3rd) leading cause of death in industrialized nations. The pathogenesis of this neurodegenerative disorder has yet to be fully elucidated. There are currently no known cures for the disease, and the best current hope is to be able to detect it early enough to impede its progress.

Of the risk factors to develop AD, age is certainly the most important factor. Persons at age 65 have a 16% chance of having AD, and this risk increases to 50% for individuals at 85 years or older. Next to age, the two main risk factors beyond genetics are military service and traumatic brain injury (TBI). For those who have served in the military, the risk of developing AD by the age of 65 years is now 50%, which then increases to over 70% in veterans over 85 years old. The key factor that is associated with military service that likely places this risk is traumatic brain injury (TBI). Those who have served in the military and have at least one reported case of TBI at any level are now shown to have a greater than 65% risk of having dementia by age 65. TBI is also a main cause of dementia in other types of heavy contact activities or occupations such as being a professional football player, in which 99% of

tested professional football players who reported at least one TBI have been shown to have dementia.

METHODS

Our previous studies have shown that we can observe brain damage via brain imaging prior to the noticeable loss of neuromotor control in model mice of neurodegeneration, such as in models of Alzheimer's Disease and in scrapie. In parallel we have also shown that a blood biomarker might be able to be used as an early predictor of AD in model mice.

Traumatic Brain Injury (TBI) is defined as an injury occurring to the brain that leads to different levels of unconsciousness. As mentioned in the introduction, TBI is now being linked to different forms of Dementia. Here we report our study to see if we might be able to predict which mice might show long-term neurodegenerative effects due to differing degrees of TBI, and what level of TBI causes further damage and earlier death to the AD model mice. Upon application of TBIs via an apparatus to effectively induce extremely mild to mild TBIs, wild-type mice and AD mouse models were tested for cognition, neuromotor control, olfactory ability, blood biomarkers and brain imaging. We have observed the long-term effects of TBI are exacerbated in the AD mouse models but that a predictor subset of lipids and of smell tests that correlate to brain damage prior might lead to earlier detection of neurodegeneration in order to define when therapy protocols should be administered.

The specific tests used to create the figures below were the SHIRPA Wire Maneuver and Handling Induced Convulsions (HIC) test. The SHIRPA Wire Maneuver Test examines the neuromuscular and locomotive activity of mice in relation to the progression of Alzheimer's Disease. Each mouse was removed from its cage by its tail and was lowered to a wire until it grasped the wire with its forelimbs. Mice were then suspended horizontally and then released from that position. HIC focuses on the seizure activity of mice, and serves to correlate seizure activity to Alzheimer's Disease progression. Each mouse was be individually withdrawn from their cage by tail suspension and it was spun clockwise or counterclockwise 360 degrees.

The severity of convulsions was then recorded. Both HIC and SHIRPA scores are collected before administering the TBIs, a week after administering the TBIs, and a month after administering the TBIs.

RESULTS AND DISCUSSION

Experiments are currently still in progress and more results are therefore forthcoming. Preliminary data, seen in Figure 1 and Figure 2, suggests that neuromotor control diminishes and epileptic activity increases for both AD and WT after the administration of five consecutive mild TBIs. Another trend that was observed is a decrease in olfactory function after the administration of five consecutive TBIs. If future data supports these findings, important implications about the effect of TBI on those at risk for AD can be made. As for blood lipid analysis and brain imaging, no preliminary data can be presented at this time due to the delay the Covid-19 pandemic has caused.

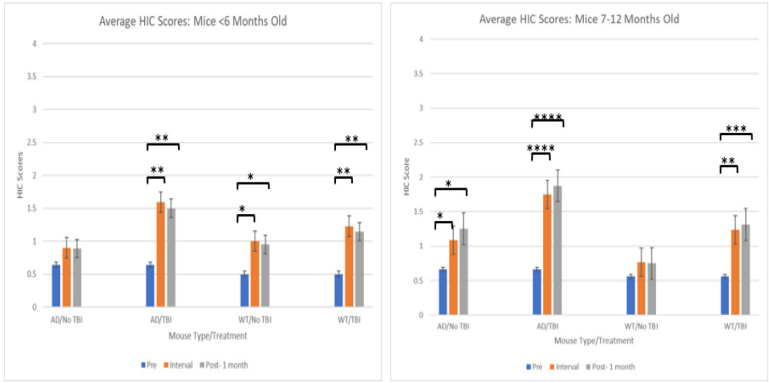

FIGURE 1: (**a-b**) Handling-Induced Convulsions were measured on younger (<6 months) and older (7-12 months) mice pre-TBI, immediately after 5x TBI treatment, and one month after the 5x-TBI treatment. HIC Score refers to a scoring system adapted from Farook et al. 2009. * = < 0.1, ** = < 0.05, *** = < 0.01, **** = < 0.001, ***** = < 0.0001.

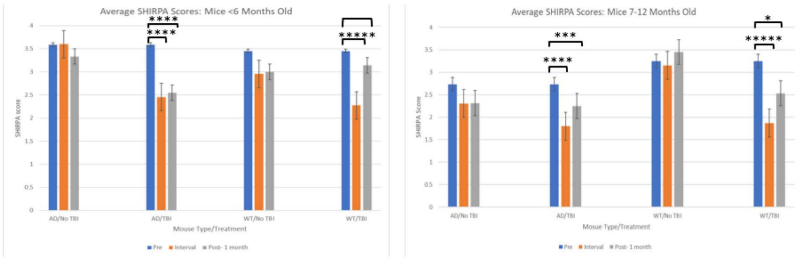

FIGURE 2: (**a-b**) SHIRPA Wire Maneuver test on younger (<6 months) and older (7-12 months) mice pre-TBI, immediately after 5x TBI treatment, and one month after the 5x-TBI treatment. SHIRPA Score refers to a scoring system from Roger et al. 2001. * = < 0.1, ** = < 0.05, *** = < 0.01, **** = < 0.001, ***** = < 0.0001.

Keywords: Alzheimer's Disease (AD), blood biomarker, neurodegeneration, neuromotor control, olfaction, traumatic brain injury (TBI)

REFERENCES

[1] Briggs, Robert et al. "Drug treatments in Alzheimer's disease." Clinical medicine (London, England) vol. 16,3 (2016): 247-53. doi:10.7861/clinmedicine.16-3-247

[2] Bryda, Elizabeth C. "The Mighty Mouse: The Impact of Rodents on Advances in Biomedical Research." *Missouri medicine* 110.3 (2013): 207–211. Print.

[3] Calamia M, Bernstein J, Keller J. 2016. I'd Do Anything for Research, But I Won't Do That: Interest in Pharmacological Interventions in Older Adults Enrolled in a Longitudinal Aging Study. Plos One. 11:e0159664.

[4] Farook, Justin M et al. "Acamprosate attenuates the handling induced convulsions during alcohol withdrawal in Swiss Webster mice." Physiology & behavior vol. 95,1-2 (2008): 267-270. doi:10.1016/j.physbeh.2008.05.020

[5] Halstead ME,Walter KD. Sport-related concussion in children and adolescents. Pediatrics 2010;126:597–615.

[6] Kane MJ, Angoa-Pérez M, Briggs DI, Viano DC, Kreipke CW, Kuhn DM. A mouse model of human repetitive mild traumatic brain injury. J Neurosci Methods. 2012 Jan 15;203(1):41-9. doi: 10.1016/j.jneumeth.2011.09.003. Epub 2011 Sep 12. PMID: 21930157; PMCID: PMC3221913.

[7] Kelleher R, Shen J. 2017. Presenilin-1 mutations and Alzheimer's disease. Proceedings of the National Academy of Sciences of The United States of America. 114:629-631.

[8] Lehmkuhl, A.M., Dirr, E.R., Fleming, S.M. Olfactory Assays for Mouse Models of Neurodegenerative Disease. J. Vis. Exp. (90), e51804, doi:10.3791/51804 (2014).

[9] Mapstone, M., Cheema, A., Fiandaca, M. et al. Plasma phospholipids identify antecedent memory impairment in older adults. Nat Med 20, 415–418 (2014). https://doi.org/10.1038/nm.3466

[10] Mez J, Daneshvar DH, Kiernan PT, et al. Clinicopathological Evaluation of Chronic Traumatic Encephalopathy in Players of American Football. JAMA. 2017;318(4):360–370. doi:10.1001/jama.2017.8334

[11] Oddo S, Caccamo A, Shepherd JD, Murphy MP, Golde TE, Kayed R, Metherate R, Mattson MP, Akbari Y, LaFerla FM. Triple-transgenic model of Alzheimer's disease with plaques and tangles: intracellular Abeta and synaptic dysfunction. Neuron. 2003 Jul 31;39(3):409-21. doi: 10.1016/s0896-6273(03)00434-3. PMID: 12895417.

[12] Pellman EJ, Viano DC, Casson IR, Tucker AM, Waeckerle JF, Powell JW, Feuer H. Concussion in professional football: repeat injuries--part 4. Neurosurgery. 2004 Oct;55(4):860-73; discussion 873-6. doi: 10.1227/01.neu.0000137657.00146.7d. PMID: 15458594.

[13] Rogers, Derek & Peters, Jo & Martin, Joanne & Ball, Simon & Nicholson, Sharon & Witherden, Abi & Hafezparast, Majid & Latcham, Judy & Robinson, Tracey & Quilter, Charlotte & Fisher, Elizabeth. (2001). SHIRPA, a protocol for behavioral assessment: Validation for longitudinal study of neurological dysfunction in mice. Neuroscience Letters. 306. 89-92. 10.1016/S0304-3940(01)01885-7.

[14] Rosen, C., Hansson, O., Blennow, K., and Zetterberg, H. (2013). Fluid biomarkers in Alzheimer's disease - current concepts. Mol. Neurodegener. 8:20. doi: 10.1186/1750-1326-8-20

[15] U.S. Newswire. US death rates from Alzheimer's disease increased 55 percent from 1999 to 2014. (2017, May 25). *U.S.Newswire*

Studies of the protective properties of the NMDA - receptor antagonist memantine on the viability of neurons in rat hippocampal culture when modeling excitotoxicity and Alzheimer's Disease

Vita Ganzha*, Nataliia Rozumna, Elena Lukyanetz

Department of Biophysics of Ion Channels, Bogomolets Institute of Physiology NASU, Kyiv, Ukraine
**V.hanzha@biph.kiev.ua.*

INTRODUCTION/MOTIVATION

Alzheimer's disease (AD) is a progressive neurodegenerative disease that affects memory, thinking, and behavior [1]. There are currently no drugs that could reduce the pathological effects of this disease, but there may be symptomatic relief that can alleviate the disease. NMDA receptors play a crucial role in both synaptic plasticity and transmission. Excessive stimulation of glutamate receptors, mainly NMDA - type, causes intense entry of calcium ions into cells, being the early key step in glutamate-induced excitotoxicity, resulting in many neurological diseases, including AD [2]. In particular, memantine, NMDA -receptor antagonists block the receptor and reduce calcium influx into the neuron, thus blocking the activation of the toxic intracellular events [3]. The purpose of this study was to find out whether memantine, the non-competitive NMDA - receptor antagonist, can protect hippocampal culture neurons from NMDA - and amyloid Aβ1–42 - induced neurotoxicity.

METHODS

This study was conducted on the cultured hippocampal cells obtained from five rats using the technique described in detail previously [4]. Modeling of the AD was carried out by 24-h-long culturing of hippocampal cells in the presence of 2 μM amyloid β1–42 (Sigma-Aldrich, USA). We used combined staining of cells by an indicator of viable and apoptotic cells, Hoechst 33258 (Sigma-Aldrich, USA), and an indicator of dead cells, propidium iodide (Sigma-Aldrich, USA). The viability of neurons was determined by counting them using confocal laser scanning microscopy, comparing cell fluorescence under control conditions, and after 24 hours of incubation with reagents (NMDA, 10 μM, Sigma-Aldrich, USA; memantine, 50 μM, Sigma-Aldrich, USA). Cells were

counted from 4 independent experiments. In each experiment, >200 cells were examined in 5 random fields for each condition. Differences among means were assessed by one-way ANOVA followed by Tukey's post hoc test. The value of P<0.05 was considered statistically significant.

RESULTS AND DISCUSSION

We found that 24-hour incubation of rat hippocampal culture neurons with NMDA or amyloid Aβ1–42 caused more than a twofold increase in the number of cells with signs of apoptosis and/or necrosis compared to the control (Fig.1, 2).

Obtained data indicated a decrease in cell viability under excitotoxicity conditions induced by NMDA or amyloid Aβ1-42 administration during AD modeling. With that, the joint application of memantine and NMDA or joint application of memantine and amyloid Aβ1–42 increased the number of living cells and decreased the number of apoptotic and necrotic neurons the hippocampal cultures (Fig.1, 2). Thus, the memantine application increased the percentage of viable cells, reducing the number of cells that died from apoptosis and/or necrosis.

We concluded that memantine could act as a neuroprotective agent against neuronal degeneration mediated by overactivation of NMDA - receptors and amyloid Aβ1–42. Despite limiting our experiments to cell culture only,

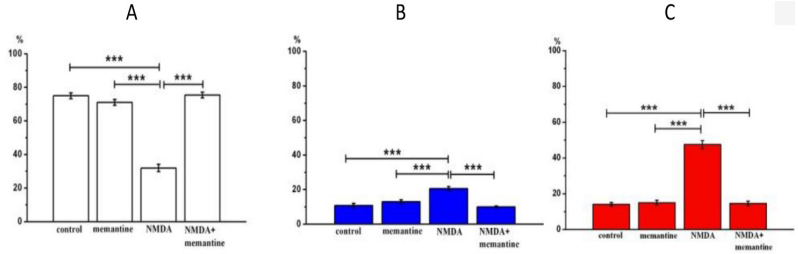

FIGURE 1: Diagrams of the mean values of the relative numbers of cytologically intact cells (**A**), cells with signs of apoptosis (**B**), and necrosis (**C**) in the culture of rat hippocampal neurons after incubation with NMDA (10 μM) and memantine (50 μM). The statistical significance of differences between the values in the groups was estimated using a Student's t-test. *** P<0,001, n= 5.

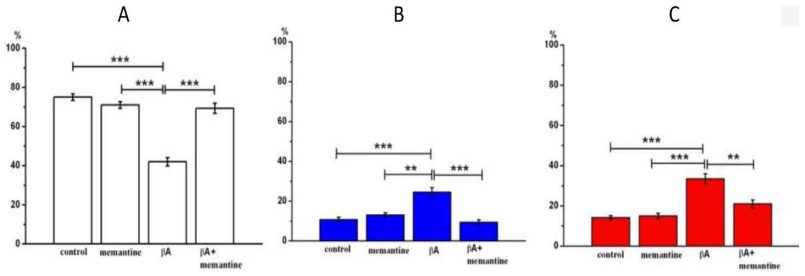

FIGURE 2: Diagrams of the mean values of the relative numbers of cytologically intact cells (**A**), cells with signs of apoptosis (**B**), and necrosis (**C**) in neurons after incubation with AB1–42 (2 μM) and memantine (50 μM) . ** P< 0,01, *** P< 0,001, n= 5.

our results show the opportunity of memantine use to reduce the neuronal loss caused by NMDA - and amyloid Aβ1–42 - induced neurotoxicity seen in patients with AD.

ACKNOWLEDGEMENTS

This study was supported by National Academy of Sciences of Ukraine (NASU) SRN 0118U007344 and NASU to support the development of priority areas of research SRN (state registration number) 0120U001281.

Keywords: Alzheimer's disease, amyloid, cell culture, hippocampal neurons, NMDA

REFERENCES

[1] Citron M. Alzheimer's disease: Strategies for disease modification. Nat Rev Drug Discov. 2010 May;9(5):387–98.

[2] Gonzalez J, Jurado-Coronel JC, Ávila MF, Sabogal A, Capani F, Barreto GE. NMDARs in neurological diseases: A potential therapeutic target. Int J Neurosci. 2015 May 4;125(5):315–27.

[3] Folch J, Busquets O, Ettcheto M, Sánchez-López E, Castro-Torres RD, Verdaguer E, et al. Memantine for the treatment of dementia: A review on its current and future applications. J Alzheimer's Dis. 2018 Jan 1;62(3):1223–40.

[4] Kravenska, E.V., Ganzha, V.V., Yavorskaya, E.N., Lukyanetz, E.A. Effect of Cyclosporin A on the Viability of Hippocampal Cells Cultured under Conditions of Modeling of Alzheimer's Disease. Neurophysiology. 2016. 48(4), 246-51.

Investigating audiovisual emotion processing using EEG

Naomi Heffer[1]*, Anke Karl[2], Krasimira Tsaneva-Atanasova[3], Chris Ashwin[1], Karin Petrini[1]

[1]Department of Psychology, University of Bath, Bath, UK
[2]Mood Disorders Centre, University of Exeter, Exeter, UK
[3]Department of Mathematics, College of Engineering Mathematics and Physical Sciences, University of Exeter, Exeter, UK
**n.r.heffer@bath.ac.uk*

INTRODUCTION/MOTIVATION

Emotions are normally expressed and perceived via multiple senses, and so in order to fully understand the link between sensory and emotional processing, it is necessary to investigate how emotions are perceived using multiple senses. The pilot study presented here aims to examine whether a small group of healthy individuals exhibit differences in brain activity responses (event-related potentials, or ERPs) when presented with emotional information from either single or multiple senses. This pilot serves as a proof of concept for a planned larger study comparing healthy individuals with individuals with trauma and PTSD.

METHODS

Participants were healthy university students (n = 5) who did not report having any psychological or neurological disorders. Participants performed an emotional oddball task where they identified rare emotional faces and voices (expressing sadness, or sadness and happiness) among a stream of frequent neutral stimuli. The task was performed in four different sensory conditions: audio-only (voices only); visual-only (faces only); audiovisual congruent (AVC, faces-voices expressing the same emotion); and audiovisual incongruent (AVI, faces-voices expressing different emotions). In addition to recording ERP data using an Enobio 8 wireless EEG system, we also measured heart rate, high-frequency heart rate variability, and skin conductance levels. These additional physiological measures aimed to determine how physiological arousal changes in the different sensory conditions and how this might relate to brain activity during processing of audiovisual emotional stimuli.

PILOT RESULTS AND RESEARCH IMPLICATIONS

The pilot results show that even based on a very small number of participants, the emotional stimuli elicit a clear oddball effect in the P300 component when perceived among a stream of neutral stimuli. The P300 is a late ERP component characterised by a positive peak occurring between 300-500ms post stimulus-onset. The 'oddball effect' refers to the increase in P300 amplitude which occurs in response to novel stimuli, and this is thought to be representative of an increase in the intensity of perceptual processing, mainly through the allocation of additional attentional resources. In the case of the present study, the oddball effect is assumed to index the additional resources required for processing emotional information in the rare stimuli, which is absent in the neutral frequent stimuli. The oddball effect may be quantified by measuring the difference in peak amplitude between the ERP waveform generated in response to frequent stimuli and rare stimuli. Comparison of effect sizes for the oddball effect in each sensory condition (i.e. Cohen's d) suggests that the oddball effect is greater in the audiovisual task conditions (AVC: d = 0.88, AVI: d = 0.87) compared to the unimodal conditions (Audio: d = 0.44, Visual: d = 0.64), see Figure 1.

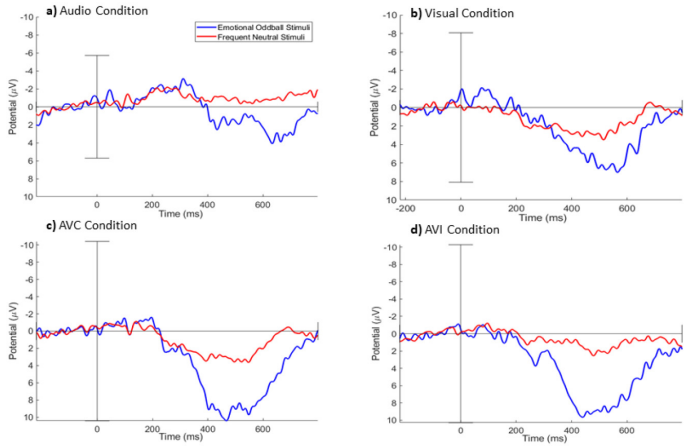

FIGURE 1: Grand average ERP waveforms (n = 5) for the Pz electrode in each of the task conditions: (**a**) audio-only; (**b**) visual-only; (**c**) audiovisual congruent (AVC); and (**d**) audiovisual incongruent (AVI). Waveforms for the emotional oddball trials are plotted in blue, and waveforms for frequent neutral trials are plotted in red. Error bars show the range in amplitude of the ERP waveform across all subjects over the whole epoch.

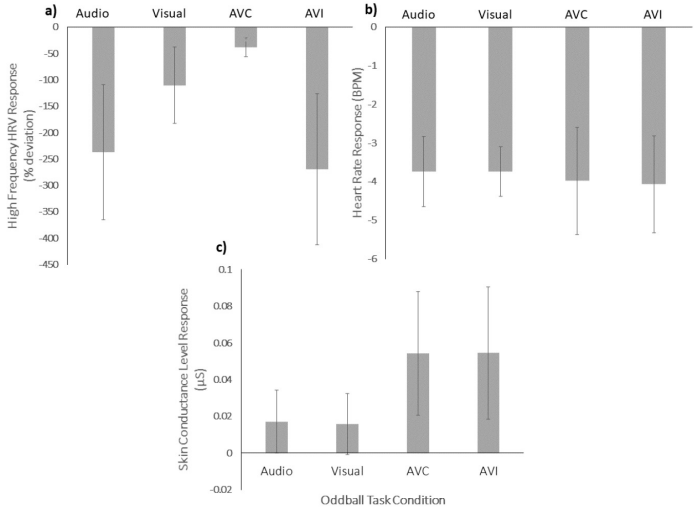

FIGURE 2: Bar graphs showing the physiological response in each task condition of the pilot study (n =5): (**a**) high frequency heart rate variability; (**b**) heart rate; and (**c**) skin conductance level. For each of the measures, the 'response' was defined as the mean level across the block of trials in each task condition minus the mean level measured over the immediately preceding one-minute baseline period. AVC = Audiovisual Congruent; AVI = Audiovisual Incongruent. Error bars represent the standard error of the mean.

The pilot results also reveal potentially interesting differences in physiological arousal across the different task conditions (see Figure 2). There was a much greater decrease in high-frequency heart rate variability in the audiovisual incongruent and audio-only conditions compared to the audiovisual congruent condition ($d \geq 0.65$ for the mean difference between the AVI/audio-only conditions and the AVC condition), which may be indicative of less effective cognitive control and/or emotion regulation during the audiovisual incongruent and audio-only conditions. The pilot results also indicate a larger increase in skin conductance levels in the audiovisual conditions relative to the unimodal conditions ($0.40 \leq d \leq 0.85$ for the mean difference between the AVI/AVC conditions and the visual-/audio-only conditions), indicative of greater sympathetic nervous activation. Overall, the pilot results are consistent with our prediction that there are meaningful differences in brain activity and physiological arousal when processing emotion from unimodal versus

audiovisual stimuli, and so place us in good stead to examine these differences in the context of PTSD when we conduct the full study.

We anticipate that the results from the full study, which will examine processing of multiple emotions (happy, angry and sad), will reveal whether any differences in ERPs between PTSD patients and controls are specific to multisensory emotional processing (i.e. differences only seen in the audiovisual task conditions), which would be consistent with existing behavioural and EEG evidence from high-anxiety individuals. We also plan to exploit the ability of ERP data to temporally discriminate between different stages of multisensory processing to assess more specifically how PTSD individuals differ from the other groups, e.g., in later attentional processes (as indexed by ERP components such as the P300) and/or earlier perceptual processes. This information will inform treatments aiming to improve socio-emotional functioning in PTSD.

ACKNOWLEDGEMENTS

This work was supported by a PhD Studentship from the Medical Research Council (MRC) under award number 2110628. Thanks go to Dr George Stothart for support and training using the EEG system and setting up the paradigm, and to Dr Meike Scheller for her support in creating the EEG data pre-processing and analysis pipelines.

Keywords: ERPs, PTSD, anxiety, oddball paradigm, skin conductance, heart rate, high-frequency heart rate variability, emotion processing, multisensory processing

REFERENCES

[1] A. Koizumi, A. Tanaka, H. Imai, S. Hiramatsu, E. Hiramoto, T. Sato, B. De Gelder, The effects of anxiety on the interpretation of emotion in the face–voice pairs, Exp Brain Res. 213 (2011) 275–282. https://doi.org/10.1007/s00221-011-2668-1.

[2] S. Campanella, D. Delle-Vigne, C. Kornreich, P. Verbanck, Greater sensitivity of the P300 component to bimodal stimulation in an event-related potentials oddball task, Clinical Neurophysiology. 123 (2012) 937–946. https://doi.org/10.1016/j.clinph.2011.10.041.

[3] G. Alba, J. Vila, B. Rey, P. Montoya, M.Á. Muñoz, The Relationship Between Heart Rate Variability and Electroencephalography Functional Connectivity Variability Is Associated With Cognitive Flexibility, Front. Hum. Neurosci. 13 (2019). https://doi.org/10.3389/fnhum.2019.00064.

A dynamical model of action selection and dopamine related movement disorders

Ayça Kepçe[1]*, Neslihan Serap Şengör[2]

[1] *Neuroscience Modelling and Research Group, Istanbul Technical University, Istanbul, Turkey*
[2] *Department of Electrical and Computer Engineering, Technical University Munich, Munich, Germany*
**ayca.kepce@tum.de*

INTRODUCTION

The action selection mechanism in humans is maintained in the loop of basal ganglia-cortex-thalamus [1,2]. This loop is mainly regulated by the neurotransmitter dopamine, which is found in dopaminergic corticostriatal neurons [3,4]. Abnormal levels of dopamine are related to movement disorders. Parkinson's disease and Huntington's disease are related to lack and excess of dopamine, respectively [5,6,7].

This study proposes an action selection model with dynamical approach, which is capable of choosing between different actions, depending on the initial conditions, dopamine levels, and stimuli. Further, by controlling the dopamine parameter, we obtain hypokinesia and hyperkinesia seen in Parkinson's and Huntington's diseases.

METHODS

The direct and indirect pathways in the cortex-basal ganglia-thalamus loop [4,7] are expressed with continuous nonlinear differential equations and activation functions, which are given below. There are two different actions (also called "channels") defined with six variables, p_i (cortex), m_i (thalamus), r_i (striatum), e_i (globus pallidus externus), n_i (subthalamic nuclei), and u_i (globus pallidus internus/substantia nigra pars reticula). The index of the variables, i denote the channel number, where $i \in \{1, 2\}$.

$$\begin{bmatrix}\dot{p_1}(t)\\ \dot{p_2}(t)\end{bmatrix} = -\begin{bmatrix}\lambda_{p1} & 0\\ 0 & \lambda_{p2}\end{bmatrix}\begin{bmatrix}p_1(t)\\ p_2(t)\end{bmatrix} + \begin{bmatrix}W_{mp1} & 0\\ 0 & W_{mp2}\end{bmatrix}\begin{bmatrix}f(m_1(t))\\ f(m_2(t))\end{bmatrix} + \begin{bmatrix}a_1\\ a_2\end{bmatrix}$$

$$\begin{bmatrix}\dot{m_1}(t)\\ \dot{m_2}(t)\end{bmatrix} = -\begin{bmatrix}\lambda_{m1} & 0\\ 0 & \lambda_{m2}\end{bmatrix}\begin{bmatrix}m_1(t)\\ m_2(t)\end{bmatrix} + \begin{bmatrix}W_{pm1} & 0\\ 0 & W_{pm2}\end{bmatrix}\begin{bmatrix}f(p_1(t))\\ f(p_2(t))\end{bmatrix} - \begin{bmatrix}W_{um1} & 0\\ 0 & W_{um2}\end{bmatrix}\begin{bmatrix}f(u_1(t))\\ f(u_2(t))\end{bmatrix}$$

$$\begin{bmatrix}\dot{r_1}(t)\\ \dot{r_2}(t)\end{bmatrix} = -\begin{bmatrix}\lambda_{r1} & 0\\ 0 & \lambda_{r2}\end{bmatrix}\begin{bmatrix}r_1(t)\\ r_2(t)\end{bmatrix} + \begin{bmatrix}W_{pr1} & 0\\ 0 & W_{pr2}\end{bmatrix}\begin{bmatrix}h(p_1(t))\\ h(p_2(t))\end{bmatrix}$$

$$\begin{bmatrix}\dot{e_1}(t)\\ e_{2(t)}\end{bmatrix} = -\begin{bmatrix}\lambda_{e1} & 0\\ 0 & \lambda_{e2}\end{bmatrix}\begin{bmatrix}e_1(t)\\ e_2(t)\end{bmatrix} - \begin{bmatrix}W_{re1} & 0\\ 0 & W_{re2}\end{bmatrix}\begin{bmatrix}f(r_1(t))\\ f(r_2(t))\end{bmatrix} + \begin{bmatrix}W_{ne1} & 0\\ 0 & W_{ne2}\end{bmatrix}\begin{bmatrix}f(n_1(t))\\ f(n_2(t))\end{bmatrix}$$

$$\begin{bmatrix}\dot{n_1}(t)\\ \dot{n_2}(t)\end{bmatrix} = -\begin{bmatrix}\lambda_{n1} & 0\\ 0 & \lambda_{n2}\end{bmatrix}\begin{bmatrix}n_1(t)\\ n_2(t)\end{bmatrix} - \begin{bmatrix}W_{en1} & 0\\ 0 & W_{en2}\end{bmatrix}\begin{bmatrix}f(e_1(t))\\ f(e_2(t))\end{bmatrix} + \begin{bmatrix}W_{pn1} & 0\\ 0 & W_{pn2}\end{bmatrix}\begin{bmatrix}f(p_1(t))\\ f(p_2(t))\end{bmatrix}$$

$$\begin{bmatrix}\dot{u_1}(t)\\ \dot{u_2}(t)\end{bmatrix} = -\begin{bmatrix}\lambda_{u1} & 0\\ 0 & \lambda_{u2}\end{bmatrix}\begin{bmatrix}u_1(t)\\ u_2(t)\end{bmatrix} - \begin{bmatrix}W_{ru1} & 0\\ 0 & W_{ru2}\end{bmatrix}\begin{bmatrix}f(r_1(t))\\ f(r_2(t))\end{bmatrix} - \begin{bmatrix}W_{eu1} & 0\\ 0 & W_{eu2}\end{bmatrix}\begin{bmatrix}f(e_1(t))\\ f(e_2(t))\end{bmatrix} + \begin{bmatrix}W_{nu1} & W_{nu21}\\ W_{nu1} & W_{nu22}\end{bmatrix}\begin{bmatrix}f(n_1(t))\\ f(n_2(t))\end{bmatrix}$$

$$f(x) = 1/(1 + e^{-3x+0.8})$$

$$h(x) = f(x - (1 - \theta))$$

The connections are expressed with W_{ijk} (from *i* to *j*, *k* designating the channel number), the stimulus and dopamine parameter are denoted with a_k (*k* is the channel number) and $\boldsymbol{\theta}$, respectively. The stimuli a can be a visual cue about a certain behavior, e.g. seeing an apple is a stimulus for the action of grabbing the apple. The dopamine parameter $\boldsymbol{\theta}$ is expressed on the cortex-striatum connection via the activation function h(x). The initial conditions can be considered of the current intrinsic state of the person about that action, e.g. being hungry for the grabbing the apple example. The values of the parameters given in Table 1 are determined in our previous work [7,8] and tuned for this model throughout the analyses.

There are four scenarios of the model's decision: selecting no action, the first action, the second action, or both actions. The decision is one of these scenarios, depending on the initial conditions, stimuli, and dopamine. If initially $p_1 > p_2$, then the first channel has a head start. When stimulus to the first channel is greater, the model "has more reasons" to choose that action. On the other hand, dopamine equally affects both channels.

RESULTS

In order to determine the parameters, several dynamical analyses are conducted: time, bifurcation, and domain of attraction analyses. The stimuli and the initial conditions would vary depending on the environment.

Table 1: Values of the parameters

Symbol	Value
$W_{um1,2}$, $W_{ru1,2}$, $W_{pr1,2}$, $W_{pn1,2}$	1
$W_{re1,2}$, $W_{en1,2}$, $W_{pm1,2}$, $W_{ne1,2}$	0.5
$W_{mp1,2}$	1.5
$W_{nu1,2}$	0.725
$\lambda_{p1,2}$, $\lambda_{m1,2}$	0.5
$\lambda_{r1,2}$, $\lambda_{e1,2}$, $\lambda_{n1,2}$, $\lambda_{u1,2}$	1
θ	$\in$ [0.1,0.95]
$a_{1,2}$	$\in$ [0.1,0.15]

Therefore, we analyzed the behavior of the model under different values of stimuli and initial conditions. Further, different values of dopamine parameter are investigated to model movement disorders.

The bifurcation analyses of *a* for different stimuli are given in Figure 1(a)-(c). The bifurcation analyses of *a* for different θ values are also investigated, no bifurcation points occurred in the range of [0.1,0.15]. Then the bifurcation graphs of θ are obtained as given in Figure 1(d) to 1(f). The results of the case a = [0.15;0.1] is symmetrical with a= [0.1;0.15].

The domain of attraction graphs for different *a* and θ values are obtained, as the one given in Figure 2. The initial values of the cortex variable of the first and second channels are located on x and y axes, respectively. Each dot represents the result of the time analysis at given initial conditions. The i^{th} action is considered to be chosen, if $p_i \geq 1$. The green (grey) dots represent both (no) actions are chosen and the blue (purple) dots represent the first (second) action is chosen.

The graphs in Figure 2 are obtained when a = [0.1, 0.1]. For θ = 0.1 the model chooses no actions, regardless of the initial conditions. Both actions are chosen for every initial condition when θ = 0.95 . For the intermediate values of θ, the model chooses the action with the greater initial value of cortex variable. If the initial values of both channels are close to each other, then the model chooses no action or both of the actions, depending on the θ value.

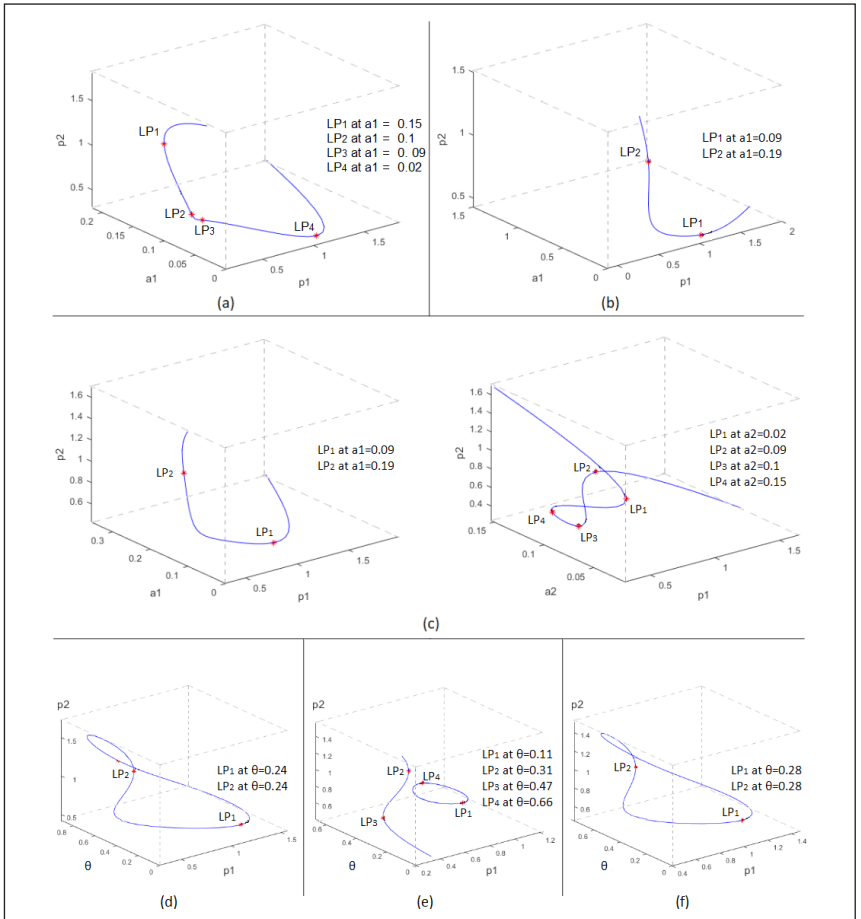

FIGURE 1: Bifurcation graphs of a and θ. LP denotes saddle-node bifurcation. For $\theta = 0.5$, bifurcation analysis of a_1 when (**a**) a = [0.1; 0.1] and (**b**) a = [0.15;0.15] . For $\theta = 0.5$, bifurcation analysis of a_1 and a_2 when a = [0.1; 0.15] Bifurcation analyses of θ, when **d**) a = [0.1; 0.1], **e**) a = [0.1; 0.15] and **f**) a = [0.15; 0.15].

For the cases that the i^{th} stimulus is greater than the other, the i^{th} action is chosen for the intermediate values of θ. No action is chosen at any of the initial conditions when $\theta = 0.1$ and both actions are chosen at every initial condition when $\theta = 0.95$.

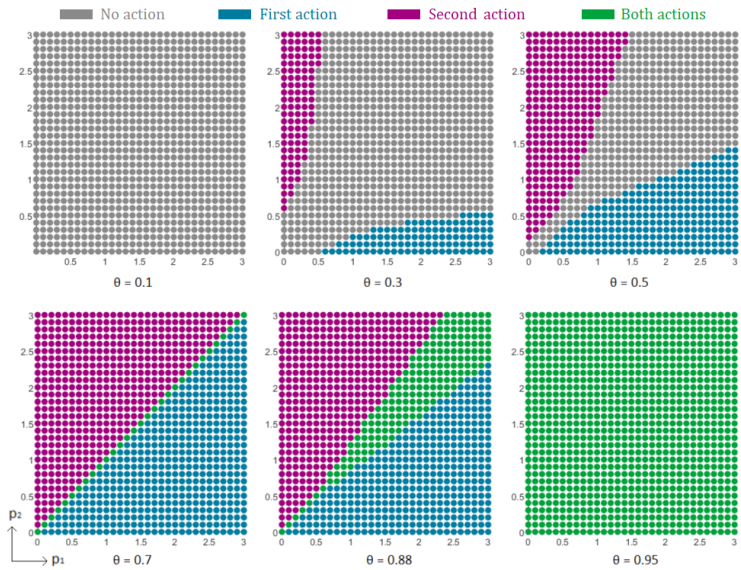

FIGURE 2: The domain of attraction graphs for and different values of a=[0.1; 0.1] and diffrent values of θ.

DISCUSSION

We proposed a dynamical model that selects actions between two choices depending on the initial conditions and the stimuli. The model should show a stable behavior as the stimuli change. Therefore, the range of the stimuli is chosen as a $\in$ [0.1, 0.15], avoiding all of the bifurcation points.

Since we wanted to replicate the hypokinetic and hyperkinetic states as teata changes, the behavior of the model should change quantitatively. Therefore, the range of dopamine parameter should contain at least one saddle-node bifurcation. Considering the bifurcation graphs given in Figure 1(d)-(f), the range is chosen as $\theta \in$ [0.1, 0.95]. For θ = 0.1 and θ = 0.95, the hypokinesia in Parkinson's and the hyperkinesia in Huntington's are obtained, respectively. For the intermediate values of θ, the model behaves as a healthy person who evaluates the situation based on the stimuli and initial conditions, and decides accordingly.

There are some deep brain stimulation (DBS) applications for treating the symptoms of these conditions [9,10]. We believe that our humble model can give intuition for developing more efficient DBS models for treating these diseases. Moreover, the model can be realized on a hardware, e.g. FPGA or a robot microcontroller, due to its simplicity.

Keywords: action selection, basal ganglia, dopamine

REFERENCES

[1] Friend, D.M. & Kravitz, A.V., 2014. Working together: basal ganglia pathways in action selection. *Trends in neurosciences*, 37(6), pp.301-303.

[2] Kropotov, J.D. & Etlinger, S.C., 1999. Selection of actions in the basal ganglia–thalamocortical circuits: Review and model. *International Journal of Psychophysiology*, 31(3), pp.197-217.

[3] Ferré, S., Fuxe, K., Fredholm, B. B., Morelli, M., & Popoli, P. (1997). Adenosine–dopamine receptor–receptor interactions as an integrative mechanism in the basal ganglia. *Trends in neurosciences*, 20(10), 482-487.

[4] Elibol, R., &, Sengör, N. S. (2015, October). A computational model of basal ganglia circuits investigating the role of dopamine on direct and indirect pathways. *In 2015 Medical Technologies National Conference (TIPTEKNO)* (pp. 1-4). IEEE.

[5] Scatton, B., Rouquier, L., Javoy-Agid, F., & Agid, Y. (1982). Dopamine deficiency in the cerebral cortex in Parkinson disease. *Neurology,* 32(9),1039-1039.

[6] Jahanshahi, A., Vlamings, R., Kaya, A. H., Lim, L. W., Janssen, M.L., Tan, S., ...& Temel, Y. (2010). Hyperdopaminergic status in experimental Huntington disease. J*ournal of Neuropathology & Experimental Neurology*, 69(9), 910-917.

[7] Kepce, A., Iris, S., Sengor, N. S. (2020, April). A Neural Network Model for the Role of Dopamine on Action Initiation and Its Realization on FPGA. *In 28th IEEE Conference on Signal Processing and Communications Applications (SIU)*. IEEE.

[8] Kepce, A., &, Sengor, N. S. (2019, October). Bifurcation Analysis of A Mass Model Related to Cortex-Basal Ganglia-Thalamus Loop. In 2019 Medical Technologies Congress (TIPTEKNO). IEEE.

[9] Little, S., Pogosyan, A., Neal, S., Zavala, B., Zrinzo, L., Hariz, M., ... & Green, A. L. (2013). Adaptive deep brain stimulation in advanced Parkinson disease. *Annals of neurology*, *74*(3), 449-457.

[10] Wojtecki, L., Groiss, S. J., Hartmann, C. J., Elben, S., Omlor, S., Schnitzler, A., & Vesper, J. (2016). Deep brain stimulation in Huntington's disease—preliminary evidence on pathophysiology, efficacy and safety. *Brain sciences*, *6*(3), 38.

Highway to a biologically-grounded neural field model of cerebellum

Roberta Maria Lorenzi[1]*, Alice Geminiani[1], Claudia A.M. Gandini Wheeler-Kingshott[1,2,3], Fulvia Palesi[1], Claudia Casellato[1], Egidio D'Angelo[1]

[1]Department of Brain and Behavioral Sciences, University of Pavia, Pavia, Italy
[2]NMR Research Unit, Queen Square MS Centre, Department of Neuroinflammation, UCL Queen Square Institute of Neurology, Faculty of Brain Sciences, London, United Kingdom
[3]Brain Connectivity Center, IRCCS Mondino Foundation, Pavia, Italy
**robertamaria.lorenzi01@universitadipavia.it*

INTRODUCTION

The brain is made of interconnected networks generating its global activity. Several modelling approaches are used to investigate the contribution of local networks to brain global dynamics. While biophysically detailed implementations allow to distinguish the contribution of single neurons to brain dynamics, they are usually too complex for large-scale simulations and need to be condensed into simpler and more abstract models. Typically, these take the form of neural masses or mean fields, which oversimply the physiological properties of an entire neuronal circuit [1,2,3]. What we propose here is an advanced mean field model of the cerebellar cortex that maintains a fundamental set of physiological and structural properties of this specific circuit.

While the cerebellum contains about 50% of all brain neurons, is deeply interconnected with the rest of the brain and remarkably contributes to generate ensemble brain dynamics 4 , the mean field models developed so far are tailored to the cerebral cortex only but may not be effective to capture cerebellar cortex properties. Indeed, the cerebellar circuit organization is peculiar and markedly differs from that of the cerebral cortex. A mean field model of the cerebellar circuit should therefore consider its complex neuronal features, multi-layer organization, quasi-crystalline geometry and local connectivity.

This work aims to develop a mean field model retaining the salient properties of the cerebellar circuit. The model will be used not just to provide theoretical insight on cerebellar network functioning but also to simulate the impact of cerebro-cerebellar interactions on whole brain dynamics in the framework of The Virtual Brain (TVB).

METHODS

The design of the cerebellar mean-filed model starts from an accurate and extensive knowledge of cerebellar anatomy and physiology. The model includes the main populations of the cerebellar cortex - Granular Cells (GrC), Golgi Cells (GoC), Molecular Layer Interneurons (MLI) and Purkinje Cells (PC) – and their connections. The connections among these neuronal populations include different excitatory, inhibitory or self-inhibitory synapses (Figure 1). Furthermore, we account for the multi-layer organization of the cerebellar cortex, where GrC layer and PC layer are the input and output layers, respectively5. The reference in functional terms is the spiking activity of neurons modelled as E-GLIF single-point neurons[6,7] optimized for each population . Population-specific firing frequencies and synaptic connections are used to calculate the conductance for each cell population (equations in Figure 1). A Transfer Function (TF) mathematical formalism[2] is used to transform population-specific spiking patterns into a time-continuous global output. This approach is inspired to that already validated for the implementation of mean-field models of isocortical circuits made of excitatory and inhibitory neurons [9–11]. Here, the mean-field TF formalism accounts also for the physiological

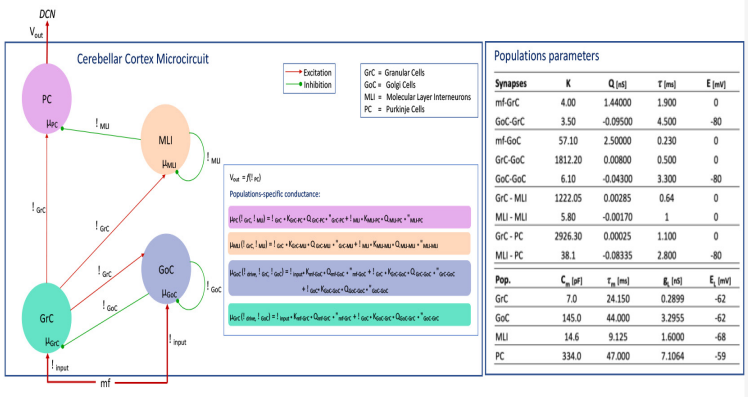

FIGURE 1: Cerebellar cortex microcircuit model. The external input ν_{input} is relayed by mf to GrC and GoC. The output activity ν_{PC} projects to the DCN. ν_{input} =external input [Hz]; for each population p or connection c: mp=conductance of each population [nS]; νp=firing rate of each population [Hz]; Kc=connections probability*cells numbers; Qc = quantal synaptic conductance [nS], τ_c=synaptic time decay [ms]. p = GrC, GoC, MLI, PC. c = mf-GrC, mf-GoC, GrC-GoC, GoC-GrC, GoC-GoC, GrC-MLI, MLI-MLI, GrC-PC, MLI-PC.

diversification of cerebellar neuronal populations and for their topological organization. GrCs and GoCs receive, through mossy fibers (mf), external synaptic input (ν_{input}) coming from other brain areas[5]. The detailed placement and connectivity generated by scaffold model approaches[8,12] are used to set connection probability (K). Detailed synaptic models (tuned and validated for each pairwise connection types) are used to set quantal synaptic conductances and synaptic time decays (Q,τ). Six different stationary ν_{input} (10, 20, 40, 60, 80, 100 Hz) are used to generate reference spiking activity in NEST for fitting the TFs.

PRELIMINARY RESULTS AND DISCUSSION

Figure1 shows the model structure and the conductance equation for each population with the explicit dependencies from the synaptic parameters K, Q and τ (values in Figure1-right). Figure2 shows our pipeline for PC. The color-map shows the behavior of the parameters used for TF fitting for either excitatory (ν_{GrC}) and inhibitory input activity (ν_{MLI}) to PC. The pipeline is extended to other populations. The final cerebellar mean-field formalism is reported in Figure2-right.

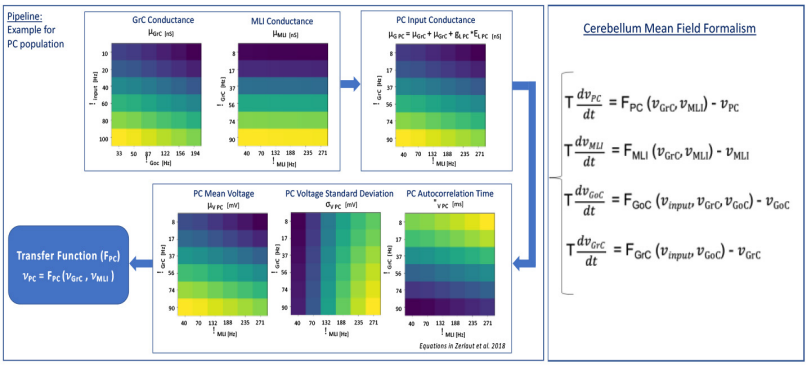

FIGURE 2: Pipeline to compute transfer function. Left: Color-map shows from yellow to blue the parameters used for Transfer Function Fitting. Population conductances assume high values for high excitations combined with low inhibition (Map bottom-left corner). PC mV follows the same conductances trend, while σ_V is higher for low excitation and high inhibition. τ_V is higher for low excitation-high inhibition. Right: Cerebellum Mean Field Equations.

Compared to the existing mean field model, our cerebellar network is built up with a bottom-up approach tailored to the specific structural and functional interactions of the neurons population in the cerebellum.

This work aims, for the first time, to implement a mean-field model of cerebellum able to reproduce its population dynamics and to investigate specific cerebellar alterations in pathologies like ataxia and autism.
This design will allow to investigate, for each population, how its activity affects the cerebellar cortex output enabling a theoretical interpretation of network functions.

The spatial localization of input stimuli from the extended brain connectome will be fundamental to understand the topological organization of cerebellar signal processing. This will require multiple modules of this cerebellar mean field, each one receiving *mf*s from specific source regions. The differentiated descriptions of synapses connecting neuronal populations will allow to account for critical factors controlling local circuit dynamics (e.g. differentiation between AMPA and NMDA receptor at excitatory synapses, or between parallel fibers and ascending axons at GrC-GoC and GrC-PC synapses). Finally, to extend the model toward the mesoscale, the TF will be extended from the cerebellar cortex to include Deep Cerebellar Nuclei (DCN).

Once an interconnected set of cerebellar mean fields will be built and validated, it will be mapped on brain atlases and integrated in TVB, in order to exploit the long-range connectome. A recent work[13] demonstrated the importance of cerebellum in whole brain dynamics by focusing on cerebro-cerebellar loop Those results will be compared with those generated with the present ad-hoc mean field. TVB-NEST co-simulations are being developed to reproduce brain activity at different levels of granularity (e.g. with single neurons or populations resolution). It will be interesting to compare the change of brain dynamics when the cerebellum is modelled as a NEST spiking node in the full TVB or as the mean field node described here.

REFERENCES

[1] Pinotsis D, Robinson P, Graben PB, Friston K. Neural masses and fields: Modeling the dynamics of brain activity. Front. Comput. Neurosci. 2014;8(NOV):2013–2015.

[2] Boustani S El, Destexhe A. A master equation formalism for macroscopic modeling of asynchronous irregular activity states. Neural Comput. 2009;21(1):46–100.

[3] DiVolo M, Romagnoni A, Capone C, Destexhe A. Biologically Realistic Mena-Field Models of Conductance-Based Networks of Spiking Neurons with Adaptation. Neural 2019;31:653–680.

[4] D'Angelo E. Physiology of the cerebellum [Internet]. 1st ed. Elsevier B.V.; 2018.Available from: http://dx.doi.org/10.1016/B978-0-444-63956-1.00006-0

[5] Gandolfi D, Pozzi P, Tognolina M, et al. The spatiotemporal organization of cerebellar network activity resolved by two-photon imaging of multiple single neurons. Front. Behav. Neurosci. 2014;8(APR):1–16.

[6] Geminiani A, Casellato C, Locatelli F, et al. Complex dynamics in simplified neuronal models: Reproducing golgi cell electroresponsiveness. Front. Neuroinform. 2018;12(December):1–19.

[7] Geminiani A, Casellato C, D'Angelo E, Pedrocchi A. Complex electroresponsive dynamics in olivocerebellar neurons represented with extended-generalized leaky integrate and fire models. Front. Comput. Neurosci. 2019;13(June):1–12.

[8] De Schepper R, Al E. The Brain Scaffold Builder, a package for structural and functional modelling of brain circuits: the cerebellar use case. *In preparation*;

[9] Kuhn A, Aertsen A, Rotter S. Neuronal Integration of Synaptic Input in the Fluctuation-Driven Regime. J. Neurosci. 2004;24(10):2345–2356.

[10] Zerlaut Y, Chemla S, Chavane F, Destexhe A. Modeling mesoscopic cortical dynamics using a mean-field model of conductance-based networks of adaptive exponential integrate-and-fire neurons. J. Comput. Neurosci. 2018;44(1):45–61.

[11] Zerlaut Y, Destexhe A. Enhanced Responsiveness and Low-Level Awareness in Stochastic Network States [Internet]. Neuron 2017;94(5):1002–1009.Available from: http://dx.doi.org/10.1016/j.neuron.2017.04.001

[12] Casali S, Marenzi E, Medini C, et al. Reconstruction and simulation of a scaffold model of the cerebellar network. Front. Neuroinform. 2019;13(May):1–19.

[13] Palesi F, Lorenzi RM, Casellato C, et al. The Importance of Cerebellar Connectivity on Simulated Brain Dynamics. Front. Cell. Neurosci. 2020;14(July):1–11.

fMRI-characteristics of pathophysiology and rTMS therapy mechanisms of chronic migraine

Kirill Markin*, Darya Frunza, Dmitriy Tarumov, Artem Trufanov

Neurology Department, S.M. Kirov Military Medical Academy, Saint-Petersburg, Russia
**vmeda.work@ya.ru*

INTRODUCTION

Migraine is one of the most important causes of disability worldwide according to the Global Burden of Disease Study 2016 [1]. Despite of various symptoms of migraine, the most common and debilitating is chronic pain, which associated with modifications at large-scale brain networks interacting. Functional magnetic resonance imaging (fMRI) allows to find out the alterations of the Salience (detecting and filtering salient stimuli), Default Mode (the main mind-wandering network which activates in resting-state), FrontoParietal (sustained attention and executive functions), Dorsal Attention (engaged during externally directed attentional tasks), SensoriMotor (associated with pain and cognition), Visual, Auditory, and Language networks interaction. Abnormal functional connectivity between these networks and subcortical regions represent the pathophysiological mechanisms of the disease. So, the clinical benefit of treatment might be defined by the modification of these abnormalities. Transcranial magnetic stimulation is one of those, which are mentioned to modify the large-scale brain networks interaction among migraine patients.

There are two primary aims of our study: 1. To investigate the pathophysiological mechanisms of chronic migraine throw the functional connectivity (FC) analysis; 2. To ascertain the efficacy of repetitive transcranial magnetic stimulation (rTMS) in chronic migraine patients.

To meet the needs of our goals, previously, we evaluated FC alterations of large-scale brain networks in chronic migraine patients. [2, 3] Then, we estimated the differences of FC before and after 5-day rTMS-therapy course compared to healthy controls. The final step of our study will be a randomized, blinded, placebo-controlled rTMS-therapy study with fMRI-control.

METHODS

At the first step of study 25 patients with chronic migraine diagnosis (ICHD-3) during the interictal period and 25 age- and sex-matched healthy controls underwent 1,5T MRI scanning. The exclusion criteria of the patient group were psychiatric and neurological disorders, contraindication to MRI, alcohol or drug (except of anti-migraine therapy) abuse. Each patient completed a test battery, which included the Numeric Rating Scale to assemble current pain intensity, the Migraine Disability Assessment Questionnaire, the Leeds Dependence Questionnaire, and the Hospital Anxiety and Depression Scale. We performed pre- and postprocessing of MRI data using "CONN functional connectivity toolbox version 19c" [4] based on MATLAB 2019b software. Primary analysis included functional realignment, unwarp, slice-timing correction, outlier identification, direct segmentation, normalization into standard MNI space, functional smoothing, and denoising. Then, ROI-to-ROI (region of interests) connectivity measures of 8 large-scale brain networks and 16 subcortical structures, involved in the pathophysiology of migraine were estimated, based on two-sample t-test of chronic migraine compared to healthy controls. We also performed the regression analysis of FC alterations and results of the test battery. False discovery rate correction $P<0,05$ was applied for all multiple comparisons.

The second step of research included rTMS interventions consisted of 30-minutes stimulation of ventrolateral prefrontal cortex and trigeminal nerve sensory branches for five days. 20 chronic migraine patients with the same inclusion and exclusion criteria before and after 5-day rTMS-therapy course were assessed with 1,5T MRI scanning during the interictal period. 29 healthy controls were included for comparison. Patients completed the same test battery immediately after each fMRI scanning. Each rTMS session included 10 Hz both sides stimulation at 60% of motor thresholds for 900 pulses. The 10 Hz protocol was administrated as trains of 60 pulses over 6,0 seconds followed by 20 seconds of rest. First analysis of fMRI data was identical to the previous step. Postprocessing included ROI-to-ROI analysis of 8 large-scale brain networks and 31 subcortical structures based on 2x2 mixed ANOVA statistics between chronic migraine group before and after rTMS course compared to healthy controls.

RESULTS AND DISCUSSION

We founded significant decrease of Numeric Rating Scale for pain intensity, Migraine Disability Assessment Questionnaire, and Leeds Dependence Questionnaire scores after rTMS-therapy. FC alterations were founded in many networks and subcortical regions, but we decided to fix attention on two mains of them.

Chronic migraine patients compared to healthy controls were characterized by increased FC between SensoriMotor and Salience Networks (T=3.46, p-FDR<0.05) (Fig.1). It can represent the higher intrinsic attention to pain stimuli in migraine. Whereas, after rTMS-therapy we observed decreased FC between these networks (F = 6.54, p-FDR<0,05) (Fig.2).

Increased FC between nucleus accumbens and Default Mode Network in chronic migraine patients (T=4.49, p-FDR<0.05) (Fig.1) was decreased after rTMS-therapy (F=9.34, p-FDR<0,05) (Fig.2). Moreover, we observed increased

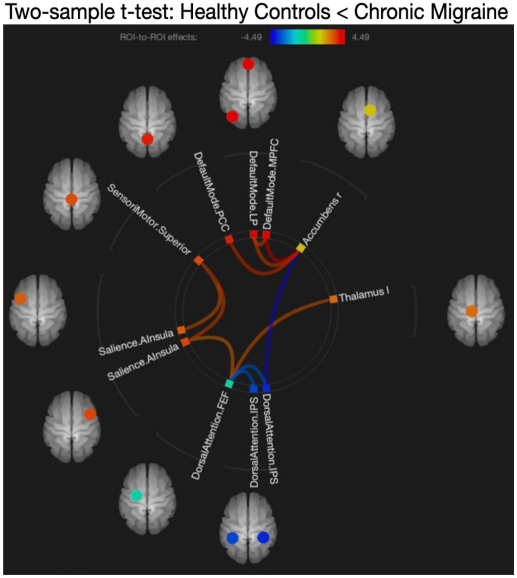

FIGURE 1: ROI-to-ROI FC ring with significant FC differences between migraine patients and healthy controls. Red indicates an increased FC; blue indicates a decreased FC.

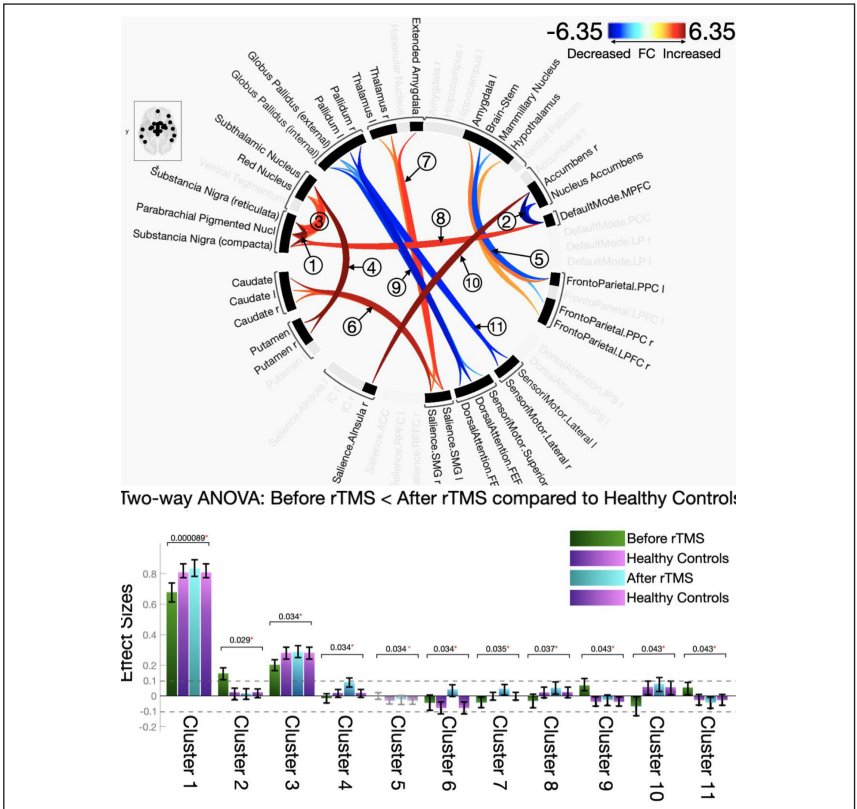

FIGURE 2: Top image: ROI-to-ROI FC ring with significant FC differences between before rTMS treatment and after rTMS treatment compared to healthy controls, where numbers from 1 to 11 denotes cluster's numbers; warmer colors represent increased FC, whereas cooler colors represent decreased FC. Bottom image: FC differences for 11 clusters that significantly differed (following correction for multiply comparisons) between before rTMS treatment and after rTMS treatment compared to healthy controls. * - pFDR < 0,05.

FC within substantia nigra after rTMS (Fig.2). Nucleus accumbens, substantia nigra, and medial prefrontal cortex (hub of Default Mode Network) are main structures of reward dopaminergic pathway. Chronic pain conditions produce the hypodophaminergic state. Thus, we think rTMS-therapy may help modify reward deficiency and anti-reward mechanisms in migraine chronification [5].

Due to these significant FC alterations, we suggest that reward system impairment during the migraine chronification leads to abnormal saliency of pain stimuli. But rTMS-therapy could re-modulate the reaction of brain pain pathways to acute pain stimuli in a healthier way and balance the reward deficiency. A limitation of our study is that we cannot claim that these results represent the effect of therapy. Thereby, we plan the 3rd part of our research - placebo-controlled study.

At the last step of research, we suppose to compare FC alterations of the large-scale brain networks and subcortical regions, involved in pathophysiological mechanisms of migraine among 60 chronic migraine patients, randomized into equal rTMS and sham-rTMS groups. Then, we consider to use the same methods of statistical analysis as in the second step of research to evaluate the efficacy of rTMS-therapy in chronic migraine patients with placebo control.

Keywords: functional connectivity, large-scale brain networks, headache, transcranial magnetic stimulation

REFERENCES

[1] GBD 2016 Headache Collaborators. Global, regional, and national burden of migraine and tension-type headache, 1990-2016: a systematic analysis for the Global Burden of Disease Study 2016. Lancet Neurol. 2018 Nov;17(11):954-976. doi:10.1016/S1474-4422(18)30322-3.

[2] Trufanov, A, Markin, K, Frunza, D, Litvinenko, I, Odinak, M. Alterations in internetwork functional connectivity in patients with chronic migraine within the boundaries of the Triple Network Model. Neurol Clin Neurosci. 2020; 8: 289– 297. doi.org/10.1111/ncn3.12423

[3] Markin, K. A common ground for pain and affective disorders among migraine patients according to internetwork disbalance. European Neuropsychopharmacology. 2020; 31(Supp.1): S50-S51. doi.org/10.1016/j.euroneuro.2019.12.069

[4] Whitfield-Gabrieli S, Nieto-Castanon A. Conn: a functional connectivity toolbox for correlated and anticorrelated brain networks. Brain Connect. 2012;2(3):125-41. doi.org/10.1089/brain.2012.0073

[5] Borsook D, Linnman C, Faria V, Strassman AM, Becerra L, Elman I. Reward deficiency and anti-reward in pain chronification. Neurosci Biobehav Rev. 2016 Sep;68:282-297. doi: 10.1016/j.neubiorev.2016.05.033

Characterization of Cyto-architecture of microglia in neurological disorders

Hasitha Nimmagadda[1], Pallavi Shrivastava[2*]

[1]Lynbrook High School, San Jose, CA, USA
[2]Laboratory of Genomics and Neurovascular Diseases, Catholic University of Santa Maria, Arequipa, Peru
**pallavitoxi@gmail.com*

INTRODUCTION/MOTIVATION

Microglia are key immune mediator cells in the brain and are known to respond to toxicity, injury and inflammation. Microglia are extensively studied in various brain pathologies for e.g. Alzheimer's disease (AD), Parkinson's disease (PD), which are neurodegenerative diseases and in trauma based injuries like Stroke and Traumatic brain injury (TBI). They act as the first line of defence in case of an injury. However, microglia do not only cause damage by releasing pro-inflammatory cytokines and reactive oxygen species, they can also exert beneficial functions e.g. homeostasis and synaptic pruning during development. The microglia are categorized into classically activated proinflammatory (M1) and alternatively activated anti-inflammatory (M2) cells. Alternatively activated M2 macrophages exhibit increased phagocytosis of apoptotic cells, which could involve activation of the scavenger receptor CD36 and inhibition of its negative regulator, toll-like receptor (TLR-4). Importantly, interleukin-10 (IL-10), an anti-inflammatory cytokine, represses inflammation and initiates repair. M1-polarized microglia is characterized by amoeboid phenotype and M2 microglia are ramified in phenotype (Figure 3). Here we investigated the polarization of microglia in different neurological disorders and characterization based on cyto-architecture changes their phenotypes. During microglial activation, the cyto-architecture of microglia changes drastically from ramified to amoeboid morphology. Here we have categorized microglia into 4 stages of activation from fully ramified microglia (resting microglia), partially ramified microglia, partially amoeboid microglia, fully amoeboid microglia (activated microglia) in neurodegenerative diseases and in traumatic brain injury. We hypothesize that changes in phenotypes of microglia can give an insight of pathological changes in early stages in neurodegenerative diseases and by targeting specific subtypes of microglia may preferentially lead to a treatment for neurodegenerative diseases. By studying the morphology of microglia and different receptors present in stages of microglia (M1 and M2) in neurological disorders may

give an insight for future therapeutic strategy for traumatic brain injuries and various neurological disorders.

METHODS

Characterization of Microglial cells in AD and PD

The confocal images were obtained from the authors of published studies on microglia in various neurological disorders. For Alzheimer's disease study, we obtained confocal images from Dr. Kathryn Hopperton (Department of Nutritional Sciences, Faculty of Medicine, University of Toronto, Toronto, Canada). For this study, 10-week-old male C57BL/6 mice were obtained from Charles River Laboratories (Saint Constant, Quebec, Canada) and Intracerebroventricular (ICV) amyloid-β (1-40) infusion was given to mice. Mice were euthanized after 28 days post-surgery. Control (wild type) and Abeta amyloid treated mice (to produce disease condition) brain samples were obtained for immunohistochemistry and brain coronal sections were stained with Ionized calcium-Binding Adapter molecule-1 (IBA-1, Wako, 1:400) and developed by using Alexa-fluor 488 (green). The 40X confocal images were taken from the CA3 region of the hippocampus. Microglial cells were counted using Fiji image-J software. For PD, we have obtained images from Dr. Ashley S. Harms, Center for Neurodegeneration and Experimental Therapeutics, Department of Neurology, The University of Alabama at Birmingham, Birmingham AL, USA. We have taken images from the published paper "Peripheral Monocyte Entry is Required for Alpha-Synuclein Induced Inflammation and Neurodegeneration in a Model of Parkinson Disease" Exp Neurol. 2018 Feb; 300: 179–187.

We used confocal images to review the cyto-architecture of microglia and characterize the stages of microglia based on circularity in AD and PD.

Statistics analysis

Microglia stained with IBA-1 were counted using Fiji image-J software and student's t-test with 95% level of confidence was used to analyze differences between control and AD groups and Control and PD groups.

RESULTS AND DISCUSSION

The confocal images data for AD showed (Figure 1) that there is a significant decrease in ramified ($p<0.001$) and partially ramified ($p<0.05$) microglia population after Aβ-amyloid injection as compared to control. In contrast, there is a significant increase in partially amoeboid ($p<0.05$) and fully amoeboid ($p<0.001$) microglia population in AD group as compared to controls. We found that Aβ-amyloid ICV injection alters the morphology of microglial cells by inducing changes in phenotypes from ramified microglia (resting stage) to amoeboid microglia (active stage) in the CA3 region of the hippocampus.

For PD (Figure 2), we found no significant changes in ramified, partially ramified and partially amoeboid microglial population in substantia nigra in Adeno-associated viruses2-synuclein (AAV2-SYN) (PD) group as compared to Adeno-associated viruses2-Green fluorescent protein (AAV2-GFP) (Control). Significant increase in the number of fully amoeboid microglial cells were found in substantia nigra in AAV2-SYN (PD) group as compared to AAV2-GFP (Control).

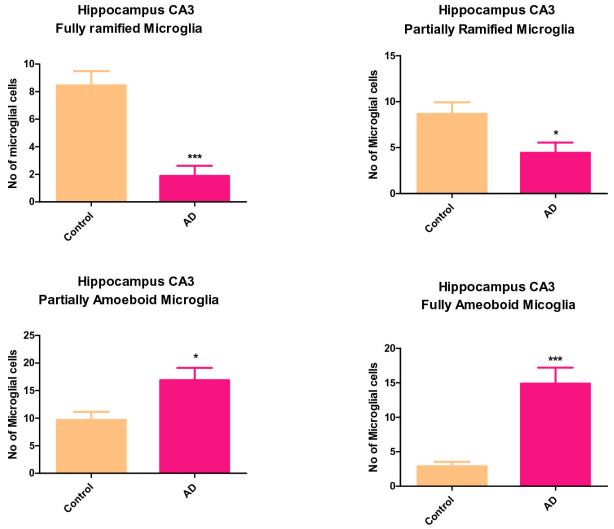

FIGURE 1: Microglia Characterization in AD.

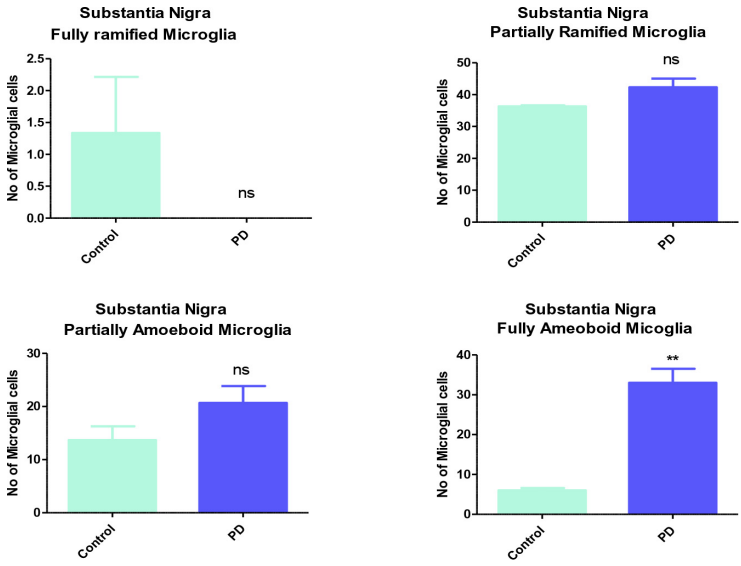

FIGURE 2: Microglia Characterization in PD.

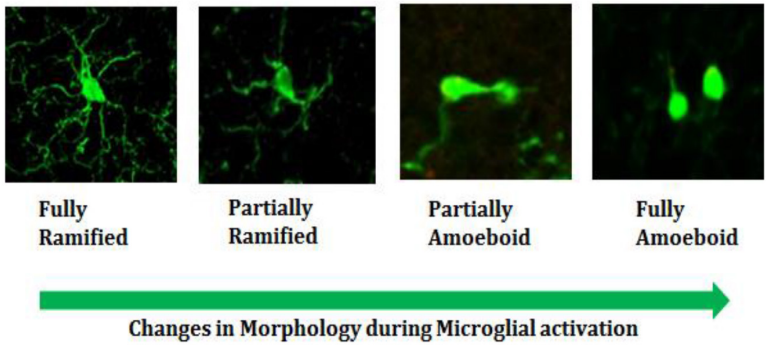

FIGURE 3: Morphological changes in microglia during activation.

These results indicate that AD has more aggressive phenotypic changes in microglia and have significant differences in ramified microglia and amoeboid microglia. However in PD there is only a significant surge in fully amoeboid microglial population as compared to controls. These results suggest that different neurological disorders like AD and PD have distinct patterns of activation of microglia with different phenotypes of microglia.

ACKNOWLEDGEMENTS

We thank Dr. Kathryn Hopperton and Dr. Ashley Harms for providing confocal images of microglia. We extend our thanks to Dr. Soyon Hong (UK Dementia Research Institute, University College London, UK) and Dr. Namas Chandra (Rutgers University, New Jersey, USA) for providing z-stack and confocal images of microglia for the study.

Keywords: Microglia, Alzheimer's disease, Parkinson's disease

REFERENCES

[1] Hopperton KE, Trépanier MO, Giuliano V, Bazinet RP. Brain omega-3 polyunsaturated fatty acids modulate microglia cell number and morphology in response to intracerebroventricular amyloid-β 1-40 in mice. J Neuroinflammation. 2016 Sep 29;13(1):257. doi: 10.1186/s12974-016-0721-5.

[2] Harms AS, Thome AD, Yan Z, Schonhoff AM, Williams GP, Li X, Liu Y, Qin H, Benveniste EN, Standaert DG. Peripheral monocyte entry is required for alpha-Synuclein induced inflammation and Neurodegeneration in a model of Parkinson disease. Exp Neurol. 2018 Feb;300:179-187. doi: 10.1016/j.expneurol.2017.11.010.

[3] Shrivastava P, Cabrera MA, Chastain LG, Boyadjieva NI, Jabbar S, Franklin T, Sarkar DK. Mu-opioid receptor and delta-opioid receptor differentially regulate microglial inflammatory response to control proopiomelanocortin neuronal apoptosis in the hypothalamus: effects of neonatal alcohol. J Neuroinflammation. 2017 Apr 14;14(1):83. doi: 10.1186/s12974-017-0844-3.

Effect of Epigallocatechin-3-gallate and curcumin on the treatment of D-galactose induced ageing mice model

Mehedi Hasan Apu, Monisha Rani Bhakta, Farzana Islam, Shuriya Farnaz, Arif Anzum Shuvo, Monjurul Kader Bakshi, Hasan Mahmud Reza*, Ashrafur Rahman*

[1]Department of Pharmaceutical Sciences, North South University, Bashundhara, Dhaka, Bangladesh
**rahman.ashrafur@northsouth.edu, hasan.reza@northsouth.edu*

INTRODUCTION

The percentage of the aging population is a global health concern and considered as a social burden. Bangladesh has 8% of its total population aged over 60, and expected to be 21% by 2050 [1]. Aging research employing the D-galactose-injected mice model has gained popularity among the researchers to investigate the safe and effective treatment options in aging induced neurodegenerative disorder like Alzheimer's disease (AD). Currently, two categories of drug-like (1) Acetylcholinesterase (AChE) inhibitors (donepezil, rivastigmine, and galantamine), and (2) an N-Methyl-D-aspartate (NMDA) receptor antagonist (memantine) are used to improve memory in aging population (AD) [2] [3]. Due to the high treatment cost and lack of effectiveness, the outcome of treatment did not reach the optimum level [3]. Studies have shown that natural compounds can be promising for the treatment of AD due to their antioxidants, anti-inflammatory properties, and cost-effectiveness [4]. Epigallocatechin-3-gallate (EGCG), prime catechin found in green tea, is becoming popular as a brain tonic because of its anti-inflammatory, antioxidative, neuroprotective role against AD [5]. However, studies show that using a combination of EGCG with cholinesterase inhibitors is the most significant future treatment option for treating AD [6resulting in neurodegeneration. Acetyl-cholinesterase (AChE]. Curcumin, a naturally occurring acetylcholinesterase, and butylcholine esterase inhibitor has a synergistic effect on epigallocatechin, but the combined approach has not yet been investigated in AD. The effect of the combination of EGCG with Curcumin on the AD-associated inflammatory biomarkers such as Superoxide Dismutase (SOD), Malondialdehyde (MDA) and Glutathione (GSH) those control the memory in the AD affected brain needs to be investigated. Therefore, it will be worthwhile to investigate the influential activity of EGCG with Curcumin in cholinergic dependent memory using several hippocam-

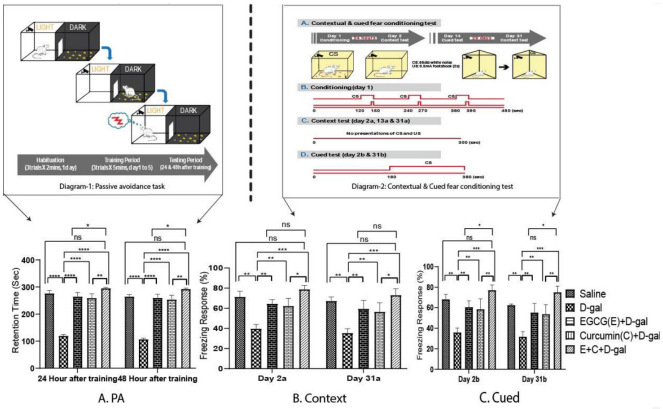

FIGURE 1: Effects of EGCG and Curcumin on (**A**) PA and (**B**), (**C**) CFC. Data was analyzed by one-way ANOVA followed by post-hoc tukey test and expressed as mean ± standard error of the mean. ns = not significant and p<0.05 considered as significant.

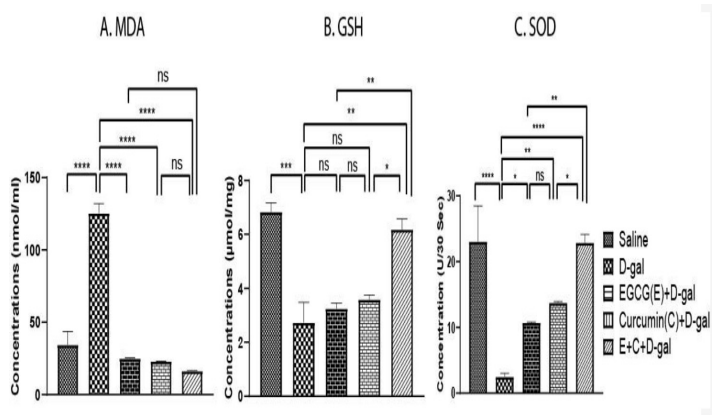

FIGURE 2: Effects of EGCG and Curcumin on oxidative stress biomarkers (A) MDA (B) GSH and (C) SOD. Data was analyzed by one-way ANOVA followed by post-hoc tukey test and expressed as mean ± standard error of the mean. ns = not significant and p<0.05 considered as significant.

pal-dependent behavioral batteries (Fig. 1) and regulation of oxidative stress biomarkers (Fig. 2).

The objective of this research is to identify a safe, inexpensive, and effective treatment option for AD by using the combination of EGCG with Curcumin for the first time through (i) establishing its cholinergic activity using hippocampal-dependent tasks in mice and (ii) identifying its influential activity in the regulation of AD-associated inflammatory biomarkers using bioassay technique.

METHOD

A. Passive Avoidance (PA)

On day 1, mice were allowed to explore both compartments named as habituation. From day 2 to day 7, the mice were exposed to a mild foot shock (US) in dark compartments. The test was then performed on days 8 to 11 (testing period), [7]. This latency time to cross through the gate between the compartments was calculated. (Diagram 1)

B. Contextual Fear Conditioning (CFC)

CFC includes keeping the animal in a novel environment, deliver an unconditioned stimulus (US: from the shocking device) associated with a conditioned stimulus (tone: CS), and then get rid of it (day 1: conditioning session). When the animal was kept in the same environment again, it showed a freezing response if it was able to recall (day 2a & 31a: context) [8]. The responses were analyzed by changing the chamber's shape (day 2b & 31b: cued session) (Diagram 1)

C. Bioassay

Oxidative biomarkers (MDA, GSH, and SOD) were measured from hippocampus.

D. Animals

Each group consists of 8 mice.
Group 1: Saline 1ml (Intra peritoneal; i.p.)
Group 2: D-gal 100 mg/kg (i.p.) [9]
Group 3: EGCG (E) 6mg/kg (Oral) [10] + D-gal 100 mg/kg (i.p)
Group 4: Curcumin (C) 200 mg/kg (Oral) [11] + D-gal 100 mg/kg (i.p)
Group 5: E: 6mg/kg (Oral) + C: 200 mg/kg (Oral) + D-gal 100 mg/kg (i.p.)

RESULTS

A. Effects of the combination of E+C on PA and CF

The D-gal mice showed an impairment of learning in the PA, CFC, whereas after administration of EGCG & Curcumin alone, the memory was improved ($P<0.001$). However, a much improvement of learning was detected in an E+C group mice compared to D-gal, EGCG, and Curcumin alone ($P<0.05$).

B. Effects of the combination of E+C on oxidative stress biomarkers

The level of oxidative stress biomarkers were changed in D-gal mice (The MDA level was remarkably increased, GSH and SOD level was significantly decreased; $P <0.05$). However, the SOD and GSH levels were increased, and MDA was decreased after administration of EGCG and Curcumin alone. The combination of E+C increased the level of GSH and SOD compared to D-gal, E+D, and C+D.

DISCUSSION

In this study, the D-gal mice exhibited low level of learning, whereas an improvement of learning was detected in mice treated with EGCG and Curcumin. The E+C treated mice group exhibited a significant learning level compared to single alone EGCG, Curcumin and D-gal. These results suggested that EGCG and Curcumin have a potential effect on learning and memory-impaired by D-gal (Fig.1). The biochemical study revealed a significant changed oxidative biomarkers in D-gal treated mice, whereas the expressions of biomarkers were minimized after using EGCG and Curcumin, suggesting EGCG [12][13] and Curcumin has the potential antioxidant properties [14]. In addition, the E+C remarkably controlled the biomarkers compared to single alone and D-gal (Fig.2). Together with the results, it could be said that E+C have a synergistic effects on memory via modulating the oxidative stress biomarkers in brain [15].

Several animal studies showed that EGCG has a pivotal role on memory improvement [16] [17]. Other studies showed that curcumin has a beneficiary role on AD [18] [19]. Study conducted on human showed that E+C had a synergistic effect on prostate cancer [14]. But there is lack of evidence to find the synergistic effect of E+C on AD. Therefore the results obtained from animal studies might be transformed in human cases in the treatment of AD

ACKNOWLEDGEMENT

The research was funded by NSU-CTRG 2019-2020 and NST 2020.

Key words: hippocampus, retention time, fear, conditioning, context, biomarkers

REFERENCES

[1] Ageing population in Bangladesh. https://ageingasia.org/ageing-population-bangladesh/

[2] Benfante R, Di Lascio S, Cardani S, Fornasari D. Acetylcholinesterase inhibitors targeting the cholinergic anti-inflammatory pathway: a new therapeutic perspective in aging-related disorders. Aging Clin Exp Res. 2019;(0123456789). https://doi.org/10.1007/s40520-019-01359-4

[3] Kaduszkiewicz H, van den Bussche H. Acetylcholinesterase inhibitors and alzheimer's disease. Encycl Neurosci. 2009;(Table 2):9–13.

[4] Ansari N, Khodagholi F. Natural Products as Promising Drug Candidates for the Treatment of Alzheimer's Disease: Molecular Mechanism Aspect. Curr Neuropharmacol. 2013;11(4):414–29.

[5] Zhang S, Zhu Q, Chen JY, OuYang D, Lu JH. The pharmacological activity of epigallocatechin-3-gallate (EGCG) on Alzheimer's disease animal model: A systematic review. Phytomedicine. 2020;79:153316.

[6] Okello EJ, Mather J. Comparative kinetics of acetyl-and butyryl-cholinesterase inhibition by green tea catechins|relevance to the symptomatic treatment of alzheimer's disease. Nutrients. 2020;12(4).

[7] Tabrizian K, Yaghoobi NS, Iranshahi M, Shahraki J, Rezaee R, Hashemzaei M. Auraptene consolidates memory, reverses scopolamine-disrupted memory in passive avoidance task, and ameliorates retention deficits in mice. Iran J Basic Med Sci. 2015;18(10):1014–9.

[8] Shoji H, Takao K, Hattori S, Miyakawa T. Contextual and cued fear conditioning test using a video analyzing system in mice. J Vis Exp. 2014;(85):1–13.

[9] Zhang X, Wang J, Xing Y, Gong L, Li H, Wu Z, et al. Effects of ginsenoside Rg1 or 17β-estradiol on a cognitively impaired, ovariectomized rat model of Alzheimer's disease. Neuroscience. 2012;220:191–200.

[10] He M, Liu MY, Wang S, Tang QS, Yao WF, Zhao HS WM. Research on EGCG improving the degenerative changes of the brain in AD model mice induced with chemical drugs. J Chinese Med Mater. 2012;1641–4. https://europepmc.org/article/med/23627134

[11] Douichene S, Djebli N, Zerrouki K. Neuroprotective effect of curcumin with a fixator of absorption against both aluminium neurotoxicity and alzheimer's disease (experimental studies in mice). International Journal of Pharmaceutical Sciences and Research. 2012 Oct 1;3(10):3837.

[12] Nikoo M, Regenstein JM, Ahmadi Gavlighi H. Antioxidant and Antimicrobial Activities of (-)-Epigallocatechin-3-gallate (EGCG) and its Potential to Preserve the Quality and Safety of Foods. Compr Rev Food Sci Food Saf. 2018;17(3):732–53.

[13] Bui TT, Nguyen TH. Natural product for the treatment of Alzheimer's disease. Journal of basic and clinical physiology and pharmacology. 2017 Sep 26;28(5):413-23.

[14] Shrikant Mishra KP. The effect of curcumin (turmeric) on Alzheimer's disease An overview Mishra S, Palanivelu K - Ann Indian Acad Neurol. 2008.

[15] Eom DW, Lee JH, Kim YJ, Hwang GS, Kim SN, Kwak JH, et al. Synergistic effect of curcumin on epigallocatechin gallate-induced anticancer action in PC3 prostate cancer cells. BMB Rep. 2015;48(8):461–6.

[16] Wu KJ, Hsieh MT, Wu CR, Wood WG, Chen YF. Green tea extract ameliorates learning and memory deficits in ischemic rats via its active component polyphenol epigallocatechin-3-gallate by modulation of oxidative stress and neuroinflammation. Evidence-Based Complementary and Alternative Medicine. 2012 Oct;2012.

[17] Stagni F, Giacomini A, Emili M, Guidi S, Ciani E, Bartesaghi R. Epigallocatechin gallate: A useful therapy for cognitive disability in Down syndrome?. Neurogenesis. 2017 Jan 1;4(1):e1270383.

[18] Mishra S, Palanivelu K. The effect of curcumin (turmeric) on Alzheimer's disease: An overview. Annals of Indian Academy of Neurology. 2008 Jan;11(1):13.

[19] Maiti P, Manna J. Dietary curcumin: a potent natural polyphenol for neurodegenerative diseases therapy. MOJ Anatomy & Physiology. 2015;1(5):127-32.

Combining K-space and modular generative adversarial network to predict the progression of Alzheimer's Disease

Shoumik Roychowdhury*

Westwood High School, Austin, Texas, USA
**shoumikitu@gmail.com*

INTRODUCTION

Alzheimer's disease (AD) is an irreversible neurodegenerative disease that progresses with time. Its main characteristics are the accumulation of amyloid plaques and neurofibrillary tangles in the brain. These plaques and tangles destroy neurons causing the loss of neurological faculties. Thus, it affects memory, thinking, and social behavior. There are approximately 44 million people living with AD in 2018 [1][2]. It is projected to double by 2060. Unfortunately, there is no current cure for this disease. Current treatments can only decelerate the progression of AD; thus, it is important for an early treatment so the disease's progression may be delayed. During its early stages, AD is challenging to detect because cognitive biomarkers do not reveal the subtle neural degeneration occurring in the brain. Over the years, researchers have identified a few categories in the AD spectrum, ranging from almost no symptoms to a complete loss of brain function. The midrange category is called Mild Cognitive Impairment (MCI)[6]. Early detection at the MCI stages can delay the onset of the disease, before irreversible damage develops. Thus, the detection of this disease early on is also an essential step towards disease prevention.

MOTIVATION

The motivation for this project comes from an observation that the cortical thickness reduces in an AD patient [4]. I hypothesize that the loss of the cortical ribbon can be predicted by using a generative network and manipulating the k-space of an MRI image [3][7].

Therefore, I propose a modular framework (Fig1) for predicting the progression of the stages of MCI and AD. The framework consists of five Conditional Deep

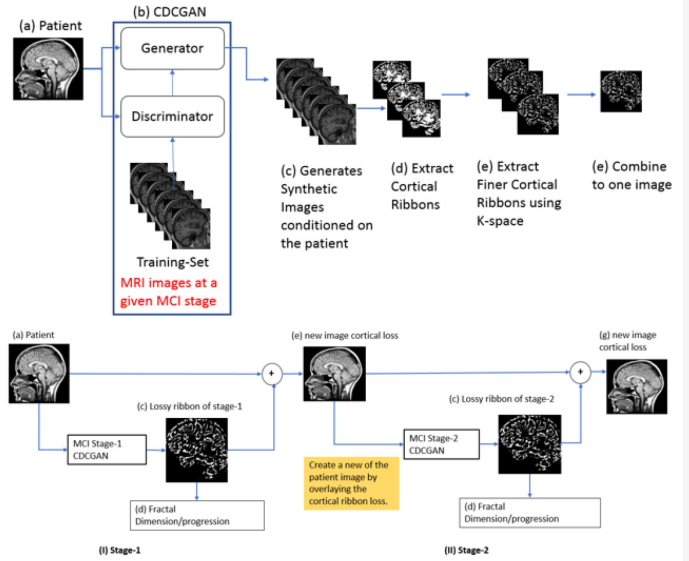

FIGURE 1: Proposed Design that shows the first two CDCGANS in the series of five.

Convolution Generative Adversarial Networks (CDCGAN). The CDCGAN is a Generative Adversarial Network which is conditioned on a reference image. Each CDCGAN predicts the deterioration in the brain for a period of six months. Thus, by the fifth CDCGAN the framework will have predicted the amount of atrophy of the first thirty months. The first CDCGAN is conditioned on the patient's initial MR image and trained on a dataset of MR images that show the deterioration of the brain after six months. This CDCGAN generates a specified number of synthetic images. From these generated brain images, the average image is calculated. Next, the cortical ribbons are extracted. After that, I apply the k-space transformation on these cortical ribbon images and under-sample by 25% in the center of the image. The under-sampling enhances the details and contrast. The fractal dimensions are computed, comparing the patient's current cortical ribbon and predicted cortical ribbon. The fractal dimension is used as a measure to calculate the predicted amount of atrophy. This process is then repeated using the second CDCGAN which uses the average image from the first CDCGAN as the new reference image

and is trained on MR images that show the deterioration of the brain after twelve months. This process is then repeated until the fifth and final CDCGAN.

METHODS

The CDCGAN consists of a generator and a discriminator. The generator uses a 1x1x16384 input noise tensor. This noise tensor is put though a series of different numbers of filters with varying kernel size until the tensor reaches dimension of 256x256x3, as this is the dimensions for an RGB 256 x 256 image. An RBG image is generated in order to not lose channel information. The generated RGB image is multiplied with the reference image (the image of the patient) to create a final conditioned image. The discriminator reverses the process. The conditioned image is added with the reference image and then a sigmoid activation function is applied. The discriminator then reverts the 256x256x3, until the tensor has dimensions, 4x4x256. Then the 4x4x256 tensor is flattened a 0 or 1 value is given to determine if the generated image fake or real.

The next step is the extraction of the cortical ribbon. First a convex hull is created and then blurred to create a new mask for the brain. The mask is applied to get rid of tissue that is not part of the brains. Next a yellow flood fill is used to calculate the blacks inside the skull. A new image is created by transposing the matrix to an image with a white background to determine a mask for the image. The mask is then applied on the Gray_cutout_image to isolate the brain itself. Lastly a banded threshold from 40-60 is conducted to isolate the cortical ribbon.

Next, we manipulate the k- space of the images by taking a 25% under-sample. This is done to compensate for the minute loss of detail in the generated images. Then the fractal dimension is calculated using the box counting method and compared to measure the predicted atrophy in the brain.

RESULTS

After the cortical ribbons have been taken and a weighted mean is calculated, the new image is combined with the old reference image. The areas of red shows where atrophy has occurred. This combined image (Fig 2) is used as the conditional image for the second CDCGAN in the series of cascaded

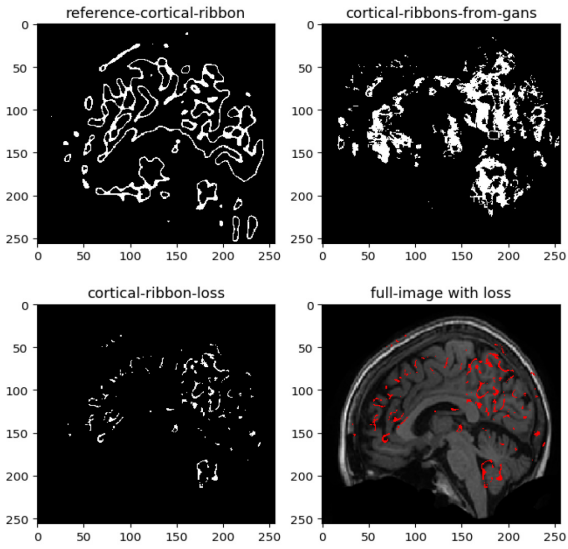

FIGURE 2: shows the final image and predicted loss.

CDCGANs. Looking at the fractal dimension of the patients we notice that the fractal dimension is decreasing, meaning that the gyri and sulci in the brain are atrophying. Therefore, my hypothesis is correct, and I can predict the loss of brain matter and the progression of AD and MCI to 85%-91%. This accuracy is compared by finding the percent change in fractal dimensions.

DISCUSSION

This method shows promise for both short and medium predictions but falls short for long term prediction. This software is created to assist doctors predict, in the short term, how AD will progress. The CDCGAN is memory intensive as training the network uses much memory. So, more memory would aid in computation. The usage of a fractal dimension as a measure is not new, but its usage to measure the human brain is a new idea and should be explored more as discussed in [10].

REFERENCES

[1] 2018 Report Alzheimer's disease facts and figures. https://www.alz.org/media/documents/alzheimers-facts-and-figures-infographic.pdf. Accessed: 2018.

[2] ADNI: Alzheimer's Disease Neuroimaging initiative, how published = http://adni.loni.usc.edu/, note = Accessed: 2019.

[3] Christopher Bowles, Liang Chen, Ricardo Guerrero, Paul Bentley, Roger N. Gunn, Alexander Hammers, David Alexander Dickie, Maria del C. Vald´es Hern´andez, Joanna M. Wardlaw, and Daniel Rueckert. GAN augmentation: Augmenting training data using generative adversarial networks. CoRR, abs/1810.10863, 2018.

[4] Youngsang Cho, Joon-Kyung Seong, Yong Jeong, and Sung Yong Shin. Individual subject classification for alzheimer's disease based on incremental learning using a spatial frequency representation of cortical thickness data. NeuroImage, 59(3):2217 – 2230, 2012

[5] M. Frid-Adar, E. Klang, M. Amitai, J. Goldberger, and H. Greenspan. Synthetic data augmentation using gan for improved liver lesion classification. In 2018 IEEE 15th International Symposium on Biomedical Imaging (ISBI 2018), pages 289–293, April 2018.

[6] Serge Gauthier, Barry Reisberg, Michael Zaudig, Ronald C Petersen, Karen Ritchie, Karl Broich, Sylvie Belleville, Henry Brodaty, David Bennett, Howard Chertkow, Jeffrey L Cummings, Mony de Leon, Howard Feldman, Mary Ganguli, Harald Hampel, Philip Scheltens, Mary C Tierney, Peter Whitehouse, and Bengt Winblad. Mild cognitive impairment. The Lancet, 367(9518):1262 – 1270, 2006.

[7] Ian J. Goodfellow, Jean Pouget-Abadie, Mehdi Mirza, Bing Xu, David Warde-Farley, Sherjil Ozair, Aaron Courville, and Yoshua Bengio. Generative adversarial nets. In Proceedings of the 27th International Conference on Neural Information Processing Systems - Volume 2, NIPS'14, pages 2672–2680, Cambridge, MA, USA, 2014. MIT Press.

[8] C. Han, H. Hayashi, L. Rundo, R. Araki, W. Shimoda, S. Muramatsu, Y. Furukawa, G. Mauri, and H. Nakayama. Gan-based synthetic brainmr image generation. In 2018 IEEE 15th International Symposium on Biomedical Imaging (ISBI 2018), pages 734–738, April 2018.

[9] Koshino Kazuhiro, Rudolf A.Werner, Fujio Toriumi, Mehrbod Som Som Javadi, Martin Gilbert Pomper, Lilja B. Solnes, Franco Verde, TakahiroHiguchi, and Steven P. Rowe. Generative adversarial networks for the creation of realistic artificial brain magnetic resonance images. In Tomography, 2018.

[10] Brown B. Hwang M. Jeon T. George A. T. King, R. D. and Alzheimer's Disease Neuroimaging Initiative. Fractal dimension analysis of the cortical ribbon in mild alzheimer's disease. NeuroImage, 53(2):471–479, 2010

Focal lesions induce large-scale percolation of sleep-like intracerebral activity in awake humans

Russo S.[1]*, Pigorini A.[1], Mikulan E.[1], Sarasso S.[1], Rubino A.[2], Zauli F.[1], Parmigiani S.[1], d'Orio P.[2], Cattani A.[1], Francione S.[2], Tassi L.[2], Lo Russo G.[2], Nobili L.[3], Sartori I.[2], Massimini M[1,4]

[1]Department of Biomedical and Clinical Sciences "L. Sacco", University of Milan, Milan, Italy
[2]"Claudio Munari" Center for Epilepsy Surgery, Ospedale Niguarda-Ca' Granda, Milan, Italy
[3]Child Neuropsychiatry, IRCCS G. Gaslini Institute
[4]IRCCS Fondazione Don Gnocchi Onlus, Milan, Italy
**simone.russo@unimi.it*

INTRODUCTION

A growing body of neuroimaging and clinical studies suggest that the consequences of focal brain lesions are not limited to local neuronal loss but that they also involve functional alterations propagating within a larger network of cortical areas (*Von Monakov 1969; Feeney and Baron 1986; Carrera and Tononi 2014*). In parallel, standard electroencephalographic recordings in brain injured subjects have consistently revealed the presence of low frequency oscillations that are prominent over the lesion (*Gloor et al. 1977*) but that can also extent to the contralateral hemisphere (*Nuwer et al. 1987; Butz et al. 2004*). Altogether, these observations raise the question of whether the generation and propagation of low-frequency neuronal activity may represent an important mechanism of large-scale network disruption after brain injury (*Fornito et al. 2015*). To address this, defining the precise nature of the electrophysiological alterations occurring after a focal lesion, their local spatial extent, and, most important, exploring their ability to percolate within a network of distant areas is of paramount importance. However, the inherent variability of pathological brain injuries, the lack of within-subject premorbid recordings, as well as the low spatial resolution of scalp EEG have so far hampered such systematic investigation.

METHODS

In our work (Russo, Pigorini et al. 2021), we overcome these limitations by studying for the first time how human intracranial activity changes after

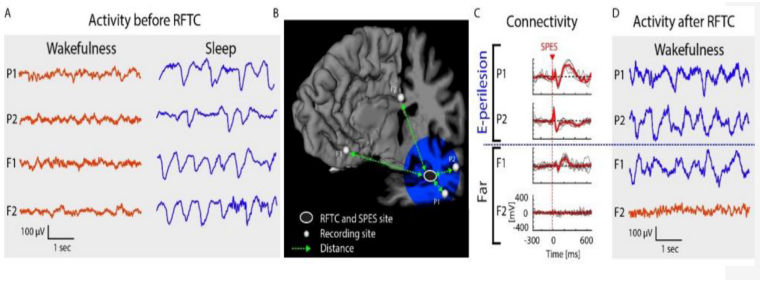

FIGURE 1: Panel (**A**): spontaneous activity of 4 exemplificative contacts during wakefulness (left column, red) and sleep (right column, blue). Panel (**B**): MRI and 3d reconstruction of the brain of the representative subject. The black ovoid and the white dots respectively depict the RFTC site and the location of the exemplificative recording contacts. The blue circle illustrates the perilesional area showing electrophysiological impairment. Green arrows illustrate the geometric distance between each recording contact and the RFTC site. Panel (**C**): CCEP recorded in each exemplificative contact by stimulating the lesioned site before RFTC (grey: trials; red: average). Panel (**D**): activity after RFTC of the four recording contacts showing a sleep-like pattern (blue traces) and a typical wakefulness pattern (red trace).

controlled surgical lesions with respect to baseline and by correlating these changes to individual long-range connectivity patterns as assessed by cortico-cortical evoked potentials (CCEPs) (*Matsumoto et al. 2017; Trebaul et al. 2018*). We analysed Stereo-ElectroEncephaloGraphic (SEEG) (*Cardinale et al. 2019*) recordings performed in 21 subjects before and after Radiofrequency-Thermocoagulation (RFTC) (*Bourdillon et al. 2016; Cossu et al. 2015; Bourdillon et al. 2017*), a surgical procedure used as therapeutic option in drug-resistant focal epilepsy. In each subject, multi-site SEEG recordings during resting wakefulness and NREM sleep (Fig. 1A and B) as well as cortico-cortical evoked potentials (Fig. 1C) were performed before RFTC and were used as a reference to characterize subsequent changes in post-RFTC activity in terms of power (Fig. 1D), amplitude and time-frequency domains (*Mukovski et al. 2007; Cash et al. 2009; Csercsa et al. 2010*; *Riedner et al. 2007*). To account for the hierarchical structure of the data, statistical comparisons were performed through hierarchical bootstrap and mixed effects models (*Aarts et al. 2014*).

RESULTS

After the lesion, intracranial activity recorded during wakefulness was characterized by an obvious intrusion of slow waves. These events matched the amplitude and time-frequency characteristics of the slow waves recorded during baseline NREM sleep in the same subject and were more prominent in the perilesional area where their power decayed exponentially within a radius of ~30 mm (β = 0.45, $p < .001$, R^2_c = 0.32, power in wakefulness before RFTC: 7.58$\pm$8.46 A.U.; power in sleep before RFTC: 23.2$\pm$2.89 A.U.; power in wakefulness after RFTC: 13.5$\pm$13.5 A.U.) (Fig. 1D, upper section). Crucially, these sleep-like slow waves were also consistently found to percolate to distant sites (up to 60 mm) through specific long-range patterns of connectivity, as predicted by CCEPs recorded in the same patients at baseline (perilesional contacts: β connectivity = 2.04, $p < .05$; β distance = -6.16, $p < .001$; R^2_m = 0.20, R^2_c = 0.38; distant contacts: β connectivity = 2.25, $p < .01$; β distance = -1.06, p = 0.06; R^2_m = 0.11, R^2_c = 0.52;) (Fig. 1D, lower section).

DISCUSSION

Given the know impact of sleep slow waves on information processing (*Sarasso et al. 2019; Nir et al. 2011; Vyazovskiy et al. 2011*) and cortical plasticity (*Tononi and Cirelli 2014*), demonstrating their occurrence and large-scale percolation within the awake brain provides a novel framework for understanding the functional and network consequences of focal brain lesions and, in turn, rehabilitation.

Keywords: Stroke, Diaschisis, SEEG, Sleep, Slow wave, NREM, local sleep

Modelling Pelizaeus-Merzbacher disease in Bioengineered neuronal organoids

Marie-Kristin Schreiber[1]*, Zoltán Ivics[2], Atilla Sebe[2], Wolfram-Hubertus Zimmermann[1], Maria-Patapia Zafeiriou[1]

[1]University Medical Centre Göttingen, Institute for Pharmacology and Toxicology, Göttingen, Germany
[2]Paul-Ehrlich-Institute, Langen, Germany.
**marie.schreiber@med.uni-goettingen.de*

INTRODUCTION

Although animal research has greatly contributed to understanding neurodegenerative diseases, translational research faces limitations due to the lack of functional studies on human tissue[1–3]. For many neurodegenerative diseases, effective treatments are missing - Pelizaeus-Merzbacher disease (PMD) represents one of them. PMD is a rare x-linked genetic disorder and hypomyelinating leukodystrophy with a prevalence ranging from 0.13 to 1.9 in 100.000 live male births[4–6]. PMD patients exhibit nystagmus, hypotonia, and cognitive impairment from infancy onwards[7], and with progressing disease, severe spasticity, ataxia and a shortened life span[6]. In PMD, myelin sheath formation is impaired, commonly caused by mutations or duplications in the proteolipid protein 1 gene (PLP1). Proteolipid protein 1 (PLP1) is essential for integrating multilamellar myelin structures[8,9]. Animal models with PLP1 mutations, PLP1-knockouts, or supernumerary autosomal copies[8–10] resulted in a better understanding of PMD pathomechanism implicating protein misfolding and axonal degeneration. To support this data with studies on human tissue, we developed a protocol for bio-engineered neuronal organoids (BENOs)[11] derived from human induced pluripotent stem cells (iPSCs). BENOs display self-organisation, normal cortical layering, excitatory and inhibitory neuron as well as glia development. Furthermore, BENOs demonstrate axonal myelination mediated by oligodendrocytes as early as day 90 of differentiation..

METHODS

For BENO generation (Fig. 1), the following hiPSC lines were used: GMP hiPSC line (TC1133, Lonza), PMD patient hiPSCs (point mutation (C.98G-A) and duplication in PLP1 gene (Xq22.3) and isogenic CRISPR/Cas9 corrected hiPSC for point mutation c.98G-A. To generate BENOs, hiPSCs are embedded in a

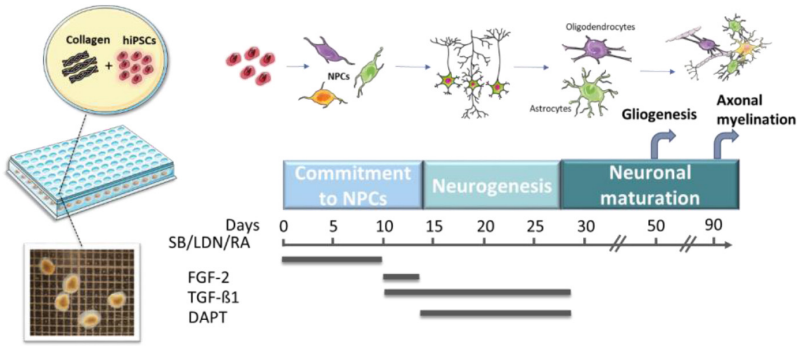

FIGURE 1: BENO generation and development from human iPSCs embedded in a defined collagen type I environment Scheme illustrates the different stages of BENO generation. Between days 0-10, neuroectodermal commitment is induced by dual smad inhibition (SB and LDN) and the presence of all-trans retinoic acid (RA). Neuronal progenitor cell growth is enhanced between days 10-14 by FGF-2 addition. Gliogenesis in BENOs is increased by addition of TGFß-1 at days 10 to 30. From day 15 to 30, DAPT is added to BENO cultures to promote neuronal differentiation. BENO development can be divided into four distinct stages: (1) Neuronal commitment to neuronal progenitor cells (NPCs) at days 3-15, (2) Neurogenesis between days 15-28, (3) Neuronal maturation from day 28 onwards and (4) Gliogenesis (day 50 onwards) such as axonal myelination (day 90 onwards). Grid 1x1 mm. Graphics were created with Servier Medical Art.

collagen matrix and neuroectodermal commitment is induced by dual SMAD inhibition (SB/LDN) and retinoic acid (RA). A complete step-by-step protocol can be obtained by Nature Exchange Protocol[12]. To investigate whether PMD BENOs resemble disease phenotype, immunofluorescence staining (CNP, PLP1, MBP and Olig2) and gene expression analysis (RT-qPCR) of *Olig2*, *CNP*, *PLP1* and *MBP* were conducted at differentiation day 60, 90 and 120.

PRELIMINARY RESULTS

We hypothesise that BENOs are suitable human models to monitor myelination and to serve as screening platforms. We investigated BENOs derived from two PMD patients (kindly provided by Dr. Zoltán Ivics, Paul-Ehrlich-Institut) with a mutation (c. 98G-A) or duplication in PLP1 gene (Xq22.3) in comparison with a well-characterised control iPSC line and a CRISPR/Cas9

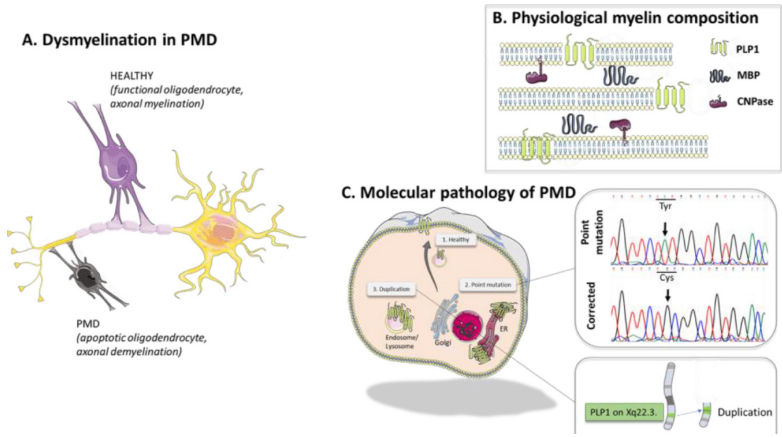

FIGURE 2: PMD Patient iPSC derived BENOs can help to elucidate the molecular pathology of the disease In a healthy individual, proteolipid protein 1 (PLP1) synthesis occurs in the endoplasmic reticulum/Golgi (**A, C**) and is endosomal transported to the plasma membrane of oligodendrocytes (**B**). 70 % of PMD cases are caused by PLP1 duplication on the X chromosome (Xq22.3.) resulting in PLP1 accumulation in late endosome/lysosome, aberrant protein transport and myelin assembly (**C**). Also common are numerous missense point mutations (amino acid change) leading to accumulation of mutant PLP1 in ER. In (**C**), chromatogram of patient A (point mutation c. 98G-A) and its corrected isogenic control is displayed. Both duplication and missense mutation phenotypes lead to oligodendrocyte apoptosis and dysfunction as well as dysmyelination. Graphics were created with Servier Medical Art.

generated isogenic control of c. 98G-A (Fig. 2). From day 90, both PMD BENOs demonstrate reduced gene expression of *Olig2* (oligodendrocyte marker) and *CNP, PLP1 and MBP* (myelin proteins). Immunofluorescence data depicts reduced numbers of Olig2-positive oligodendrocytes, decreased neuronal innervation and signs of neuronal damage. BENOs of the isogenic control exhibit a similar phenotype, suggesting that the mutation c. 98G-A is not solely responsible for the observed phenotype. To investigate whether additional point mutations in PLP1 gene or other myelination related are disease causing, we will sequence genes associated with PMD on the patient iPSC (c.98G-A). If no mutations are identified, whole exome sequencing will be performed.

OUTLOOK

In future experiments, we aim to: (1) identify the causing mutations, (2) understand the pathomechanism underlying the disease phenotype and (3) develop therapeutic approaches for PMD in BENOs such as screening platforms to identify factors that ensure enhanced myelination or oligodendrocyte survival and proliferation.

Keywords: Pelizaeus-Merzbacher disease, Cortical organoids, Neurodegenerative diseases, Myelination, Oligodendrocytes, Drug screening assays

REFERENCES

[1] Qian, X. *et al.* Brain-Region-Specific Organoids Using Mini-bioreactors for Modeling ZIKV Exposure. *Cell* **165**, 1238–1254 (2016).

[2] Wang, H. Modeling Neurological Diseases With Human Brain Organoids. *Front. Synaptic Neurosci.* **10**, 1–14 (2018).

[3] Quadrato, G., Brown, J. & Arlotta, P. The promises and challenges of human brain organoids as models of neuropsychiatric disease. *Nat. Med.* **22**, 1220–1228 (2016).

[4] Heim, P. *et al.* Leukodystrophy incidence in Germany. *Am. J. Med. Genet.* (1997) doi:10.1002/(SICI)1096-8628(19970905)71:4<475::AID-AJMG20>3.0.CO;2-C.

[5] Bonkowsky, J. L. *et al.* The burden of inherited leukodystrophies in children. *Neurology* (2010) doi:10.1212/WNL.0b013e3181eee46b.

[6] Numata, Y. *et al.* Epidemiological, clinical, and genetic landscapes of hypomyelinating leukodystrophies. *J. Neurol.* (2014) doi:10.1007/s00415-014-7263-5.

[7] Inoue, K. PLP1-related inherited dysmyelinating disorders: Pelizaeus-Merzbacher disease and spastic paraplegia type 2. *Neurogenetics* (2005) doi:10.1007/s10048-004-0207-y.

[8] Garbern, J. Y. Pelizaeus-Merzbacher disease: Genetic and cellular pathogenesis. *Cellular and Molecular Life Sciences* (2007) doi:10.1007/s00018-006-6182-8.

[9] Woodward, K. J. The molecular and cellular defects underlying Pelizaeus-Merzbacher disease. *Expert Reviews in Molecular Medicine* (2008) doi:10.1017/S1462399408000677.

[10] Mayer, J. A. *et al.* Modeling the natural history of Pelizaeus-Merzbacher disease. *Neurobiol. Dis.* (2015) doi:10.1016/j.nbd.2014.12.023.

[11] Zafeiriou, M. P. *et al.* Developmental GABA polarity switch and neuronal plasticity in Bioengineered Neuronal Organoids. *Nat. Commun.* (2020) doi:10.1038/s41467-020-17521-w.

[12] Zafeiriou, M. & Blenkle, A. Generation of Bioengineered Neuronal Organoids (BENOs) from human pluripotent stem cells. Natue Exchange Protocols (2020)

Effect of Psilocybin on neural oscillations and signal diversity in EEG and their psychological correlates

Faissal Sharif*, David Erritzoe, Laura Kärtner, Christopher Timmermann

Department of Brain Sciences, Faculty of Medicine, Imperial College London, London, United Kingdom
**fs419@ic.ac.uk*

INTRODUCTION/MOTIVATION

Research interest in psychedelics has grown significantly in the last decade, with numerous studies exploring their ability to induce acute changes in states of consciousness [1]. These drastic physiological changes can translate into long-term psychological changes and could potentially be leveraged for psychotherapy [2,3,4]. As with all psychedelics, the effects of psilocybin, a tryptamine alkaloid contained in certain mushroom species, are mediated by serotonin 2A (5-HT2A) receptor agonism [5]. This mechanism has been implicated in the reduction of spectral power, particularly in the alpha band, as well as the increase of EEG signal diversity (entropy) under psychedelics [5,6,7]. Till date, few studies have replicated these findings and investigated their relationship with acute psychological effects of psilocybin. This study aimed to investigate the effects of high doses of psilocybin on spectral power, entropy, acute and long-term psychological effects such as emotional insight and ego dissolution, and how they are associated.

METHODS

In this within-subject study, 28 psychedelic-naive subjects received 1 mg (low dose, LD) and 25 mg (high dose, HD) of psilocybin, during two dosing days, four weeks apart. During each dosing day, four repeated acute measures of emotional insight, richness of imagery and strength of emotion were accompanied by resting-state EEG (RS-EEG) measures. Further, acute ego dissolution ratings and long-term changes in psychological insight at 2- and 4-weeks post-dosing were assessed. RS-EEG data was analysed for changes in power and entropy through Lempel-Ziv Complexity (LZs).

RESULTS AND DISCUSSION

All acute psychological measures were significantly increased in the HD compared to the LD. Similarly, long-term measures of psychological insight were increased after 25 mg psilocybin and stable over four weeks post-dosing. Widespread decreases in power were observed in alpha, and to a lesser extent, in theta and beta bands, after the HD and were accompanied by an increase of LZs (Figure 1, 2). Increases in gamma power correlated with acute measures of strength of emotion. Together, these findings largely support previous work on psychedelics and provide important insights into the neurobiological basis of the psychedelic experience under psilocybin, and their relation to acute and long-term psychological measures, further substantiating mechanistic aspects of psilocybin psychotherapy.

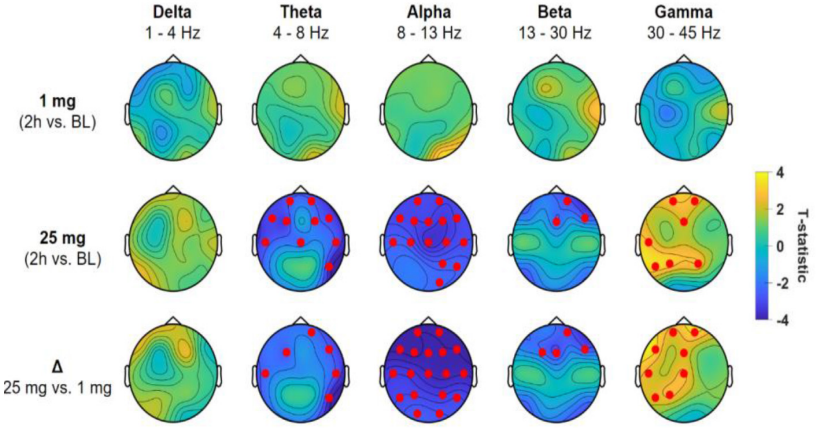

FIGURE 1: Topographic Spectral Power changes in LD and HD conditions (n = 19). Results of paired t-tests with false discovery rate (FDR) and cluster correction are presented. Comparisons of peak (2h post-dosing) vs. baseline spectral power in 1 mg, 25 mg, as well as comparisons between conditions (**Δ**) are shown. Significance is indicated as < .05 (red dot). Abbreviations: BL, baseline.

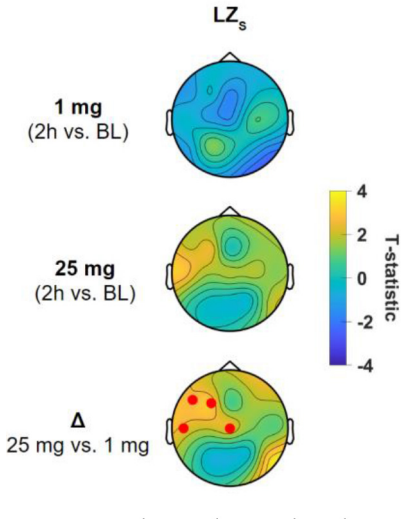

FIGURE 2: Topographic Lempel-Ziv Complexity changes in LD and HD conditions (n = 19). Results of t-tests with FDR and cluster correction are presented. Comparisons of peak (2h post-dosing) vs. baseline LZs activity in 1 mg, 25 mg, as well as comparisons between conditions (Δ) are shown. Significance is indicated as < .05 (red dot). Abbreviations: LZs , Lempel-Ziv Complexity; BL, baseline.

ACKNOWLEDGEMENTS

The author would like to thank Dr David Erritzøe and Laura Kärtner, who provided outstanding supervision and support throughout this project. Meg Spriggs, Dr Chris Timmermann and Dr Fernando Rosas provided crucial technical supervision and training on resting-state EEG data processing and analysis. University tuition and living expenses of the author have been funded entirely through the Klaus Murmann Fellowship Programme offered by the Foundation of German Business, under the umbrella of the Federal Ministry of Education and Research of Germany.

Keywords: Psychedelics, Psilocybin, EEG, Entropy, Lempel-Ziv, Alpha

REFERENCES

[1] Heal, D.J., Henningfield, J., Frenguelli, B.G., Nutt, D.J., et al. (2018) Psychedelics - Re-opening the doors of perception. *Neuropharmacology*. 142, 1–6.

[2] Johnson, M.W., Garcia-Romeu, A., Cosimano, M.P. & Griffiths, R.R. (2014) Pilot study of the 5-HT2AR agonist psilocybin in the treatment of tobacco addiction. *Journal of psychopharmacology* . 28 (11), 983–992.

[3] Bogenschutz, M.P., Forcehimes, A.A., Pommy, J.A., Wilcox, C.E., et al. (2015) Psilocybin-assisted treatment for alcohol dependence: a proof-of-concept study. *Journal of psychopharmacology* . 29 (3), 289–299.

[4] Erritzoe, D., Roseman, L., Nour, M.M., MacLean, K., et al. (2018) Effects of psilocybin therapy on personality structure. *Acta psychiatrica Scandinavica*. 138 (5), 368–378.

[5] Carhart-Harris, R.L., Leech, R., Hellyer, P.J., Shanahan, M., et al. (2014) The entropic brain: a theory of conscious states informed by neuroimaging research with psychedelic drugs. *Frontiers in human neuroscience*. 8, 20.

[6] Muthukumaraswamy, S.D., Carhart-Harris, R.L., Moran, R.J., Brookes, M.J., et al. (2013) Broadband cortical desynchronization underlies the human psychedelic state. *The Journal of neuroscience: the official journal of the Society for Neuroscience*. 33 (38), 15171–15183.

[7] Timmermann, C., Roseman, L., Schartner, M., Milliere, R., et al. (2019) Neural correlates of the DMT experience assessed with multivariate EEG. *Scientific reports*. 9 (1), 16324.

Esculetin attenuates restraint stress-induced anxiety-like and depressive-like behaviours and cognitive impairments in mice by impeding neuroinflammation and up-regulation of BDNF level

Kunjbihari Sulakhiya[1]*, Shalini Shukla[1], Chandana C Barua[2]

[1] Department of Pharmacy, Neuropharmacology Research Lab, Indira Gandhi National Tribal University (IGNTU), Amarkantak, India

[2]Department of Pharmacology and Toxicology, Assam Agricultural University, Guwahati, India

**kunj@igntu.ac.in*

INTRODUCTION/MOTIVATION

Converging lines of evidence suggest that stress plays important role in the pathogenesis of neuropsychiatric disorders including anxiety, depression and cognitive impairments. These stressful events influence various cellular and molecular pathways resulting in neuroinflammation, oxido-nitrosative stress and altered synaptic plasticity of the brain (Sulakhiya et al., 2016a). Stress promotes release of pro-inflammatory cytokines including of Interleukin-1β (IL-1β), Tumor necrosis factor-α (TNF-α) in the brain which further causes release of reactive oxygen species (ROS) thereby altering the synaptic plasticity of the brain (Sulakhiya et al., 2014). Antidepressant drugs including imipramine, clomipramine, fluoxetine, and trazodone are employed to treat depression and associated behavioural anomalies by inhibiting neuroinflammation and oxidative stress. But, currently used antidepressants are of synthetic origin having marginal efficacy compared to placebo, and also having slow onset of actions and side effects problem. Therefore, there is an utmost need for novel drugs or augmentation therapies with higher efficacy and lower side effects. Esculetin (ESC), a coumarin derived potent antioxidant, also possesses, anti-inflammatory, antidepressant, anti-anxiety and neuroprotective potential by inhibiting neuroinflammation and oxidative stress (Sulakhiya et al., 2016b). Therefore, considering the antioxidant and neuroprotective effect of ESC, the present study was conducted to evaluate the protective effect of ESC pre-treatment against restraint stress (RS)-induced behavioural and biochemical changes in mice.

METHODS

Male Swiss Mice (n=10) were pre-treated with esculetin (50 mg/kg, Body Weight) or imipramine (IMI; 30 mg/kg) orally for 14 days and subjected to RS for 3 h/day for 14 days to induce behavioural and biochemical changes. After 40 min of RS procedure, mice were subjected to Open Field Test (OFT) test, Tail suspension test (TST) and Novel object recognition test (NORT) to assess anxiety- and depressive-like behaviors, and cognitive impairments (Jangra et al., 2016; Sulakhiya et al., 2016). Following behavioral studies, mice were sacrificed to isolate hippocampus (HC) for the analysis of interleukin-1β (IL-1β), Tumor necrosis factor-α (TNF-α), Brain derived neurotrophic factor (BDNF), Malondialdehyde (MDA), glutathione (GSH) and nitrite level using ELISA and Spectrophotometer. All data are presented as mean ± S.E.M. and compared by one-way ANOVA followed by Tukey's test as post hoc test. The results were considered significant at $P<0.05$. GraphPad Prism 5.0 Version for Windows, GraphPad Software was used to perform statistical analysis (San Diego, CA, USA).

RESULTS AND DISCUSSION

Chronic RS significantly decreased both open arms entries and duration in EPM ($P<0.01$), increased immobility time in TST ($P<0.001$) and decreased recognition index in NORT ($P<0.001$) in mice which was significantly alleviated by ESC ($P<0.05$) and IMI ($P<0.01$) pre-treatment (Table 1). Hippocampal IL-1β, TNF-α, MDA & nitrite level were increased significantly ($P<0.001$) after RS in mice which were prevented by chronic pre-treatment of ESC and IMI (Table 2). Furthermore, ESC ($P<0.05$) and IMI ($P<0.01$) pre-treatment significantly restored hippocampal GSH, and BDNF level in RS subjected mice (Table 2). The protection offered by esculetin against RS might be due to its antioxidant and anti-inflammatory activity. In conclusion, results suggested that ESC provided alleviating effect against RS-induced anxiety-and depressive-like behaviours, and cognitive dysfunction as well as neurochemical alterations by impeding neuroinflammation, oxido-nitrosative stress and by up-regulation of BDNF level in mouse hippocampus. Currently, numerous plant derived antioxidants such as quercetin, resveratrol, berberine, theaflavins are used as nutraceuticals for the prevention of various diseases including depression. These molecules interact with several biochemical pathways involved in the pathogenesis of diseases. In similar manner esculetin can be used as nutraceuticals for the management of various neurological disorders because of

its wide pharmacological properties. Thus, ESC may be potential therapeutic agent for the prevention and treatment of stress related psychiatric and memory disorders. Still, many features needed to be addressed such as pharmacokinetics and pharmacodynamics including proper dosage, dose-response relationships, duration of action, exact mechanisms of action and other such related aspects of nutraceuticals.

Table 1: Effect of chronic pre-treatment of ESC on restraint stress (RS)-induced behavioural changes in mice

Behavioral Tests	Unstressed + VEH	Unstressed + ESC	Stressed + VEH	Stressed + ESC	Stressed + IMI
EPM – Open Arm Entries (in %)	23.50±3.49	23.17±3.33	8.26±2.52##	20.00±1.69*	22.83±2.45**
EPM- Open Arm Duration (in %)	14.33±2.11	12.67±2.34	3.50±0.99##	11.33±1.70*	12.67±1.45**
TST – Immobility Time (in sec)	197.7±8.57	189.3±7.94	262.5±11.16##	212.5±10.06*	203.3±13.70**
NORT – Recognition Index (in %)	74.67±7.19	70.83±7.19	38.83±3.45##	68.50±3.21**	72.67±4.46**

Values are expressed as Mean±S.E.M (n=6). **##**P<0.01 Vs Unstressed + VEH group and *P<0.05, **P<0.01 Vs Stressed + VEH group.

Table 2: Effect of chronic pre-treatment of ESC on restraint stress (RS)-induced biochemical changes in mice

Parameters	Unstressed + VEH	Unstressed + ESC	Stressed + VEH	Stressed + ESC	Stressed + IMI
IL-1β level (in pg/ml)	1.26±0.05	1.25±0.04	3.28±0.09###	2.90±0.09*	2.65±0.12**

TNF-α level (pg/ml)	1.56±0.05	1.55±0.04	2.52±0.08###	2.00±0.14*	1.70±0.08***
MDA level (nmol MDA/mg of protein)	3.18±0.58	3.36±0.04	6.68±0.46###	4.51±0.05*	4.00±0.05**
Nitrite level (μM/mg of protein)	0.86±0.20	0.67±0.11	2.57±0.15###	1.48±0.20**	1.28±0.17**
GSH level (mM/mg of protein)	0.09±0.006	0.10±0.012	0.02±0.003###	0.05±0.004*	0.06±0.004**
BDNF level (pg/mg of protein)	92.70±12.11	92.70±13.44	43.28±6.47	77.70±7.74*	82.27±8.30**

Values are expressed as Mean±S.E.M (n=3). ##P<0.01 Vs Unstressed + VEH group and *P<0.05, **P<0.01, P<0.001 Vs Stressed + VEH group.

ACKNOWLEDGEMENTS

Authors are very thankful to the Department of Pharmacy, Indira Gandhi National Tribal University, Amarkantak for necessary support. We would like to thank to NIPER, Guwahati for providing facilities to carry out some work.

Keywords: Antioxidant, Esculetin, Depression, Neuroinflammation, Cognitive impairment, Restraint stress

REFERENCES

[1] Sulakhiya K, Kumar P, Jangra A, Dwivedi S, Hazarika NK, Baruah CC, Lahkar M. Honokiol abrogates lipopolysaccharide-induced depressive like behavior by impeding neuroinflammation and oxido-nitrosative stress in mice. European journal of pharmacology. 2014 Dec 5;744:124-31.

[2] Sulakhiya K, Patel VK, Saxena R, Dashore J, Srivastava AK, Rathore M. Effect of Beta vulgaris Linn. leaves extract on anxiety-and depressive-like behavior and oxidative stress in mice after acute restraint stress. Pharmacognosy research. 2016a Jan;8(1):1.

[3] Sulakhiya K, Keshavlal GP, Bezbaruah BB, Dwivedi S, Gurjar SS, Munde N, Jangra A, Lahkar M, Gogoi R. Lipopolysaccharide induced anxiety-and depressive-like behaviour in mice are prevented by chronic pre-treatment of esculetin. Neuroscience Letters. 2016b Jan 12;611:106-11.

[4] Sulakhiya K, Kumar P, Gurjar SS, Barua CC, Hazarika NK. Beneficial effect of honokiol on lipopolysaccharide induced anxiety-like behavior and liver damage in mice. Pharmacology Biochemistry and Behavior. 2015 May 1;132:79-87.

[5] Jangra A, Dwivedi S, Sriram CS, Gurjar SS, Kwatra M, Sulakhiya K, Baruah CC, Lahkar M. Honokiol abrogates chronic restraint stress-induced cognitive impairment and depressive-like behaviour by blocking endoplasmic reticulum stress in the hippocampus of mice. European Journal of Pharmacology. 2016 Jan 5;770:25-32.

Amplified Mnemonic discrimination and attenuated generalization are associated with positive schizotypy

Ágota Vass[1,2]*, Ágnes Szőllősi[1,2]*, Mihály Racsmány[1,2]*, Bertalan Polner[1]*

[1]Department of Cognitive Science, Budapest University of Technology and Economics, Budapest, Hungary
[2]Institute of Cognitive Neuroscience and Psychology, Research Centre for Natural Sciences, Budapest, Hungary
**vass.agota@ttk.hu; bpolner@cogsci.bme.hu; aszollosi@cogsci.bme.hu; mracsmány@cogsci.bme.hu*

INTRODUCTION/MOTIVATION

According to the hippocampal dysfunction theory, memory impairments and positive symptoms of schizophrenia such as hallucinations and delusions might be attributable to an unbalance in the interplay of two main hippocampal computational mechanisms, pattern separation and pattern completion[1]. Behavioural studies in patients with schizophrenia have come to disparate findings when testing the hippocampal dysfunction theory and are not devoid of some of the limitations and confounds that are commonly encountered in schizophrenia research, such as small samples and the unclear effect of medication on cognitive performance[2][3][4]. As schizotypy is increasingly considered to be a useful construct for conceptualizing the development and expression of schizophrenia[5], the present study aims to overcome the limitations of previous studies by investigating the relationship between positive schizotypy and pattern separation and pattern completion. Some of the most important advances of the current study include examination of a larger sample of individuals free from confounding effects of medication and disease burden.

METHODS

The relationship was examined in a sample of healthy individuals (N=71, M[age]= 24.0, SD[age] = 5.1, 53 females) varying in terms of self-reported unusual experiences measured by the short Oxford-Liverpool Inventory of Feelings and Experiences (O-LIFE) questionnaire. Additionally, participants completed the Mnemonic Similarity Task where they were presented with images of

everyday objects. On a subsequent memory test that immediately followed the encoding phase, they saw old and new images and visually similar images (lures) to the ones they saw before. The response options were old, new, and similar. A series of linear regression analyses were carried out to examine the relationship between lure discrimination index and false recognition of lures (putative behavioural indicators of pattern separation and pattern completion, respectively) and positive schizotypy. Elementary perceptual deficits were statistically corrected for and assessed with a Perceptual Discrimination (PD) test. Participants also completed the General Mental Health Questionnaire-12, the Current Psychotic Experiences Questionnaire, the Athen Insomnia Scale and the State Trait Anxiety Inventory to control for further intra-individual differences. We tested the specificity of the relationship between memory performance and positive schizotypy by including general mental health, insomnia, anxiety and the negative and disorganized schizotypy sub-dimensions in the regression models as additional predictors, respectively.

RESULTS AND DISCUSSION

Resemblance between positive schizotypy and schizophrenia could not be detected at the level of behavioural performance. Positive schizotypy was associated with enhanced mnemonic discrimination ($\beta = 0.017$, $R^2 = 0.10$, $F(1, 69) = 7.67$, $p < .01$) and attenuated false recognition of lures ($\beta = -0.018$, $R^2 = 0.17$, $F(1, 69) = 14.33$, $p < .01$), and these results remained robust when controlling for perceptual deficits and further intra-individual differences. We addressed possible underlying mechanisms that might cause a lower false recognition of lures (e.g. impaired ability to generalize, false alarms and schizophrenia and schizotypy and the aging brain in schizophrenia) and enhanced mnemonic discrimination (the fragmented phrene) in schizophrenia and schizotypy.

ACKNOWLEDGEMENTS

Bertalan Polner was supported by the BME-Biotechnology FIKP grant of EMMI (BME FIKP-BIO), and by the National Research, Development and Innovation Office (NKFI/OTKA K 128599).

Ágnes Szőllősi was supported by the ÚNKP-20-4 New National Excellence Program of the Ministry for Innovation and Technology from the source of the National Research, Development and Innovation Fund.

Keywords: schizotypy, hippocampus, pattern separation, pattern completion

REFERENCES

[1] Tamminga, C. A., Southcott, S., Sacco, C., Wagner, A. D., & Ghose, S. (2012). Glutamate dysfunction in hippocampus: Relevance of dentate gyrus and CA3 signaling. Schizophrenia Bulletin, 38(5), 927-935.

[2] Das, T., Ivleva, E. I., Wagner, A. D., Stark, C. E., & Tamminga, C. A. (2014). Loss of pattern separation performance in schizophrenia suggests dentate gyrus dysfunction. Schizophrenia Research, 159(1), 193-197.

[3] Martinelli, C., & Shergill, S. S. (2015). Clarifying the role of pattern separation in schizophrenia: The role of recognition and visual discrimination deficits. Schizophrenia Research, 166(1–3), 328–333.

[4] Kraguljac, N. V., Carle, M., Frölich, M. A., Tran, S., Yassa, M. A., White, D. M., Reddy, A., & Lahti, A. C. (2018). Mnemonic Discrimination Deficits in First-Episode Psychosis and a Ketamine Model Suggests Dentate Gyrus Pathology Linked to N-Methyl-D-Aspartate Receptor Hypofunction. Biological Psychiatry: Cognitive Neuroscience and Neuroimaging, 3(3), 231–238.

[5] Ettinger, U., Mohr, C., Gooding, D. C., Cohen, A. S., Rapp, A., Haenschel, C., & Park, S. (2015). Cognition and brain function in schizotypy: A selective review. Schizophrenia Bulletin, 41(suppl 2), S417-S426.

II Organisation, structure and function of neural systems

Does the brain cause behaviour?

Abalo-Rodríguez, Inés[1]*, Estal-Muñoz, Víctor[2]*, Pérez-Álvarez, Marino[3]*

[1]Department of Experimental Psychology, Complutense University of Madrid, Madrid, Spain
[2]Department of Biological and Health Psychology, Autonomous University of Madrid, Madrid, Spain
[3]Department of Psychology, University of Oviedo, Oviedo, Spain
**iabalo@ucm.es; victor.estal@uam.es; marino@uniovi.es;*

INTRODUCTION/MOTIVATION

Neuroscientists care about behaviour. According to the guidelines of the BRAIN project, "it is no exaggeration to say that nothing in neuroscience makes sense except in the light of behaviour" (p. 15) [1]. Therefore, it becomes essential to discuss the type of relationship that exists among the brain and behaviour. In multiple cases, this relationship is proposed to be causal, thus understanding the brain as the *cause* of behaviour. For instance, the objective III.4 of the BRAIN project, according to their guidelines, is in fact "demonstrating causality" of the brain over behaviour (p. 83). Other examples of this issue are the studies that attribute causality to the brain when talking about racist behaviour [2] or gender differences [3, 4]. Hence, the aim of this abstract is to critically analyse the correctness of attributing a causal role to the brain when talking about behaviour and under which circumstances, if any, it is in fact acceptable to do it.

METHODS

In this abstract, we are presenting a conceptual discussion of the causal role attributed to the brain over behaviour. Thus, the methodology employed will be the one used in philosophy. To this end, (1) we will first define *behaviour* in a broader sense, including both "internal cognitive processes" as well as externally observable actions. This conceptualization is in line with the suggestion made by several neuroscientists [e.g. 1] as well as the theoretical framework Behaviour Analysis [5, 6]. We will then (2) conceptualize what a *cause* is and what the requirements that need to be met in an experiment to

conclude that "*A* causes *B*" are. These requirements are: (i) manipulation of A, (ii) randomization and (iii) temporal precedence of *A* over *B* [7, 8]. Finally, we will (3) revise the research conducted in neuroscience in the light of these requirements. In line with other authors [9], we will argue that the existing methodology does not meet the requirements (i) and (ii), and faces several difficulties when meeting (iii). Causal statements imply that we can directly control the variables of interests and randomize their conditions, which is unfortunately not the case when studying the brain. Moreover, the temporal precedence of the brain activity over the studied behaviour cannot be always ensured. This fact, together with the plasticity of the brain, raises the question of what the cause and the consequence are when studying the relationship among the brain and behaviour. Finally, (3) we will conclude that the existing methods and data allows us to talk about correlations but not causation.

RESULTS AND DISCUSSION

As a conclusion of the former points, we will argue that, while it is correct to understand the brain as the cause of behaviour under certain circumstances (e.g. in neurological disorders: a brain malfunction *causes* an observed behavioural symptom such as loss of memory), we should be cautious when making these attributions in all the other cases. First of all, because of the aforementioned methodological limitations, which prevent us from making these interpretations. Correlation is not causation, and unfortunately enough, existing research on the brain does not generally enable us to establish a causal relationship over behaviour. Moreover, and more importantly, there is a theoretical mistake that should be avoided when interpreting these results. We should be aware that the brain activity that correlates with the observed behaviour is in fact a *description* at a biological level of that very same behaviour, rather than the *explanation*. Such a brain activity is of course necessary for that behaviour to happen, but attributing a causal role to it is in fact misleading [10, 11]. According to the well stablished framework of Behaviour Analysis, the cause of behaviour relies instead on the learning processes and history of the organism [5, 12]. Except from specific circumstances, the brain does *not cause*, but rather *enables* behaviour. Establishing such a distinction is essential in order to guide research in neuroscience and to properly interpret the phenomena that we are studying.

Keywords: brain, behaviour, cause, causal relationship, behaviour analysis

REFERENCES

[1] Bargmann, C., Newsome, W., Anderson, A., Brown, E., Deisseroth, K., Donoghue, J., & Sanes, J. (2014). BRAIN 2025: a scientific vision. Brain Research through Advancing Innovative Neurotechnologies (BRAIN) Working Group Report to the Advisory Committee to the Director, NIH.

[2] Smith, J. A., Marsh, J., & Mendoza-Denton, R. (2010). Are we born racist?: New insights from neuroscience and positive psychology. Beacon Press.

[3 Baron-Cohen, S. (2005, January). The essential difference: The male and female brain. In Phi Kappa Phi Forum (Vol. 85, No. 1, pp. 23-26). National Forum: Phi Kappa Phi Journal.

[4] Brizendine, L. (2006). The female brain. Broadway Books.

[5] Foxan-Parga, M. X. (Ed.) (2020). Análisis funcional de la conducta humana. Concepto, metodología y aplicaciones. Pirámide.

[6] Skinner, B. F. (1953). Science and human behavior. Simon and Schuster.

[7] Mosteller, F., & Tukey, J. W. (1977). Data analysis and regression: a second course in statistics.

[8] León, O. G., & Montero, I. (2003). Métodos de investigación en psicología y educación.

[9] Jazayeri, M., & Afraz, A. (2017). Navigating the Neural Space in Search of the Neural Code. Neuron, 93(5), 1003-1014.

[10] Fuchs, T. (2011). The brain--A mediating organ. Journal of Consciousness studies, 18(7-8), 196-221.

[11] Fuchs, T. (2017). Ecology of the brain: The phenomenology and biology of the embodied mind. Oxford University Press.

[12] Pérez Álvarez, M. (2011). El mito del cerebro creador: cuerpo, conducta y cultura.

Measuring Phase-amplitude coupling in amygdala-stimulated pilocarpine-treated rats

Ádám-József Berki*, Réka-Barbara Bod, István Mihály, Károly Orbán-Kis and Tibor Szilágyi

Department of Physiology, Faculty of Medicine, George Emil Palade University of Medicine, Pharmacy, Science, and Technology of Târgu Mureș, Târgu Mureș, Romania
**berki.adam-jozsef@stud15.umftgm.ro*

INTRODUCTION/MOTIVATION

Temporal lobe epilepsy (TLE) is a debilitating neurological disorder that is medically intractable in about one-third of the cases, which calls for new therapeutic approaches [1]. Deep brain stimulation (DBS) is a promising therapeutic alternative for these cases. [2] However, biomarkers are needed to elucidate its mechanism of action and to optimize stimulation protocols [3]. The analysis of electrophysiological signals has been widely applied to investigate the oscillatory behavior of epileptic networks. Phase-amplitude coupling (PAC) is a form of cross-frequency coupling, and it is a useful tool to characterize network excitability. It was proposed to use the PAC strength between slow and fast oscillations as a marker of epileptogenesis as well as to develop phase-dependent stimulation algorithms, based on continuous measurement of PAC values [4], [5]. In the present study we hypothesize that low-frequency stimulation of the amygdala modulates the coupling of oscillatory components, and by this, it could alleviate the pathological synchrony between neural networks in the epileptic tissue.

METHODS

The lithium-pilocarpine model of TLE was used to induce status epilepticus (SE) in male Wistar rats [6]. Continuous video monitoring was used during the whole duration of the chronic period (3 months). Spontaneous epileptic seizures were recorded after a 2-3 week-long latent period. 8 weeks after SE recording electrodes were implanted bilaterally in the hippocampus as well as a stimulating electrode in the left basolateral amygdala of pilocarpine-treated (DBS-Pilo, N=10) and age-matched control animals (N=7). Following a 10 day-long post-surgical recovery DBS-Pilo and control animals (DBS-Control,

N=4) were stimulated daily with 4 packages of 50 seconds trains for 10 days (4Hz, 500mA, 0.1ms biphasic pulses, with 5-minute pauses between packages). The 3 remaining control rats (SHAM-Control) were recorded but not stimulated. From each daily 30-minute long hippocampal recording the first and last 5-minute intervals were extracted and analyzed offline. To measure the PAC, a time-resolved phase-amplitude coupling measure (tPAC) was applied by using the Brainstorm Toolbox for MATLAB [7]. The frequency for phase was represented by delta oscillations (1–4 Hz) and the frequency for amplitude consisted of the following frequency domains: 30–100 Hz for gamma, 100–150 Hz for High Frequency Oscillations (HFOs), 150–250 Hz for ripples, and 250–600 Hz for fast ripples.

RESULTS

The coupling strength before the stimulation was significantly higher ($p<0.05$) in the epileptic animals compared to controls in almost all studied frequency bands (delta-gamma, delta-ripple and delta-fast ripple), in both hemispheres, except the delta-HFO PAC on the right hippocampal recordings.

Table 1: Maximum PAC between delta (1-4 Hz) and fast (30-600 Hz) oscillations

Electrode position	Group	Delta-Gamma	Delta-HFO	Delta-Ripple	Delta-Fast ripple
L.H.	Control	$1.70 \times 10^{-2} \pm 9 \times 10^{-4}$	$1.90 \times 10^{-2} \pm 1 \times 10^{-3}$	$1.47 \times 10^{-2} \pm 1.1 \times 10^{-3}$	$1.09 \times 10^{-2} \pm 6 \times 10^{-4}$
	DBS-Pilo Before	$2.51 \times 10^{-2} \pm 2 \times 10^{-3}$	$2.40 \times 10^{-2} \pm 1.8 \times 10^{-3}$	$2.51 \times 10^{-2} \pm 2 \times 10^{-3}$	$1.91 \times 10^{-2} \pm 1.7 \times 10^{-3}$
	DBS-Pilo After	$2.14 \times 10^{-2} \pm 1.7 \times 10^{-3}$	$2.13 \times 10^{-2} \pm 1.6 \times 10^{-3}$	$2.01 \times 10^{-2} \pm 1.4 \times 10^{-3}$	$1.58 \times 10^{-2} \pm 1.5 \times 10^{-3}$
R.H.	Control	$1.66 \times 10^{-2} \pm 5 \times 10^{-4}$	$1.93 \times 10^{-2} \pm 1.1 \times 10^{-3}$	$1.48 \times 10^{-2} \pm 4 \times 10^{-4}$	$1.12 \times 10^{-2} \pm 5 \times 10^{-4}$
	DBS-Pilo Before	$2.31 \times 10^{-2} \pm 1.8 \times 10^{-3}$	$2.33 \times 10^{-2} \pm 1.8 \times 10^{-3}$	$2.41 \times 10^{-2} \pm 2.1 \times 10^{-3}$	$1.73 \times 10^{-2} \pm 1.2 \times 10^{-3}$
	DBS-Pilo After	$1.95 \times 10^{-2} \pm 1.2 \times 10^{-3}$	$2.00 \times 10^{-2} \pm 1.2 \times 10^{-3}$	$2.07 \times 10^{-2} \pm 1.3 \times 10^{-3}$	$1.47 \times 10^{-2} \pm 1 \times 10^{-3}$

Control: PAC values of the control animals during the first 5-minute periods of daily recordings;
DBS-Pilo Before: PAC values of DBS-Pilo group during the 5-minute periods before the stimulation trains;
DBS-Pilo After: PAC values of DBS-Pilo group during the 5-minute periods after the stimulation trains. All values are the averages of the 10-day recordings (mean ± S.E.M.).
L.H.: left hippocampus; R.H.: right hippocampus.

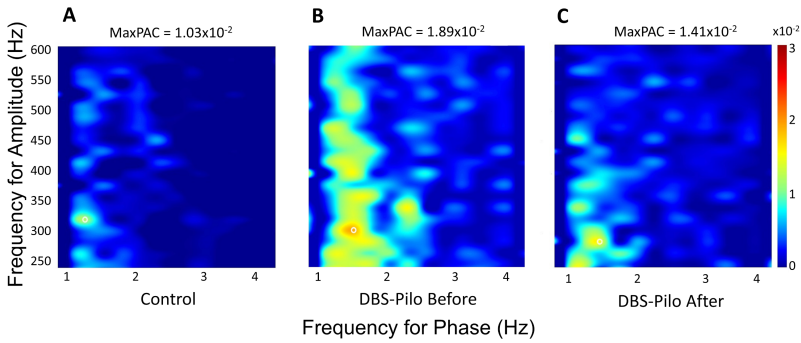

FIGURE 1: Representative comodulograms of individual animals showing the PAC strength between delta and fast-ripple frequency pairs. The coupling strength is color-coded (scale bar on the right). (**A**) Comodulogram of a SHAM-Control animal. (**B**) The epileptic animals exhibited a stronger MaxPAC (white circle) which (**C**) was reduced after DBS.

The pre-stimulation and post-stimulation values were compared from all groups to evaluate the effect of DBS on PAC. A significant decrease ($p<0.05$) was found in every frequency pair in the DBS-Pilo group, except the delta-HFO coupling measured in the left hippocampus. After the DBS, the decreased PAC values still differed significantly ($p<0.05$) from those measured in controls, except for the delta-gamma PAC (Table 1., Figure 1.). The PAC strength did not change in the DBS-Control group after the stimulation.

DISCUSSION

The measurement of PAC was an effective way to evaluate the interictal hippocampal electrical activity. First, we showed that PAC strength is elevated in pilocarpine treated animals compared to healthy ones, indicating the presence of interictal hypersynchrony. The difference was most outstanding in the delta-fast ripple coupling that further highlights the relevance of fast ripples in the diagnosis of epilepsy [8]. The present study also tested the effects of low-frequency stimulation (LFS) on the phase-amplitude coupling to reveal possible mechanisms of neuromodulation. We demonstrated for the first

time, that amygdala LFS decreases the pathologically elevated hippocampal PAC in the pilocarpine model of TLE. We consider that the reduction of coupling strength could be an essential mechanism that diminishes the interictal hypersynchrony and hyperexcitability. We remark that LFS did not decrease the PAC strength to the values detected in controls and that LFS was not influencing the PAC in healthy rats.

Measuring PAC is a promising tool to characterize the large-scale electrical activity, and it may be used in the diagnosis of epilepsy and also to monitor and to optimize the therapeutic effect of DBS in epilepsy.

ACKNOWLEDGEMENTS

Ádám-József Berki was supported by the ELTE Márton Áron Special College.

Keywords: temporal lobe epilepsy, pilocarpine, amygdala, deep brain stimulation, EEG, phase-amplitude coupling

REFERENCES

[1] J. A. French. Refractory epilepsy: Clinical overview. *Epilepsia*, vol. 48, no. SUPPL. 1, pp. 3–7, 2007.

[2] R. Fisher *et al.* Electrical stimulation of the anterior nucleus of thalamus for treatment of refractory epilepsy. *Epilepsia*, vol. 51, no. 5, pp. 899–908, 2010.

[3] M. Jakobs, A. Fomenko, A. M. Lozano, and K. L. Kiening. Cellular, molecular, and clinical mechanisms of action of deep brain stimulation—a systematic review on established indications and outlook on future developments. *EMBO Mol. Med.*, vol. 11, no. 4, pp. 1–18, 2019.

[4] Y. Salimpour and W. S. Anderson. Cross-frequency coupling based neuromodulation for treating neurological disorders. *Front. Neurosci.*, vol. 13, no. FEB, pp. 1–13, 2019.

[5] S. Samiee, M. Lévesque, M. Avoli, and S. Baillet. Phase-amplitude coupling and epileptogenesis in an animal model of mesial temporal lobe epilepsy. *Neurobiol. Dis.*, vol. 114, pp. 111–119, 2018.

[6] G. Curia, D. Longo, G. Biagini, R. S. G. Jones, and M. Avoli. The pilocarpine model of temporal lobe epilepsy. *J. Neurosci. Methods*, vol. 172, no. 2, pp. 143–157, 2008.

[7] F. Tadel, S. Baillet, J. Mosher, D. Pantazis, and R. Leahy. Brainstorm: A user-friendly application for MEG/EEG analysis. *Comput. Intell. Neurosci.*, vol. 2011, p. 879716, Apr. 2011.

[8] J. G. R. Jefferys *et al.*, Mechanisms of physiological and epileptic HFO generation. *Prog. Neurobiol.*, vol. 98, no. 3, pp. 250–264, 2012.

Synaptology of human temporal neocortex: 3D-ultrastructural analyses

Nicolás Cano-Astorga[1,2] *, Javier DeFelipe[1,2,3], Lidia Alonso-Nanclares[1,2,3]

[1]Laboratorio Cajal de Circuitos Corticales, Centro de Tecnología Biomédica, Universidad Politécnica de Madrid, Madrid, Spain
[2]Instituto Cajal, Consejo Superior de Investigaciones Científicas (CSIC), Madrid, Spain
[3]Centro de Investigación Biomédica en Red sobre Enfermedades Neurodegenerativas (CIBERNED),ISCIII, Madrid, Spain
**cano-astorga@cajal.csic.es*

INTRODUCTION

Brain organization is extremely complex and our current knowledge it is far from being completed. The cerebral cortex attracts the researcher´s attention because is where cognitive process takes place. To understand how neuronal circuits contribute to the functional organization of the cerebral cortex, a detailed ultrastructural analysis of neuronal connectivity is required. In particular, Brodmann area 21 is involved in high-level cognitive functions like language [1]. This region is a highly connected cortex that integrates and distributes the information in many circuits [2]. These circuits are mainly established by cortico-cortical layer III projecting neurons, which process the information through synapses [3]. We have performed a detailed three-dimensional ultrastructural analysis of the neuropil, the region where most of the synapses are located. The goals of this study were to provide data about synaptic characteristics.

METHODS

Human brain tissue samples were obtained from 8 control individuals (3 women and 5 men, whose ages ranged between 24 to 53 years old). Ultrastructural images were obtained using FIB/SEM, which removes 20 nm-thick layers of material and images the exposed surface. This procedure is continuously repeated, leading to fully reconstruct of a given volume [4]. The volume obtained by the FIB/SEM was analyzed using EspINA software [5]. Each synapse was individually identified and classified -by the user- as asymmetric (AS; excitatory) or symmetric (SS; inhibitory) based on its prominent or thin post-synaptic density, respectively [6] (Figure 1). Once a synapse was

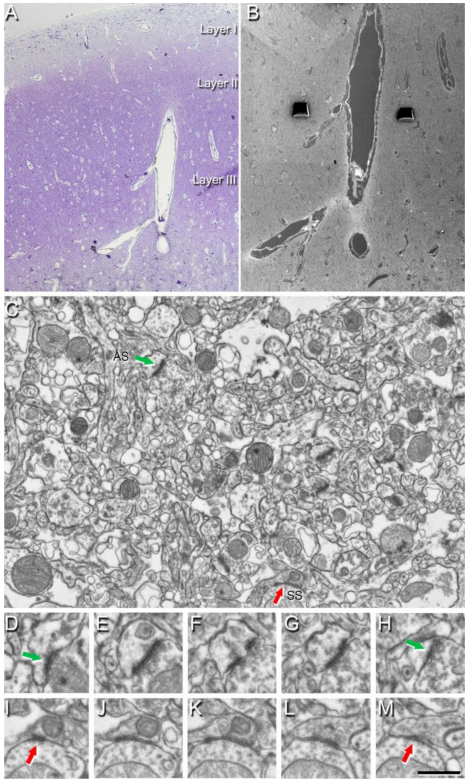

FIGURE 1: Correlative light/electron microscopy analysis of layer III of the Brodmann area 21. (**A**) Delimitation of layers is based on the staining pattern of 1 µm-thick semithin section, stained with toluidine blue, which is adjacent to the block for FIB/SEM imaging (B). (**B**) SEM image with higher magnification of the blood vessels in A to illustrate the block surface with trenches made in the neuropil where FIB/SEM analyses was performed. (**C**) Serial image obtained by FIB/SEM showing the neuropil of an autopsy case (AB3), two synapses are indicated as examples of asymmetric (AS, green arrow) and symmetric synapses (SS, red arrow). Synapse classification was based on the examination of the full sequence of serial images; an AS with prominent postsynaptic density can be visualized in **D-H**, and an SS with thin postsynaptic density, in **I-M**. Scale bar shown in M indicates 160 µm in A, 100 µm in B, 950 nm in C, and 550 nm in D-M.

visually identified, EspINA reconstructs it semi-automatically in 3D. Based on this 3D reconstructed synapse, morphologic categories (macular, perforated, horseshoe or fragmented) were done attending to its shape [7]. EspINA also

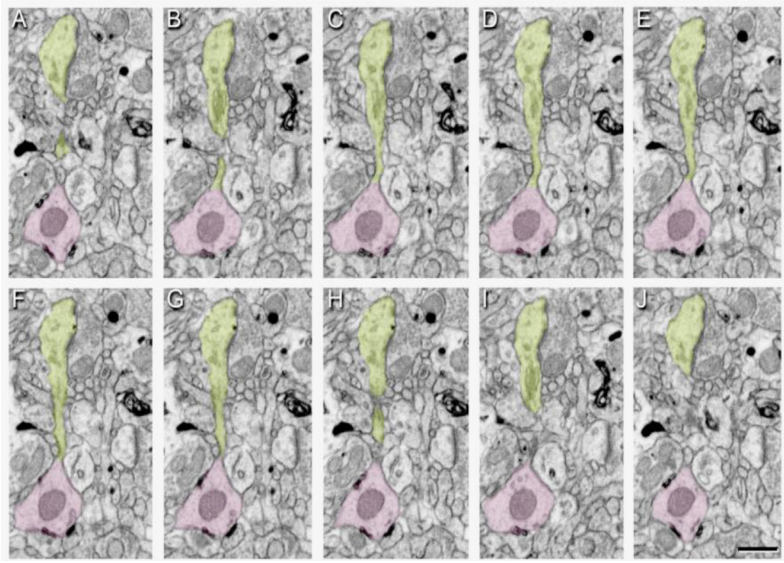

FIGURE 2: FIB/SEM images from serial sections made in a biopsy case (H38) to illustrate a dendritic shaft (pink) with one dendritic spine emerging from the shaft (in green). Scale bar shown in J indicates 500 nm in **A-J**.

provides the area of the synaptic apposition surface (SAS) [8] and the position of its centroids [9], which allows analyzing the synaptic size and its spatial 3D distribution, respectively. Moreover, the postsynaptic targets (dendritic spines or dendritic shafts) of the synapses were clearly determined [10] (Figure 2).

RESULTS AND DISCUSSION

Preliminary results based on 11158 μm^3 examined tissue sample and 4945 synapses showed a mean synaptic density of 0.60 synapses/μm^3, most synapses were AS (93.33%) versus SS (6.67%), which concur with human related literature [11].

Macular-shape synapses were the most frequent (83.30%) following by perforated (11.69%), horseshoe (3.86%) and fragmented (1.15%), being the macular shape-synapses smaller than perforated, horseshoe and fragmented synapses, which concur with current hypothesis.

Furthermore, the spatial distribution study showed that synaptic spatial distribution pattern corresponds to a random pattern, in which the synapses can occupy any location of the space, which could be an intrinsic characteristic of cortical circuit´s organization. Finally, the study of the postsynaptic elements revealed that most AS were established on dendritic spines heads (66.7%), whereas most SS were established on dendritic shafts (90.1%). In the human cerebral cortex, it has been reported that the percentage of AS established on dendritic spines range between 47%-85% [12-15]. However, this percentage is about 80% in non-human primates [16-18], and 90% in rats and mice [10,17,19].

BIBLIOGRAPHY

[1] Xu Y, Lin Q, Han Z, He Y, Bi Y. 2016. Intrinsic functional network architecture of human semantic processing: Modules and hubs. NeuroImage 132:42–55. DOI: https://doi.org/10.1016/j.neuroimage.2016.03.004

[2] Felleman DJ, Xiao Y, and McClendon E. 1997. Modular Organization of Occipito-Temporal Pathways: Cortical Connections between Visual Area 4 and Visual Area 2 and Posterior Inferotemporal Ventral Area in Macaque Monkeys. J Neurosci 17:3185-3200. DOI: https://doi.org/10.1523/JNEUROSCI.17-09-03185.1997

[3] Thomson A and Lamy C. 2007. Functional maps of neocortical local circuitry. Front in Neurosci 1:19-42. DOI: https://doi.org/10.3389/neuro.01.1.1.002.2007

[4] Merchán-Pérez A, Rodríguez JR, Alonso-Nanclares L, Schertel A, DeFelipe J. 2009. Counting synapses using FIB/SEM microscopy: a true revolution for ultrastructural volume reconstruction. Front Neuroanat 3:18. DOI: https://doi.org/10.3389/neuro.05.018.2009

[5] Morales J, Alonso-Nanclares L, Rodríguez JR, DeFelipe J, Rodríguez A, Merchán-Pérez A. 2011. Espina: a tool for the automated segmentation and counting of synapses in large stacks of electron microscopy images. Front Neuroanat 18:18. DOI: https://doi.org/10.3389/fnana.2011.00018

[6] Colonnier M. 1968. Synaptic patterns on different cell types in the different laminae of the cat visual cortex. An electron microscope study. Brain Res 9:268–287. DOI: https://doi.org/10.1016/0006-8993(68)90234-5

[7] Santuy A, Rodríguez J, DeFelipe J, Merchán-Pérez A. 2018a. Study of the size and shape of synapses in the juvenile rat somatosensory cortex with 3D electron microscopy. Eneuro 5:e0377-17. DOI: https://doi.org/10.1523/ENEURO.0377-17.2017

[8] Morales J, Alonso-Nanclares L, Rodríguez JR, DeFelipe J, Rodríguez A, Merchán-Pérez A. 2011. Espina: a tool for the automated segmentation and counting of synapses in large stacks of electron microscopy images. Front Neuroanat 18:18. DOI: https://doi.org/10.3389/fnana.2011.00018

[9] Merchán-Pérez A, Rodríguez JR, González S, Robles V, DeFelipe J, Larrañaga P, Bielza C. 2014. Three-dimensional spatial distribution of synapses in the neocortex: a dual-beam electron microscopy study. Cereb Cortex 24:1579–1588. DOI: https://doi.org/10.1093/cercor/bht018

[10] Santuy A, Rodriguez JR, DeFelipe J, Merchán-Pérez A. 2018b. Volume electron microscopy of the distribution of synapses in the neuropil of the juvenile rat somatosensory cortex. Brain Struct Funct 223:77–90. DOI: https://doi.org/10.1007/s00429-017-1470-7

[11] DeFelipe J, Alonso-Nanclares L, Arellano JI. 2002. Microstructure of the neocortex: Comparative aspects. J Neurocytol 31:299-316. DOI: https://doi.org/10.1023/a:1024130211265

[12] Yakoubi R, Rollenhagen A, von Lehe M, Shao Y, Sätzler K, Lübke JHR. 2018. Quantitative Three-Dimensional Reconstructions of Excitatory Synaptic Boutons in Layer 5 of the Adult Human Temporal Lobe Neocortex: A Fine-Scale Electron Microscopic Analysis. Cereb Cortex 29:2797–2814. DOI: https://doi.org/10.1093/cercor/bhy146

[13] Yakoubi R, Rollenhagen A, von Lehe M, Miller D, Walkenfort B, Hasenberg M, Sätzler K, Lübke JHR. 2019. Ultrastructural heterogeneity of layer 4 excitatory synaptic boutons in the adult human temporal lobe neocortex. eLife 20 8:e48373. DOI: https://doi.org/10.7554/eLife.48373

[14] Domínguez-Álvaro M, Montero-Crespo M, Blazquez-Llorca L, DeFelipe J, Alonso-Nanclares L. 2019. 3D Electron Microscopy Study of Synaptic Organization of the Normal Human Transentorhinal Cortex and Its Possible Alterations in Alzheimer's Disease. eNeuro 6:1-17. DOI: https://doi.org/10.1523/ENEURO.0140-19.2019

[15] Domínguez-Álvaro M, Montero-Crespo M, Blazquez-Llorca L, DeFelipe J, Alonso-Nanclares L. 2020. 3D ultrastructural study of synapses in the human entorhinal cortex. Cereb cortex bhaa233. DOI: https://doi.org/10.1093/cercor/bhaa233

[16] Peters A, Sethares C, Luebke JI. 2008. Synapses are lost during aging in the primate prefrontal cortex. Neurosci 152:970-981. https://doi.org/10.1016/j.neuroscience.2007.07.014

[17] Hsu A, Luebke JI, Medalla M. 2017. Comparative ultrastructural features of excitatory synapses in the visual and frontal cortices of the adult mouse and monkey. J Comp Neurol 525:2175–2191. DOI: https://doi.org/10.1002/cne.24196

[18] Dumitriu D, Hao J, Hara Y, Kaufmann J, Janssen WGM, Lou W, Rapp PR, Morrison JH. 2010. Selective changes in thin spine density and morphology in monkey prefrontal cortex correlate with aging-related cognitive impairment. J Neurosci. 30:7507-7515. https://doi.org/10.1523/JNEUROSCI.6410-09.2010

[19] Calì C, Wawrzyniak M, Becker C, Maco B, Cantoni M, Jorstad A, Nigro B, Grillo F, De Paola V, Fua P, Knott GW. 2018. The effects of aging on neuropil structure in mouse somatosensory cortex—A 3D electron microscopy analysis of layer 1. PLoS ONE 13:e0198131. DOI: https://doi.org/10.1371/journal.pone.0198131

The secretome of Mesenchymal Stem Cells induces synapse formation in Central Nervous System neurons

Joana Correia[1]*, Ricardo Faria[1]*, Diogo Tomé[1,2], Marta Dias[1], Filipa Costa[1], Sofia C. Serra[3,4], António J. Salgado[3,4], Ramiro D. Almeida[1,2]

[1]iBiMED - Institute of Biomedicine, Department of Medical Sciences, University of Aveiro, Aveiro, Portugal
[2]CNC - Center for Neuroscience and Cell Biology, University of Coimbra, Coimbra, Portugal
[3]Life and Health Sciences Research Institute (ICVS), School of Medicine, University of Minho, Braga, Portugal
[4]ICVS/3B's - PT Government Associate Laboratory, Braga/Guimarães, Portugal
**These authors contributed equally to this work.*
**joanarcorreia@ua.pt*

INTRODUCTION

Mesenchymal stem cells (MSC) are self-renewing, multipotent precursors present in the stromal fraction of several adult tissues, including bone marrow, dental pulp, adipose tissue, placenta and umbilical cord (Nombela-Arrieta et al., 2011). They have drawn intense interest for the last few years, due to their regenerative effects in the nervous system (Gögel et al., 2011). In fact, MSCs transplantation into injured spinal cord promoted its regeneration and functional recovery (Hofstetter et al., 2002; Ide et al., 2010; Liu et al., 2013). Recent studies attribute the regenerative potential of MSCs to their paracrine activity instead of their ability to differentiate into neuronal or glial cells (Crigler et al., 2006; Konala et al., 2016). Several molecules with neuroregulatory properties, including neurotrophic factors, chemokines, cytokines and extracellular matrix proteins, as well as microvesicles and exosomes were identified in MSCs secretome (Martins et al. 2017; Pires et al., 2016). Thus, administration of the secretome into spinal cord injury sites can be a solution to surpass some of the disadvantages associated with MSCs grafting, such as, the high number of cells required for transplantation and low survival rate when delivered into a damaged tissue.

The establishment of the neuronal circuitry after injury requires that axon growth be accompanied by synapse formation to achieve functional recovery. However, until now the synaptogenic potential of MSCs secretome is still poorly characterized. Moreover, recent studies have shown that the secretome of MSCs isolated from different tissue sources may present

significant variation. In this work we aimed to investigate the effects of the secretome of different populations of mesenchymal stem cells, namely the human umbilical cord perivascular cells (HUCPVC) bone marrow (BMSCs), adipose tissue (ASCs), on synapse formation of CNS neurons.

METHODS

Hippocampal or cortical neurons were stimulated with the secretome of mesenchymal stem cells from different origins at a final concentration of 2x. After stimulation, cells were fixed for 10 minutes in 4% paraformaldehyde and washed three times (each 5 minutes) in PBS. After that, cells were permeabilized with PBS-Triton X-100 0.25% for 10 minutes, and then washed with PBS. Next, to prevent non-specific binding, cells were blocked with 3% bovine serum albumin (BSA) for 40 minutes. Primary antibodies solution was prepared in 3% BSA and incubated with the cells overnight at 4ºC. After the incubation, the preparations were washed three times with PBS and incubated with the secondary antibodies solution at room temperature for 1h protected from the light (this solution was also prepared in 3% BSA). After the incubation, the preparations were washed again twice with PBS-Triton X-100 0.1% and then washed with PBS. Lastly, the coverslips were mounted with ProLong mounting media with DAPI in glass slides. The antibodies used were: β-III Tubulin (mouse), Synapsin (rabbit), anti-mouse and anti-rabbit Alexa-conjugated secondary antibodies 568 and 488, respectively.

RESULTS AND DISCUSSION

To determine the effect of the secretome of mesenchymal stem cells from different origins in synapse formation of central nervous system neurons, we stimulated neurons with conditioned media from the different cells at a final concentration of 2x. The formation of presynaptic clusters was assessed by immunostaining against the SV marker. β-III Tubulin immunostaining was used as an axonal marker. HUCPVC and ASC secretome treatment increased the number of synapsin puncta per axon length in cortical (Figure 1) and hippocampal (Figure 2) axons. BMSC secretome treatment only showed an effect in hippocampal neurons.

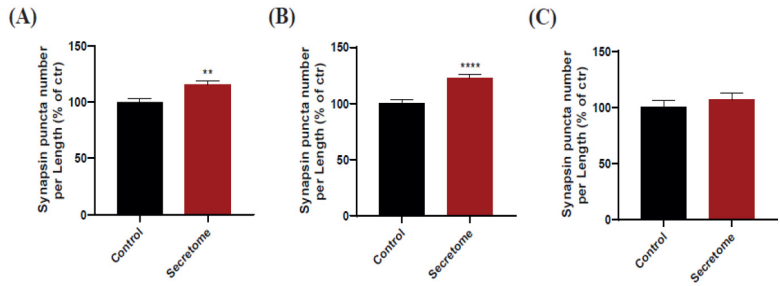

FIGURE 1: ASC and HUCPVC secretome induces synapse formation in cortical neurons.
(**A-C**) Quantification of synapsin puncta number per axonal length. Results show that global application of ASC (A) and HUCPVC (**B**) secretome significantly increases the number of synapsin puncta. No effect was observed when neurons were stimulated with BM (**C**). Puncta analysis was performed with Image J 1.45e software. Results are expressed as % of control. Bars represent the mean ± SEM of at least 45 images from randomly selected areas of 3 independent experiments; (A) ** represents p = 0.0037 and (B) **** represents p < 0.0001 by unpaired t-test when compared to Ctr.

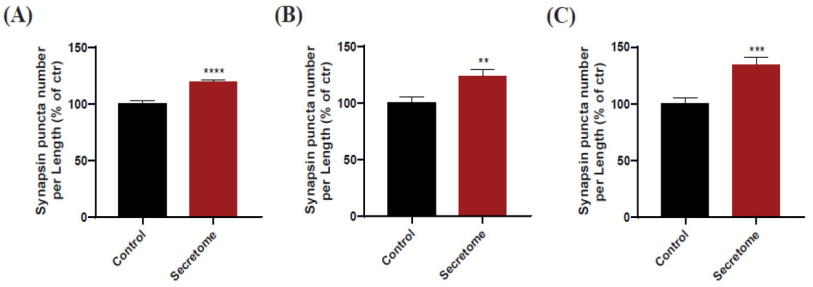

FIGURE 2: ASC, HUCPVC and BMSC secretome induces synapse formation in hippocampal neurons.
(**A-C**) Quantification of synapsin puncta number per axonal length. Results show that global application of ASC (A), HUCPVC (**B**) and BMSC (**C**) secretome significantly increases the number of synapsin puncta. Puncta analysis was performed with Image J 1.45e software. Results are expressed as % of control. Bars represent the mean ± SEM of at least 45 images from randomly selected areas of 4 independent experiments; (A) **** represents p < 0.0001 ; (B) ** represents p = 0.0054 and (C) *** represents p = 0.0001 by unpaired t-test when compared to Ctr.

We demonstrated that application of mesenchymal stem cell secretomes to both rat cortical and hippocampal neurons induces an enhancement of synaptic vesicle clustering, a hallmark of synapse formation. However, the secretome of BMSC only showed an effect on hippocampal neurons, which suggests that secretomes of distinct sources may have dissimilar effects in different neuronal populations. Overall, these results show that the secretome HUCPVC, ASC and BMSC have synaptogenic properties and may constitute a new approach to tackle traumatic and degenerative CNS pathologies.

ACKNOWLEDGEMENTS

This work was supported by Fundação para a Ciência e Tecnologia (FCT) through the individual PhD grants SFRH/BD/139368/2018 (DT) and SFRH/BD/141092/2018 (MD).

Keywords: secretome, mesenchymal stem cells, adipose stem cells, bone marrow stem cells, human umbilical cord perivascular cells, cortical neurons, synapse, hippocampal neurons, synaptogenesis

REFERENCES

[1] Crigler, L. et al. (2006) 'Human mesenchymal stem cell subpopulations express a variety of neuro-regulatory molecules and promote neuronal cell survival and neuritogenesis', Experimental Neurology, 198(1), pp. 54–64. doi: 10.1016/j.expneurol.2005.10.029.

[2] Gögel, S., Gubernator, M. and Minger, S. L. (2011) 'Progress and prospects: stem cells and neurological diseases', Gene Therapy, 18(1), pp. 1–6. doi: 10.1038/gt.2010.130.

[3] Hofstetter, C. P. et al. (2002) 'Marrow stromal cells form guiding strands in the injured spinal cord and promote recovery', Proceedings of the National Academy of Sciences, 99(4), pp. 2199–2204. doi: 10.1073/pnas.042678299.

[4] Ide, C. et al. (2010) 'Bone marrow stromal cell transplantation for treatment of sub-acute spinal cord injury in the rat', Brain Research. Elsevier B.V., 1332, pp. 32–47. doi: 10.1016/j.brainres.2010.03.043.

[5] Konala, V. B. R. et al. (2016) 'The current landscape of the mesenchymal stromal cell secretome: A new paradigm for cell-free regeneration', Cytotherapy. Elsevier Inc., 18(1), pp. 13–24. doi: 10.1016/j.jcyt.2015.10.008.

[6] Liu, J. et al. (2013) 'Acellular spinal cord scaffold seeded with mesenchymal stem cells promotes long-distance axon regeneration and functional recovery in spinal cord injured rats', Journal of the Neurological Sciences. Elsevier B.V., 325(1–2), pp. 127–136. doi: 10.1016/j.jns.2012.11.022.

[7] Martins, L. F., Costa, R. O., Pedro, J. R., Aguiar, P., Serra, S. C., Teixeira, F. G., Sousa, N., Salgado, A. J., & Almeida, R. D. (2017) 'Mesenchymal stem cells secretome-induced axonal outgrowth is mediated by BDNF', Scientific Reports, 7(1), pp. 1–13. doi:10.1038/s41598-017-03592-1

[8] Nombela-Arrieta, C., Ritz, J. and Silberstein, L. E. (2011) 'The elusive nature and function of mesenchymal stem cells', Nature Reviews Molecular Cell Biology. Nature Publishing Group, 12(2), pp. 126–131. doi: 10.1038/nrm3049.

[9] Pires, A. O. et al. (2016) 'Unveiling the Differences of Secretome of Human Bone Marrow Mesenchymal Stem Cells, Adipose Tissue-Derived Stem Cells, and Human Umbilical Cord Perivascular Cells: A Proteomic Analysis', Stem Cells and Development, 25(14), pp. 1073–1083. doi: 10.1089/scd.2016.0048.

Ubiquitin-proteasome system participates in the local regulation of presynaptic function

Filipa J. Costa[1]*, Maria J. Pinto[2]*, Ramiro D. Almeida[1,2]

[1]Department of Medical Sciences, Institute of Biomedicine (iBiMED), University of Aveiro, Aveiro, Portugal
[2]CNC - Center for Neuroscience and Cell Biology, University of Coimbra, Coimbra, Portugal
**These authors contributed equally to this work.*
**fjcosta@ua.pt*

INTRODUCTION

Throughout development, the establishment of functional synaptic contacts is pivotal for the correct wiring of neurons and, ultimately, for proper brain function in adulthood. Presynaptic differentiation corresponds to one of these events. Differentiation of the presynaptic terminal is a complex and rapid event that normally occurs in spatially specific axonal regions distant from the soma; thus, it is believed to be dependent on intra-axonal mechanisms [1]. Therefore, it is of utmost importance to fully comprehend the cascade of events comprising synapse formation and function.

Interestingly, accumulating evidence shows that ubiquitin-proteasome system (UPS) has a crucial role in synapse formation, maintenance and function [2]. One of these evidence is that the ubiquitinated proteins are highly enriched at the Drosophila neuromuscular junction (NMJ), with aggregates of ubiquitin (Ub) conjugates surrounding the active zone, the region responsible for neurotransmitter release [3].

Furthermore, several presynaptic proteins, mainly synaptic vesicle (SV)-associated or active zone proteins, are present in their ubiquitinated form in the adult rat brain [4]. On the other hand, the ataxia mice with a loss-of-function mutation in the proteasome-associated deubiquitinating enzyme Usp14, have an inability to mobilize SVs for fusion and a reduced size of presynaptic button [5]. Such changes are associated with reduced levels of protein ubiquitination in the synaptic compartment [6] , mainly due to an accelerated loss of ubiquitin by proteasome degradation [7]. These studies identify a critical role for ubiquitin homeostasis in presynaptic function, specifically in the release of neurotransmitters.

However, little efforts have been made to discern the role of ubiquitin signaling in this process. In this study we investigated the role of polyubiquitination system in the presynaptic formation and function.

METHODS

Hippocampal neurons were plated in microfluidic chambers. After 7 day *in culture,* neurons were stimulated with ubiquitin-proteasome system or protein synthesis inhibitors.

For detection and quantification of polyubiquitinated proteins, neurons were tagged with lipophilic FM 5-95 lypophilic styryl dye (FM-dye) in imaging medium, at room temperature (RT). Image acquisition was performed using a spinning disk confocal imaging system configured for a motorized inverted microscope driven by iQ 3.1 software. Confocal microscopy associated with a spinning disk system allows high resolution fluorescent images to be acquired from living cells *in vivo* [8].

After cell imaging, hippocampal neurons were fixed for 10 min in 4 % paraformaldehyde (PFA) and 4% sucrose, at RT. Neurons were washed three times with PBS solution, permeabilized for 5 min with 0.25% Triton X-100 diluted in PBS, washed three times with PBS, and then blocked for 30 min in 3% bovine serum albumin (BSA) diluted in PBS. After that, cells were incubated with Alexa Fluor 405 anti-MAP2, Alexa Fluor 488 anti-Bassoon and Alexa Fluor 568 anti-TAU diluted in blocking solution overnight, at 4 °C. Cells were then washed twice with 0.1% Triton X-100 in PBS and once with PBS 1x. The preparations were cured at 4°C, protected from light. After cured, coverslips were sealed with nail polish and kept at 4 °C until microscopy analysis. The preparations were visualized in Zeiss LSM 510 confocal microscope with a 40x objective.

RESULTS AND DISCUSSION

We show that accumulation of an on-site pool of polyubiquitinated proteins acts as a local "hub" for presynaptic assembly. Using a microfluidic system, we observed that specific inhibition of the proteasome in axons boosts formation of presynaptic clusters. Strikingly, assembly of presynaptic clusters upon contact with a postsynaptic partner occurs in parallel to a site-specific decrease in proteasome activity. Moreover, accumulation of polyubiquitinated

conjugates significantly increased the number of presynaptic clusters. Lastly, we identify a role for different proteolytic-related Ub chains in the differentiation of presynaptic terminals. It is important to note that this study is still ongoing. Therefore, the results described have not yet been shown.

In this study, we propose a new on-site UPS-related mechanism controlling formation of presynaptic sites [9]it is believed to be dependent on intra-axonal mechanisms. However, the full nature of the local events governing presynaptic assembly remains unknown. Herein, we investigated the involvement of the ubiquitin-proteasome system (UPS. Our results suggest a model in which transient and local reduction of proteasome activity after contact with a postsynaptic partner leads to an onsite accumulation of proteins in their polyubiquitinated state (K48 and K11), which in turn functions as a nesting platform for the clustering of presynaptic material and subsequently, presynaptic differentiation (Figure 1) [9]it is believed to be dependent on intra-axonal mechanisms. However, the full nature of the local events governing presynaptic assembly remains unknown. Herein, we investigated the involvement of the ubiquitin-proteasome system (UPS. We further hypothesize that transient enrichment of proteasome-related polyubiquitinated proteins may act as a hub for the recruitment of SV protein transport vesicles and piccolo-Bassoon transport vesicles (PTVs) and formation of en passant boutons (Figure 1). On the other hand, K11, K29 and K63 polyubiquitin-chains participate in the release of synaptic vesicles.

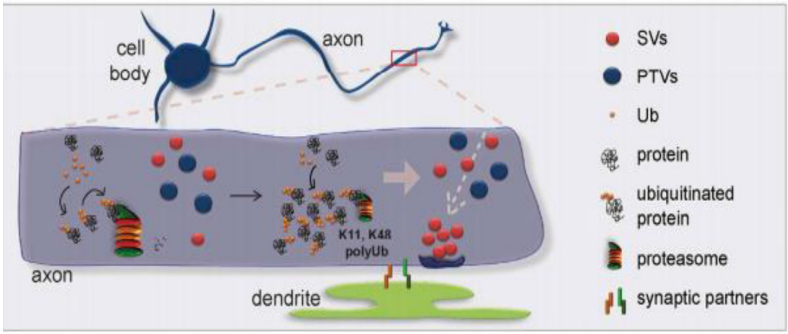

FIGURE 1: Inhibition of the proteasome by polyubiquitinated proteins (K11 and K48) leads to the recruitment of SV and PTVs necessary for the formation of presynaptic sites.

Together, these findings identify a new and unexpected role for polyubiquitinated proteins and demonstrate that UPS acts locally to regulate the assembly of new presynapses. The understanding and identification of the mechanisms underlying the synaptic function in normal neurodevelopment, serve as a support to understand how these mechanisms are affected in neuronal disorders.

Keywords: Ubiquitin-proteasome system (UPS), Synaptic transmission, Polyubiquitination, Microfluidic chambers

REFERENCES

[1] Y. Jin and C. C. Garner, "Molecular mechanisms of presynaptic differentiation," *Annu. Rev. Cell Dev. Biol.*, vol. 24, pp. 237–262, 2008.

[2] Pinto, M.J., D. Tome, and R. D. Almeida, "The ubiquitinated axon: local control of axon development and function by ubiquitin," *Under Revis.*

[3] X. Tian and C. Wu, "The role of ubiquitin-mediated pathways in regulating synaptic development, axonal degeneration and regeneration: Insights from fly and worm," *J. Physiol.*, vol. 591, no. 13, pp. 3133–3143, 2013.

[4] C. H. Na, D. R. Jones, Y. Yang, X. Wang, Y. Xu, and J. Peng, "Synaptic protein ubiquitination in rat brain revealed by antibody-based ubiquitome analysis," *J. Proteome Res.*, vol. 11, no. 9, pp. 4722–4732, 2012.

[5] B. J. Bhattacharyya, S. M. Wilson, H. Jung, and R. J. Miller, "Altered neurotransmitter release machinery in mice deficient for the deubiquitinating enzyme Usp14," *Am. J. Physiol. - Cell Physiol.*, vol. 302, no. 4, pp. 698–708, 2012.

[6] P. Chen *et al.*, "The proteasome-associated deubiquitinating enzyme Usp14 is essential for the maintenance of synaptic ubiquitin levels and the development of neuromuscular junctions," *J. Neurosci.*, vol. 29, no. 35, pp. 10909–10919, 2009.

[7] P. Chen *et al.*, "Ubiquitin homeostasis is critical for synaptic development and function," *J. Neurosci.*, vol. 31, no. 48, pp. 17505–17513, 2011.

[8] P. Lam, R. S. Fischer, W. D. Shin, C. M. Waterman, and A. Huttenlocher, "Spinning disk confocal imaging of neutrophil migration in Zebrafish," *Methods Mol Biol*, pp. 219–233, 2014.

[9] M. J. Pinto *et al.*, "The proteasome controls presynaptic differentiation through modulation of an on-site pool of polyubiquitinated conjugates," *J. Cell Biol.*, vol. 212, no. 7, pp. 789–801, 2016.

Study of patho-connectomics using innovative approaches in functional magnetic resonance imaging data analysis (PhD project presentation)

Lucianna Couto[1, 2]*, Sofia Reimão[1], Alexandre Andrade[2]

[1]Faculty of Medicine of the University of Lisbon (FMUL), University of Lisbon (UL), Lisbon, Portugal
[2]Institute of Biophysics and Biomedical Engineering (IBEB), Faculty of Sciences of the University of Lisbon (FCUL), University of Lisbon (UL), Lisbon, Portugal
**lucianna.couto@edu.ulisboa.pt*

INTRODUCTION/MOTIVATION

Scientific advances in the fields of *in vivo* neuroimaging, graph theory, computational modelling, study of brain diseases, among others, led to the development of a specific research field called connectomics. Briefly, connectomics refers to the study of connectomes, i.e., maps of brain networks showing the detailed structural and functional connectivity between brain regions across multiple spatial-temporal scales [1]–[3]. In this context, patho-connectomics, i.e., the study and diagnosis of brain diseases using connectomics, is a field of increasing relevance. This approach is based on the idea that a focal injury affects the whole brain by causing disruptions in brain networks.

In order to obtain *in vivo* neuroimaging data to map human connectomes, the most common technique is the functional magnetic resonance imaging (fMRI), which consists in monitoring changes in brain tissue oxygenation (Blood Oxygen Level Dependent, i.e., BOLD effect) under specific situations [2]–[4]. The potential for using connectivity measures other than correlation coefficient, as well as applying techniques to bring the BOLD signal closer to its neural origin, thereby mitigating the effect of unpredictable hemodynamic responses, remains mostly unexplored. Furthermore, automated, connectome-based diagnosis of brain diseases, including estimation of the probability of evolving to more severe stages and resorting to artificial intelligence, has been a very active topic.

Therefore, this PhD project is a methodological investigation that aims to: (a) evaluate whether there are significant changes in the connectomes of healthy and diseased subjects obtained from the use of non-standard connectivity

metrics and from the deconvolution of the hemodynamic component of the BOLD signal in fMRI data analysis, and, if so, to evaluate whether these changes are globally distributed or focused on specific brain regions/networks; and (b) assess whether the adoption of these methodological innovations provide significant improvements in automated diagnosis of specific diseases.

METHODS

In this PhD project, fMRI data will be obtained mainly from existing databases in the host lab, as well as publicly available databases. The use of innovations will encompass: (a) incorporation of innovative functional connectivity measures that are complementary to correlation coefficient, such as coherence, mutual information, and transfer entropy [5]; (b) incorporation of information regarding the hemodynamic response, using deconvolution approaches, such as total activation [6] and blind deconvolution [7]; and (c) evaluation of improvements in the efficiency of automated diagnosis and biomarker identification of a disease. The main software packages that will be adopted include: GraphVar, MULtiple connectivity ANalysis (MULAN), and in-house codes.

RESULTS AND DISCUSSION

The expected results of this PhD project are: (a) a comprehensive, statistically-informed assessment of how the adoption of non-standard connectivity metrics and the use of deconvolution approaches might affect the connectomes in healthy subjects and specific diseases; (b) an evaluation of whether these innovative methodological approaches provide a significant improvement in the performance of classifiers in diagnosing selected diseases; and (c) an enriched patho-connectomics analysis framework that will be made available to the scientific community, with the potential for application in a wide range of diseases.

ACKNOWLEDGEMENTS

Funding: PhD Scholarship: University of Lisbon (UL) and Faculty of Medicine of the University of Lisbon (FMUL).

Keywords: Connectomes, Patho-connectomics, fMRI data, Connectivity metrics, Deconvolution

REFERENCES

[1] G. Deco and M. L. Kringelbach, "Great expectations: Using whole-brain computational connectomics for understanding neuropsychiatric disorders", Neuron, vol. 84, 2014.

[2] A. Fornito, A. Zalesky, and M. Breakspear, "The connectomics of brain disorders", Nat. Rev. Neurosci., vol. 16, 2015.

[3] A. Fornito and E. T. Bullmore, "Connectomics: A new paradigm for understanding brain disease", Eur. Neuropsychopharmacol., vol. 25, 2015.

[4] J. E. Chen and G. H. Glover, "Functional Magnetic Resonance Imaging Methods", Neuropsychol. Rev., vol. 25, no. 3, pp. 289–313, 2015.

[5] H. E. Wang, C. G. Bénar, P. P. Quilichini, K. J. Friston, V. K. Jirsa, and C. Bernard, "A systematic framework for functional connectivity measures", Front. Neurosci., vol. 8, 2014.

[6] F. I. Karahanoğlu, C. Caballero-Gaudes, F. Lazeyras, and D. Van De Ville, "Total activation: fMRI deconvolution through spatio-temporal regularization", Neuroimage, vol. 73, pp. 121–134, Jun. 2013.

[7] G.-R. Wu, W. Liao, S. Stramaglia, J.-R. Ding, H. Chen, and D. Marinazzo, "A blind deconvolution approach to recover effective connectivity brain networks from resting state fMRI data", Med. Image Anal., vol. 17, pp. 365–374, 2013.

Dephasing the speaking brain: Cleaning covert sentence production activation maps with a phase-based fMRI data analysis

Iñigo De Vicente, Eneko Uruñuela, Maite Termenon, César Caballero-Gaudes*

Signal Processing in Neuroimaging lab, Basque Center on Cognition, Brain and Language, San Sebastián-Donostia, Spain
**c.caballero@bcbl.eu*

INTRODUCTION/MOTIVATION

The spatial resolution in conventional gradient-echo functional MRI (fMRI) experiments is largely confounded by the blood-oxygenation level dependent (BOLD) signal changes emanating from large draining veins [1]. These macrovascular effects limit precise localization of the neuronal activity, which fundamentally occurs at the level of smaller veins and capillaries. Previous studies have observed that the phase of the fMRI signal captures BOLD changes in voxels with large vessels but not in voxels located within the microvasculature [2]. Thus, by performing a linear regression between the phase and magnitude BOLD signals, the signal contribution coming from large veins can be estimated, and subsequently removed from the original magnitude time-series. Here, we aim at investigating the performance of this phase-based denoising method on a covert sentence production task, where part of the observed activations in Broca's area may be biased towards macrovasculature contained in the Sylvian fissure [3]. We analyze the performance of two fitting algorithms, ordinary least-squares (OLS) [2] and orthogonal distance regression (ODR) [4], by comparing the conventional magnitude-based activation maps against those obtained after suppressing the contributions from macrovascular veins.

METHODS

T2*-weighted multiband gradient-echo echo-planar images (TR = 850ms, TE = 35ms, flip angle = 56º, multiband acceleration factor = 6, voxel size = 2.4 x 2.4 x 2.4 mm^3, matrix size = 88 x 88 mm^2, 452 volumes) were collected in 23 subjects in a fMRI experiment while they performed a covert sentence production task in Spanish [5]. All analyses were performed using AFNI [6]

and in-house python scripts. Magnitude and phase fMRI signals were independently preprocessed prior to phase-based OLS [2] or ODR [4] denoising (which also required automatic filtering of respiratory-related fluctuations). Subject-level analyses were based on a general linear regression model which included the timings of the sentence production paradigm to model the task-evoked BOLD fluctuations, as well as the polynomials and motion-derived regressors to account for low-frequency trends and motion, and computed at the individual subject's space with 3dREMLfit to account for voxelwise temporal correlations. Separate GLM analyses were performed on the RAW preprocessed magnitude (i.e. without any phase-based denoising), and after the two phase-denoised methods (OLS-denoised and ODR-denoised). Group-level statistics comparing the different preprocessing strategies (RAW, OLS, ODR) were obtained with a mixed effects model using 3dMEMA [7].

RESULTS AND DISCUSSION

Both OLS and ODR algorithms estimated phase-magnitude correlations in similar regions, showing low coefficient of determination (R^2) values in white-matter voxels with reduced vasculature, and large R^2 values close to large veins, such as the superior sagittal sinus (see Figure 1). The R^2 maps matched the temporal standard deviation maps of the magnitude signal, which generally reflect physiological noise of large vessels. ODR outperformed OLS in terms of estimation accuracy, thus resulting in more effective removal of large draining effects. When comparing standard activation maps against those obtained after performing phase-based denoising, we found significant signal suppression in individual subjects and at the group-level (see Figure 2). As hypothesized, the larger effects of macrovascular contributions were observed in areas of the inferior frontal gyrus, particularly in the left pars orbitalis which is located adjacent to the Sylvian fissure and may thus contain large macrovascular signals. Our results demonstrate that previous covert sentence production studies can be biased towards macrovascular sources contained in the pars orbitalis. As such, we show that phase-based

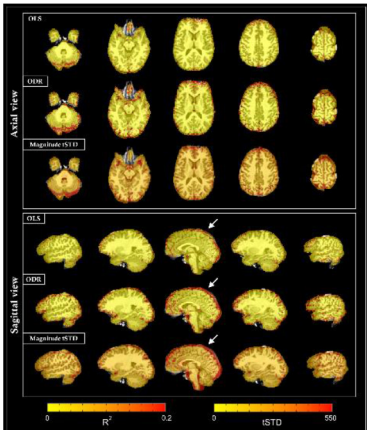

FIGURE 1: R2 maps of both OLS and ODR fitting methods and temporal standard deviation (tSTD) map shown in the axial and sagittal planes for a representative subject. Arrows highlight the apparent pattern of the superior sagittal sinus.

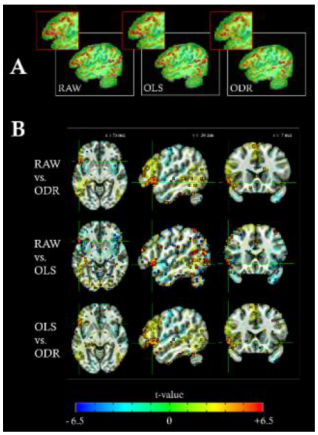

FIGURE 2: (**A**) Sagittal slice showing activations from a representative subject at the left pars orbitalis. The activation maps correspond to: (left) RAW analysis, (middle) OLS phase-based denoising, (right) ODR phase-based denoising. (**B**) Group-level effects of denoising in the activation maps at the left pars orbitalis. The maps depict significant differences using a mixed effects model between the analysis approaches: (top) RAW vs. ODR phase-based denoising, (middle) RAW vs. OLS phase-based denoising, (bottom) OLS vs. ODR phase-based denoising.

denoising methods have the potential to improve the accuracy of standard fMRI activation maps.

Keywords: Vein suppression, large draining veins, macrovascular bias, phase BOLD fMRI, phase regression, phase denoising, speech production

REFERENCES

[1] Hoogenraad, F. G., Hofman, M. B., Pouwels, P. J., Reichenbach, J. R., Rombouts, S. A., & Haacke, E. M. (1999). Sub-millimeter fmri at 1.5 tesla: correlation of high resolution with low resolution measurements. *Journal of Magnetic Resonance Imaging: An Official Journal of the International Society for Magnetic Resonance in Medicine*, 9(3), 475–482.

[2] Delion, M., Mercier, P., & Brassier, G. (2016). Arteries and veins of the sylvian fissure and insula: microsurgical anatomy. In *Advances and technical standards in neurosurgery* (pp. 185–216). Springer .

[3] Menon, R. S. (2002). Postacquisition suppression of large-vessel bold signals in high-resolution fmri. *Magnetic Resonance in Medicine: An Official Journal of the International Society for Magnetic Resonance in Medicine*, 47(1), 1–9.

[4] Curtis, A. T., Hutchison, R. M., & Menon, R. S. (2014). Phase based venous suppression in resting-state bold ge-fmri. *Neuroimage*, 100, 51–59.

[5] Mazoyer, B., Zago, L., Jobard, G., Crivello, F., Joliot, M., Perchey, G., ... & Tzourio-Mazoyer, N. (2014). Gaussian mixture modeling of hemispheric lateralization for language in a large sample of healthy individuals balanced for handedness. *PloS one*, 9(6), e101165.

[6] Cox, R. W. (1996). AFNI: software for analysis and visualization of functional magnetic resonance neuroimages. Computers and Biomedical research, 29(3), 162-173.

[7] Chen, G., Saad, Z. S., Nath, A. R., Beauchamp, M. S., & Cox, R. W. (2012). FMRI group analysis combining effect estimates and their variances. Neuroimage, 60(1), 747-765.

Synaptogenic effect of human umbilical cord perivascular cells' secretome in cortical and hippocampal neurons

Ricardo Faria[1]*, Diogo Tomé[1,2]*, Joana Correia[1], Marta Dias[1], Filipa Costa[1], Sofia C. Serra[3], António J. Salgado[3], Ramiro D. Almeida[1,2]

[1]iBiMED - Institute of Biomedicine, Department of Medical Sciences, University of Aveiro, Aveiro, Portugal

[2]CNC – Center for Neuroscience and Cell Biology, University of Coimbra, Coimbra, Portugal

[3]Life and Health Sciences Research Institute (ICVS), School of Medicine, University of Minho, Braga, Portugal

**These authors contributed equally to this work*

**ricardof@ua.pt*

INTRODUCTION/MOTIVATION

Throughout development, neurons exhibit an intrinsic growth capacity that allows their axons to grow and establish correct synaptic contacts. However, once the synaptic connections have been established, the developmental growth capacity of central nervous system (CNS) neurons declines. This loss, together with environment changes, largely accounts for the failure of adult CNS neurons to regenerate [1,2]. Therefore, it is crucial to investigate the key molecules and mechanisms involved in axonal elongation and synapse formation. Mesenchymal stem cells (MSC) are important for neuronal survival and repair and these regenerative properties are largely linked to the expression and release of a wide range of molecules (neurotrophic factors and cytokines) and microvesicles, the secretome [3]. We have recently shown that MSC secretome promotes axonal outgrowth of CNS neurons [4], but its effects on synaptogenesis remain elusive. In this work we aimed to uncover the effects of the secretome of a population of mesenchymal progenitors residing in the Wharton Jelly of the umbilical cord, known as human umbilical cord perivascular cells (HUCPVC), on synapse formation of CNS neurons.

METHODS

Primary cultures of rat embryonic cortical and hippocampal neurons were prepared as previously described [5]. The neuronal cultures were stimulated with the HUCPVCs' conditioned medium, which was previously collected and concentrated to 100 times by ultracentrifugation [6]. Immunocytochemistry

was performed using antibodies against synapsin and β-III tubulin. Fluorescent images of fixed cells were obtained with a Zeiss LSM-880 with airyscan with a 63x oil objective. Synapsin puncta and axonal length quantification were performed using ImageJ/Fiji software.

For calcium imaging experiments, cells were incubated for 30-40 min at 37ºC and 5% CO2 with 5 µM of Fluo-4 AM (excitation wavelength of 488 nm, Invitrogen) in saline solution, containing 0.2% of Pluronic F127 (Molecular Probes) to load the dye into the cells. Imaging was performed in saline solution (see above) at 37ºC in a humidified atmosphere to avoid medium evaporation. All settings, including exposure time and laser power, were conserved during the entire experiment. Calcium levels were monitored every second. Following a 200 s control period, cells were challenged with 2.5 mM KCl to induce membrane depolarization.

RESULTS AND DISCUSSION

We first evaluated the effect of HUCPVC secretome in presynaptic assembly. Cortical and hippocampal neurons were stimulated with HUCPVC secretome at both 2 times and 5 times and the formation of presynaptic clusters was assessed (Fig. 1). Secretome treatment increased the number of synapsin puncta per axon length at both 2 times (122.38%, $p<0.0001$) and 5 times (143.48%, $p<0.0001$) in cortical axons (Fig. 1A and 1C). This synaptogenic effect of HUCPVC secretome was also observed in hippocampal neurons with an increase in both 2 times (123.4%, $p<0.05$) and 5 times (129.48%, $p<0.001$) (Fig. 1B and 1D). Taken together, these data show that HUCPVC secretome induces an increase in synaptic vesicles (SV) clustering along the axonal shaft of both hippocampal and cortical neurons, indicating that HUCPVC secretome promotes the formation of new synapses in CNS neurons.

We next sought to investigate if the new synapses induced by HUCPVC secretome were functional. For this purpose, we assessed the global synaptic activity of hippocampal cultures by calcium imaging. Hippocampal neurons were treated with HUCPVC secretome and intracellular calcium levels were then monitored by loading the cells with the calcium dye Fluo-4 AM (Fig. 2). Basal activity was recorded over a period of 200 seconds. To determine possible changes in synaptic activity between the two groups, neurons

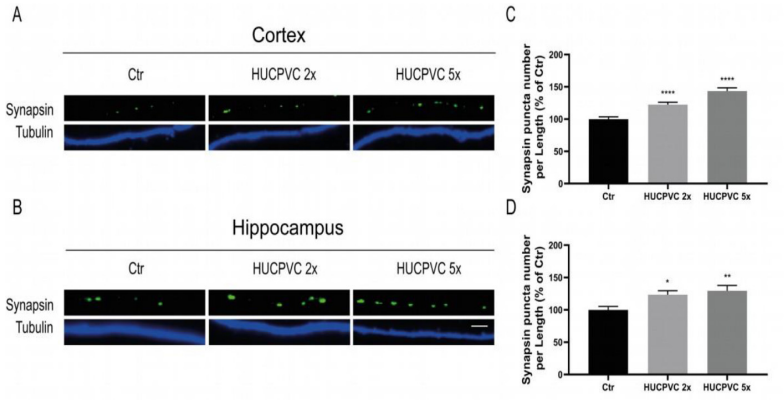

FIGURE 1: HUCPVC secretome induces synapse formation in CNS neurons. (A, B) Effect of HUCPVC secretome in presynaptic assembly. CNS neurons were stimulated with HUCPVC secretome, and the formation of presynaptic clusters was assessed by immunocytochemistry using an antibody against the synaptic vesicle markers synapsin (green), axons were detected using an antibody against tau (blue). (C-D) Quantification of synapsin (C, D) puncta number per axonal length. Results show that application of secretome at a concentration of 2 times and 5 times significantly increases the number of synapsin puncta, demonstrating that secretome stimulation induces the formation of new synapses in both cortical and hippocampal neurons. Results are expressed as % of control. Bars represent the mean ± SEM of at least 50 images from randomly selected areas of 3 independent experiments in the cortex and at least 30 images and 2 independent experiments in the hippocampus. The scale bar is 2,5 µm.

were then challenged with 2.5 mM KCl to induce membrane depolarization. A quick rise in intracellular calcium levels was observed in the cell bodies of both control (Fig. 2A) and secretome-treated hippocampal neurons (Fig. 2B), as a result of the opening of voltage-dependent calcium channels. The elevated calcium gradually returned to levels close to basal level. The magnitude of the calcium response after plasma membrane depolarization was significantly higher (114.39%, $p<0.0001$) in the secretome-treated neurons, when compared to control neurons (Fig. 2C). These data indicate that HUCPVC secretome enhances global synaptic activity in cultured hippocampal neurons, suggesting that the new synapses induced by HUCPVC secretome are functional. Together, our results demonstrate that MSC secretome has synaptogenic properties and revealing a potential role of the secretome to act locally in axonal regenerative therapies.

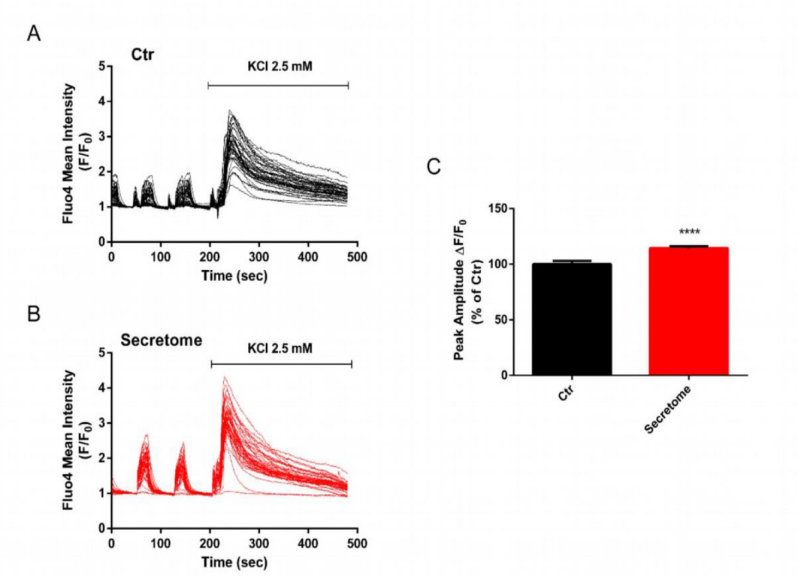

FIGURE 2: HUCPVC secretome enhances KCl-evoked calcium influx in hippocampal neurons. (**A, B**) Representative Fluo-4 AM fluorescent traces (one trace per neuron) obtained from hippocampal neurons after treatment with HUCPVC secretome. Hippocampal neurons were stimulated with HUCPVC secretome. Calcium influx induced by KCl-evoked plasma membrane depolarization was accessed by loading the cells with the calcium indicator Fluo-4 AM. (**C**) Averaged calcium response to KCl stimulation. Results show that global application of HUCPVC secretome significantly enhances the mean peak amplitude (ΔF/F0) of KCl-evoked calcium signals, indicating that HUCPVC secretome induces an increase in global synaptic activity in hippocampal neurons. Results are expressed as % of control. Bars represent the mean ± SEM of 307 neurons randomly selected of 3 independent experiments.

ACKNOWLEDGMENTS

This work was supported by Fundação para a Ciência e Tecnologia (FCT) through the individual PhD grants SFRH/BD/139368/2018 (DT) and SFRH/BD/141092/2018 (MD).

Keywords: Mesenchymal stem cells, Secretome, Synapse formation, Calcium imaging, Synaptic activity

REFERENCES

[1] F.M. Mar, A. Bonni, M.M. Sousa, *EMBO reports* **15**,254-263 (2014).

[2] K. Kadomatsu, K. Sakamoto, *Archives of Biochemistry and Biophysics* **558**, 36-41 (2014).

[3] V.B.R. Konala, M.K. Mamidi, R. Bhonde, A.K. Das, R. Pochampally, R. Pal, *Cytotherapy* **18**, 13-24 (2016).

[4] L.F. Martins, R.O. Costa, J.R. Pedro, P. Aguiar, S.C. Serra, F.G. Teixeira, N. Sousa, A.J. Salgado, R.D. Almeida, *Scientific Reports* **7**, 1-13 (2017).

[5] M.J. Pinto, P.L. Alves, L. Martins, J.R. Pedro, H.R. Ryu, N.L. Jeon, A.M. Taylor, R.D. Almeida, *Journal of Cell Biology* **212**, 789-801 (2016).

[6] A.O. Pires, B.M. Pinheiro, F.G. Teixeira, S.I. Anjo, S.R. Samy, E.D. Gomes, S.C. Serra, N.A. Silva, B. Manadas, N. Sousa, A.J. Salgado, *Stem Cells and Development* **25**, 1073-1083 (2016).

Hippocampal proteomic analysis to unravel the axonal proteome of rat axons

José Felgueiras[1]*, Rui Vitorino[1], Ramiro Almeida[1,2]*

[1]Department of Medical Sciences, iBiMED - Institute of Biomedicine, University of Aveiro,Aveiro, Portugal
[2]CNC – Center for Neuroscience and Cell Biology, University of Coimbra, Coimbra, Portugal
**joao.macedo@ua.pt; ramirodalmeida@gmail.com*

INTRODUCTION/MOTIVATION

The growth cone and the presynapse can be locate far away from the cell body. Information and the supply of cellular components have to travel long distances to reach these subdomains. This distance poses a challenge to the nerve cell. Axonal transport partially addresses these needs.[1]–[3]. However, considering the complex neuronal architecture and the axonal length, it would take an unsuitable time to transport cargos from the cell body to distal axons. Local mRNA translation solves some of these challenges and nowadays it is well accepted a synergy of both mechanisms. They work tightly to regulate the axonal proteome, and as a consequence to control vital axonal functions such as, axonal pathfinding synaptic plasticity and nerve regeneration. Local mRNA translation has a central role in modulating the axonal proteome [4]–[6].

The axonal proteome is composed by the entire repertoire of the proteins present in axons at a given moment. However, the identification of this repertoire with contamination of cell bodies or dendrites has been hampered by the lack of a suitable technique that can separate axons from this other structures. In this study we cultured hippocampal neurons in microfluidic chambers to isolate axons from soma and dendrites. A pure population of axons was isolated and subsequently analysed by mass spectrometry. Using bioinformatic tools we investigated the identity of the proteins present in these pure axonal extracts. We found proteins related to the cytoskeleton, plasma membrane and the synapse. We also found proteins associated with neurological disorders, suggesting that this set of proteins can be further analysed to study disease-related mechanisms. In our study we analysed the (pure) axonal proteome of developing hippocampal neurons and we have identified new proteins that may have an important role in neuronal physiology and disease.

METHODS

In order to identify the protein content in distal axons we cultured rat embryonic hippocampal neurons in microfluidic chambers. These microfluidic devices allow the isolation of pure axonal lysates with contamination of other cellular structures like soma or dendrites. The resulting protein extracts were digested, and peptide lysates were then analysed using an Orbitrap Fusion Lumos mass spectrometer coupled to an EasyLC (Fig.1).

The results were first analysed using a combination of Proteome Discoverer and MaxQuant to catalogue the axonal proteome and construct a more reliable analysis. Additionally, we run a Gene ontology (GO) analysis and a secretome analysis. The GO analysis allowed us to obtain a more detailed knowledge about each category group of the listed proteins, providing information in the form of biological process, molecular function and cellular component.

To obtain a comprehensive understanding of the axonal proteome we next used both a broad disease-database (DisGeNET) and specific disease-data-

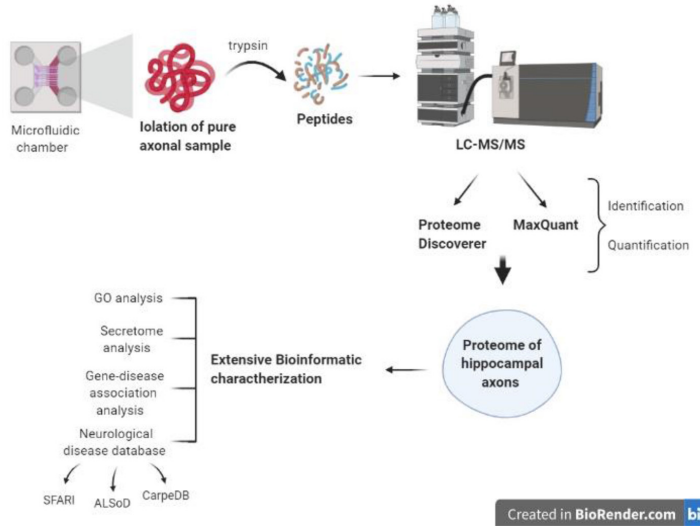

FIGURE 1: Outline of the experimental design used.

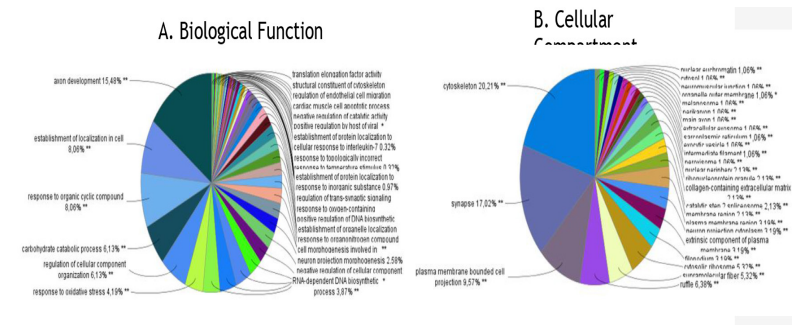

FIGURE 2: Functional annotation. (**A**) biological function and (**B**) cellular compartment analysis of the rat hippocampal axonal proteome (Cytoscape, ClueGo).

bases (Sfari, CarpeDB and ALSoD) to search for different neuropathologies fingerprints, which may identify future targets or patterns. Since all these platforms contain collections of genes associated with human diseases, we then compared our dataset of proteins with each repository. This allows us to build a gene-disease association map, reviling the relevant proteins associated with multiple neurological disorders.

RESULTS AND DISCUSSION

We first sought to identify and categorize the axonal proteome obtained by Mass spectrometry (Fig.2). The results show that both axoplasmic transport and local translation are enriched in rat hippocampal axons. We were able to identify proteins that showcase local translation activity in axons, such as ribosomal proteins, initiation factors, elongation factors, RNA-binding proteins, Golgi apparatus proteins, and endoplasmic reticulum chaperones (Fig.2A). From the GO analysis, we confirmed that both cytoskeletal-associated proteins and axonogenic proteins were highly enriched within the proteome found in axons of hippocampal rat neurons (Fig.2B). There was also presence of various biosynthetic processes in the axon, reinforcing the active local protein production. Interestingly, the analysis also revealed that almost 40% of proteins are predicted as secreted proteins.

We next aimed to identify the proteins associated with different neurodegenerative diseases, such as Autism spectrum disorders, Amyotrophic Lateral Sclerosis and Epilepsy. This panel gathers several proteins involved in important biological processes, such as axonal and synaptic function and development. Thus, these results suggest that dysregulation of intra-axonal translation might be linked to the pathogenesis of neurological disorders. Overall, this study deepens the current knowledge on the proteome content of hippocampal axons and gathers information about the fingerprint of several disorders, opening new possibilities for exploring new targets.

Keywords: Axonal proteome, Local protein synthesis, Quantitative proteomics, Neurological disorders

REFERENCES

[1] E. M. Chudinova and E. S. Nadezhdina, "Interactions between the Translation Machinery and Microtubules," *Biochem.*, vol. 83, pp. 176–189, 2018.

[2] J. T. Kevenaar and C. C. Hoogenraad, "The axonal cytoskeleton: From organization to function," *Front. Mol. Neurosci.*, vol. 8, no. AUGUST, pp. 1–12, 2015.

[3] S. Brunholz, S. Sisodia, A. Lorenzo, C. Deyts, S. Kins, and G. Morfini, "Axonal transport of APP and the spatial regulation of APP cleavage and function in neuronal cells," *Exp. Brain Res.*, vol. 217, no. 3–4, pp. 353–364, 2012.

[4] A. C. Lin and C. E. Holt, "Local translation and directional steering in axons," *EMBO J.*, vol. 26, no. 16, pp. 3729–3736, 2007.

[5] E. Kim and H. Jung, "Local protein synthesis in neuronal axons: Why and how we study," *BMB Rep.*, vol. 48, no. 3, pp. 139–146, 2015.

[6] V. Rangaraju, S. tom Dieck, and E. M. Schuman, "Local translation in neuronal compartments: how local is local?," *EMBO Rep.*, vol. 18, no. 5, pp. 693–711, 2017.

Relating slow waves from different measurement techniques through an adaptable pipeline

Robin Gutzen[1,2]*, Giulia De Bonis[3], Elena Pastorelli[3,4], Cristiano Capone[3], Chiara De Luca[3,4], Glynis Mattheisen[5], Anna Letizia Allegra Mascaro[6,7], Francesco Resta[6], Francesco Saverio Pavone[6], Maria V. Sanchez-Vives[8,9], Maurizio Mattia[10], Sonja Grün[1,2], Andrew Davison[5], Pier Stanislao Paolucci[3], Michael Denker[1]

[1]Institute of Neuroscience and Medicine (INM-6) and Institute for Advanced Simulation (IAS-6) and JARA-Institute Brain Structure-Function Relationships (INM-10), Jülich Research Centre, Jülich, Germany
[2]Theoretical Systems Neurobiology, RWTH Aachen University, Aachen, Germany
[3]Instituto Nazionale di Fisica Nucleare (INFN), Sezione di Roma, Rome, Italy
[4]Ph.D. Program in Behavioural Neuroscience, "Sapienza" University of Rome, Rome, Italy
[5]Unité de Neurosciences, Information et Complexité, Neuroinformatics Group, CNRS FRE, Gif-sur-Yvette, France
[6]European Laboratory for Non-linear Spectroscopy (LENS), University of Florence, Florence, Italy
[7]Istituto di Neuroscienze, CNR, Pisa, Italy
[8]Institut d'Investigacions Biomèdiques August Pi i Sunyer (IDIBAPS), Barcelona, Spain
[9]Institució Catalana de Recerca i Estudis Avanc, ats (ICREA), Barcelona, Spain
[10]Istituto Superiore di Sanità, (ISS), Rome, Italy
**r.gutzen@fz-juelich.de*

INTRODUCTION/MOTIVATION

Today's neuroscientific research landscape excels in an unprecedented richness of data and methodologies. On the one hand, this enables scientific progress by enabling a variety of new methodological approaches and analytical findings. On the other hand, the diversity makes it more difficult to relate complementary yet different approaches, to make the results comparable, and to incorporate them into models. In other words: making scientific progress by building a cumulative understanding based on existing results. The phenomenon of slow cortical waves is a prime example of this scenario. During sleep or anesthesia, they are persistently observed by various measurement techniques in various species [1,2], as well as being expressed in various models. There is an increasing amount of such data shared publicly and a wide basis of findings in the literature analyzing slow waves, and investigating their relevance [3]. However, the heterogeneity of analytical methods, tools, data formats, metadata, and even terminologies makes it difficult to form a coherent understanding.

METHODS

Here, we present an adaptable and reusable analysis pipeline to support quantitative statistical comparisons on the level of slow-wave characteristics. The key objective of the pipeline is to bring together existing methods, standards, and tools in a flexible and modular manner in order to serve the requirements of a wide range of datasets and research questions. Thus, the main goal is not to apply new methods but rather to reconcile existing ones in a common framework that enables their comparison or complementary usage, enabling trustworthy integration and synthesis of knowledge across scales. The reusability and extendability of each of the pipeline components are furthermore promoted by building entirely on open-source tools, such as the workflow manager Snakemake (RRID:SCR_003475), the Neo (RRID:SCR_000634) library for data representation [4], the Elephant (RRID:SCR_003833) analysis toolbox, and the EBRAINS Knowledge Graph (https://kg.ebrains.eu) for capturing the pipeline execution.

RESULTS AND DISCUSSION

The pipeline design enables the creation of application-tailored and reproducible analyses of slow-wave activity. We demonstrate the analysis and comparison of slow-wave characteristics using ECoG [5,6,7] and Calcium Imaging [8.9] data of anesthetized mice (see Figure 1). While the 'same methods - different data' approach enables a fair comparison between datasets, the pipeline equally enables 'same data - different methods' benchmarking.

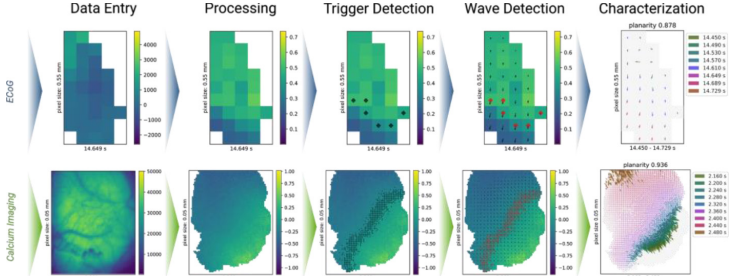

FIGURE 1: Sequential processing stages and corresponding exemplary outputs of the analysis pipeline applied to a wave front recorded using ECoG data (top) and calcium imaging (bottom). By use of largely common components for both data types, the resulting characterization of the vector field showing wave propagation (right) is comparable on a quantitative level.

Finally, we discuss how the individual elements can be reused, rearranged, or extended to help derive analysis pipelines for similar research endeavors and amplify collaborative research. Our prototype already illustrates not only the benefits of sharing data, but also how the integration of such pipelines may become more seamless and automatized when data and metadata are published in well documented standardized formats.

ACKNOWLEDGEMENTS

This project has received funding from the European Union's Horizon 2020 Framework Programme for Research and Innovation under Specific Grant Agreement No. 785907 (Human Brain Project SGA2) and 945539 (Human Brain Project SGA3), and by the Helmholtz Association Initiative and Networking Fund under project number ZT-I-0003.

Keywords: slow waves, reproducibility, spatiotemporal propagation, brain states, anesthesia, wide-field calcium imaging, MEA electrophysiology

REFERENCES

[1] Adamantidis, A. R., Herrera C. G., and Gent T. C. (2019) "Oscillating circuitries in the sleeping brain." Nature Reviews Neuroscience 1-17. doi: 10.1038/s41583-019-0223-4

[2] Alkire, M. T., Hudetz A. G. , and Tononi G. (2008) "Consciousness and anesthesia." Science 322.5903: 876-880. doi: 10.1126/science.1149213

[3] Sanchez-Vives, M. V., Massimini, M., and Mattia, M. (2017) "Shaping the default activity pattern of the cortical network". Neuron, 94(5), 993-1001. doi: 10.1016/j.neuron.2017.05.015

[4] Garcia, S., Guarino, D., Jaillet, F., Jennings, T., Pröpper, R., Rautenberg, P.L., Rodgers, C.C., Sobolev, A., Wachtler, T., Yger, P., et al. (2014). Neo: an object model for handling electrophysiology data in multiple formats. Frontiers in Neuroinformatics 8, 10. doi: 10.3389/fninf.2014.00010

[5] Dasilva, M., Camassa, A., Navarro-Guzman, A., Pazienti, A., Perez-Mendez, L., Zamora-López, G., Mattia, M. & Sanchez-Vives, M. V. (2020). Modulation of cortical slow oscillations and complexity across anesthesia levels. NeuroImage, 224, 117415.

[6] Sanchez-Vives, M. (2019) "Cortical activity features in transgenic mouse models of cognitive deficits (Williams Beuren Syndrome)" [Data set]. EBRAINS. doi: 10.25493/DZWT-1T8

[7] De Bonis, G. et al. (2019) "Analysis pipeline for extracting features of cortical slow o scillations". Frontiers in Systems Neuroscience 13:70. doi: 10.3389/fnsys.2019.00070

[8] Resta, F., Allegra Mascaro, A. L., and Pavone, F. (2020). Study of Slow Waves (gSWs) propagation through wide-field calcium imaging of the right cortical hemisphere of GCaMP6f mice [Data set]. EBRAINS. doi: 10.25493/3E6Y-E8G

[9] Celotto, M. et al. (2020) "Analysis and Model of Cortical Slow Waves Acquired with Optical Techniques". Methods and Protocols 3.1:14. doi: 10.3390/mps3010014

Morphological alterations of pyramidal neurons from the contralesional hemisphere after ischemic stroke

Sergio Plaza-Alonso[1,2], Asta Kastanauskaite[1,2], Susana Valero-Freitag[3], Nikolaus Plesnila[3], Farida Hellal[3], Javier DeFelipe[1,2,4], Paula Merino-Serrais[1,2]

[1]Laboratorio Cajal de Circuitos Corticales, Centro de Tecnología Biomédica, Universidad Politécnica de Madrid, Madrid, Spain
[2]Instituto Cajal, Consejo Superior de Investigaciones Científicas (CSIC), Madrid, Spain
[3]Experimental Stroke Research, Institute for Stroke and Dementia Research, Cluster for Systems Neurology, University of Munich Medical Center, Munich, Germany
[4]Centro de Investigación Biomédica en Red sobre Enfermedades Neurodegenerativas (CIBERNED), ISCII, Madrid, Spain
**serplalo@cajal.csic.es*

INTRODUCTION

Stroke is one of the major causes of death and disability worldwide[1]. With over 80 million prevalent cases globally, the world is facing a modern epidemic[2].

Much emphasis has been placed on clarifying the pathological aspects and consequences of the focal lesion, the infarct core. However, interesting studies indicate that, after stroke, remote regions connected to the infarcted area are also affected. This process, known as diaschisis, is present among others, in the contralateral hemisphere, affecting the performance of the whole brain and may be implicated in the suppression of functional recovery after stroke[3–5].

Given this, the main goal of the present study was to analyze possible micro-anatomical alterations of pyramidal neurons in layer III from the contralesional somatosensory cortex-barrel field (BF) in the ischemic stroke mice model 'tMCAo'. These alterations could provide new insights into the understanding of the pathology and lead us to new therapy approaches.

METHODS

The transient middle cerebral artery occlusion mice stroke model (tMCAo) and the correspondent SHAM-control mice were used (20 weeks old, 18 male

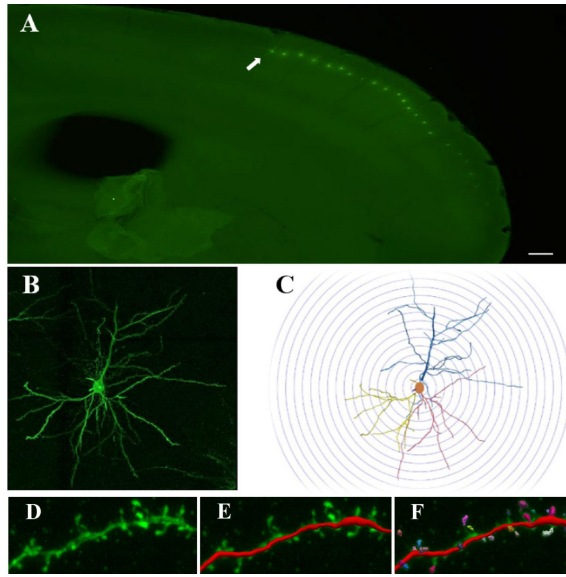

FIGURE 1: (**A**) Panoramical overview of LY injected pyramidal neurons (in green) from a SHAM somatosensory cortex transversal section (right hemisphere). (**B**) Detail of a LY injected neuron from Fig 1A. (indicated with a white arrow). Neuronal and spine structure were 3D reconstructed using confocal microscopy and visualizce with Neurolucida 360 software. (**C**) 3D tracing model of the pyramidal neuron from Fig. 1B. Concentric spheres represent the segments made by Sholl Analysis to estimate the data. (**D**) Detail of a LY injected apical dendrite from a SHAM mouse. (**E-F**) 3D trace of the dendrite branch (in red) and dendritic spines from Fig 1D.

animals). 594 pyramidal neurons, located in the contralesional somatosensory cortex-barrel field (layer III) were individually injected with Lucifer Yellow (LY). LY injected cells were then 3D reconstructed using confocal microscopy and morphological parameters were analysed with Neurolucida 360 software[6] (Figure 1).

Several morphometric parameters were analysed in apical and basal dendritic trees. First, we evaluated the complexity of the dendritic arborization in both, apical and basal dendritic tree by measuring: dendritic length; dendritic volume; number of intersections; dendritic surface; number of nodes and dendritic diameter, as a function of the distance from the soma (Sholl analysis - 30 cells per group). This analysis creates a 3D scaffold of concentric spheres that normalize measures, thus allowing a reliable comparison between groups (Figure 1C).

Then, spine morphology was analysed through different morphometric parameters, such as dendritic spine density; dendritic spine length and dendritic spine volume, in apical and basal dendritic trees. This data was studied as a function of the distance from the soma (Sholl analysis), as an average per dendrite and as a frequency distribution analysis (minimum of 21 dendrites per group).

Statistical analysis

Mann-Whitney test was used to compare averages (mean ± SEM); Kolmogorov – Smirnov test was used in the frequency distribution analysis; Two-way ANOVA followed by a post–hoc Bonferroni comparison was used to compare values when presented as a function of the distance from the soma (Sholl analysis).

RESULTS/DISCUSSION

Apical dendritic tree shows less neuronal complexity in tMCAo animals: significant decrease in dendritic length (Figure 2A), number of intersections (Figure 2C), and dendritic surface (Figure 2D) of the apical dendritic tree were found in tMCAo compared with SHAM mice. No changes were found in basal dendritic tree analysis in any parameter.

Apical and basal dendrites show alterations in spine morphology: Frequency distribution analysis reveals significant changes in spine length and volume in both apical and basal dendritic trees between groups. No differences were found in Sholl and average analysis.

The complexity of the neuronal dendritic structure determines their biophysical properties, thus influencing their functional capacity and potential for plastic change. In addition, dendritic spines, being the main post-synaptic element, are targets of most excitatory synapses in the cerebral cortex and their morphology could determine synaptic strength and learning rules[7–9]. Therefore, alterations of spine morphology and neuronal complexity could affect neuronal function. Furthermore, the morphological alterations found in this study could play an important role in the recovery of the patient, since most of the post-ictus rehabilitation therapies rely on the neuronal and circuit potential for plasticity of the areas both close to the infarct core and symmetrically located in the contralateral hemisphere[10,11]. Thus, the alterations found in this stroke model are of great interest and should be further

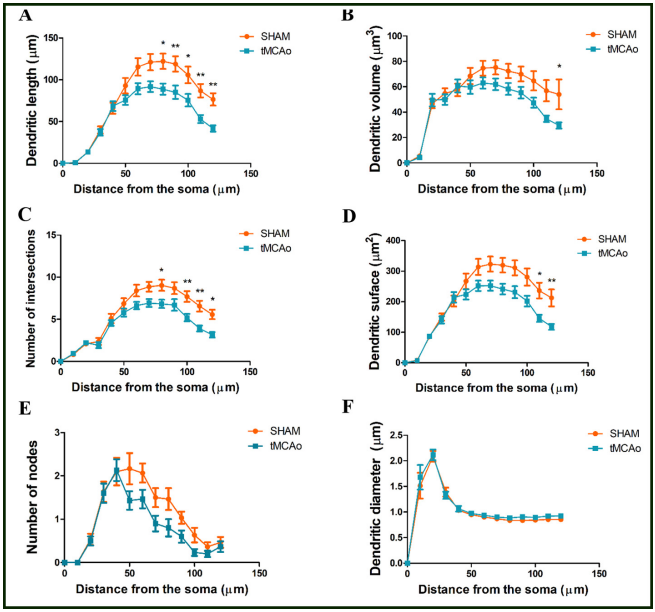

FIGURE 2: Reduction in the apical dendritic tree complexity. Results from Apical Dendritic Tree morphological Sholl analysis. Significant decreases were found in several parameters (Dendritic Length; Number of intersection; Dendritic Surface and Dendritic Volume) from tMCAo mice model, compared to SHAM. Two-way ANOVA (repeated measures) and post-hoc Bonferroni test were used to analyze the data. N= 30 cells per group (tMCAo, SHAM). Data is shown as mean ± SEM. *p<0.05; **p<0.01.

analysed. In fact, we are currently extending the areas of study to perform these analyses. Specifically, we are planning to include the contralateral hippocampus and the secondary somatosensory cortex, both areas in which the ischemic lesion may have a different impact.

Keywords: Ischemic stroke, intracellular injection, 3D reconstruction, neuronal complexity, dendritic spine length and volume, somatosensory cortex

REFERENCES

[1] Donnan GA, Fisher M, Macleod M, Davis SM. Stroke. Lancet (London, England). 2008 May;371(9624):1612–23.

[2] Global, regional, and national burden of neurological disorders, 1990-2016: a systematic analysis for the Global Burden of Disease Study 2016. Lancet Neurol. 2019 May;18(5):459–80.

[3] Buetefisch CM. Role of the Contralesional Hemisphere in Post-Stroke Recovery of Upper Extremity Motor Function. Front Neurol. 2015;6:214.

[4] Duering M, Righart R, Csanadi E, Jouvent E, Hervé D, Chabriat H, et al. Incident subcortical infarcts induce focal thinning in connected cortical regions. Neurology. 2012 Nov;79(20):2025–8.

[5] Silasi G, Murphy TH. Stroke and the connectome: how connectivity guides therapeutic intervention. Neuron. 2014 Sep;83(6):1354–68.

[6] Benavides-Piccione R, Regalado-Reyes M, Fernaud-Espinosa I, Kastanauskaite A, Tapia-González S, León-Espinosa G, et al. Differential Structure of Hippocampal CA1 Pyramidal Neurons in the Human and Mouse. Cereb Cortex. 2019 Jul 2.

[7] Benavides-Piccione R, Fernaud-Espinosa I, Robles V, Yuste R, DeFelipe J. Age-based comparison of human dendritic spine structure using complete three-dimensional reconstructions. Cereb Cortex. 2013 Aug;23(8):1798–810.

[8] van Elburg RAJ, van Ooyen A. Impact of Dendritic Size and Dendritic Topology on Burst Firing in Pyramidal Cells. PLOS Comput Biol. 2010 May 13;6(5):e1000781.

[9] Stuart GJ, Spruston N. Dendritic integration: 60 years of progress. Nat Neurosci. 2015 Dec;18(12):1713–21.

[10] Carmichael ST. Plasticity of cortical projections after stroke. Neuroscientist. 2003 Feb;9(1):64–75.

[11] Gerloff C, Bushara K, Sailer A, Wassermann EM, Chen R, Matsuoka T, et al. Multimodal imaging of brain reorganization in motor areas of the contralesional hemisphere of well recovered patients after capsular stroke. Brain. 2005 Dec 19;129(3):791–808.

Cytoarchitectonic mapping of the human inferior colliculi

Rönna, C.-J.[1]*, Brandstetter, A.[1], Mohlberg, H.[1], Amunts, K.[1,2]

[1]Institute of Neuroscience and Medicine (INM-1), Research Centre Jülich, Jülich, Germany
[2]C. and O. Vogt Institute for Brain Research, University Hospital Düsseldorf, Heinrich Heine University Düsseldorf, Düsseldorf, Germany
**coco-june.roenna@outlook.com*

INTRODUCTION

It is an essential part of the Human Brain Project to get a deeper understanding of the brain's structural organization (Amunts, 2019). A 3D atlas is an important prerequisite for new insights into structure-function relationships. This requires the identification and mapping of a large number of areas of the cerebral cortex and subcortical nuclei. One of the nuclei that has not yet been submitted to the BigBrain atlas is the inferior colliculus (IC). It is located in the midbrain and is a few millimeters in diameter. As part of the sensory circuit, the IC receives auditory input from the brainstem and sends output to the mediate geniculate body and further on to the temporal lobe (Winer & Schreiner, 2005). The present, ongoing study is investigating the human IC in one of the BigBrain models (Amunts et al., 2013, 2020). This approach enables us to better characterize the 3D shape and position of the IC, also to reveal its internal organization. The mapping will be continued in nine other brains. The data will be implemented in the EBRAINS interactive AtlasViewer, a 3D atlas based on our first BigBrain data set (https://interactive-viewer.apps.hbp.eu/?templateSelected=Big+Brain+%28Histology%29&parcellationSelected=Cytoarchitectonic+Maps).

METHODS

Histological sections of a human postmortem brain (thickness 20 micrometers) cut in the coronal plane and stained for cell bodies (Merker, 1983) were analyzed in the so-called second BigBrain data set, where each section of a total of 7404 was histologically processed and the stack was 3D-reconstructed (Amunts et al., 2020). In our study, the borders of the IC of both hemispheres were delineated in digitized sections using the in-house software OnlineSectionTracer. As each region of the brain has its distinct

cytoarchitectonic pattern, depending on the shape, size and density of its neurons, such patterns could be observed at the border between two adjacent brain regions. These were applied to annotate the structures on 11 sections in each hemisphere at a distance of every 30th section, i.e. a distance of 600µm between two adjacent sections. For further observations, the EBRAINS interactive AtlasViewer was used. The software allowed to visualize the three cutting planes i.e. coronal, sagittal and horizontal, and to explore them simultaneously in relationship to the surface representation of the brain.

RESULTS

The IC was located ventrally to the superior colliculus and laterally to the periaqueductal gray (PAG) (Fig.1). It is roundly shaped at caudal and middle levels. At anterior levels, the IC seems to have "edges" and "notches". Cytoarchitectonically the IC consists of two regions. One subdivision has a high neuronal density and was identified as the central nucleus of the IC, i.e. ICC (Fig. 1). The ICC was dorsally covered by a region with a lower density of neurons, the peripheral nucleus of the IC, i.e. ICP (Fig. 1).

DISCUSSION

Two subdivisions of the IC could be identified based on cytoarchitectonic criteria and its borders were delineated in one brain: the central and the peripheral nuclei of the IC. These nuclei are not visible in routine MR images, due to lower resolution and lower contrast in MR imaging. Therefore, small structures, like the IC require a histological approach. Other studies reported that the IC comprises three substructures: the central nucleus, the dorsal cortex and the external nucleus (Winer & Schreiner, 2005). Our analyses showed a similar cytoarchitecture between dorsal cortex and external nucleus and were therefore combined (ICP).

The BigBrain data sets used in the study is a benefit for small brain structures of only a few millimeters: The distance between sections could be decreased at any time of the investigation, to get a detailed look on the structure or to gain more annotated sections. In addition, 3D reconstructions of a structure can be performed more precisely if every section is available and it enables us to run further investigations later on, such as deep-learning based approaches to automatically annotate the structure.

The delineations are currently stored in our in-house software for annotations "OnlineSectionTracer". It is planned to complement the current mapping by a 3D reconstruction of the structure and analyzing histological sections of nine additional brains to capture inter-subject variability of the IC. The results will be used to compute probabilistic maps showing variability in space and extent, and will be published through the interactive AtlasViewer of EBRAINS and the Julich Brain Atlas (https://interactive-viewer.apps.hbp.eu/?templateSelected=MNI+Colin+27&parcellationSelected=JuBrain+Cytoarchitectonic+Atlas&cNavigation=0.0.0.-W000..2_ZG29.-ASCS.2-8jM2._aAY3..BSR0..86T%7E.14VKq%7E.L8Nk..3GAA).

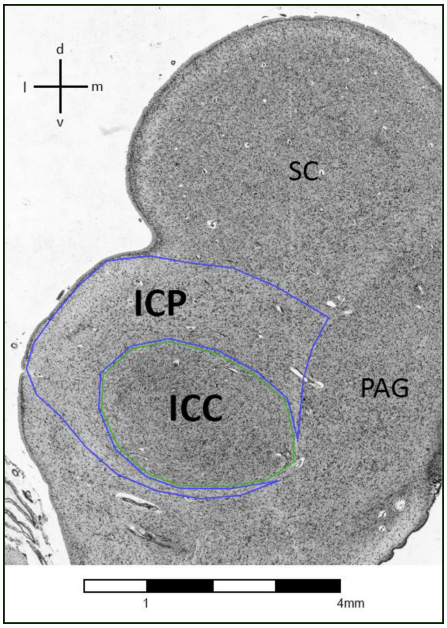

FIGURE 1: Coronal view of the mesencephalon of the human brain at the level of the inferior colliculus (IC) and its subdivisions, i.e. central nucleus of the IC (ICC) and the peripheral nucleus of the IC (ICP). SC - superior colliculus, PAG - periaqueductal gray, d - dorsal, v - ventral, m - medial, l – lateral.

Keywords: Inferior Colliculi, Mapping, Neuroanatomy, Human Brain Project

REFERENCES

[1] Amunts K., Knoll A. C., Lippert T., Pennartz C. M. A., Ryvlin P., Destexhe A., Jirsa V. K., D'Angelo E., Bjaalie J. G. (2019). *The Human Brain Project – Synergy between neuroscience, computing, informatics and brain-inspired technologies.* Plos Biology, 17(7): e3000344 doi.org/10.1371/journal.pbio.3000344

[2] Amunts, K., Lepage, C., Borgeat, L., Mohlberg, H., Dickscheid, T., Rousseau, M.-E., Bludau, S., Bazin, P.-L., Lewis, L.B., Oros-Peusquens, A.-M., Shah, N. J., Lippert, T., Zilles, K. & Evans, A. C. (2013). BigBrain: An Ultrahigh-Resolution 3D Human Brain Model. Science Vol. 340, No. 6139, pp. 1427 – 1475 doi: 10.1126/science.1235381

[3] Amunts, K., Mohlberg, H., Bludau, S. & Zilles, K. (2020). Julich-Brain: A 3D Probabilistic Atlas of the Human Brain's Cytoarchitecture. Science Vol. 369, No. 6506, pp. 988 - 992 doi.org/10.1126/science.abb4588

[4] Merker, B. (1983). Silver staining of cell bodies by means of physical development. Journal of Neuroscience Methods 9: 235-241.

[5] Winer, J. A. & Schreiner, C. E. (2005). The Central Auditory System: A Functional Analysis.

[6] In J. A. Winer & C. E. Schreiner (Ed.) The Inferior Colliculus (pp. 21 & 23). New York, NY: Springer

Investigating non-invasive deep brain stimulation using temporally interfering electric fields

Dimitrios Stoupis*

Department of Physics, Aristotle University of Thessaloniki, Thessaloniki, Greece
**dstoupis@auth.gr*

INTRODUCTION/MOTIVATION

Treating brain diseases or suppressing their symptoms by electric stimulation is not a trivial task. Different methods exist for stimulating structures deep in the brain, but usually these are invasive, posing considerable risk for the overall health of the individual. This is one of the main reasons there is wide research activity in non-invasive methods for deep brain stimulation. The problem of most non-invasive methods is the lack of focality to stimulate a small target area. An emerging technique in the field of applied neuroscience is the Transcranial Temporal Interference Stimulation (tTIS), showing promising results [1], [2]. The great advantage of this method is the high penetration depth it can achieve, without affecting the surrounding areas, thus making it ideal for targeted deep brain stimulation. The benefits of this method can be utilized to study the response pattern through EEG signals by stimulating a very small area of choice non-invasively. The current work presents the development of a software tool capable of importing realistic human head models derived from medical imaging data and creating a personalized treatment plan for tTIS. This work is ongoing with the aim of optimizing the treatment plan of the tTIS to stimulate specific targets inside the brain.

METHODS

The software tool was developed in Python and it is available in GitLab [3]. Initially, to verify the code that has been developed, a replication simulation was run on the sphere model reported in [1]. Subsequently, the code was applied in anatomically realistic models taken from the Population Head Model repository (PHM) [4], [5]. More specifically, all the models were meshed with the help of the PyMesh library using a tetrahedral mesh suitable for the implementation of the Finite Element Method (FEM). The electrodes were placed on the surface of the head, following the 10-20 international standard, using the code developed by [6]. Eventually, the Laplace equation was solved

to extract the potential in the different areas of the model and the resulting internal electric field, by utilizing the FEM solvers of SfePy [7]. The dielectric properties of the tissues used in the models were taken from [8] at the frequency of 1 kHz used for creating the temporal interference in the PHM.

RESULTS AND DISCUSSION

There was very good agreement between the results obtained in [1] inside the sphere model and the results with the code developed in this work (Figure 1), therefore the code can be considered as validated/verified.

The result of the temporal interference envelop, using electrodes P4, F7 for the VCC and GND, respectively, of the first frequency pair (1 kHz) and electrodes P3, F8 for the second frequency pair (1.04 kHz) can be seen in (Figure 2). One important observation that came up from the results obtained with PHM is that, as expected, the distribution of the electric field varies significantly between different models, using the same electrode pair (of the 10-20 system). Therefore, optimization methods need to be applied to maximize the electric field in deep areas of interest in the brain. This optimization will be performed in the near future for the different head models of the PHM [4], [5] to study the variations and the difficulties or traits that will arise.

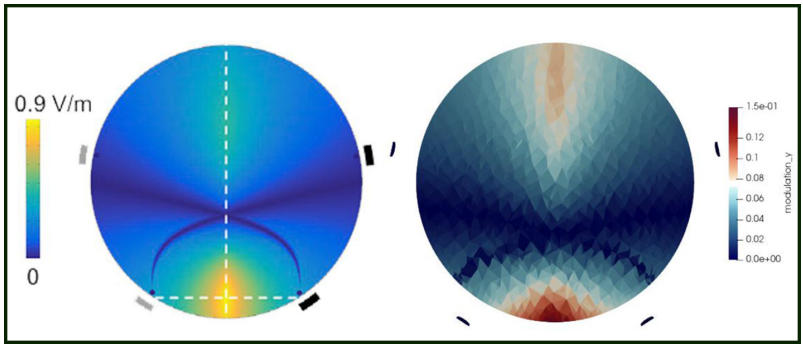

FIGURE 1: Comparison of the results from Grossman et al. (left) and the present work(right).

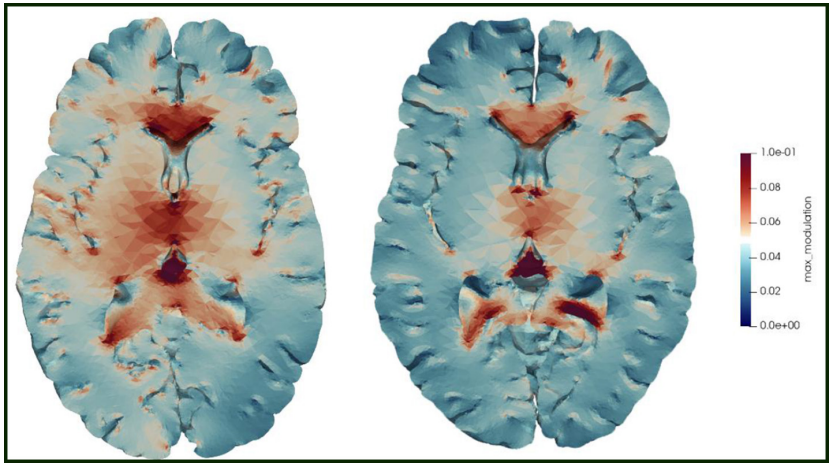

FIGURE 2: Comparison of the temporal interference envelop, using electrodes P4, F7 for the VCC and GND respectively of the first frequency pair (1 kHz) and electrodes P3, F8 for the second frequency pair (1.04 kHz), based on the 10-20 standard.

ACKNOWLEDGEMENTS

This research work is part of the author's thesis, supervised by Prof. Theodoros Samaras.

The results presented in this work have been produced using the Aristotle University of Thessaloniki (AUTh) High Performance Computing Infrastructure and Resources.

Keywords: neuroscience, temporal interference, finite elements, deep brain stimulation

REFERENCES

[1] N. Grossman, D. Bono, N. Dedic, S. B. Kodandaramaiah, A. Rudenko, H.-J. Suk, A. M. Cassara, E. Neufeld, N. Kuster, L.-H. Tsai, A. Pascual-Leone and E. S. Boyden, "Noninvasive Deep Brain Stimulation via Temporally Interfering Electric Fields," Cell, vol. 169, p. 1029–1041.e16, 6 2017.

[2] S. Rampersad, B. Roig-Solvas, M. Yarossi, P. P. Kulkarni, E. Santarnecchi, A. D. Dorval and D. H. Brooks, "Prospects for transcranial temporal interference stimulation in humans: A computational study," NeuroImage, vol. 202, p. 116124, 11 2019.

[3] D. Stoupis, "tACS Temporal Interference - Project ID: 18467592," [Online]. Available: https://gitlab.com/dimst23/tacs-temporal-interference. [Accessed 5 11 2020].

[4] E. G. Lee, W. Duffy, R. L. Hadimani, M. Waris, W. Siddiqui, F. Islam, M. Rajamani, R. Nathan and D. C. Jiles, "Investigational Effect of Brain-Scalp Distance on the Efficacy of Transcranial Magnetic Stimulation Treatment in Depression," IEEE Transactions on Magnetics, vol. 52, p. 1–4, 7 2016.

[5] E. G. Lee, P. Rastogi, R. L. Hadimani, D. C. Jiles and J. A. Camprodon, "Impact of non-brain anatomy and coil orientation on inter- and intra-subject variability in TMS at midline," Clinical Neurophysiology, vol. 129, p. 1873–1883, 9 2018.

[6] P. Giacometti, K. L. Perdue and S. G. Diamond, "Algorithm to find high density EEG scalp coordinates and analysis of their correspondence to structural and functional regions of the brain," Journal of Neuroscience Methods, vol. 229, p. 84–96, 5 2014.

[7] R. Cimrman, V. Lukeš and E. Rohan, "Multiscale finite element calculations in Python using SfePy," Advances in Computational Mathematics, vol. 45, p. 1897–1921, 5 2019.

[8] C. Gabriel, "Compilation of the Dielectric Properties of Body Tissues at RF and Microwave Frequencies.," Defense Technical Information Center, 1996.

Uncovering statistical links between gene expression and structural connectivity patterns in the mouse brain

Nestor Timonidis[1]*, Alberto Llera[2], Paul H.E. Tiesinga[1]

[1]Donders Centre for Neuroscience, Radboud University Nijmegen, Nijmegen, the Netherlands
[2]Donders Centre for Cognitive Neuroimaging, Radboud University Nijmegen, Nijmegen, the Netherlands
**n.timonidis@donders.ru.nl*

INTRODUCTION/MOTIVATION

Finding links between genes and structural connectivity is of the utmost importance for unravelling the underlying mechanism of the brain connectome [1,2]. In this study we identify links between the gene expression [3] and the axonal projection density [4] in the mouse brain, by applying a modified version of the Linked ICA method [5] to volumetric data from the Allen Institute for Brain Science for identifying independent sources of information, also referred to as components, that link both modalities at the voxel level (fig. 1).

METHODS

The gene expression and projection density datasets comprised of 3318 genes from *in situ hybridization* experiments and 498 injections from *tract-tracing* experiments on wild-type mice, respectively, which were registered to the Allen Reference Atlas in 200 μm^3 resolution [9]. In order to account for the high variance of projection densities, we performed separate local analyses on sets of projections from the three most densely sampled brain areas, namely the visual cortex, the caudoputamen and the midbrain reticular nucleus. We determined those brain areas, injections and genes that were most involved in components that link both gene expression and projection density modalities (fig. 2), while we validated their biological context through enrichment analysis [6, 7]. In order to assess the reproducibility of the results, we took pairwise correlations between the local analyses and the global analysis obtained using all 498 available projections, and we estimated their significance using Pearson's rho. A similar procedure was followed when comparing results with factorisations obtained using the Dictionary Learning and Sparse Coding technique (DLSC) [8].

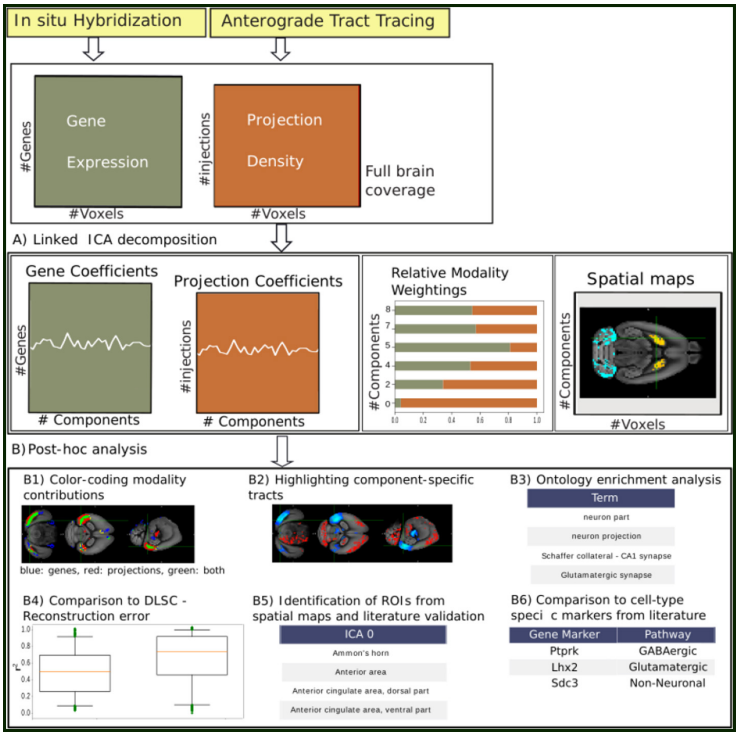

FIGURE 1: Schematic overview of the Linked ICA analysis workflow. The analysis is based on volumes of the gene expression and projection density modalities, from which we obtain using Linked ICA (**A**) a number of independent components that link both modalities. Each component comprises of coefficients of genes and projection patterns, the relative modality weightings and a spatial map, with the dimensionality of each structure defined as shown in the schema. Components of interest are the ones with a non-zero value of explained variance for both modalities. This example corresponds to the local analysis of the visual cortex projection set, in which the components of interest were 0, 2, 4, 5, 7 and 8. (**B**) Post-hoc analysis of the obtained results. (**B1**) The contribution of the modalities to the spatial maps is highlighted using a color-coding scheme, in which green corresponds to voxels with high shared variance, red corresponds to voxels dominated by projection density variance and blue corresponds to voxels dominated by gene expression variance (see fig. 2 for more details about the color-coding procedure). (**B2**) We highlight tracts formed by specific components, by taking the inner product between the projection density dataset and the coefficients of the component of interest. (**B3**) Ontology enrichment analysis is applied to the gene coefficients in order to find significant functional annotations. (**B4**) Results are being compared to the ones obtained from DLSC. (**B5,B6**) We validate by comparison with literature a number of identified regions of interest from the spatial maps (B5) and a number of cell-type-specific gene markers (B6).

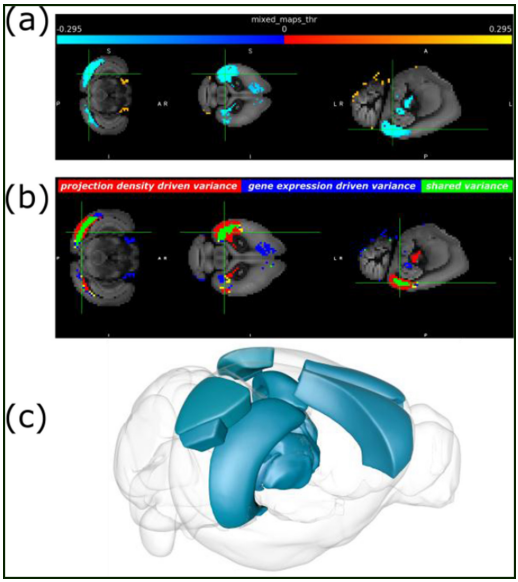

FIGURE 2: Spatial map visualizations of highlighted brain areas with high variance in component 0 of the visual cortex projections analysis. Components are ordered in terms of explained variance, hence component 0 is the most important in the analysis (numbering starts from zero). (**a**) Shared spatial map, in which the blue-to-lightblue color represents voxels with large negative values (below 1st-percentile) and the red-to-yellow color represents voxels with large positive values (above 99th-percentile), see colorbar. The spatial map is z-scored, meaning that positive and negative values represent standard deviations from the mean. A number of highlighted subcortical areas give the impression of being located outside of brain space. This is explained by the low density of the Nissl volume in these areas, which serves as the anatomical template. The template has been plotted overlaid with the spatial map, based on CCF v3.0 [9]. The highlighted areas include the primary visual area, lateral visual area, secondary motor area, polymodal association cortex of thalamus and ammon's horn, suggesting patterns of cortico-cortical, cortico-thalamic and cortico-hippocampal connections. (**b**) Color-coded spatial map used to identify which modality drives the component's variation in the regions of interest. Green corresponds to voxels with high shared variance, red corresponds to voxels dominated by projection density variance and blue corresponds to voxels dominated by gene expression variance. The color-coding was obtained by taking the inner product between each data modality and the respective coefficients of a component of interest, resulting in modality-specific maps. Afterwards, we thresholded these two maps and the spatial map obtained from the analysis using the 1st and 99th percentiles. Finally, we overlaid all thresholded maps together and defined groups of voxels with variance driven by either each independent modality or both, which were then colored accordingly. (**c**) Nissl stain volume representation of the highlighted areas using a screen shot from the Scalable Brain Atlas Composer, a 3D brain visualization tool [10]. Areas with less than 10 voxels of high variance were not visualized with the SBA composer.

RESULTS AND DISCUSSION

The results were highly reproducible when compared to the global and DLSC analyses. Moreover, the reconstruction of the gene expression and projection density datasets yielded r^2 scores of 0.68 and 0.64, respectively. Regarding the biological context, we identified representing components associated with literature-validated cortico-midbrain and cortico-striatal projections, whose gene subsets were enriched with annotations for neuronal and synaptic function and related developmental and metabolic processes. Hence, Linked ICA yielded reproducible independent components that were preserved under increasing data variance.

Taken together, we have developed and validated a novel paradigm for linking gene expression and structural projection patterns in the mouse mesoconnectome, which can power future studies aiming to relate genes to brain function.

ACKNOWLEDGEMENTS

Parts of this research have received funding from the European Union's Horizon 2020 Framework Programme for Research and Innovation under Grant Agreement No 785907 (Human Brain Project SGA2) and the FLAG ERA project FIIND (NWO054-15-104).

Keywords: linked ICA, axonal projections, gene expression, matrix factorisation, dictionary learning and sparse coding, mouse brain, connectomics, spatial transcriptomics, machine learning, tract-tracing, in situ hybridization

REFERENCES

[1] Henry, A. M. and Hohmann, J. G. (2012). High-resolution gene expression atlases for adult and developing mouse brain and spinal cord. *Mammalian Genome*, 23(9):539–549.

[2] Kang, H. J., Kawasawa, Y. I., et al (2011). Spatio-temporal transcriptome of the human brain. *Nature*, 478(7370):483–489.

[3] Lein, E. S. et al. (2007). Genome-wide atlas of gene expression in the adult mouse brain. *Nature*, 445:168–176.

[4] Oh, S. W. et al. (2014). A mesoscale connectome of the mouse brain. *Nature*, 508:207–214.

[5] Groves, A. R., Beckmann, C. F., Smith, S. M., and Woolrich, M. W. (2011). Linked independent component analysis for multimodal data fusion. *NeuroImage*, 54(3):2198–2217.

[6] Rivals, I., Personnaz, L., Taing, L., and Potier, M. C. (2007). Enrichment or depletion of a go category within a class of genes: which test? *Bioinformatics*, 23(4):401–407.

[7] Ogata, H., Goto, S., Sato, K., Fujibuchi, W., Bono, H., and Kanehisa, M. (1999). Kegg: Kyoto encyclopedia of genes and genomes. *Nucleic Acids Research*, 27(1):2934

[8] Mairal, J., Bach, F., Ponce, J., and Sapiro, G. (2010). Online learning for matrix factorization and sparse coding. *Journal of Machine Learning Research*, 11:19–60.

[9] Wang, Q., Ding, S.-L., Li, Y., Royall, J., et al (2020). The allen mouse brain common coordinate framework: A 3d reference atlas. *Cell*, 181(4):936 – 953.e20.

[10] Bakker, R., Tiesinga, P., and Kotter, R. (2015). The scalable brain atlas: Instant web-based access to public brain atlases and related content. *Neuroinformatics*, 13(3):353:366.

Comparing effective connectivity during different HCP tasks

Polina Turishcheva[1]*, Sunreeta Bhattacharya[2], Arsenii Onuchin[3], Polina Rusina[4]

[1]Data Science, Innopolis University, Innopolis, Russia
[2]Biological Science, Indian Institute of Science, Bangalore, India
[3]Phycological Science, MSU, Moscow, Russia
[4]Biological Science, MSU, Moscow, Russia
**havegreatsuccessq@gmail.com*

INTRODUCTION/MOTIVATION

A network node's functionality is governed by its interconnections with other nodes. By using graph analyses it would be possible to identify whether similar connection patterns in neuronal nodes tend to exhibit similar functionality and by using effective connectivity we can try to define the influence of one node to another. It is also interesting to find specific task-dependent changes in effective cortical network properties because they are not fully investigated yet. Pareto analysis of top keywords in fMRI articles showed that there is only one paper about effective connectivity to 10 papers about functional one ([1]). Human Connectome Project is a wonderful dataset to solve to compare connectivity graphs during different tasks. It contains records for 8 tasks: resting state, motor, language, working memory, gambling, relational, social, emotion. Further description is provided in [2].

METHODS

We used fMRI data provided by Neuromatch Academy. It contained preprocessed BOLD signals for 339 anonymized subjects with Glasser parcellation [3] and divided by HCP tasks. We processed it in the following way:

1. Filtered initial data to physiologically relevant frequencies: from 0.02 Hz to 0.15 Hz.

2. Calculated Granger Causality matrix for each HCP task for each person independently (order=1 because HCP dataset frequency is 0.72 Hz).

As this graph is a directed one we have used only one direction, ignoring the complementary graph. (The complementary one could also be useful and in further studies we plan to compare the influence of a direction.) One of the most popular model-dependent effective connectivity methods in modern neuroscience is Dynamic Causal Modelling. While Granger Causality application to fMRI signals caused debates in the scientific community [4,5], it was acknowledged to be reasonable to use it ([6]). We chose it because DCM estimation is biased by assumed input shapes and exact numbers. Granger Causality does not have this drawback ([4]).

3. Averaged matrixes among tasks. The results are in Fig.1.

4. Choose a threshold. The choice was made based on the average clustering coefficient, average shortest path, and the number of edges. We changed the threshold in the range of 0.05-0.20 with the step of 0.01 and measured these properties. For average clustering coefficient and the number of edges the trends in all 8 graphs were the same, however, the behavior of graphs for different tasks crucially differed for the average shortest path for the threshold>0.08, hence, it was chosen for further analyses.

In figure 1, the representation signifies the obvious differences in connectivity across tasks, but manual analysis is not applicable. Note that nodes may be in different places in the circle. The picture allows only to estimate the

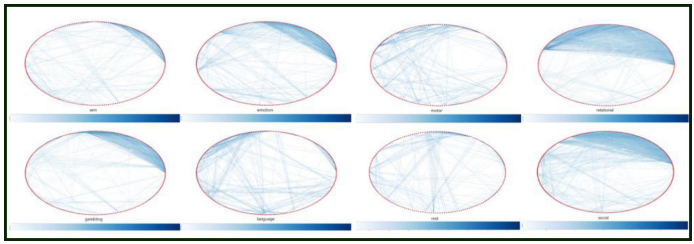

FIGURE 1: Effective connectivity graphs for different HCP task and resting state, averaged among subjects. (Threshold = 0.08., 360 nodes).

differences in connectivity patterns and their strength because darker shade corresponds to higher connectivity (range = (0.08; 0.5)).

To characterize those graphs the following metrics were selected (For a detailed description of metrics, see [1,7]):

- Small-world property sigma and omega coefficients
- Average clustering coefficient
- Number of cliques
- Maximum cliques size
- Edge density
- Node centralities
- Degree distribution among functional networks' nodes

RESULTS AND DISCUSSION

We have experienced problems with computations due to the big amount of data and the absence of optimized libraries, therefore, our work is still in process. Our plans imply creating more effective python libraries, especially for small-world property coefficients and node centralities. And we also plan to test our metrics based on a random graph. We suppose that the whole set of metrics would allow us to define the task being executed and a random graph with close properties is a nice way to challenge our assumption.

Table 1: For now we have complete results

edge density	average clustering	maximum clique	degree distribution
resting state=0.007	resting state=0.356	resting state=motor=5	resting state=6257
motor=0.008	motor=0.281		motor=6945,
language=0.009	language=0.402	language=6	language=33341
working memory=0.010	working memory=0.417	working memory=8	working memory=293196
gambling=0.014	gambling=0.349	gambling=11	
relational=0.021	relational=0.409	relational=25	
social=0.21	social=0.317	social=18	
emotion=0.013	emotion=0.470	emotion=10	emotion=9690897

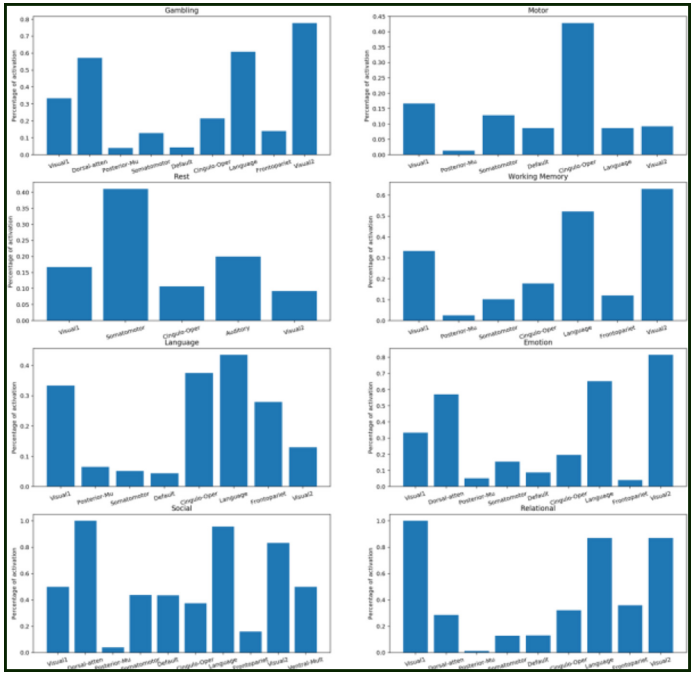

FIGURE 2: Normalized degrees distributions among functional networks (determined by Glasser parcellation) during different tasks. Const=20.

In Fig.2 one can see the results of the following analysis: We calculated the number of nodes in a functional network with a degree >= const and divided it into the overall number of nodes in the corresponding network. We run Kolmogorov-Smirnov test to compare these normalized degree distributions. p = 0.001 after Bonferroni correction (initially p=0.05). Language and working memory tasks showed close distributions (p=0.86), the same for gambling and emotion (p=0.86). Those 2 couples may be explained by a natural connection between the tasks: gambling implies some emotional feedback and the language task require working memory functionality. Surprisingly, the motor task and the resting state were close either (p = 0.62). The possible explanation is that both do not require a lot of cognitive activity and distributions are close because of default network domination. Those 3 couples also have close values for edge densities and maximum clique, but these correspondences do not hold for average clustering coefficient.

However, further investigations are needed to prove these explanation hypotheses. It is also worth mentioning that the distribution for the social task appeared to be unlike anyone else according to Kolmogorov-Smirnov test. We use the KS test to compare the similarity of degree distributions during different tasks. This test was chosen because it shows how different are empirical distributions and it also non-parametric, which is useful in case of unknown distributions.

ACKNOWLEDGEMENTS

This project was started as a part of Neuromatch Academy 2020. We are grateful to our neuromatch mentors Alexandre Hyafil, Kayson Fakhar, and Neuromatch Academy organizers.

Keywords: Granger Causality, effective connectivity, graph analyses, multi-level organization of the brain

REFERENCES

[1] Karwowski, W., Vasheghani Farahani, F., Lighthall, N. (2019). Application of graph theory for identifying connectivity patterns in human brain networks: a systematic review. frontiers in Neuroscience, 13, 585.

[2] Glasser, M. F., Smith, S. M., Marcus, D. S., Andersson, J. L., Auerbach, E. J., Behrens, T. E., ... Robinson, E. C. (2016). The human connectome project's neuroimaging approach. Nature neuroscience, 19(9), 1175-1187.

[3] Glasser, M. F., Coalson, T. S., Robinson, E. C., Hacker, C. D., Harwell, J., Yacoub, E., ... Smith, S. M. (2016). A multi-modal parcellation of the human cerebral cortex. Nature, 536(7615), 171-178

[4] Friston, K. J. (2011). Functional and effective connectivity: a review. Brain connectivity, 1(1), 13-36.

[5] Roebroeck, A., Formisano, E., Goebel, R. (2011). The identification of interacting networks in the brain using fMRI: model selection, causality and deconvolution. Neuroimage, 58(2), 296-302

[6] Friston, K. (2011). Dynamic causal modeling and Granger causality Comments on: The identification of interacting networks in the brain using fMRI: Model selection, causality and deconvolution. Neuroimage,58(2-2), 303.

[7] Bullmore, E., Sporns, O. (2009). Complex brain networks: graph theoretical analysis of structural and functional systems. Nature reviews neuroscience, 10(3), 186-198

III Brain simulation and brain-inspired architectures

Structural and functional modelling of the cerebellar circuit using the brain scaffold builder

Robin De Schepper*, Alice Geminiani, Alberto Antonietti, Stefano Masoli, Martina Rizza, Egidio D'Angelo, Claudia Casellato

Department of Brain and Behavioral Sciences, Universita degli Studi di Pavia, Pavia, Italy
**robingilbert.deschepper@unipv.it*

INTRODUCTION

Efficient modelling of the brain requires a computational framework with general strategies that should be able to incorporate experimental data at different scales and encompass a variety of microcircuit organizations [1]. To this end we have developed the Brain Scaffold Builder (BSB) for structural and functional modelling of the brain. The BSB framework provides an organized staged workflow, multiple interchangeable general strategies for cell placement and connectivity, a configuration system capable of including neuronal and synaptic models at different levels of detail and support for multiple simulators with transparent parallel simulations and data storage. The cerebellar network lends itself well to test the effectiveness of this approach, thanks to the intricate topology of the microcircuit with many unique modelling challenges. Here we reconstruct for the first time a functional network of the entire cerebellar cortex at subcellular resolution, using morphologically realistic conductance-based multi-compartmental neuron models of the Purkinje cell, Golgi cell, granule cell, stellate and basket cells [2]. The reconstruction unifies a collection of scattered experimental references into a functioning scaffold model of the cerebellar cortex with the power to predict missing information. Effortlessly, using the BSB framework, the same network model was simulated on a point-neuron backend, allowing to investigate different levels of functional granularity. All simulations were validated against experimental data, demonstrating that data-driven models can effectively capture the impact of subcellular and cellular properties on neuronal circuit computation.

METHODS

The BSB's (https://github.com/dbbs-lab/bsb) design allows easy incorporation of user-defined rules and allows to change neuron and synaptic mechanisms. The BSB builds on the first version of a microcircuit scaffold builder [3], [4]. In the placement module, cell types are representations of neuronal populations and configure how their somas should be positioned in the volume and what morphologies represent them in 3D space; the provided placement strategies are Particle placement, Satellite placement, Parallel array placement. In the connectivity module, connection types configure which strategies should be used to connect cells of specific types; the provided connectivity strategies are Capped probability cloud, Touch detection, Voxel (or fiber) intersection. The simulation configuration determines which simulator to use and sets simulator-dependent settings: *cell models* (such as point or multicompartmental models) and *connection models* (such as synapse models or gap junction models). Interfaces to a multicompartmental neuron model simulator (NEURON) and a point-neuron simulator (NEST) have been implemented.

RESULTS AND DISCUSSION

Using this framework, a mouse cerebellar cortex microcircuit was reconstructed and simulated. The example here reported refers to a volume of 300 µm along x, 200 µm along z, and the whole cortex thickness along y (130 µm of granular layer, 15 µm of Purkinje layer, 150 µm of molecular layer). So, the reconstructed volume was 17.7·10-3 mm^3 and contained about 30 ˙ 000 neurons (Figure 1 – A, B). We developed two functional variants for simulations: using specific biophysically detailed compartmental neuronal models and extended generalized leaky integrate and fire point-neuron models [5]resonance and phase-reset - which are thought to play a critical role in controlling neural network dynamics. Although these properties emerge from detailed representations of molecular-level mechanisms in \"realistic\" models, they cannot usually be generated by simplified neuronal models (although these may show spike-frequency adaptation and bursting, both constrained by experimental measurements and reproducing multiple observations from electrical recordings in vivo and in vitro. A spatiotemporal stimulation pattern was applied at the input stage of the network (the mossy fibers - *mf*): 10 impulses over a period of 100ms following a Poisson distribution given to 4 *mf*s in the center of the transverse plane, thus activating about 80 glomeruli, which represents a realistic functional unit. Thanks to the separation between

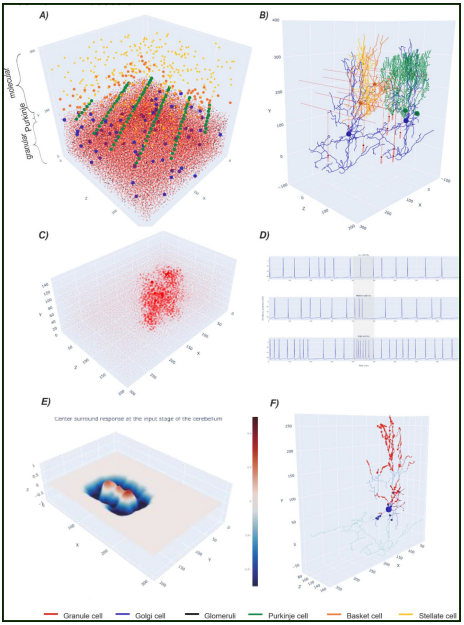

FIGURE 1: (**A**) 3D placement of all cells as spheres with specified radius into the defined volume (300 µm x, 200 µm z, 295 µm y), including Granular, Purkinje and Molecular layers. y represents the thickness, along which ascending axons run; z is the direction along which parallel fibers run. (**B**) Some cells are depicted with full detailed morphologies. (**C**) All the placed granular cells, with different size and opacity based on the level of activation generated by the stimulation pattern (100 Hz on 4 mfs for 100 ms -grey transparent rectangle). (**D**) Membrane voltage traces at soma of 3 GoCs in a different relative position with respect to the activity spot: the low activity GoC (**F**) receives 30% of its aa synapses and 5% of its pf synapses from GrCs with at least 2 excited dendrites. (**E**) center-surround response of the granule cells to mossy fiber stimulation. The balance between excitation (red) and inhibition (blue) is reported similar to how it is reported in Mapelli & D'Angelo 2007.

the model reconstruction and simulation, the same network architecture (cell positions, pairwise connections) was simulated at two levels of resolution, as a multicompartmental network and a point-neuron network. The emerging network dynamics showed good agreement with in-vivo recordings for firing rate metrics and spatial-temporal patterns (Figure 1 – C-F).

The spatiotemporal characteristics of neuronal outputs are determined by the geometry of its axon arborization, of its dendritic tree, the pattern of its innervation, and its electrical properties. For the cerebellar circuit, these

geometrical and morphological features were considered in network building through the BSB. The BSB allowed to fill gaps in knowledge, providing a new "ground truth" about circuit properties by binding the many parameters characterizing the cerebellar network into a single coherent functional construct. Thanks to a cross-validation of structural principle and functional responses (such as center-surround responses in the granular layer; vertical organization in the Purkinje layer and feedforward and lateral inhibition in the molecular layer), the resulting cerebellar structure is robust and could represent a source of structural estimations.

The framework, provided as an open-source python package, can be applied to other microcircuits including those of the cerebral cortex, hippocampus and basal ganglia. Outside of these immediate scientific results the framework will also drive the development and distribution of better written code, will help the neuroscience field to converge on shared, well adopted and validated tools and will stimulate a move away from heterogenous and concurrently developed code for the same purposes. It will drastically reduce the time, effort and resources spent on developing models and allow the field instead to progress and break ground on state of the art discoveries.

ACKNOWLEDGEMENTS

This project/research has received funding from the European Union's Horizon 2020 Framework Programme for Research and Innovation under the Specific Grant Agreement No. 945539 (Human Brain Project SGA3).

This research was supported by the EBRAINS research infrastructure, funded from the European Union's Horizon 2020 Framework Programme for Research and Innovation under the Specific Grant Agreement No. 945539 (Human Brain Project SGA3).

Keywords: cerebellum, model, scaffold, simulation, reconstruction, cortex

REFERENCES

[1] E. D'Angelo and C. Gandini Wheeler-Kingshott, "Modelling the brain: Elementary components to explain ensemble functions," *Riv. del nuovo Cim.*, vol. 40, no. 7, pp. 273–333, 2017.

[2] M. Ito, "Cerebellar circuitry as a neuronal machine," *Prog. Neurobiol.*, vol. 78, no. 3–5, pp. 272–303, 2006.

[3] S. Casali, E. Marenzi, C. Medini, C. Casellato, and E. D'Angelo, "Reconstruction and Simulation of a Scaffold Model of the Cerebellar Network," *Front. Neuroinform.*, vol. 13, p. 37, May 2019.

[4] A. Geminiani, A. Pedrocchi, E. D'Angelo, and C. Casellato, "Response dynamics in an olivocerebellar spiking neural network with nonlinear neuron properties," *Front. Comput. Neurosci.*, vol. 13, no. 68, 2019.

[5] A. Geminiani, C. Casellato, F. Locatelli, F. Prestori, A. Pedrocchi, and E. D'Angelo, "Complex dynamics in simplified neuronal models: reproducing Golgi cell electroresponsiveness," *Front. Neuroinform.*, vol. 12, no. 88, pp. 1–19, 2018.

A homeostatic mechanism for plasticity in heterogeneous spiking networks

Timo Gierlich[1]*, Akos F. Kungl[1], Andreas Baumbach[1], Mihai A. Petrovici[1,2]

[1]Kirchhoff Institute for Physics, Heidelberg University, Heidelberg, Germany
[2]Department of Physiology, University of Bern, Bern, Switzerland
**gierlich@kip.uni-heidelberg.de*

INTRODUCTION/MOTIVATION

Even compared to today's computer architectures, the human brain keeps impressing us with its robustness, speed, low-energy consumption and learning capabilities. Understanding these properties at a mechanistic level that is on the level of neurons and synapses and capturing these advantages in neuromorphic hardware [1, 2] is still an ongoing quest. A major challenge on the way is noise and parameter variability. To increase both biological plausibility and hardware compatibility, models need to take into account that neuronal systems show inherent parameter variation [3, 4, 5] and omnipresent temporal noise, which requires a large degree of computational robustness. Hence, robust learning rules are required to compensate for this variability and to enable reliable operation and learning. Further, homeostatic mechanisms are crucial to keep the neural network in its working regime and to compensate for variations in the environment [6]. In this work, we address this problem within a model of spike-based Bayesian inference. We propose an anti-Hebbian spike-timing-dependent plasticity (STDP) learning rule that could keep the effect of reciprocal synaptic connections between two neurons symmetric, which is often an implicit but important assumption in models of the brain [7, 8, 9].

METHODS

Recent work suggests that the human brain executes perception based on Bayesian inference on noisy and ambiguous input data [10, 11]. The neural sampling theory interprets the brain's neural activity as a sampling process from a probability distribution that represents a learned model of our environment [8, 10] (fig. 1b). In this theory, we view the neural activity as a process of scanning over network-states whereby the time spent in a certain state is proportional to its probability. Our approach uses a model of sampling with

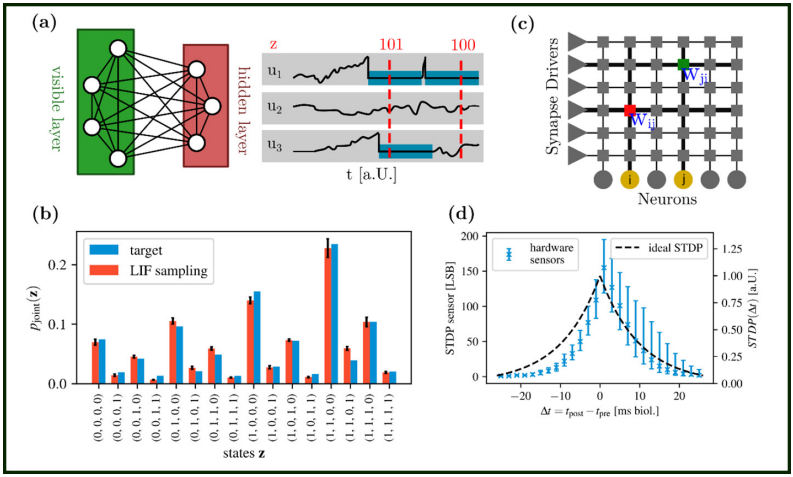

FIGURE 1: (**a**) Left: Exemplary architecture of a sampling network. Right: The dynamics of the membrane potentials of leaky integrate-and-fire neurons are interpreted as binary states. If a neuron is refractory (blue shaded part), it is identified with z=1, otherwise with z=0. (**b**) Illustration of sampling: A high-dimensional probability distribution (blue) is sampled via the dynamics of the spiking network. (**c**) Illustration of the implication of a heterogeneous substrate on the required symmetry of a network: In a neuromorphic hardware, for example, reciprocal connections are made of distinct synapse and neuron circuits. (**d**) Measurements of a symmetric STDP curve in the BrainScaleS-2 neuromorphic system [20] show considerable variations.

spiking neurons (fig 1a) [8, 9, 12, 13]. This model requires the effect of reciprocal synaptic connections to be symmetric, which a priori may not be the case both in biological neural networks and analog neuromorphic substrates. Moreover, in a local learning rule weight updates also need to be symmetric, which is not necessarily fulfilled in heterogeneous systems, because the plasticity mechanisms belonging to each synapse are physically distinct (fig. 1c and d). Consequently, a robust learning rule should incorporate a symmetrization mechanism to fulfill the requirement of the ideal abstract model.

In this work, we propose an anti-Hebbian learning algorithm based on STDP [14] that can establish homeostasis during training (fig. 2a, orange curve). We simulated the networks with SBS [15], a python framework for spike-based sampling using the numerical simulator NEST [16].

RESULTS AND DISCUSSION

We consider a two-neuron system with the connection from neuron 1 to neuron 2 W_{21} being larger than the reciprocal connection W_{12}. On average, neuron 2 will spike more often directly after neuron 1 than vice versa (fig. 2a, blue curve), which results in a net negative update of W_{21} (and a positive one of W_{12}) and hence move the two weights closer to each other.

Numerical simulations of a two-neuron system consisting of stochastic spiking neurons connected by unequal weights revealed that the symmetrization algorithm only functions for equal bias or zero mean weight (see fig 2b and c). For example, in the regime of high positive weights, the algorithm results in a solution where the weight from the low-bias neuron to the high bias neuron is stronger than its reciprocal counterpart. This happens because the

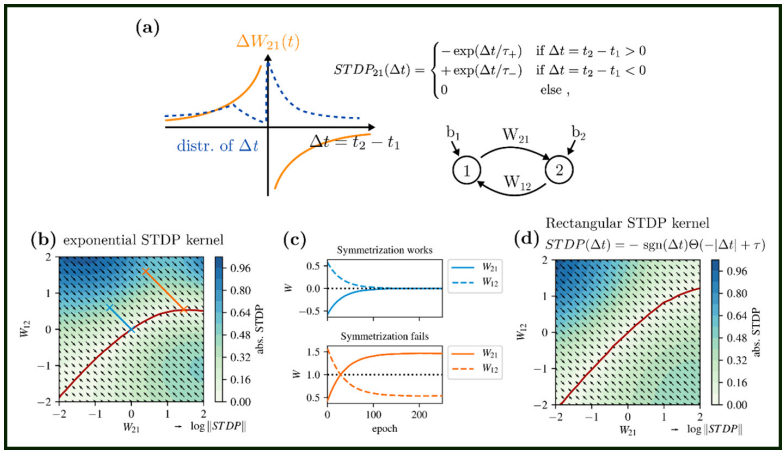

FIGURE 2: (**a**) Motivation of the symmetrization algorithm. Distribution of intervals between spikes from presynaptic neuron 1 to postsynaptic neuron 2 (blue dashed line). Here, W21 > W12, which results in many small positive intervals and hence, many large negative updates. Weighting the blue curve with the anti-symmetric exponential kernel (orange) results in a net negative weight update for W21. (**b**) Phase plane diagram of weight updates with exponential STDP kernel. For a fixed set of biases b1 = 1.0 and b2 = 0.0 we calculate the weight update for every combination of W12 and W21. The arrows indicate the direction of the update, while the colormap in the background marks its absolute value. The stable attractor plotted in the red — this is where the algorithm converges to — deviates from the diagonal, which would be the desired outcome. (**c**) Time evolution of symmetrization. The trajectories are marked in (c). (**d**) Phase plane diagram with a rectangular STDP kernel. An appropriate kernel choice can mitigate the deviation from the desired symmetric outcome.

exponential shape of the postsynaptic potential makes the instantaneous firing rate of the postsynaptic neuron peak directly after the incoming spike. We conclude that the unequal base firing rates of the neurons together with this strong non-linear response gives rise to this unexpected behavior.

Our preliminary results suggest that an appropriate choice of STDP kernels (instead of the exponential in the original scheme) could mitigate this effect. Above that, classical tools from machine learning such as regularization and sparsity targets could help to keep the weights small while conserving activity in the hidden layer.

Until now, implementations of sampling on neuromorphic hardware [13, 17, 18] relied on the time-consuming computation of model parameter updates on an external CPU. To exploit the energy and speed advantages of neuromorphic hardware, we aim for a fully on-chip implementation of spike-based sampling together with a local STDP-based learning rule and a symmetrization mechanism on the BrainScaleS-2 neuromorphic platform [19].

ACKNOWLEDGEMENTS

This work has received funding from the European Union 7 th Framework Programme under grant agreement 604102 (HBP), the Horizon 2020 Framework Programme under grant agreements 720270, 785907, 945539 (HBP) and the Manfred Stärk Foundation, Germany. The authors acknowledge support by the state of Baden-Württemberg through bwHPC and the German Research Foundation (DFG) through grant no INST 39/963-1 FUGG (bwForCluster NEMO).

Keywords: learning, plasticity, spiking neurons, heterogeneous systems, homeostasis, Bayesian inference, sampling, neuromorphic hardware

REFERENCES

[1] Roy, Kaushik, Akhilesh Jaiswal, and Priyadarshini Panda. 2019. "Towards Spike-Based Machine Intelligence with Neuromorphic Computing." Nature 575 (7784): 607–17. https://doi.org/10.1038/s41586-019-1677-2.

[2] Schuman, Catherine D., Thomas E. Potok, Robert M. Patton, J. Douglas Birdwell, Mark E. Dean, Garrett S. Rose, and James S. Plank. 2017. "A Survey of Neuromorphic Computing and Neural Networks in Hardware," May. http://arxiv.org/abs/1705.06963.

[3] Marder, Eve, and Jean Marc Goaillard. 2006. "Variability, Compensation and Homeostasis in Neuron and Network Function." Nature Reviews Neuroscience 7 (7): 563–74. https://doi.org/10.1038/nrn1949.

[4] Pfeil, Thomas, Andreas Grübl, Sebastian Jeltsch, Eric Müller, Paul Müller, Mihai A. Petrovici, Michael Schmuker, Daniel Brüderle, Johannes Schemmel, and Karlheinz Meier. 2013. "Six Networks on a Universal Neuromorphic Computing Substrate." Frontiers in Neuroscience 7 (7 FEB): 1–17. https://doi.org/10.3389/fnins.2013.00011.

[5] Petrovici, Mihai A., Bernhard Vogginger, Paul Müller, Oliver Breitwieser, Mikael Lundqvist, Lyle Muller, Matthias Ehrlich, et al. 2014. "Characterization and Compensation of Network-Level Anomalies in Mixed-Signal Neuromorphic Modeling Platforms." PLoS ONE 9 (10). https://doi.org/10.1371/journal.pone.0108590.

[6] Zenke, Friedemann, Guillaume Hennequin, and Wulfram Gerstner. 2013. "Synaptic Plasticity in Neural Networks Needs Homeostasis with a Fast Rate Detector." PLoS Computational Biology 9 (11). https://doi.org/10.1371/journal.pcbi.1003330.

[7] Hopfield, John J. 2018. "Neural Networks and Physical Systems with Emergent Collective Computational Abilities." Feynman and Computation 79 (April): 7–19. https://doi.org/10.1201/9780429500459.

[8] Buesing, Lars, Johannes Bill, Bernhard Nessler, and Wolfgang Maass. 2011. "Neural Dynamics as Sampling: A Model for Stochastic Computation in Recurrent Networks of Spiking Neurons." PLoS Computational Biology 7 (11). https://doi.org/10.1371/journal.pcbi.1002211.

[9] Petrovici, Mihai A., Johannes Bill, Ilja Bytschok, Johannes Schemmel, and Karlheinz Meier. 2016. "Stochastic Inference with Spiking Neurons in the High-Conductance State." Physical Review E 94 (4). https://doi.org/10.1103/PhysRevE.94.042312.

[10] Fiser, József, Pietro Berkes, Gergő Orbán, and Máté Lengyel. 2010. "Statistically Optimal Perception and Learning: From Behavior to Neural Representations." Trends in Cognitive Sciences 14 (3): 119–30. https://doi.org/10.1016/j.tics.2010.01.003.

[11] Aitchison, Laurence, and Máté Lengyel. 2017. "With or without You: Predictive Coding and Bayesian Inference in the Brain." Current Opinion in Neurobiology 46: 219–27. https://doi.org/10.1016/j.conb.2017.08.010.

[12] Probst, Dimitri, Mihai A. Petrovici, Ilja Bytschok, Johannes Bill, Dejan Pecevski, Johannes Schemmel, and Karlheinz Meier. 2015. "Probabilistic Inference in Discrete Spaces Can Be Implemented into Networks of LIF Neurons." Frontiers in Computational Neuroscience 9 (JAN): 1–11. https://doi.org/10.3389/fncom.2015.00013.

[13] Kungl, Akos F., Sebastian Schmitt, Johann Klähn, Paul Müller, Andreas Baumbach, Dominik Dold, Alexander Kugele, et al. 2019. "Accelerated Physical Emulation of Bayesian Inference in Spiking Neural Networks." Frontiers in Neuroscience 13 (November). https://doi.org/10.3389/fnins.2019.01201.

[14] Neftci, Emre, Srinjoy Das, Bruno Pedroni, Kenneth Kreutz-Delgado, and Gert Cauwenberghs. 2014. "Event-Driven Contrastive Divergence for Spiking Neuromorphic Systems." Frontiers in Neuroscience 7 (8 JAN). https://doi.org/10.3389/fnins.2013.00272.

[15] Oliver Breitwieser, Andreas Baumbach, Agnes Korcsak-Gorzo, Johann Klähn, Max Brixner, & Mihai Petrovici. (2020, February 24). sbs: Spike-based Sampling (v1.8.2) (Version v1.8.2). Zenodo. http://doi.org/10.5281/zenodo.3686015

[16] Gewaltig, Marc-Oliver, and Markus Diesmann. 2007. "NEST (NEural Simulation Tool)." Scholarpedia 2 (4): 1430. http://www.scholarpedia.org/article/NEST_(NEural_Simulation_Tool).

[17] Dold, Dominik, Ilja Bytschok, Akos F. Kungl, Andreas Baumbach, Oliver Breitwieser, Walter Senn, Johannes Schemmel, Karlheinz Meier, and Mihai A. Petrovici. 2019. "Stochasticity from Function — Why the Bayesian Brain May Need No Noise." Neural Networks 119 (November): 200–213. https://doi.org/10.1016/j.neunet.2019.08.002.

[18] Czischek, Stefanie, Andreas Baumbach, Sebastian Billaudelle, Benjamin Cramer, Lukas Kades, Jan M. Pawlowski, Markus K. Oberthaler, et al. 2020. "Spiking Neuromorphic Chip Learns Entangled Quantum States." http://arxiv.org/abs/2008.01039.

[19] Billaudelle, S., Y. Stradmann, K. Schreiber, B. Cramer, A. Baumbach, D. Dold, J. Goltz, et al. 2020. "Versatile Emulation of Spiking Neural Networks on an Accelerated Neuromorphic Substrate," 1–1. https://doi.org/10.1109/iscas45731.2020.9180960.

Modelling cerebellar nuclei and NucleoCortical pathways

Massimo Grillo[1]*, Alice Geminiani[1,2], Alberto Antonietti[1,2], Egidio D'Angelo[2,3], Alessandra Pedrocchi[1]

[1]Department of Electronics, NEARLab, Information and Bioengineering, Politecnico di Milano, Milan, Italy
[2]Department of Brain and Behavioral Sciences, University of Pavia, Pavia, Italy
[3]Brain Connectivity Center, IRCCS Mondino Foundation, Pavia, Italy
**massimo.grillo@polimi.it*

INTRODUCTION/MOTIVATION

The cerebellum is a subcortical structure, whose main role in motor control is learning and coordination [1] From an anatomical point of view, it can be subdivided into two major layers: cortex and deep nuclei. The cerebellar cortex processes input sensorimotor information and then, conveys signals toward the Deep Cerebellar Nuclei (DCN), which constitute the sole output stage of the cerebellum [2]. However, the information does not flow only from the cerebellar cortex to the cerebellar nuclei, since it was found that some DCN neurons project back to the cerebellar cortex, forming the so called NucleoCortical (NC) pathways [3]–[5].

In order to investigate the behaviour of DCN neurons during the execution of sensorimotor tasks, in-silico models of the cerebellum are often exploited. Available models of the cerebellar circuit include Spiking Neural Networks, inspired to anatomical and functional features of mouse cerebellum, such as: cells morphologies, anatomical connections, and electrophysiological behaviour of neurons and synapses [6], [7]we have built an olivocerebellar Spiking Neural Network (SNN. The most recent models of the DCN include only 2 out of 6 neuron types identified in literature [8] and projections from the input stage of the cerebellum towards the nuclei, without any backward connection (NC pathways). Since a detailed implementation of the cerebellar nuclei is crucial when simulating complex sensorimotor tasks, the aim of this work was to update the current in-silico DCN layer by including the NC

pathways, which required the implementation of a new neural population in the DCN layer: the Glycinergic-Inactive (Gly-I) neurons.

METHODS

In order to replicate the functional behaviour of neurons inside an in-silico model, Spiking Neural Networks can be exploited. Recently, the neural simulator NEST has been developed within the Human Brain project and it represents a shared platform for Brain simulation [9]. For our purpose, the electroresponsive properties of Gly-I neurons were replicated through a single-point neuron model, the Extended-Generalized Leaky Integrate and Fire (E-GLIF) model [10], [11]resonance and phase-reset – which are thought to play a critical role in controlling neural network dynamics. Although these properties emerge from detailed representations of molecular-level mechanisms in "realistic" models, they cannot usually be generated by simplified neuronal models (although these may show spike-frequency adaptation and bursting. This model can reproduce complex electrophysiological behaviours with limited computational cost, thanks to a system of ordinary differential equations, which describe the dynamics of membrane potential and two intrinsic currents of the neuron. The model includes some electrophysiological parameters, extracted from literature, and other optimizable parameters, tuned through an optimization algorithm implemented in Matlab. Specifically, in order to implement Gly-I neurons, before running the optimization algorithm, a specific stimulation protocol with current steps was designed, allowing to evaluate their main electroresponsive features: no autorhythm, linear current-frequency relationship and high spike frequency adaptation [12]. After that, several optimizations were launched in order to find the best set of parameters which minimized the difference between the desired spike times and the actual times at which the E-GLIF membrane potential reached threshold; this way, the target firing rates for the different input current values in the stimulation protocol were fitted. Finally, the parameters were verified with NEST through single-neurons simulations, in which one Gly-I neuron was stimulated with the same protocol used during optimization and its firing rates were computed after the stimulation onset (instantaneous firing rate) and near the end of each stimulation step (Steady-State firing rate).

At this point, by exploiting the cerebellar scaffold tool (https://github.com/dbbs-lab/bsb) [6], [7], [13]connect them synaptically, and endow neurons and synapses with biologically-grounded mechanisms. The scaffold model can keep neuronal morphology separated from network connectivity, which can in turn be obtained from convergence/divergence ratios and axonal/dendritic field 3D geometries. We first tested the scaffold on the cerebellar microcircuit, which presents a challenging 3D organization, at the same time providing appropriate datasets to validate emerging network behaviors. The scaffold was designed to integrate the cerebellar cortex with deep cerebellar nuclei (DCN, Gly-I neurons have been placed inside the DCN layer scaffold model, by defining the layer position, neuron density, and morphological properties. Considering the convergence and divergence ratios, they have been connected to other neurons inside the scaffold: Purkinje Cells and Mossy fibers, pre-synaptic neurons that provide inhibitory and excitatory inputs respectively [8], but also Golgi cells (GoCs) inside the cerebellar cortex, post-synaptic population inhibited by the activity of Gly-I neurons [4]. The synaptic parameters of the NC pathway were set considering that a Gly-I burst lasting around 50 ms caused a suppression in 25% of GoCs [4].

RESULTS AND DISCUSSION

In Figure 1, we can notice the behaviour of Gly-I model at rest and when stimulated by depolarizing current with increasing amplitude.

At rest, no spiking activity was generated, while, when depolarized, the instantaneous firing rate increased almost linearly from around 20 Hz to 135 Hz. We can also notice that the Steady-State firing rate is much lower than the instantaneous firing rate, showing a high spike frequency adaptation: the firing rate strongly decreases from stimulation onset to the end of stimulation phase.

After the implementation of these neurons as E-GLIF models, they have been placed inside the cerebellum scaffold and connected with other neurons. In particular, Gly-I neurons received input signals coming from Mossy fibers

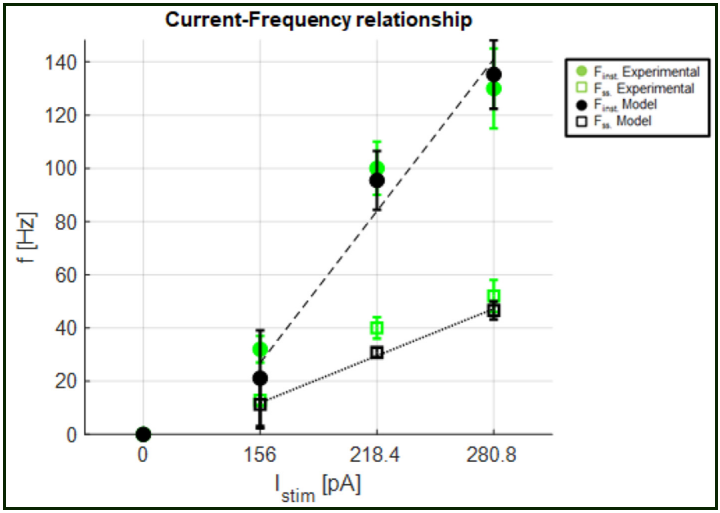

FIGURE 1: Current-Frequency relationship of Gly-I neuron during NEST simulations in two conditions: rest and depolarized by currents with increasing amplitude. Both instantaneous (dots) and Steady-State (squares) firing rates have been reported considering their average value among 50 simulations along with their standard deviation. Black symbols refer to model outcomes, whereas green symbols represent the experimental behaviour. The model values have been linearly interpolated (black lines).

and Purkinje cells and projected outside the DCN layer toward the cerebellar cortex, reaching 25% of GoCs, see Figure 2.A. The synaptic strength of the NC pathway made by Gly-I neurons has been properly tuned in order to replicate the suppression effect on GoCs: the population firing rate of GoCs decreases from 8.52 $\pm$ 0.82 Hz to 1.30 $\pm$ 0.71 Hz, see Figure 2.B.

To sum up, we here enhanced previous models of the cerebellar DCN layer adding a new neural population that projects back to the cerebellar cortex. The model will be exploited for more accurate simulations of complex cerebellum-driven tasks, where integration of input sensorimotor signals and cerebellar output feedback occurring in the cerebellar cortex is supposed to play a key role [5][14]. In addition, following the experimental characterization of the other neuron types in the DCN, the model will be further updated.

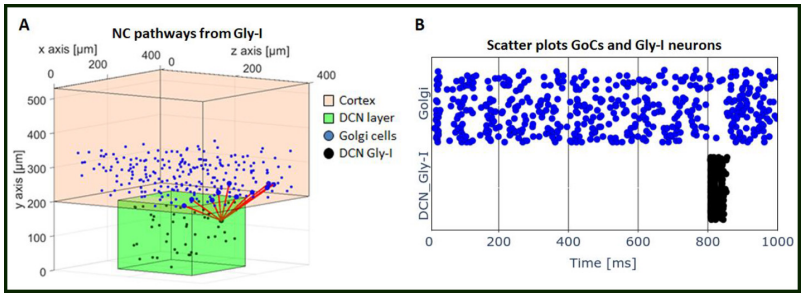

FIGURE 2: (**A**) Representation of the cerebellar cortex (pink), DCN layer (green) and NC pathways (redlines) connecting one Gly-I neuron (black dot) to several GoCs (blue dots) in the cerebellar cortex. (**B**) Scatter plots of GoCs and Gly-I neurons, showing the inhibitory effect of a glycinergic burst on GoCs activity.

Keywords: Computational Neuroscience, Spiking Neural Networks, Cerebellum, NucleoCortical pathways

REFERENCES

[1] S. G. Lisberger, "The neural basis for learning of simple motor skills," *Science (80-.).*, 1988.

[2] J. F. Medina, W. L. Nores, T. Ohyama, and M. D. Mauk, "Mechanisms of cerebellar learning suggested by eyelid conditioning," *Current Opinion in Neurobiology*. 2000.

[3] B. D. Houck and A. L. Person, "Cerebellar loops: A review of the nucleocortical pathway," *Cerebellum*. 2014.

[4] L. Ankri *et al.*, "A novel inhibitory nucleo-cortical circuit controls cerebellar Golgi cell activity," *Elife*, 2015.

[5] Z. Gao *et al.*, "Excitatory Cerebellar Nucleocortical Circuit Provides Internal Amplification during Associative Conditioning," *Neuron*, 2016.

[6] A. Geminiani, A. Pedrocchi, E. D'Angelo, and C. Casellato, "Response Dynamics in an Olivocerebellar Spiking Neural Network With Non-linear Neuron Properties," *Front. Comput. Neurosci.*, 2019.

[7] S. Casali, E. Marenzi, C. Medini, C. Casellato, and E. D'Angelo, "Reconstruction and simulation of a scaffold model of the cerebellar network," *Front. Neuroinform.*, 2019.

[8] M. Uusisaari and T. Knöpfel, "Functional classification of neurons in the mouse lateral Cerebellar Nuclei," *Cerebellum*, 2011.

[9] J. M. Eppler, M. Helias, E. Muller, M. Diesmann, and M. O. Gewaltig, "PyNEST: A convenient interface to the NEST simulator," *Front. Neuroinform.*, 2009.

[10] A. Geminiani, C. Casellato, F. Locatelli, F. Prestori, A. Pedrocchi, and E. D'Angelo, "Complex dynamics in simplified neuronal models: Reproducing golgi cell electroresponsiveness," *Front. Neuroinform.*, 2018.

[11] A. Geminiani, C. Casellato, E. D'Angelo, and A. Pedrocchi, "Complex electroresponsive dynamics in olivocerebellar neurons represented with extended-generalized leaky integrate and fire models," *Front. Comput. Neurosci.*, 2019.

[12] M. Uusisaari and T. Knöpfel, "GlyT2+ neurons in the lateral cerebellar nucleus," *Cerebellum*, 2010.

[13] R. De Schepper *et al.*, "The Brain Scaffold Builder, a package for structural and functional modelling of brain circuits: the cerebellar use case."

[14] B. D. Houck and A. L. Person, "Cerebellar premotor output neurons collateralize to innervate the cerebellar cortex," *J. Comp. Neurol.*, 2015.

A Multi-layer microcircuit model of somatosensory cortex with multiple interneuron classes

Han-Jia Jiang[1,2]*, Sacha J van Albada[1,2]

[1]Institute of Neuroscience and Medicine (INM-6) and Institute for Advanced Simulation (IAS-6) and JARA Institute Brain Structure-Function Relationships (INM-10), Jülich Research Centre, Jülich, Germany
[2]Institute of Zoology, University of Cologne, Cologne, Germany
**h.jiang@fz-juelich.de*

INTRODUCTION/MOTIVATION

Three major classes of GABAergic inhibitory interneurons play critical and distinct roles in the regulation of cortical network dynamics and signal processing [1, 2]. The mechanisms of regulation are linked to the anatomical and physiological diversity of these interneurons. While experimental studies provide realistic observations, neuronal network simulations with parameters from experimental data can aid in direct exploration of the mechanisms and conveniently test hypotheses. Therefore, we develop a microcircuit model of mouse somatosensory (barrel) cortex incorporating three major classes of interneurons as a tool to study cortical network dynamics and sensory signal processing.

METHODS

The simulation software NEST 2.16.0 [3] is used to create a multi-layer (L2/3, L4, L5, and L6) cortical microcircuit model adapted from [4]. The neuron model is the leaky-integrate-and-fire neuron model with exponentially decaying post-synaptic currents (PSC). The network includes populations of excitatory (Exc) cells and three classes of interneurons: parvalbumin (PV), somatostatin (SOM) and vasoactive intestinal peptide (VIP) cells. The layer-specific numbers of each cell type are based on the data of a mouse barrel column [5, 6]. Cell-type-specific membrane parameters are according to the measurements in [7]. Probabilities of recurrent connections are determined from experimental data of paired recordings or algorithmic estimates by [8]. Each neuron receives optimized background inputs with cell-type-specific numbers of connections. Two hundred thalamic cells are created and connected to Exc and PV cells with layer-specific probabilities to test the network responses to a 10-ms transient thalamic input of 100 spikes/s.

The weights of excitatory recurrent connections are set according to local intracortical unitary excitatory postsynaptic potentials (uEPSPs) [5], while those of inhibitory connections are multiplied by a relative inhibitory strength (g). The background and thalamic inputs are only excitatory, with weights according to thalamocortical uEPSPs [9]. Synaptic short-term plasticities (STPs) are included in the recurrent connections according to the Tsodyks model. The STP parameters of different connections are individually fitted to match the experimentally measured STPs.

RESULTS AND DISCUSSION

The ground-state firing rates of the populations in the optimized model are comparable to those of *in vivo* data from [10], although some deviations remain (Figure 1A). Over a range of external input and relative inhibitory

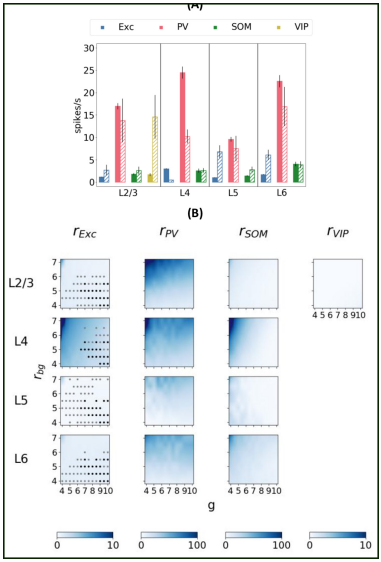

FIGURE 1: Network ground states (**A**) Ground-state firing rates with the optimized parameters. Filled and hatched bars show simulation and experimental data [10], respectively. Error bars show SEMs. (**B**) Ground states over different parameters. Firing rates (spikes/s) of all populations over different levels of relative inhibitory strength (g) and external input (r_{bg}, spikes/s) are shown by color. Dots in the first column show the range where the simulation data fulfill the criteria from [11] (gray: fit in that particular layer, black: fit in all layers).

strengths, the model is able to fulfill the criteria on firing rates, spiking irregularity, and pairwise correlations of spike counts derived in [11] (Figure 1B). The changes of firing rates in L2/3 in response to activation of PV, SOM, and VIP cells show their respective roles of inhibition and disinhibition (Figure 2A), as observed in most experimental studies. In addition, the model with STPs shows clearer multi-layer spiking responses to simulated transient thalamic input as compared to a version without STPs (Figure 2B). Further mechanistic analysis of the model may reveal the mechanisms behind these results and explore the specific roles of different interneuron types in state-dependent modulation of sensory signal processing. As a model of barrel cortex, it is particularly suited to studying whisker sensation, but it may also provide insights into the contributions of the distinct interneuron types to other sensory processes, such as visual discrimination learning [12].

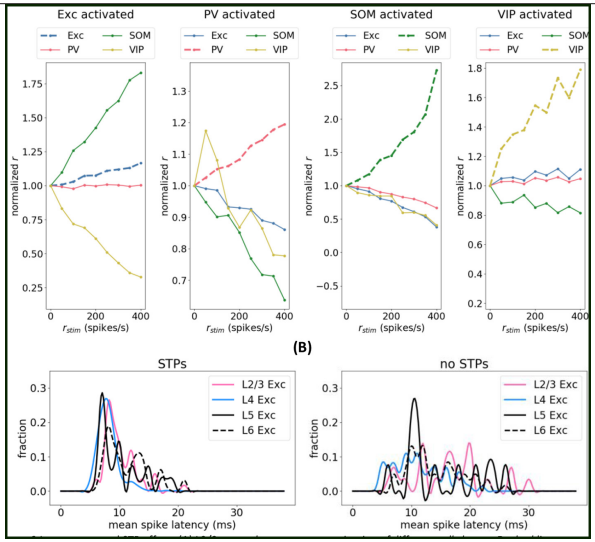

FIGURE 2: Interneuron and STP effects (**A**) L2/3 network responses to activation of different cell classes. Dashed lines represent stimulated populations. r_{stim}: firing rate of stimulus. (**B**) Multi-layer responses of Exc cells to the thalamic input, showing the distribution of cells in terms of mean spike latency (n of repetitions=10, bin=1 ms). The model with STPs (left) shows more obvious peaks of spiking activity in most layers.

ACKNOWLEDGMENTS

This project has received funding from the European Union's Horizon 2020 Framework Programme for Research and Innovation under Specific Grant Agreement No. 945539 (Human Brain Project SGA3). We thank Guanxiao Qi, Alexander van Meegen, Aitor Morales-Gregorio, Renato Duarte, and Dirk Feldmeyer for helpful discussions.

Keywords: interneuron, somatosensory cortex, microcircuit

REFERENCES

[1] Karnani, M. M., Agetsuma, M., & Yuste, R. (2014). A blanket of inhibition: functional inferences from dense inhibitory connectivity. Current Opinion in Neurobiology, 26, 96-102.

[2] Tremblay, R., Lee, S., & Rudy, B. (2016). GABAergic interneurons in the neocortex: from cellular properties to circuits. Neuron, 91(2), 260–292.

[3] Linssen, C., Lepperød, M. E., Mitchell, J., Pronold, J., Eppler, J. M., Keup, C., Peyser, A., Kunkel, S., Weidel, P., Nodem, Y., Terhorst, D., Deepu, R., Deger, M., Hahne, J., Sinha, A., Antonietti, A., Schmidt, M., Paz, L., Garrido, J., Ippen, T., Riquelme, L., Serenko, A., Kühn, T., Kitayama, I., Mørk, H., Spreizer, S., Jordan, J., Krishnan, J., Senden, M., Hagen, E., Shusharin, A., Vennemo, S. B., Rodarie, D., Morrison, A., Graber, S., Schuecker, J., Diaz, S., Zajzon, B., & Plesser, H. E. (2018). NEST 2.16.0. doi: 10.5281/zenodo.1400175

[4] Potjans, T. C. & Diesmann, M. (2014). The cell-type specific cortical microcircuit: Relating structure and activity in a full-scale spiking network model. Cerebral Cortex 24(3), 785–806.

[5] Lefort, S., Tomm, C., Sarria, J. C. F., & Petersen, C. C. (2009). The excitatory neuronal network of the C2 barrel column in mouse primary somatosensory cortex. Neuron, 61(2), 301-316.

[6] Lee, S., Hjerling-Leffler, J., Zagha, E., Fishell, G., & Rudy, B. (2010). The largest group of superficial neocortical GABAergic interneurons expresses ionotropic serotonin receptors. Journal of Neuroscience, 30(50), 16796-16808.

[7] Neske, G. T., Patrick, S. L., & Connors, B. W. (2015). Contributions of diverse excitatory and inhibitory neurons to recurrent network activity in cerebral cortex. Journal of Neuroscience, 35(3), 1089-1105.

[8] Markram, H., Muller, E., Ramaswamy, S., Reimann, M. W., Abdellah, M., Sanchez, C. A., ... & Kahou, G. A. A. (2015). Reconstruction and simulation of neocortical microcircuitry. Cell, 163(2), 456-492.

[9] Bruno, R. M., & Sakmann, B. (2006). Cortex is driven by weak but synchronously active thalamocortical synapses. Science, 312(5780), 1622-1627.

[10] Yu, J., Hu, H., Agmon, A., & Svoboda, K. (2019). Recruitment of GABAergic interneurons in the barrel cortex during active tactile behavior. Neuron, 104(2), 412-427.

[11] Maksimov, A., Diesmann, M., & van Albada, S. J. (2018). Criteria on balance, stability, and excitability in cortical networks for constraining computational models. Frontiers in Computational Neuroscience, 12, 44.

[12] Khan, A. G., Poort, J., Chadwick, A., Blot, A., Sahani, M., Mrsic-Flogel, T. D., & Hofer, S. B. (2018). Distinct learning-induced changes in stimulus selectivity and interactions of GABAergic interneuron classes in visual cortex. Nature neuroscience, 21(6), 851-859.

Dimensionality reduction: From theory to practical approach with hierarchical temporal memory and principal components analysis

Yong Hoon Lee*, Javaan S. Chahl

School of Engineering, University of South Australia, Adelaide, Australia
**sanghanp@hotmail.com*

INTRODUCTION/MOTIVATION

Dimensionality reduction is a popular and highly effective data modelling algorithm employed not only in unsupervised machine learning but in biological brains as well[2]. Avoiding high computational complexity, performance degradation and, data over-fitting are possible benefits for unsupervised learning[1]. Moreover, saving energy, increasing memory capacity, representing complex data in an easier way for subsequent layers can be seen as advantages for biological brains[2]. A number of strategies and algorithms have been proposed and have proven useful in some applications such as classification, yet extracting meaningful models by processing data in high dimensions to train and operate for real world tasks is still challenging. In this research, we investigate a Hierarchical Temporal Memory (HTM) framework, which has a neuroscience foundation, together with a successful unsupervised machine learning framework: Principal Components Analysis (PCA). With this investigation, we offer theoretical analysis to provide a comprehensive idea of dimensionality reduction and experimental outcomes of real world problem conducted with the MNIST dataset. More importantly, we analyze the potential for synergistic interactions from which both frameworks can benefit each other.

METHODS

In order to investigate the performance, the Modified National Institute of Standards and Technology's (MNIST) handwritten digits dataset was used.[3]

1. Training algorithms

   (1) Principal components analysis (PCA) implementation

   Step1> Create X = 60,000 × 784 data matrix using the MNIST training dataset. Each row vector of the matrix is a digit image with 784 pixels.

$$X = [\, x_1, x_2, x_3, .. x_{60000} \,]^T$$

Step2> In order to create the covariance of X, the average digit matrix of the dataset is calculated as following.

$$\Psi = (1/60000) \Sigma\, x_i \quad (\text{where } i=1,2,3... \ 60000)$$

then, calculate difference of each digit image from the average matrix.

$$\Phi = X - \Psi$$

Step3> Calculate covariance matrix of the matrix X.

$C_X = (1/60000) \Sigma\, \Phi\, \Phi^T$ (where i=1,2,3... 60000 and C_X is 784 x 784 symmetric matrix)

Step4> By analyzing the cumulative explained variance, 44 highest valued eigenvectors components (which is enough to account for 80% of the data variance) among 784 components are selected for projecting the dataset into new space. So, create PCA matrix Ω which has size of 784 x 44.

Step5> Create the reduced dataset

$Y = X\Omega^T$ (where the dimension of new dataset Y is 60000 x 44)

(2) Hierarchical temporal memory (HTM) implementation

We employ two software frameworks to implement this function: OpenCV and the Numenta Platform for Intelligent Computing (NuPIC). OpenCV plays the role of basic image processing functions such as data acquisition, thresholding and retina filtering. On the other hand, the NuPIC is an open source project which implements the computational theory of HTM[4]. The NuPIC receives the binarised output of OpenCV and undergoes training to generate sparse distributed representations (SDRs).

We also employ the biological retina inspired image enhancement framework to investigate the possibility of performance improvements of the HTM. Though a biological retina performs various imperative functions on the incoming visual data, we focus on image pre-processing functions which could facilitate the processing of the subsequent layers. The retina model

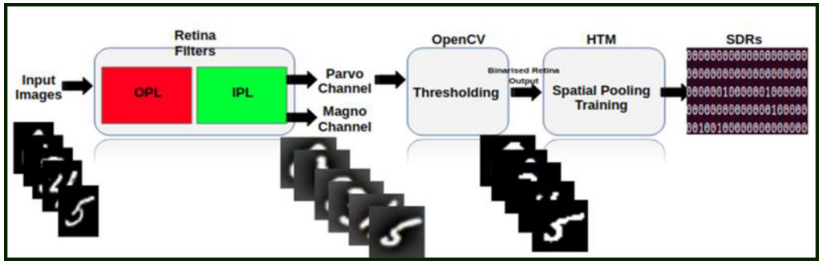

FIGURE 1: Software flow the HTM framework for generating the reduced dataset named SDRs

we employ is based on the model of Jeanny Herault [5]. The retina output is passed to the next layer through 2 different channels: parvo and magno. The former channels are inspired by the fovea which plays the role of detail detecting and the latter channels are related to peripheral vision which is specialized to detect motion [6][7][8]. As we can see from Fig.1, the MNIST dataset images are enhanced by the retina filters at the first stage. Then, the outputs of the parvo channel are converted into binary images to be a proper input to the HTM framework. With those binary images, the HTM framework establishes and keeps updating the synaptic connections to generate SDRs for the subsequent layers.

2. Classification using Support Vector Machine (SVM)
   The Support vector machine (SVM) classifier (python libraries) was employed to evaluate the performance of employed dimensional reduction frameworks. For the PCA, the classifier model is fitted using 60,000 training dataset and then the classification result is extracted using 10,000 test dataset. In case of the HTM, the synaptic connections are established by training the framework with 60,000 training dataset firstly, then the SDRs of 10,000 test dataset digits are generated. Fitting the classifier model and extracting classifier result are conducted using these SDRs generated from the 10,000 test dataset.

RESULTS AND DISCUSSION

We conduct the dimensionality reductions and classification experiments on an Ubuntu 18.04 platform with python (for PCA and SVM) and C++ (for image processing and HTM) programming language.

Table 1: Experiment result of two dimensional reduction frameworks and the HTM + PCA interwinded pipeline

	Principal Components Analysis	Hierarchical Temporal memory (Columns, Active columns)	HTM(400,80) + PCA
Classification Accuracy	70% variance : 98.3% 80% variance : 98.7% 85% variance : 98.6% 90% variance : 98.5% 95% variance : 98.5%	(100,20) : 81.5% (200,40) : 87.4% (300,60) : 91% (400,80) : 93.3%	70% variance : 90.7% 80% variance : 95.7% 85% variance : 97.3% 90% variance : 98.5% 95% variance : 99.0%
Training Time (sec)	70% variance : 0.04 80% variance : 0.05 85% variance : 0.06 90% variance : 0.07 95% variance : 0.08	(100,20) : 350 (200,40) : 406 (300,60) : 456 (400,80) : 489	70% variance : 0.52 80% variance : 0.42 85% variance : 0.41 90% variance : 0.40 95% variance : 0.41
Classification Time (sec)	70% variance : 27 80% variance : 45 85% variance : 61 90% variance : 87 95% variance : 144	(100,20) : 11 (200,40) : 18 (300,60) : 26 (400,80) : 34	70% variance : 4 80% variance : 8 85% variance : 12 90% variance : 21 95% variance : 32

From the Table 1, it is concluded that standalone PCA outperforms standalone HTM framework in image classification task. However, the interwined HTM + PCA pipeline shows more promising results that are similar or better classification accuracy with significantly decreased classification time. These findings suggest that proper use of the HTM, inspired by computational principles of the neocortex [10], as a data pre-processing for reducing dimension could be beneficial and effective for artificial intelligent (AI) applications or building practical intelligent systems.

For future tasks, it looks necessary to model the mathematical frameworks for optimizing the parameter values of our customized HTM. In addition, it also seems vital to migrate the HTM to a parallel computing platform such as NVIDIA CUDA [8] to boost the performance which will allow the HTM to conduct data pre-processing tasks for practical supervised and reinforcement learning systems which require real-time capability. Finally, the temporal memory (TM) component will be investigated to find a solution to build an intelligent framework with prediction capability which the HTM theory claims is the true source of intelligence of the human-being [9].

Keywords: dimensionality reduction, principal components ananysis, hierarchical temporal memory, machine learning

REFERENCES

[1] Ethem Alpaydin. Introduction to Machine Learning - 3rd Edition. The MIT Press, Cambridge, Massachusetts, United States America, 2014.

[2] Robert Calderbank, Sina Jafarpour, and Robert Schapire. Compressed learning: Universal parse dimensionality reduction and learning in the measurement domain. Preprint, 2009.

[3] Yann LeCun, Corinna Cortes, and Christopher J.C Burgers. The mnist database of handwritten digits. http://yann.lecun.com/exdb/mnist/. Accessed: 2020-02-20.

[4] J. Hawkins, S. Ahmad, S. Purdy, and A. Lavin. Biological and machine intelligence (bami). Initial online release 0.4, 2016.

[5] Herault Jeanny. Vision: Image, Signals and Neural Networks-model of Neural Processing in Visual Perception. World Scientific, 2010.

[6] Helga Kolb. How the retina works: Much of the construction of an image takes place in the retina itself through the use of specialized neural circuits. American Scientist, pages pp.28 – 35, 2003.

[7] Adrien Wohrer. The vertebrate retina: a functional review. [Research Report] RR-6532, INRIA, inria-00280693, 2008.

[8] Cleomar Pereira da Silva, Douglas Mota Dias, Cristiana Bentes, and Marco Aurlio Cavalcanti Pacheco. Evolving gpu machine code. Journal of Machine Learning Research, pages pp.673 – 712, 2015.

[9] Jeff Hawkins and Sandra Blakeslee. On Intelligence. Times Books, New York, United States of America, 2004.

[10] Cui Y, Ahmad S and Hawkins J. The HTM Spatial Pooler—A Neocortical Algorithm for Online Sparse Distributed Coding. Front. Comput. Neurosci. 11:111. doi: 10.3389/fncom.2017.00111, 2017.

Hybrid 3D/Inkjet printed organic neuromorphic transistors and neural networks

Tanyaradzwa Mangoma[1]*, George Malliaras[2], Ronan Daly[1]*****

[1]Department of Engineering, Institute for Manufacturing, Charles Babbage Road, Cambridge CB3 0FS, UK

[2]Electrical Engineering, University of Cambridge, JJ Thomson Ave, Cambridge CB3 0FA, UK

**tm617@cam.ac.uk; **gm603@cam.ac.uk; ***rd439@eng.cam.ac.uk*

INTRODUCTION

In recent years, neuromorphic properties have been found in organic electrochemical transistors (OECTs) based on organic electronic materials such as poly(3,4ethylenedioxythiophene) doped with polystyrene sulfonate (PEDOT:PSS) [1]. OECTs comprise of a simple architecture; a source and drain electrode, bridged by an organic semiconducting film which is then submerged in an ionic solution. On application of a gate voltage (V_G), ions from the electrolyte enter the semiconductor, changing its doping state and conductivity, which in turn changes the current that flows between the source and the drain (drain current, I_D) [2]. On repeated voltage pulses at the gate, ions accumulate in the semiconductor, have a cumulative effect on the drain current. This emulates Hebbian learning whereby synaptic connections become more efficient upon repeated stimulation of the post-synaptic by the pre-synaptic neuron (neurons that fire together wire together)[3]. In OECTs, the pre-synaptic neuron and the post-synaptic current are emulated by the gate voltage and drain current, respectively. Leveraging these properties, functions such as synaptic plasticity, orientational selectivity and homeoplasticity have been emulated in OECTs[1], [4], [5].

Applications of neuromorphic OECTs have been widely identified in bioelectronics; a field where facile design change and rapid, low-cost fabrication are essential for the successful translation to industry[6]. The simple structure of OECTs lends itself particularly well to additive manufacturing techniques, which can facilitate the development of neuromorphic devices for bioelectronics.

Here, we show a hybrid additive manufacturing approach to fabricating neuromorphic OECT devices. We combine 3D printing of commercially available printing filaments with inkjet printing of semiconducting thin films to create

OECT architectures. We go on to demonstrate spiking plasticity and adaptation to exhibit neuromorphic behaviour in OECTs.

METHOD

Material, device design and fabrication

Devices were designed using Autodesk Inventor CAD software and converted to g.code using CURA 3D printing software. A dual extrusion Ultimaker 3 3D printer was used to deposit insulating and conducting polymer filament. Thermoplastic co-polyester (TPC), trade named Natural FLEX 45, from RS components was chosen as the insulating material[7]. A composite Polylactide Resin (PLA) incorporated with carbon black from Proto-Pasta was used to form conducting components of the device[8].

Clevios PEDOT: PSS from Heraeus Epurio was inkjet printed using a Fuji Film Dimatix Materials Printer DMP-2850 [9][10]. 0.01M Phosphate buffered saline (PBS) solution is used as the electrolyte material. The solution was formed by adding a PBS pellet from Sigma Aldrich to DI water[11].

Characterization

A Keysight B1500a semiconductor device analyser was used to obtain transistor and neuromorphic characteristics of the device[12]. A silver-silver chloride electrode was used to apply the pulses at the gate of the device.

RESULTS

OECT devices and neural networks were designed and printed. Figure 1 shows an illustration and images of a single additively manufactured OECT device. The devices were biased as shown in Fig. 1a. Fig. 1b and 1c show images of a single OECT device before the well is attached. The device architecture was incorporated into neural networks based on the same principles.

Figure 2 shows results obtained from the OECTs demonstrating neuromorphic behaviour. Hebbian learning was captured using spike-timing-dependent plasticity (STDP)[1]. A pair of 500mV pulses were applied at the gate at a constant V_D of -500mV. Resulting I_D shows an amplitude difference between the response to the pulses, validating the learning nature of the devices (Fig 3a insert). Figure 2a shows the depression percentage of the post synaptic current,

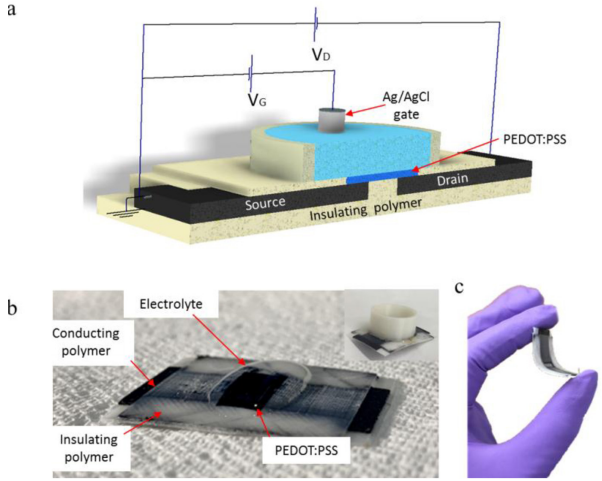

FIGURE 1: An additively manufactured OECT device (**a**) Schematic of the designed OECT (**b**) Images of the 3D and inkjet printed device. Inset shows device after with a well attached for electrolyte containment, (**c**) illustrating device flexibility[[13].

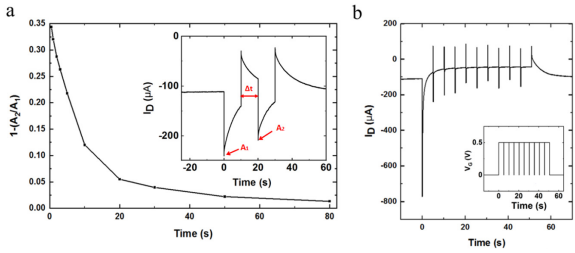

FIGURE 2: Neuromorphic properties of the printed device. (**a**) ID depression percentage as a function of pulse interval Δt. Frequency resolution can be seen in the learning characteristics of the device (insert) A pair- pulsed-depression response at Δt= 10s. (**b**) Adaptation in OECTs. A train of VG pulses is applied to the device and the ID is measured as a function of time. The device initially gives a STDP and subsequently adapts[13].

expressed as $1-\left[\frac{A2}{A1}\right]$ where A_1 and A_2 correspond to the amplitude of the first and second I_D values. This is plotted as a function of Δt. From the plot, the measured depression percentages show that the learning properties in the device are frequency dependant (i.e. shows muscle memory[14], [15]).

Synaptic depression decreases in responsiveness on application of strong and high frequency stimuli. This is termed sensory adaptation[16], [17]. Studies in visual[18], auditory[19] and olfactory[20] functions have shown that adaption is an efficient learning mechanism that tracks rapid information changes while encoding its basic context[1]. Figure 2b shows adaptation of the device. A train of 10s long, 500mV gating pulses with 100ms intervals were applied to the device. After the first pulse, the drain current of the device changes to a new steady-state. On application of the subsequent pulses, only the basic context of rapid information changes is captured.

DISCUSSION

Organic neuromorphic devices based on OECTa could be used in bioelectronics as an adaptive sensing and diagnostic tool. Herein, we have highlighted an accessible and AM technique that can be used to fabricate OECTs with neuromorphic properties. These devices exhibit spiking plasticity and adaptation. The use of additive manufacturing opens an avenue where rapid design change and rapid, low-cost fabrication can be achieved to make novel devices for bioelectronic. It is hoped that the finding from this paper initiates the use of additive manufacturing technologies for bioelectronics and neuromorphic computing.

ACKNOWLEDGEMENTS

This work was funded by the EPSRC Centre for Doctoral Training in Ultra Precision Engineering (EP/L016567/1). The authors gratefully acknowledge the contributions members from the Bioelectronics and Fluids in Advanced Manufacturing groups (Department of Engineering, University of Cambridge) for their help.

Keywords: organic electrochemical transistor, additive manufacturing, neuromorphic, 3D printing, neural network, AI hardware

REFERENCES

[1] P. Gkoupidenis, N. Schaefer, B. Garlan, and G. G. Malliaras, 'Neuromorphic Functions in PEDOT:PSS Organic Electrochemical Transistors', *Adv. Mater.*, vol. 27, no. 44, pp. 7176–7180, Nov. 2015, doi: 10.1002/adma.201503674.

[2] D. A. Bernards and G. G. Malliaras, 'Steady-State and Transient Behavior of Organic Electrochemical Transistors', *Adv. Funct. Mater.*, vol. 17, no. 17, pp. 3538–3544, Nov. 2007, doi: 10.1002/adfm.200601239.

[3] D. O. Hebb, *The Organization of Behavior: A Neuropsychological Theory*. Psychology Press, 2005.

[4] P. Gkoupidenis, S. Rezaei-Mazinani, C. M. Proctor, E. Ismailova, and G. G. Malliaras, 'Orientation selectivity with organic photodetectors and an organic electrochemical transistor', *AIP Adv.*, vol. 6, no. 11, p. 111307, Nov. 2016, doi: 10.1063/1.4967947.

[5] P. Gkoupidenis, D. A. Koutsouras, and G. G. Malliaras, 'Neuromorphic device architectures with global connectivity through electrolyte gating', *Nat. Commun.*, vol. 8, 15448, May 2017, Accessed: Apr. 20, 2020. [Online]. Available: https://pure.mpg.de/pubman/faces/ViewItemOverviewPage.jsp?itemId=item_3178698.

[6] E. R. W. van Doremaele, P. Gkoupidenis, and Y. van de Burgt, 'Towards organic neuromorphic devices for adaptive sensing and novel computing paradigms in bioelectronics', *J. Mater. Chem. C*, vol. 7, no. 41, pp. 12754–12760, 2019, doi: 10.1039/C9TC03247A.

[7] 'RS Components | Electronic and Electrical Components'. https://uk.rs-online.com/web/ (accessed Apr. 06, 2020).

[8] 'Conductive PLA', *ProtoPlant, makers of Proto-pasta*. https://www.proto-pasta.com/pages/conductive-pla.

[9] 'Dimatix Materials Printer DMP-2850 | Deposition Products | Industrial Inkjet Printheads | Fujifilm USA'. http://www.fujifilmusa.com/products/industrial_inkjet_printheads/deposition-products/dmp-2800/index.html (accessed Aug. 29, 2018).

[10] 'Heraeus Epurio Home'. https://www.heraeus.com/en/hep/home_ec/home_ec_page.html?gclid=CjwKCAjwpqv0BRABEiwA-TySwTvdP5iOxACMi5kNavRv90HN6ES-4trO-2L6Nstovx83j4uYatFmEfRoCGokQAvD_BwE (accessed Apr. 06, 2020).

[11] 'United Kingdom | Sigma-Aldrich'. https://www.sigmaaldrich.com/united-kingdom.html (accessed Apr. 06, 2020).

[12] 'B1500A Semiconductor Device Parameter Analyzer and Measurement Modules | Keysight (formerly Agilent's Electronic Measurement)'. https://www.keysight.com/en/pc-2250789/b1500a-semiconductor-device-analyzer?cc=GB&lc=eng.

[13] 'Hybrid 3D/Inkjet-Printed Organic Neuromorphic Transistors - Mangoma - - Advanced Materials Technologies - Wiley Online Library'. https://onlinelibrary.wiley.com/doi/full/10.1002/admt.202000798 (accessed Dec. 14, 2020).

[14] 'Neural Correlates of Motor Memory Consolidation | Science'. https://science.sciencemag.org/content/277/5327/821 (accessed Apr. 06, 2020).

[15] P. J. E. Attwell, S. F. Cooke, and C. H. Yeo, 'Cerebellar Function in Consolidation of a Motor Memory', *Neuron*, vol. 34, no. 6, pp. 1011–1020, Jun. 2002, doi: 10.1016/S0896-6273(02)00719-5.

[16] W. G. Regehr, 'Short-Term Presynaptic Plasticity', *Cold Spring Harb. Perspect. Biol.*, vol. 4, no. 7, p. a005702, Jul. 2012, doi: 10.1101/cshperspect.a005702.

[17] S. Chung, X. Li, and S. B. Nelson, 'Short-term depression at thalamocortical synapses contributes to rapid adaptation of cortical sensory responses in vivo', *Neuron*, vol. 34, no. 3, pp. 437–446, Apr. 2002, doi: 10.1016/s0896-6273(02)00659-1.

[18] D. Gilden, R. Blake, and G. Hurst, 'Neural Adaptation of Imaginary Visual Motion', *Cognit. Psychol.*, vol. 28, no. 1, pp. 1–16, Feb. 1995, doi: 10.1006/cogp.1995.1001.

[19] S. M. Anstis and S. Saida, 'Adaptation to auditory streaming of frequency-modulated tones', *J. Exp. Psychol. Hum. Percept. Perform.*, vol. 11, no. 3, pp. 257–271, 1985, doi: 10.1037/0096-1523.11.3.257.

[20] T.-Y. Chen and K.-W. Yau, 'Direct modulation by Ca²⁺-calmodulin of cyclic nucleotide-activated channel of rat olfactory receptor neurons', *Natur*, vol. 368, no. 6471, pp. 545–548, Apr. 1994, doi: 10.1038/368545a0.

A brain-inspired meta-learning control architecture to solve conflictual decisions in robots

Federica Robertazzi[1,2]*, Guido Schillaci[1,2], Egidio Falotico[1,2]

[1]The BioRobotics Institute, Sant'Anna School of Advanced Studies, Viale Rinaldo Piaggio, Pontedera, Italy

[2]Department of Excellence in Robotics and AI, Sant'Anna School of Advanced Studies, Viale Rinaldo Piaggio, Pontedera, Italy

**federica.robertazzi@santannapisa.it*

INTRODUCTION/MOTIVATION

Meta-learning – also known as learning how to learn – is a field of research in machine learning techniques that allows to replicate the flexible and efficient learning of human intelligence. These general-purpose machine learning systems are able to (i) generalize across tasks, objects and environments, (ii) build upon previous experience and learn new things more quickly starting from simple concepts before trying to learn more complex ones, (iii) perform tasks without a large dataset and with long-tail distributions, in order to face successfully in real world settings [1]. Meta-learning approaches can be divided into the following categories: recurrent models, metric learning, learning optimizers. This work falls within this third category.

Here, we present a brain-inspired meta-learning control model of basal ganglia that performs an action selection and decision-making task within a Stroop test, in which we generate a conflictual instance between prefrontal cortex and motor output in a robot/simulated agent. This type of task is important in the context of planning of motor actions in a real scenario where elements of tasks can be conflictual.

The proposed model takes inspiration from the control architecture developed by Khamassi et al. [2] for action selection and endowed with a meta-learning framework based on neuromodulation theory proposed by Doya et al. [3]. In particular we extend the reference control architecture [2] with a meta-learning hyperparameter optimization that reproduces the action of neuromodulators in the human brain.

METHODS

The model architecture shown in Figure 1 consists of twelve modules. Three modules process the inputs (visual perception and external reward) and outputs (motor commands) of the system.

The others represent different brain regions: Posterior Parietal Cortex (PPC), Anterior Cingulate Cortex (ACC), Ventral Tegmental Area (VTA), Lateral Prefrontal Cortex (LPFC), Striatum, Substantia Nigra reticulata (SNr), Thalamus, Substantia Nigra compacta (SNc), Premotor Cortex (PMC). They are constituted by firing rate neurons where the output of the differential equation of each neuron is mapped from 0 to 1 with a sigmoid activation function.

The communication between neurons is only inter-layers (i.e. no intra-layer recurrent connections) mediated by one-to-one excitatory or inhibitory synapses.

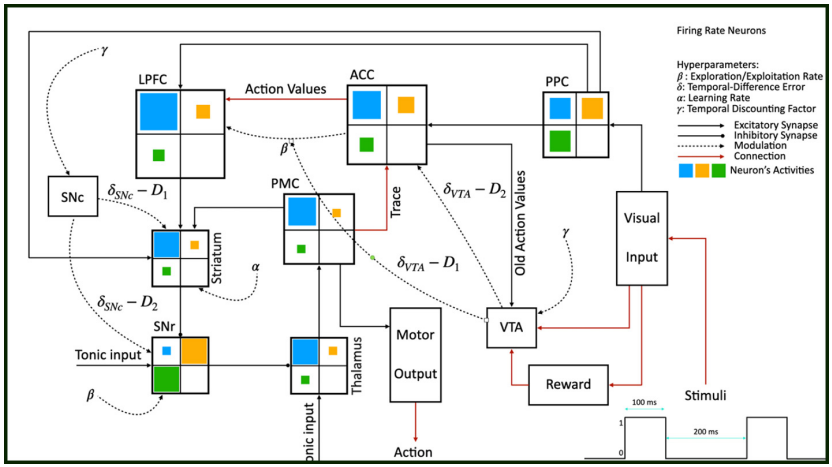

FIGURE 1: shows the model architecture inspired by Khamassi et al. [2] and the meta-learning mechanism based on principles of Doya's neuromodulation theory [3]: Posterior Parietal Cortex (PPC), Anterior Cingulate Cortex (ACC), Ventral Tegmental Area (VTA), Lateral Prefrontal Cortex (LPFC), Striatum, Substantia Nigra reticulata (SNr), Substantia Nigra compacta (SNc), Thalamus and Premotor Cortex (PMC), visual perception, reward perception and motor output. It also shows excitatory (black arrow) or inhibitory (dashed arrow) synapses, reinforcement learning and meta-learning mechanisms. Stimuli are fed in the model by simulating a square wave (amplitude=1, duration=100 ms, inter-stimuli interval=200 ms) for each neuron.

Reinforcement learning is implemented in the ACC layer and the meta-leaning, inspired by the neuromodulation theory, is based on the following hyperparameters: (i) dopamine receptors D1, regulating the exploration-exploitation beta parameter with an inverse linear function that relates dopamine to the entropy of the probability distribution of the actions [4], (ii) dopamine receptors D2, regulating the striatum neuron's excitability [4] and (iii) serotonin, regulating dopamine with a logarithmic function accounting for a differential effect both in space into the striatum and in the reward temporal scale [5].

We implemented a Stroop test task composed by two different types of trials equally distributed: Go trials and No-Go trials [6]. In the former trials the simulated agent goes in the direction that maximizes the expectation of the associated reward, while in the latter ones an unexpected hold signal occurs after a certain delay from the appearance of the stimulus. We used two neurons to encode two different stimuli in two different opposite directions, e.g. left and right, and one neuron to encode the action of stay or return to the starting point.

Stimuli are fed in the model by simulating a square wave (amplitude=1, duration=100 ms, inter-stimuli interval=200 ms, see Figure 1) for each neuron.

RESULTS AND DISCUSSION

We show that a meta-learning mechanism based on this framework is able to reproduce the conflictual instance between motor planning and action execution.

In Go trials when the target appears the simulated agent goes to reach it, instead in No-Go trials it produces a suppression of the motor command sent to the cortex, provoking and inducing the return or remaining in the starting position (see Figure 2).

The results are obtained pooling 10 simulations with 1000 stimuli/simulation. The training period is defined as the time required to achieve a fixed value threshold (-0.25). After that we have the test period where the model embedded (i.e. learning to react) the hold signal.

In particular, we compute: the reaction time (i.e. the time to reach the pick of the PMC neuron associated to the chosen direction) in Go trials (training:

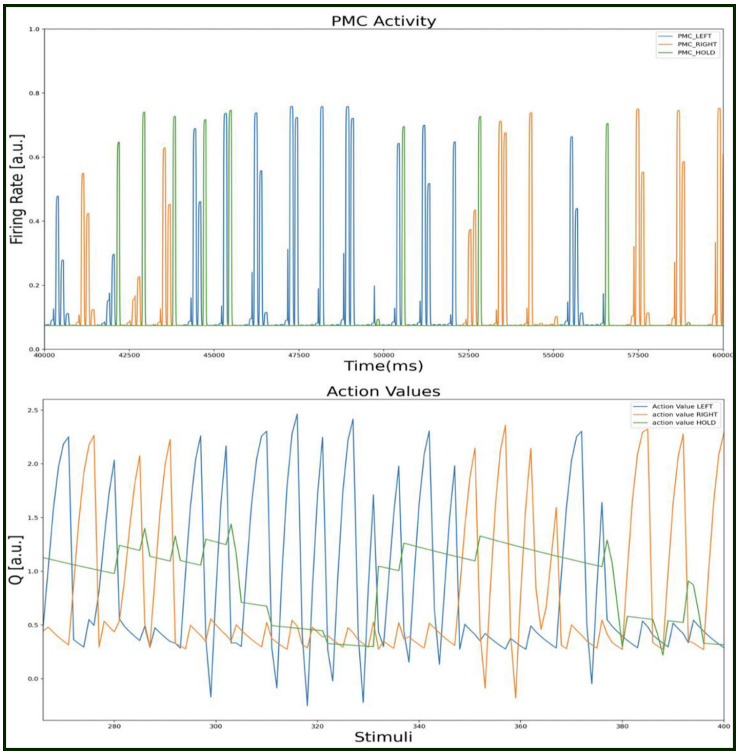

FIGURE 2: (Top) PMC neurons' activities in a window ranging from 40 to 60 seconds: two neurons codify stimuli (blue and yellow) and one the hold signal (green). (Bottom) The action value of each neuron is activated when the corresponding action is selected.

50,16±1,67 ms vs test: 49,29±0,43 ms) and No-Go trials (training: 50,02±1,61 ms vs test: 61,88±1,84 ms); the Stop Signal Reaction Time (SSRT) (i.e. the difference between the reaction time and the delay of the hold signal) (training: 16,09 ±9,44 ms vs test: 29,76±3,20 ms), the percentage of correct inhibition (training: 0% vs test: 55,35±10,99%) and the global accuracy (training: 50,88±16,15 vs test: 77,93±4,36%). After the learning phase, we obtained an increase of correct inhibition of No-Go trials because of the action of the meta-learning mechanism that adjusts the value of hyperparameters accordingly and an increase of the global accuracy as well. We also obtained a shift towards greater values of SSRT during the learning phase meaning that

the simulated agent is more capable to counteract the motor command in No-Go trials.

Keywords: meta-learning, brain-inspired control, basal ganglia, action selection, decision-making

REFERENCES

[1] Finn, C. & Abbel, P. & Levine, S. (2017). Model-Agnostic Meta-Learning for Fast Adaptation of Deep Network

[2] Khamassi, Mehdi & Lallee, Stephane & Enel, Pierre & Procyk, Emmanuel & Dominey, Peter. (2011). Robot Cognitive Control with a Neurophysiologically Inspired Reinforcement Learning Model. Frontiers in neurorobotics. 5. 1. 10.3389/fnbot.2011.00001.

[3] Doya K. Metalearning and neuromodulation. Neural Netw. 2002 Jun-Jul;15(4-6):495-506. doi: 10.1016/s0893-6080(02)00044-8. PMID: 12371507.

[4] Humphries MD, Khamassi M, Gurney K. Dopaminergic Control of the Exploration-Exploitation Trade-Off via the Basal Ganglia. Front Neurosci. 2012 Feb 6;6:9. doi: 10.3389/fnins.2012.00009. PMID: 22347155; PMCID: PMC3272648.

[5] Tanaka, Saori & Doya, Kenji & Okada, Go & Ueda, Kazutaka & Okamoto, Yasumasa & Yamawaki, Shigeto. (2004). Prediction of immediate and future rewards differentially recruits cortico-basal ganglia loops. Nat Neurosci 7: 887-893. Nature neuroscience. 7. 887-93. 10.1038/nn1279.

[6] Turner, Robert & Pasquereau, Benjamin. (2017). A selective role for ventromedial subthalamic nucleus in inhibitory control. eLife. 6. 10.7554/eLife.31627.

Tuning to resonances: Homeostatic plasticity in the olivocerebellar system

Elías Mateo Fernández Santoro*, Mario Negrello*, Thijs Hoedemakers*

Neuroscience, Erasmus MC, Rotterdam, The Netherlands
**e.fernandezsantoro@erasmusmc.nl; m.negrello@erasmusmc.nl; t.hoedemakers@outlook.com*

INTRODUCTION/MOTIVATION

The Olivocerebellar system plays a central role in supervised and unsupervised motor learning, crucially contributing to the coordination, precision and accurate timing of movements. Despite early conceptions of the system as strictly feed-forward, it is in fact composed by multiple feedforward and feedback loops [1,2]. The main loop consists of two inhibitory projections from Purkinje cells (PCs) to deep cerebellar nuclei to inferior olive (IO) and a powerful excitatory feedback connection, via climbing fibers [3,4,5]. We are motivated to model this loop as we are interested in the role of induced IO reverberations and electrotonic coupling on PC homeostatic synaptic plasticity [12].

METHODS

We developed a model to study the dynamics of plasticity of this closed loop when Purkinje cells are subjected to stochastic input. This model is endowed with biophysically plausible IO cells, with both resonant and oscillatory dynamics. Our experiments inquire on the role of induced IO reverberations and electrotonic coupling on PC homeostatic synaptic plasticity (PC-PF), which is incorporated through Spike-Timing Dependent Plasticity (STDP). We attempt to gauge the contribution of conductivity of the IO gap junctions has on the input dynamics of the olivocerebellar loop. Our circuit model has 20 IO cells, 10 PCs and 10 cerebellar nuclear cells (Fig 1.A). The detailed Inferior Olive model is a two compartmental HH type model with simple calcium dynamics [6] and both the PC and DCN are adaptive exponential models [7]. We model the synapses of this resonant system between the IO, PC and DCN according to physiological results [8,9,10]. When the IO spikes the PC pauses its simple spike train induced by an update of the adaptive part of the adex model (through the CS-PC synapse). The input comes from the PF onto the PC. The PC inhibits the DCN model which in

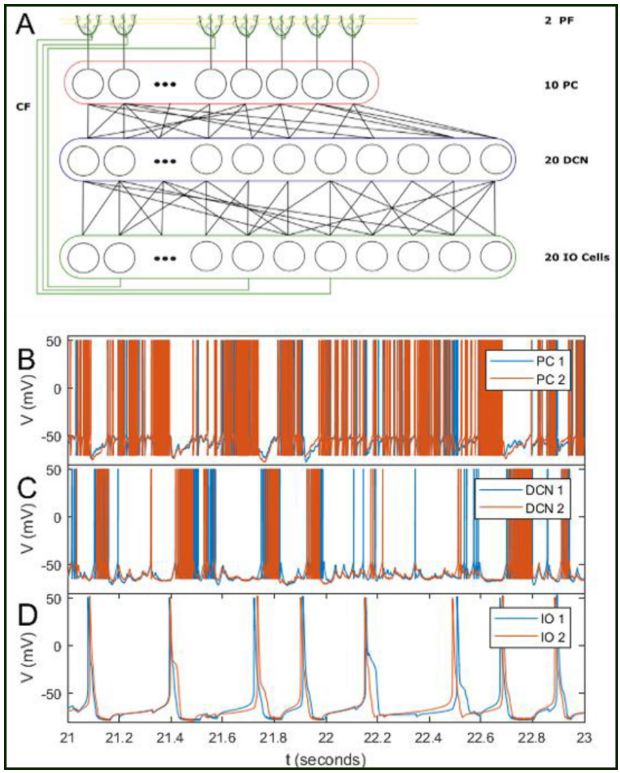

FIGURE 1: Schematic representation of the olivocerebellar system (A) and response of each cell of the cerebellar loop for a 2 seconds window of time (B, C and D). A: PCs are connected, with a 1:10 ratio, to deep cerebellar nuclei (DCN), which are connected with a 1:10 ratio to inferior olive (IO) cells. 10 randomly selected IO cells are connected with 1:1 ratio to PCs via climbing fibers (CF). B: the PCs response, C: the DCN response and D: the IO response of coupled cells.

turn has a small input on the IO when it spikes. Hence, when the PC pauses due to the IO spike, the DCN spikes and gives a larger input to the IO (which sometimes leads to a reset of the IO). This is shown in Fig 1.B. The Spike-Timing Dependent Plasticity (STDP) that integrates all pre- and post-synaptic spike times. Two different simulations are performed on Brian [11] both for the coupled and uncoupled scenarios. The STDP is used only in the second type of simulation. Both types of simulations use the same PF synaptic input stream (modeled as an Ornstein-Uhlenbeck process), which is applied twice during the second type of simulation. The second half of the latter is interpreted as the response of a trained loop.

RESULTS AND DISCUSSION

While this work is still in progress, our hypotheses are that specific frequencies that evoke a resonance in the olivary nucleus become encoded in the PC weights (at PF-PC synapse), rendering the system able to promote inputs with specific frequency components. We also hypothesize that some particular frequency components may be at the control of resonance and IO synchronicity. Initial results of the model indicate frequency selectivity observed as peaks of the spike triggered averages (STA) as seen in Fig 2. We also find that the selectivity is reduced when olivary cells are decoupled. This may indicate that in the presence of strong coupling, PCs are separating temporal patterns. We are conducting an extensive parameter space analysis to verify the hypothesis that Purkinjes can selectively learn specific frequencies, in a type of unsupervised learning.

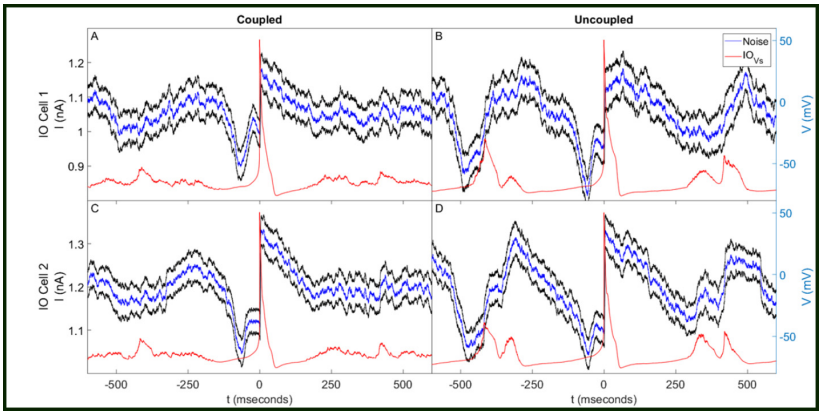

FIGURE 2: CS Triggered Noise Averages for coupled (A and C) and uncoupled (B and D) scenarios for both before (A and B) and after (C and D) STDP. The left vertical axis shows the current of the PSC of PC 1 and the right axis the membrane potential of IO 1. The upper and lower black lines represent the confidence interval of the average PSC. A lower variability in CS period is seen for the uncoupled scenario (B and D) as the average shows membrane potential peaks before and after the CS. The coupled scenario (A and C) is seen to have less variability in the PSC preceding the drop at 100ms.

Keywords: Olivocerebellar system, Homeostatic plasticity, Encoding of frequencies

REFERENCES

[1] Llinas, R.R. and Negrello, M.N. (2015). Cerebellum., 10.4249/scholarpedia.4606

[2] Eccles, J., Ito, M., and Szentagothai, J. (2013). The Cerebellum as a Neuronal Machine. Springer Berlin Heidelberg, 10.1113/expphysiol.1968.sp001975

[3] Lang, E.J., Apps, R., Bengtsson, F., and Cerminara, N.L. (2017). The roles of the olivocerebellar pathway in motorlearning and motor control a consensus paper. The Cerebellum, 16(1):230–252., 10.1007/s12311-016-0787-8

[4] Marr, D. and Thach, W. T. (1991). A Theory of Cerebellar Cortex, pages 11–50. Birkhauser Boston, Boston, MA., 10.1113/jphysiol.1969.sp008820

[5] Tang, T., Suh, C. Y., Blenkinsop, T. A., and Lang, E. J. (2016).Synchrony is key: Complex spike inhibition of the deep cerebellar nuclei. The Cerebellum, 15(1):10–13., 10.1007/s12311-015-0743-z

[6] Schweighofer, N., Doya, K., and Kawato, M. (1999). Elec-trophysiological properties of inferior olive neurons: Acompartmental model. The American Physiological Society.

[7] Brette, R. and Gerstner, W. (2005). Adaptive ExponentialIntegrate-and-Fire Model as an Effective Description ofNeuronal Activity.J Neurophysiol, 94.

[8] Marieb, E. N. and Hoehn, K. (2013). Human Anatomy & Physiologoy. 9th edition.

[9] Kandel, E., Schwartz, J., and Jessell, T. (2000a). Principles of Neural Science, Fourth Edition. McGraw-Hill Companies, Incorporated

[10] Eccles, J., Ito, M., and Szentagothai, J. (2013). The Cerebellum as a Neuronal Machine. Springer Berlin Heidelberg.

[11] Goodman, Dan and Romain Brette (2008). "NEUROINFORMATICS Brian: a simulator for spiking neural networks in Python". In: 2.1.

[12] Kistler WM, De Zeeuw CI. Dynamical working memory and timed responses: the role of reverberating loops in the olivo-cerebellar system. Neural Comput. 2002 Nov;14(11):2597-626. doi: 10.1162/089976602760407991. PMID: 12433292.

Cerebro-cerebellar interactions: *in vivo* and *in silico* tools co-design

Francesco Jamal Sheiban[1]*, Alessandra Maria Trapani[1], Alice Geminiani[1,2], Egidio Ugo D'Angelo[2,3], Alessandra Pedrocchi[1]

[1]NEARLab (Department of Electronics, Information and Bioengineering, DEIB), Politecnico di Milano, Milan, Italy
[2]Department of Brain and Behavioural Sciences, University of Pavia, Pavia, Italy
[3]IRCCS Mondino Foundation, Pavia, Italy
**francescojamal.sheiban@polimi.it*

INTRODUCTION

A major goal of contemporary neuroscientific research is to design experimental protocols for animal studies coupled with *in vivo* neural recordings to gather data so to investigate the brain mechanisms underlying behaviour [1]. Moreover, replicating those experiments *in silico* lets researchers develop and test computational models of the different brain areas involved and validate them against collected data. By faithfully reproducing biological features, such models can be used to test and/or suggest neurophysiological/pathological hypotheses and be eventually translated to clinical scenarios [1].

Recent findings ascribe cognitive functions to the cerebellum [2] that might be linked to cerebro-cerebellar interactions, though experimental tools and complementary computational models that investigate these connections in an exhaustive way are missing in literature [3]. The aim of this study is therefore the co-design of *in vivo* and *in silico* behavioural protocols and tools to be eventually used to investigate the functional role of cerebro-cerebellar interactions in motor learning tasks.

METHODS

Following this approach, the work presented here involves: (i) the implementation of a custom experimental setup for "reach-to-grasp" *in vivo* experiments on adult mice; (ii) the design of a neurorobotic setup to replicate the protocol *in silico*, including a virtual environment and a robotic subject embodying

a functional spiking neural network; (iii) the simulation of a behavioural task execution using the neurorobot.

The target behavioural protocol of this study is a "reach-to-grasp" movement to collect water droplets at two possible locations, marked by an anticipatory directional (left/right) cue. For the *in vivo* experimental procedure, water deprived mice are trained to reach the reward after a time-varying delayed go-cue (i.e., a sound) from a fixed starting point, by associating the direction of an early stimulus to the reward location.

Thus, a sensorized cage was designed to house animal during the task execution and automatically deliver the protocol stimuli with precise timings via integrated sensors and actuators. The overall system was controlled by an Arduino ® Mega 2560 board communicating with a user-friendly graphical interface designed for setting protocol parameters and monitoring task execution in real-time.

Along with the implementation of the *in vivo* apparatus, the behavioural protocol was reconstructed on the NeuroRobotics Platform (NRP) [4]. The *in silico* task was designed to closely mimic its *in vivo* counterpart by employing the iCub humanoid robot and providing the same environmental stimuli via custom-designed transfer functions.

This virtual implementation also required the design of a brain network model of integrate-and-fire neurons driving the neurorobot movements, with constant synaptic weights tuned via a trial-and-error procedure. The reconstructed model, designed following biological findings, included two identical modules (to discriminate the directional stimuli) and feedback loops between premotor and frontal cortices [5][6], motor thalamus [7][8] and cerebellum [9] to reproduce short-term memory and temporal decisions mechanisms. More specifically, cortical areas consisted of the medial prefrontal cortex (mPFC), the secondary (ALM) and primary (CFA, RFA) motor cortex and the primary somatosensory cortex (vS1) regions. The thalamic areas comprised nuclei from the ventral lateral (VL, VAL) and posterior (VPM) regions (Figure 1).

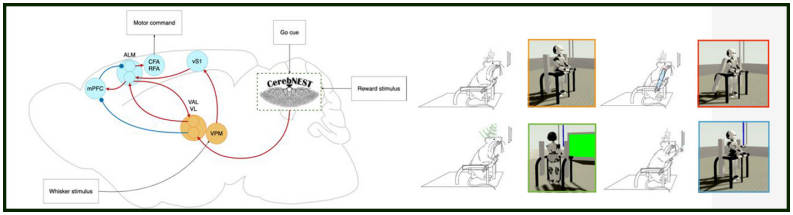

FIGURE 1: *In vivo* and *in silico* protocols co-execution. The iCub robot, when provided with a SNN composed of two identical modules, whose structure is schematically reported in the figure [left], successfully performed the behavioural task as it was designed to be executed *in vivo* [right]. The virtual subject waited in standing position with its hand on a fixed starting point (orange box), receiving a somatosensory stimulus on its shoulder (red box) simulating the *in vivo* directional stimulus (a whisker touch). Then, the robot waited motionless until a go-cue (green box) signalled reward availability, upon which it performed the grasping movement (blue box) mirroring the somatosensory stimulus direction.

RESULTS AND DISCUSSION

As a result of the *in vivo* and *in silico* co-design, we released and tested the first prototype of the experimental set-up, adjusting the components design to adapt it to real-case scenarios and completing the hardware circuitry along with the real-time communication between the software and the micro-controller. Then, the entire experimental protocol was correctly executed *in silico* by the neurorobot using a scaled-down neural network of the designed brain model (Figure 1).

Concerning the *in silico* protocol reconstruction, we managed to provide the same *in vivo* experimental stimuli to the neurorobot, implementing different transfer functions to carry signals from the environmental and robotic sensors to the spiking neural network.

Monitoring the activity of the tuned spiking neural network, we evaluated the capability of reproduce spiking responses supposed to occur at the beginning and end of cerebellum-driven learning. Specifically, we assessed that the premotor cortex/thalamus loop, the medial prefrontal cortex and the motor cortex were able to sustain preparatory activity, block impulsive actions and drive movement execution, respectively, once provided with the expected cerebellar activity at the end of learning, as opposed to being disconnected from the cerebellar module (Figure 2).

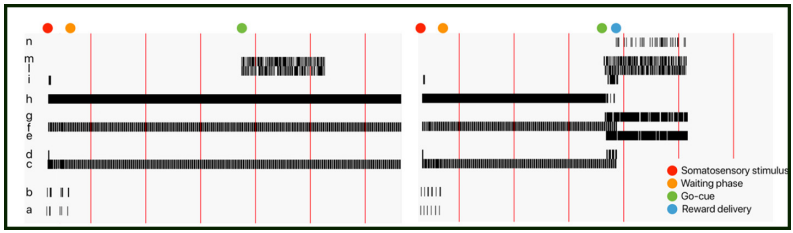

FIGURE 2: Sensorimotor signals encoding in the network. The spike activity recorded without [left] and with [right] the supposed post-learning cerebellar input dynamics to the cerebral nodes. Without these inputs, the ALM/VL-VLA loop (c-f) and mPFC area (h) are not silenced upon go-cue exhibition (l-m), thus their sustained activity persists after the screen is set to green. Conversely, with the proper cortico-cerebellar connections, the go signals cause the inhibitory VL-VLA areas (e-g) to stop the mPFC and subsequent ALM-premotor (d) and CFA-RFA (i) activation drives the neurorobot in correctly performing the movement.

These results represent a solid basis on which to continue the co-design of in vivo and in silico protocols, improving the prototype of the experimental set-up, acquiring animal data, refining the neural network model (e.g., scaling up the network and embedding distributed plasticity) and simulating the full learning protocol, eventually exploiting high-performance computing resources.

ACKNOWLEDGMENTS

This work is supported by CerebNEST and RisingNet projects within the European Union's Horizon 2020 Framework Programme for Research and Innovation under the Specific Grant Agreement No. 945539 (Human Brain Project SGA3). We thank Ileana Montagna, PhD, Department of Brain and Behavioral Sciences, University of Pavia, for the experimental setup design support.

Keywords: Neurorobotics Platform, experimental co-design, brain modelling

REFERENCES

[1] J. N. Crawley and A. Holmes, "Behavioral Neuroscience," Current Protocols in Neuroscience, no. April, pp. 1–2, 2011.

[2] E. D. Angelo and S. Casali, "Seeking a unified framework for cerebellar function and dysfunction : from circuit operations to cognition," Frontiers in Neural Circuits, vol. 6, no. January, pp. 1–23, 2013.

[3] M. J. Wagner and L. Luo, "Neocortex – Cerebellum Circuits for Cognitive Processing," Trends in Neurosciences, vol. 43, no. 1, pp. 42–54, 2020.

[4] E. Falotico, L. Vannucci, A. Ambrosano, and U. Albanese, "Connecting Artificial Brains to Robots in a Comprehensive Simulation Framework: The Neurorobotics Platform," Frontiers in Neurorobotics, vol. 11, no. January, pp. 1–19, 2017.

[5] A. Saiki, R. Kimura, T. Samura, Y. Fujiwara-Tsukamoto, and Y. Sakai, "Different Modulation of Common Motor Information in Rat Primary and Secondary Motor Cortices," PLOS ONE, vol. 9, no. 6, pp. 1–13, 2014.

[6] M. Murakami, H. Shteingart, Y. Loewenstein, Z. F. Mainen, "Distinct Sources of Deterministic and Stochastic Components of Action Timing Decisions in Rodent Frontal Cortex," Neuron, vol. 94, no. 4, pp. 908–919., 2017.

[7] Z. V. Guo, H. K. Inagaki, K. Daie, S. Druckmann, C. R. Gerfen, and K. Svoboda, "Maintenance of persistent activity in a frontal thalamocortical loop," Nature, 2017.

[8] N. Sakayori, S. Kato, M. Sugawara, S. Setogawa, H. Fukushima, R. Ishikawa, S. Kida, and K. Kobayashi, "Motor skills mediated through cerebellothalamic tracts projecting to the central lateral nucleus," Molecular Brain, pp. 1–12, 2019

[9] F. P. Chabrol, A. Blot, T. D. Mrsic-Flogel, "Cerebellar Contribution to Preparatory Activity in Motor Neocortex," Neuron, vol. 103, no. 3, pp. 506–519, 2019.

NO production and diffusion model in the granular layer of the cerebellum

Alessandra Trapani[1*], Alberto Antonietti[1,2], Giovanni Naldi[3], Egidio D'Angelo[2], Alessandra Pedrocchi[1]

[1]Department of Electronics Information and Bioengineering, Politecnico di Milano, Milano, Italy
[2]Department of Brain Behavioral Science, Università di Pavia, Pavia, Italy
[3]Department of Environmental Science and Policy, Università di Milano, Milano, Italy
**alessandramaria.trapani@polimi.it*

INTRODUCTION

Since the discovery of Nitric Oxide (NO) acting as an intracellular messenger in the brain [1], there is growing evidence that NO is responsible for the coordination of synaptic activity, both excitatory and inhibitory [2]. Cellular types that can produce NO molecules have been found in the cerebral cortex [3], hippocampus [4] and in the cerebellum [1],[5]. In the granular layer of the cerebellum, NO notably acts as a retrograde messenger, being produced in the Granule Cells (GrCs) and regulating the neurotransmitter release probability of the mossy fiber (*mf*) terminals [5]. As NO synthesized in response to an external stimulus diffuses freely across the cell membrane, spreading rapidly in the extracellular space, it is able to provide a type of neural communication that goes beyond the mere synaptic transmission [6]. In the past few years, an increasingly number of studies (reviewed in [2]) suggested that certain stimulation patterns of a closely-packed group of neurons, containing neuronal NO synthase (nNOS) enzyme, may generate a diffuse cloud of NO, thus acting as a volume transmitter, with a relatively large area of influence. On the other hand, isolated stimuli would just lead to a local effect of the NO signal, exerting classical communication through single anatomical synaptic connection [7]. The aim of this work was to replicate the NO diffusive properties in the granular layer of the cerebellum. Therefore, we developed a model able to simulate the production and diffusion of NO molecules to be integrated in a 3D realistic inspired cerebellar model [8].

METHODS

NO production model: The dynamic of NO production depends on complex biochemical reaction cascade [9]. For simplicity we split the reaction cascade

in two differential equations. The equation that we design for describing the Ca^{2+}/calmodulin binding is reported below.

$$\frac{dCalm2C(t)}{dt} = -\frac{Calm2C(t)}{\tau_c} + \left[Ca^{2+}\right]\delta_{spike}.$$

Where τ_c is a time constant describing the decay of Calm2C concentration after a spike of Ca^{2+} has entered the cell.

We modeled the activation of nNOS enzyme with another differential equation:

$$\frac{dnNOS(t)}{dt} = -\frac{nNOS(t)}{\tau_{n1}} + \frac{1}{\tau_{n2}}\left(\frac{Calm2C(t)}{Calm2C(t)+1}\right)$$

Where τ_{n1} and τ_{n2} are time constants describing the dynamics of nNOS decay and activation respectively. Here we assume that the amount of NO produced is proportional to the amount of active nNOS.

NO diffusion model: To model the NO diffusion, we used the heat diffusion equation as in [10], modified to take into account the activity of the NO source ($S(\boldsymbol{x},t)$) and the NO consumption ($-\lambda C_{no}(\boldsymbol{x},t)$) in the extracellular space [7]. Note also that thanks to low molecular weight and non-polarity, NO can be considered to diffuse isotropically through the tissue, meaning that the diffusion coefficient (D) is constant [11].

$$\frac{\partial C_{no}(x,t)}{\partial t} = D\nabla^2 C_{no}(x,t) - \lambda C_{no}(x,t) + S(x,t)$$

In order to solve this equation, we had to adopt some simplification on the geometry of the problem. We modelled each individual source of NO as a point source, from which the NO diffuses uniformly in all directions. Thus, we can safely assume radial symmetry to compute the diffusion profile in space.

A spike train stimulates NMDA receptors. Ca^{2+} enters in the intracellular space through the NMDA receptor. Ca^{2+} react with calmodulin and the concentration of Calm2C (calmodulin/calcium bounded) increase. This induces a catalytic activation of nNOS enzyme that starts producing NO using oxygen and reducing NADPH to catalyse the conversion of arginine to citrulline.

$$\frac{\partial C_{no}(r,t)}{\partial t} - D\nabla^2 C_{no}(r,t) + \lambda C_{no}(r,t) = S(t)$$

We are going to compute C_{no} with respect to the distance *r* from the source, not to ***x*** (3D coordinates). This means that the source will have a fixed location in *r = 0* and it will be described by just its evolution in time, hence S(t). Moreover, due to the rapid decay in the NO concentration (high inactivation rate), we can assume a finite domain with boundaries condition being $C_{no}(r,t) \approx 0$. We computed the solution of the diffusion equation using the Green's function [12] and numerically integrating the resulting equation. Thanks to the linearity of the problem, we can represent the action of multiple sources by simply summing each of their contribution, with respect to given points of observation.

RESULTS AND DISCUSSION

As shown in Figure 1, the system of differential equations we designed for describing the synthesis process were compared with the results obtained in NEURON through the Reaction&Diffusion module [13]. We used the simulation obtained with NEURON as reference, given its ability in simulating the biochemical reactions involved in the NO synthesis in the intracellular space. Unlike the complex reaction cascade simulated in NEURON, our production function is able to replicate the synthesis process in two steps only, that depend on the timing of spike events. This implementation is compatible with the NEST simulation environment [14], that will be used to simulate the overall activity of the cerebellar network. In Figure 2 we reported the NO signal, resulting from the production and diffusion simulation of a single source stimulated with different spike patterns. As we can see from its space profile, single active source will affect only the nearest *mf* terminal, even at high frequencies stimuli, acting as a classical second messenger. However, if more than one neighbouring GrCs receive stimuli that are close in time, the area of influence of the NO signal expands and triggers a volume transmitter action involving clusters of neurons.

This model will be used as a starting point to integrate the diffusive properties of NO in a STDP plasticity model [15] and build a NO-dependent diffusive plasticity reflecting the experimental evidence found in [5], regarding the role of NO in LTP mechanisms in the granular layer.

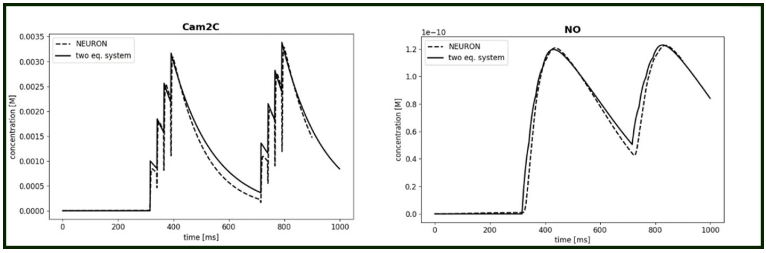

FIGURE 1: Dash curves refer to results obtained using NEURON simulation environment, while solid line curves to our two-equations system. In the right panel Ca^{2+}/calmodulin concentrations are compared while in the left panel the resulting NO concentrations produced by a single source.

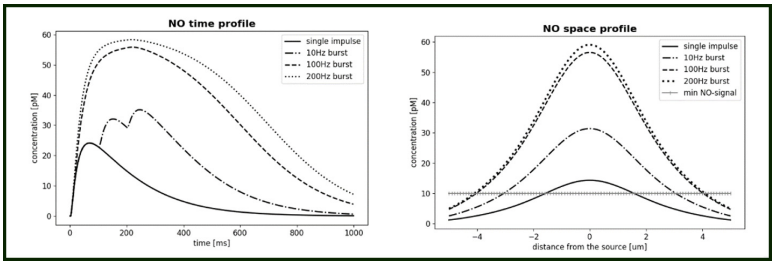

FIGURE 2: Time (right panel) and space (left panel) profile of NO signal generated by a single source located in a granule cell stimulated at different frequencies (burst length fixed at 200 ms). (left panel) Observational point at 200 nm from the source. (right panel) Space profiles referred to t = 210 ms. 10 pM is the minimum NO concentration to trigger plasticity effects.

ACKNOWLEDGEMENTS

Simulations in NEURON were implemented by Stefano Masoli, Department of Brain and Behavioral Sciences, University of Pavia, Pavia, Italy. This research has received funding from the HBP Partnering Project (CerebNEST).

Keywords: nitric oxide, cerebellum, diffusion, simulation

REFERENCES

[1] J. Garthwaite, S. L. Charles, and R. Chess-Williams. "Endothelium-derived relaxing factor release on activation of NMDA receptors suggests role as intercellular messenger in the brain". In: Nature 336.6197 (1988), pages 385–388. ISSN: 0028-0836. DOI: 10.1038/336385a0. URL: http://www.nature.com/articles/336385a0

[2] N. Hardingham, J. Dachtler, and K. Fox. "The role of nitric oxide in pre-synaptic plasticity and homeostasis". In: Frontiers in Cellular Neuroscience 7.OCT (2013), pages 1–19. ISSN: 16625102. DOI: 10.3389/fncel.2013.00190

[3] J. R. Steinert et al. "Nitric Oxide Is a Volume Transmitter Regulating Postsynaptic Excitability at a Glutamatergic Synapse". In: Neuron 60.4 (2008), pages 642–656. ISSN: 08966273. DOI: 10.1016/j.neuron.2008.08.025. URL: http://dx.doi.org/10.1016/j.neuron.2008.08.025

[4] B. M. Pigott and J. Garthwaite. "Nitric oxide is required for L-type Ca^{2+} channel-dependent long-term potentiation in the hippocampus". In: Frontiers in Synaptic Neuroscience 8.JUN (2016), pages 1–10. ISSN: 16633563. DOI: 10.3389/ fnsyn .2016.00017

[5] A. Maffei et al. "NO enhances presynaptic currents during cerebellar mossy fiber - Granule cell LTP". In: Journal of Neurophysiology 90.4 (2003), pages 2478–2483. ISSN: 00223077. DOI: 10.1152/jn.00399.2003

[6] J. R. Steinert et al. "Nitric Oxide Is an Activity-Dependent Regulator of Target Neuron Intrinsic Excitability". In: Neuron 71.2 (2011), pages 291–305. ISSN: 08966273. DOI: 10.1016/j. neuron.2011.05.037. URL: http://dx.doi.org/10.1016/j.neuron.2011.05.037

[7] J. Garthwaite. "From synaptically localized to volume transmission by nitric oxide". In: Journal of Physiology 594.1 (2016), pages 9–18. ISSN: 14697793. DOI: 10.1113/JP270297

[8] S. Casali et al. "Reconstruction and simulation of a scaffold model of the cerebellar network". In: Frontiers in Neuroinformatics 13 (2019). ISSN: 16625196. DOI: 10.3389/fninf.2019.00037

[9] C. N. Hall and J. Garthwaite. "Trans-synaptic signalling by nitric oxide". In: Dendritic Neurotransmitter Release (2005), pages 283–300. DOI: 10.1007/0-387-23696-1 19

[10] A. Philippides et al. "Modeling cooperative volume signaling in a plexus of nitric oxide synthase-expressing neurons". In: Journal of Neuroscience 25.28 (2005), pages 6520–6532. ISSN: 02706474. DOI: 10.1523/JNEUROSCI.1264- 05.2005

[11] K. C. Wood et al. "Picomolar nitric oxide signals from central neurons recorded using ultrasensitive detector cells". In: Journal of Biological Chemistry 286.50 (2011), pages 43172– 43181. ISSN: 00219258. DOI: 10.1074/jbc.M111.289777

[12] H. Carslaw and J. Jaeger. Conduction of heat in solids. Oxford University Press, 1959

[13] NEURON simulator. URL: https://neuron.yale.edu/neuron/

[14] NEST simulator. URL: https://www.nest-simulator.org/

[15] A. Antonietti et al. "Implementation of an Advanced Frequency-Based Hebbian Spike Timing Dependent Plasticity". In: Proceedings of the Annual International Conference of the IEEE Engineering in Medicine and Biology Society, EMBS November (2019), pages 3005–3009. ISSN: 1557170X. DOI: 10.1109/EMBC.2019.8856489

Modelling neural dynamics on neuromorphic hardware

Mollie Ward[1]*, Oliver Rhodes[1]

[1] Department of Computer Science, University of Manchester, Manchester, UK
**Correspondence: mollie.ward@manchester.ac.uk*

INTRODUCTION AND MOTIVATION

Accurate and efficient simulation of neural activity has long been a goal in computational neuroscience research. Neuromorphic computing aims to provide platforms for energy-efficient exploration of computational neuroscience through simulation of Spiking Neural Networks (SNNs): networks of individual neuron models designed to mimic biological networks[1,2]. These SNNs generally incorporate a simple model called the Leaky Integrate-and-Fire (LIF) model[3] which simplifies a number of biological features resulting in the loss of a range of neuronal characteristics including the ability to compute operations such as XOR. Incorporation of more biologically accurate dynamics onto neuromorphic systems could be therefore be fundamental to further understanding of the brain.

LIF neurons are modelled as point processes with a single term describing membrane conductance. In reality, neurons are not this simple and more complex models exist describing these simplified features: ion-channels governing membrane conductance can be described using mathematical approximations, and the cable equation captures complex, elongated structures incorporating branched dendritic extensions[3] through multi-compartment models[4,5] (Figure 1).

However, increasing the complexity of models increases computational costs; large-scale simulations of SNNs with complex neuron models[4], while effective, consume megawatts of power simulating small regions of the brain (0.29 mm^3)[4,6]. This is not mimicked in the brain which demonstrates a remarkable ability for large amounts of fine-scale computation at a fraction of the power (up to 20 Watts), much faster than these SNNs[1,7]. Neuromorphic systems provide a potential solution by mimicking the brain, enabling real-time simulations by using processors which are less complex than those used in standard computing platforms[1,8]. However, use of these processers limits the

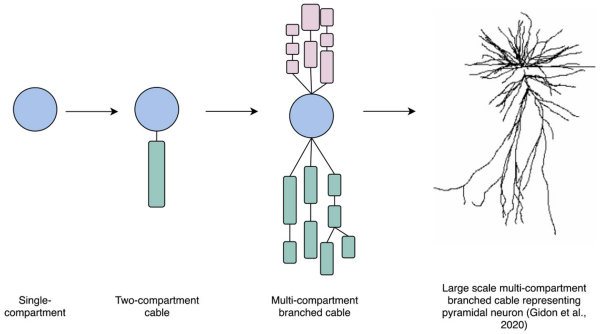

FIGURE 1: Neuron models increasing in complexity. Neurons are approximated as a number of compartments, each described by a single membrane potential. The simplest model is a single compartment model e.g. LIF model. Detailed neuronal morphologies can be captured with multicompartment models e.g. Gidon et al.5 's pyramidal cell (far right).

complexity of modelling available; some platforms have energy-efficient hard-coded circuitry, limiting flexibility of trialling new models. Implementation of complex models is therefore a challenge as mathematical operations such as exponentials and divides are not often available yet feature heavily in the models.

Here, the advantages and challenges of implementing more biologically realistic models on neuromorphic hardware while aiming to maintain energy-efficiency are explored. Requirements for accurate and efficient ion-channel modelling are demonstrated with an example of how these dynamics can be incorporated into a multi-compartment model, giving single neurons XOR-solving properties never before demonstrated on neuromorphic hardware.

METHODS

The SpiNNaker neuromorphic platform[9] is used due to its software programmable nature and flexibility, enabling exploration of different neural models incorporating operations such as exponentials and divisions.

The basic equation for all single-compartment neurons includes a term, i_m, describing the current per unit area (nA/mm^2). In Integrate-and-Fire models,

i_m consists of a single passive leakage term which can be expanded to include ion-channel conductances in more complex models, described by calculating the current conducted by the channel:

$$i_m = \bar{g}P(V - E)$$

Where $\bar{g}$ is the single channel open conductance per unit area (mS/mm^2), P is the probability that the channel is open and E is the reversal potential (mV). Potassium and sodium channel currents are modelled as $\bar{g}_K n^4 (V - E_K)$ and $\bar{g}_{Na} m^3 h (V - E_{Na})$ where and are activation parameters for each channel respectively; sodium channels also have an inactivation parameter, h. These conductances were originally described by Hodgkin and Huxley[10] and are here modelled on SpiNNaker[9] with testing in voltage-clamping experiments and comparison with a reference floating-point Python implementation.

A two-compartment reference model is built based on the multi-compartment neuron model described by Gidon et al. 2020[5]our knowledge of active dendrites has been almost entirely acquired from studies of rodents. In this work, we investigated the dendrites of layer 2 and 3 (L2/3. This model is constructed in the NEURON simulator, along with a version in Python to explore accuracy and performance. The soma incorporates sodium (I_{Na}) and potassium (I_K) currents and the dendrite features a calcium (I_{Ca}) current responsible for dendritic calcium action potentials (dCaAPs) when the membrane potential crosses -36 mV. Membrane potential in each compartment, μ, is governed by the cable equation:

$$c_m \frac{dV_\mu}{dt} = -i_m + \frac{I_e^\mu}{A_\mu} + g_{\mu,\mu\pm1}(V_{\mu\pm1} - V_\mu)$$

Where c_m is the specific membrane capacitance (nS/mm^2, I_e^μ), is the electrode current (nA), A_μ is the total surface area (mm^2) and $g_{\mu,\mu+1}$ is internal coupling conductance (nS/mm^2).

RESULTS AND DISCUSSION

Despite additional mathematical complexity, SpiNNaker[9] is able to accurately model the potassium and sodium channel conductances. Terms m, n and h

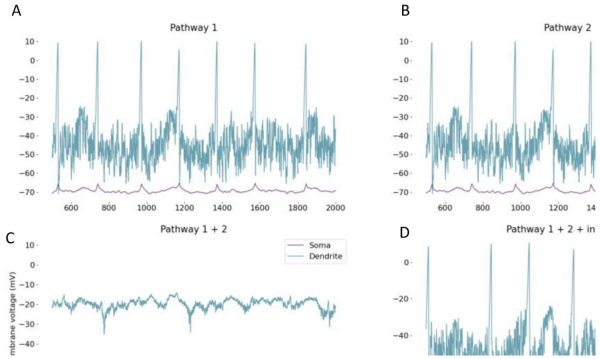

FIGURE 2: Two compartment dendrite-soma model in NEURON[9] environment demonstrating XOR properties. (**A**) Stimulation of a single pathway with 15 excitatory synaptic connections results in the dendritic compartment firing dCaAPs. (**B**) As (A) with separate, identical pathway. (***C***) Stimulation of both pathways results in the loss of dCaAPs. (**D**) dCaAPs restored when both pathways are stimulated with 15 inhibitory synapses.

are described by differential equations and solving them requires a number of calculations including divisions and an exponential. Simplifying assumptions which give a biologically faithful model were sought, including treating variables exhibiting small changes as constant, enabling pre-calculation of certain costly operations and removing three sets of exponential and divide operators.

The two-compartment model under exploration contains a variety of these ion-channel conductances and hence illustrates an example of the dynamic properties a neuron can exhibit when incorporating conductances. The model contains a dendritic compartment with XOR-solving capabilities (Figure 2; A-D). The calcium-channel current suppresses the amplitude of action potentials when the input strength is increased above a threshold, giving capabilities to a single neuron which would previously have required a network solution.

FUTURE WORK

The two-compartment model built in NEURON[11] and Python will be implemented on SpiNNaker[9] and efforts made to improve efficiency; the feasibility of using a lookup table to pre-calculate certain voltage-dependent operations

involved in the calculation of activation parameters is under investigation which will significantly increase the efficiency of the models described.

Addition of these dynamics onto neuromorphic hardware will enable replication of a wide range of neuronal firing characteristics observed in biology; efficient and accurate implementation of these models are therefore of interest to both computational neuroscience and AI communities.

Keywords: neuromorphic computing, neuron modelling, brain simulation, Hodgkin-Huxley model, Spiking Neural Networks, SpiNNaker

REFERENCES

[1] Roy, K., Jaiswal, A. & Panda, P. Towards spike-based machine intelligence with neuromorphic computing. Nature 575, 607–617 (2019).

[2] Furber, S. Large-scale neuromorphic computing systems. J. Neural Eng. 13, (2016).

[3] Dayan, P. & Abbott, L. F. Theoretical Neuroscience: Computational and Mathematical Modeling of Neural Systems. (The MIT Press, 2005).

[4] Markram, H. et al. Reconstruction and Simulation of Neocortical Microcircuitry. Cell 163, 456–492 (2015).

[5] Gidon, A. et al. Dendritic action potentials and computation in human layer 2/3 cortical neurons. Science (80-.). 367, 83–87 (2020).

[6] Wallace, S., Vishwanath, V., Coghlan, S., Lan, Z. & Papka, M. E. Measuring power consumption on IBM Blue Gene/Q. Proc. - IEEE 27th Int. Parallel Distrib. Process. Symp. Work. PhD Forum, IPDPSW 2013 853–859 (2013). doi:10.1109/IPDPSW.2013.269

[7] Cox, D. D. & Dean, T. Neural networks and neuroscience-inspired computer vision. Curr. Biol. 24, R921–R929 (2014).

[8] Rhodes, O. et al. Real-time cortical simulation on neuromorphic hardware. Philos. Trans. R. Soc. A Math. Phys. Eng. Sci. 378, (2020).

[9] Furber, S. B., Galluppi, F., Temple, S. & Plana, L. A. The SpiNNaker project. Proc. IEEE 102, 652–665 (2014).

[10] Hodgkin, A. L. & Huxley, A. F. A quantitative description of membrane current and its application to conduction and excitation in nerve. J. Physiol 117, (1952).

[11] Hines, M. L. & Carnevale, N. T. The NEURON Simulation Environment. Neural Comput. 9, 1179–1209 (1997).

IV Cognitive and behavioral neuroscience

How affective looming sounds modulate the whole-body action preparation within peripersonal space: The case of stepping congruent/incongruent to affect

Mehrdad Bahadori*, Paola Cesari

Department of Neuroscience, Biomedicine, and Movement Sciences, University of Verona, Verona, Italy
**Mehrdad.bahadori@univr.it*

INTRODUCTION/MOTIVATION

The peripersonal space (PPS) has found to have specific sensory-motor representation in the brain. Previous literature has dedicated two functions to sensory-motor behavior within PPS: a rapid sensory-motor interface for defensive purpose, and a sensory-motor interface serving goal-directed actions [1]. In this study, we investigate how the different affective (positive, negative, and neutral) looming sounds (approaching either from left or right) stopping at different distances (close and far) within the PPS, modulate action preparation in a whole-body movement as stepping. We were expecting that action preparation strategies were following motivational direction; e.g. stepping faster toward (away from) a positive (negative) approaching sound. To measure action preparation as a reflection of a feed-forward command from the motor cortex, force, and electromyographic premotor reaction times (PRTs) have been measured [2]. Additionally, step width, step duration, and maximum velocity have been registered by recording kinematics via motion capture.

METHODS

Sixteen right leg dominant participants have participated in the experiment. Emotional sounds were selected from the IADS dataset having different levels of induced valence and arousal. Five positive and five negative sounds have been selected from the IADS database [3]. As neutral sound, different colors of noises (5 sounds: red, pink, white, blue, and violet noise) were selected [4]. The sounds were modulated in a way that they were approaching either

from the left (-80°) or the right (80°) side with zero degrees of elevation from the ear canal filtered by using KEMAR HRTF provided by CIPIC dataset [5]. Participants were standing barefoot putting each foot on one of the two side-by-side force plates. The two different experimental conditions for action were defined based on the stepping direction according to the approaching sound direction: 1) stepping toward the approaching sound 2) stepping away from the approaching sound. The force premotor reaction time (FPRT) and electromyography premotor reaction time data (EPRT) considering Tibialis Anterior (TA), Adductor (AD), Rector Femoris (RF), and Gluteus Medius (GM), have been registered, along with kinematics data. The FPRT was defined as the time difference between the sound offset and the onset of force changes, while the EPRT for each muscle have been defined as the time difference between the sound offset and the onset of the muscle activity (considering the standing leg) (Figure 1). For statistical analysis, a separate repeated measures ANOVA was deployed for each variable by considering Action (toward/away) × Emotion (positive/negative/neutral) × Distance (close/far) as within-subjects variables.

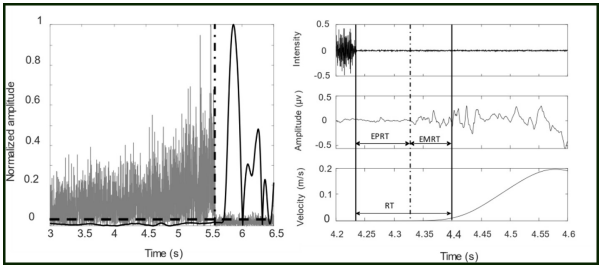

FIGURE 1: left) detecting force onset procedure in one trial, to calculate the FPRT by subtracting it from the offset of the sound. The grey signal is the normalized sound stimuli, the black signal is the normalized absolute value of the force, the vertical dash-dot line is the offset of the sound, and the horizontal dash line is the threshold of force initiation. The first sample in force signal exceeding the threshold after the sound offset is considered as the force onset. right) the variables calculated from EMG analysis. The graphs are showing the sound intensity, EMG activity of one muscle, and velocity of the moving leg in one trial from top to bottom respectively. The first and last solid vertical lines are showing the sound offset and kinematics onset respectively. The vertical dash-dot line shows the onset of EMG activity. The EPRT is the time between offset of the sound and onset of EMG activity, the EMRT it the time between onset of the muscle activity and onset of the kinematic, and the RT (Reaction Time) is the time between offset of the sound and the onset of the kinematics.

RESULTS AND DISCUSSION

The results revealed prompter step while reacting to closer sounds compared to further sounds, regardless of the emotional content of the sounds and Action (Figure 2). This result is in line with previous studies, which show the enhanced motor cortex activation while an external stimulus is very close to the body [6, 7]. Furthermore, our results showed that the PRTs were being modulated by the emotional content of the sound. The results showed that FPRT (Figure 2) and EPRT in all anticipatory muscles was shorter while reacting to neutral sounds compared to both positive and negative sounds, which might be due to lower perceptual load given the simpler sound composition in terms of frequency components [8]. Interestingly, FPRT and EPRT of GM muscle in standing leg for negative sound was shorter than positive sound. Previous studies suggest that, while emotions are closely linked to actions, negative events require more prompt reactions and need to be more crucially prepared [9].

Importantly, the results revealed shorter FPRTs and EPRTs in the far distance while reacting to negative sounds compared to positive sounds. Previous studies have concluded the expansion of PPS followed by negative emotions, by measuring different behavioral and neurophysiological variables [4, 10]. It is shown that time-to-collision underestimation is enhanced for individuals who are fearful of the threatening stimulus and the size of the underestimation is linked to individuals' level of threat-related anxiety [11, 12]. If PPS is extended, the distance between the feared object and PPS boundaries is

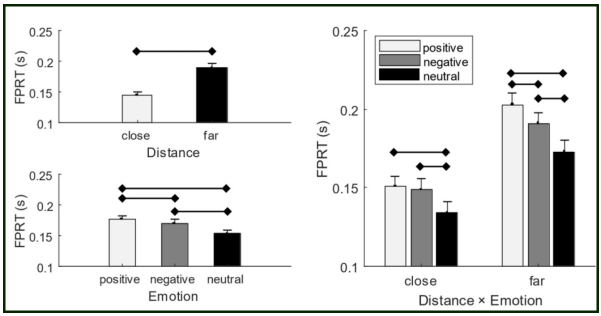

FIGURE 2: The FPRTs of standing leg for different Emotions (positive/negative/neutral) Distances (close/far) and their interactions. The error bars show the standard error and the black lines show a significant difference at the level of α<0.05.

smaller, consequently, the entrance within the PPS occurs sooner. Thus, the fact that an approaching negative stimulus is perceived as colliding sooner seems coherent with the PPS boundaries being farther. Concludingly, in line with the above-mentioned studies, the results showed that the whole-body PPS space is extended in presence of negative emotion which leads to promoter whole-body movement such as stepping.

Besides, the data revealed that the step width was larger when sounds were closer to the body compared to the far distances. Importantly, the post-hoc analysis showed that the step length did not change for positive sound in the close and far distance, but it was bigger for negative and neutral sounds in close distance compared to far distance. According to distance regulation hypothesize, the changes in the physical proximity of an actor to the outside world follows the approach and avoidance behavior [13]. Accordingly, since a stimulus within PPS triggers a flight behavior as well as an induced negative emotion by the stimuli, the steps were larger while reacting to a stimulus very close to the body or negative but not positive one.

In this experiment, the data did not show any significant difference in Action condition in none of the measured variables. However, we think that one of the reasons that we did not find any difference in Action is due to using sounds instead of images, since reactions to emotional images have found to be stronger [14] and more immediate [15] compared to sounds; thus our stimuli were not sufficient enough to drive stepping, which is a sophisticated motor task [16], in direction of approach and avoidance behavior.

To conclude, this study showed that the movement preparation of stepping, as a whole-body sophisticated movement, in presence of the external stimuli is modulated based on the distance of the stimuli within PPS and the affects induced by the stimuli. The results add new evidence about the role of PPS as a movement regulating factor and how affects induced by external stimuli modulate these multisensory-motor regulations within PPS.

Keywords: Peripersonal space, looming sound, emotion, reaction time, motivation

REFERENCES

[1] Rizzolatti, G., L. Fogassi, and V. Gallese, Motor and cognitive functions of the ventral premotor cortex. Current opinion in neurobiology, 2002. 12(2): p. 149-154.

[2] Santos, M.J., N. Kanekar, and A.S. Aruin, The role of anticipatory postural adjustments in compensatory control of posture: 2. Biomechanical analysis. Journal of Electromyography and Kinesiology, 2010. 20(3): p. 398-405.

[3] Bradley, M.M. and P.J. Lang, The International Affective Digitized Sounds (; IADS-2): Affective ratings of sounds and instruction manual. University of Florida, Gainesville, FL, Tech. Rep. B-3, 2007.

[4] Ferri, F., et al., Emotion-inducing approaching sounds shape the boundaries of multisensory peripersonal space. Neuropsychologia, 2015. 70: p. 468-475.

[5] Algazi, V.R., et al. The cipic hrtf database. in Proceedings of the 2001 IEEE Workshop on the Applications of Signal Processing to Audio and Acoustics (Cat. No. 01TH8575). 2001. IEEE.

[6] Camponogara, I., N. Komeilipoor, and P. Cesari, When distance matters: Perceptual bias and behavioral response for approaching sounds in peripersonal and extrapersonal space. Neuroscience, 2015. 304: p. 101-108.

[7] Cléry, J., et al., Neuronal bases of peripersonal and extrapersonal spaces, their plasticity and their dynamics: knowns and unknowns. Neuropsychologia, 2015. 70: p. 313-326.

[8] Bahadori, M., et al., Action planning and affective states within the auditory peripersonal space in normal hearing and cochlear-implanted listeners. Neuropsychologia (under revision), 2020.

[9] Borgomaneri, S., V. Gazzola, and A. Avenanti, Temporal dynamics of motor cortex excitability during perception of natural emotional scenes. Social cognitive and affective neuroscience, 2013. 9(10): p. 1451-1457.

[10] Ruggiero, G., et al., The effect of facial expressions on peripersonal and interpersonal spaces. Psychological research, 2017. 81(6): p. 1232-1240.

[11] Brendel, E., et al., Threatening pictures induce shortened time-to-contact estimates. Attention, Perception, & Psychophysics, 2012. 74(5): p. 979-987.

[12] Vagnoni, E., S.F. Lourenco, and M.R. Longo, Threat modulates perception of looming visual stimuli. Current biology, 2012. 22(19): p. R826-R827.

[13] Chen, M. and J.A. Bargh, Consequences of automatic evaluation: Immediate behavioral predispositions to approach or avoid the stimulus. Personality and social psychology bulletin, 1999. 25(2): p. 215-224.

[14] Bradley, M.M. and P.J. Lang, Affective reactions to acoustic stimuli. Psychophysiology, 2000. 37(2): p. 204-215.

[15] Thierry, G. and M.V. Roberts, Event-related potential study of attention capture by affective sounds. Neuroreport, 2007. 18(3): p. 245-248.

[16] Rocchi, L., et al., Step initiation in Parkinson's disease: influence of initial stance conditions. Neuroscience letters, 2006. 406(1-2): p. 128-132.

Processing visual ambiguity in fractal patterns: Is pareidolia a sign of creativity?

Antoine Bellemare Pepin[1]*, Yann Harel[2], Geneviève Mageau[2], Karim Jerbi[2]

[1]Department of Music, Concordia University, Montreal, Canada
[2]Department of Psychology, Université de Montréal, Montreal, Canada
antoine.bellemare9@gmail.com

INTRODUCTION/MOTIVATION

Creativity is a multifaceted ability that leads to novel and purposeful artifacts. Characterizing creativity experimentally within the framework of cognitive neuroscience has proven challenging. While most studies have focused on divergent thinking abilities [1], [2], emerging work also points to perceptual abilities as a potential basis for creativity. We therefore hypothesized that differences in high- and low-creative individuals could be reflected in pareidolia, i.e., the perception of recognizable forms in noisy or ambiguous stimuli. Pareidolia can be seen as the perceptual counterpart of divergent thinking, in that it relies on finding multiple solutions within a single problem space. This perceptual phenomenon has mostly been studied in the context of face detection [3], [4], [5], although more recent studies relied on natural scenery images [6] or generative stimuli [7], [8], [9]. Only one study investigated how pareidolia relates with creativity, demonstrating that fluency on a divergent thinking task significantly predicts fluency and originality in a Divergent Pareidolia Task [6]. Moreover, past research points to fractal dimension, an indicator of statistical complexity, as likely environmental predictor of pareidolia [8]. However, no study has been investigating the interaction of creativity and stimulus properties in the emergence of pareidolic percepts.

METHODS

In the present study, we set out to quantify the relation between performance on a pareidolia perception task and individual creativity levels (measured with a series of standard questionnaires) across a sample of 50 participants. We designed a pareidolia task in which participants were asked to perceive as many recognizable forms as possible in ambiguous stimuli. Our stimuli

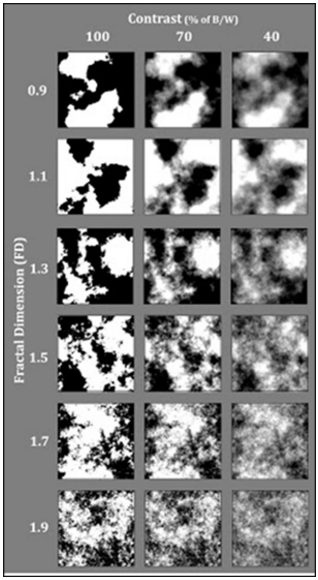

FIGURE 1: Stimuli generated with Fractional Brownian Motion algorithm. The X-axis represents the three levels of constrast, ranging from full black and white (left), to 20% of black and 20% white (right). The Y-axis represents the fractal dimention of Stimuli, ranging from 0.9 to 1.9.

consisted in generated synthetic cloud-like images where we control the level of complexity by modulating their fractal dimension (FD), as well as their contrast level by thresholding the grayscale image at three different luminance levels (see Fig. 1). To model the interaction between creativity, fractal dimension and contrast in predicting pareidolia, we used Generalized Linear Mixed Effects Models (GLMM), which are regression models that allow using non-normally distributed dependent variables and including random effects to model variables from different nested levels [10]. Low- and mid-contrast images were grouped together to make the variable as binomial. To achieve a good fit of data with a GLMM, successive models were constructed and compared with each other while level of complexity was increased at each iteration. To quantify the significance of a model over another, ANOVAs were computed between the Akaike Information Criterion (AIC) of two models.

RESULTS AND DISCUSSION

Our preliminary analyses revealed that pareidolic perceptions arise more often and more rapidly when the ambiguous image had lower FD and higher contrast, validating that situational factors influence pareidolia. Results from our main analyses then revealed that high-creative individuals are generally more prone to experience pareidolia, and to perceive a higher number of objects when it occurs. We further show that both FD and contrast interact with creativity in predicting pareidolia, in that (1) the difference between low- and high-creatives in predicting pareidolia is amplified for images with lower FDs, and (2) images with lower contrast decrease pareidolia occurrences for low- more than for high- creatives. We further demonstrate that for high-contrast images, differences between low- and high-creatives are smaller for images of intermediate FDs and larger for images of low and high FDs in predicting pareidolia (see Fig. 2).

These results show that both FD and contrast are promising visual features to manipulate in order to investigate pareidolic perception and its putative modulations with creativity. It further suggests that creativity might be related to perception of meaningful patterns in ambiguous stimuli, and that intermediate FDs (1.3-1.5), which facilitate pareidolia especially for low-creatives,

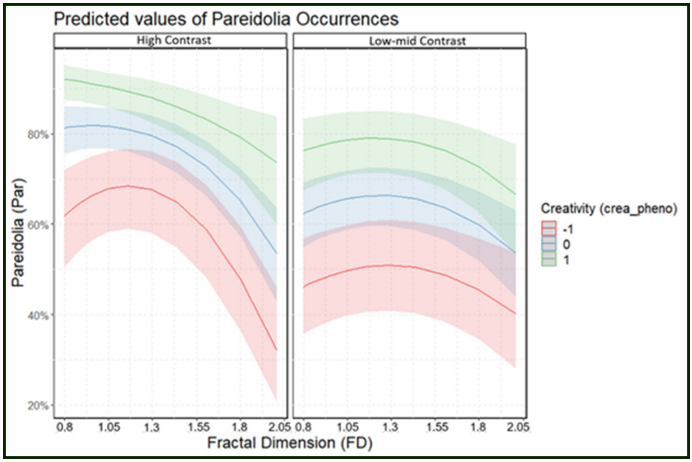

FIGURE 2: Predicted probabilities of the interaction between FD, Contrast and Creativity on pareidolia occurrences. Creativity values (-1, 0, 1) represent modelled z scores; creativity was entered in the model as a continuous variable.

might constitute an optimal situational factor for engaging in pareidolia in general population. Interestingly, intermediate FDs have been associated with perception of beauty and aesthetic preferences [11], suggesting that pareidolia might be accompanied by aesthetic experience. Our research shows that creativity is related to altered perceptual processes, as evidenced by the observed differential pareidolic response to varying levels of FD and contrast between high- and low-creative individuals. The present findings extend our understanding of the perception-creation link and open new exciting questions in studying creative behavior in humans.

ACKNOWLEDGEMENTS

I would like to thank my parents, for love, and the Universe, for life. And all the co-authors without whom this project would not have been possible.

Keywords: creativity, perception, fractal dimension, pareidolia, phenomenology

REFERENCES

[1] Guilford, J. P. (1950). Creativity. American Psychologist, 5, 444–454. doi:10.1037/h0063487

[2] Weisberg, R. W. (2006). Creativity: Understanding innovation in problem solving, science, invention, and the arts. John Wiley & Sons.

[3] Hong, K., Chalup, S. K., King, R. A., & Ostwald, M. J. (2013, April). Scene perception using pareidolia of faces and expressions of emotion. In 2013 IEEE Symposium on Computational Intelligence for Creativity and Affective Computing (CICAC) (pp. 79-86). IEEE.

[4] Liu, J., Li, J., Feng, L., Li, L., Tian, J., & Lee, K. (2014). Seeing Jesus in toast: neural and behavioral of face pareidolia. Cortex, 53, 60-77.

[5] Lee, J. (2016). I See Faces: Popular pareidolia and the proliferation of meaning.

[6] Diana, L., Frei, M., Chesham, A., de Jong, D., Chiffi, K., Nyffeler, T., ... & Müri, R. M. (2020). A divergent approach to pareidolias—Exploring creativity in a novel way. Psychology of aesthetics, creativity, and the arts.

[7] Rogowitz, B. E., & Voss, R. (1990, October). Shape perception and low-dimension fractal boundary contours. In Human Vision and Electronic Imaging: Models, Methods, and Applications (Vol. 1249, pp. 387-394). International Society for Optics and Photonics.

[8] Bies, A. J., Kikumoto, A., Boydston, C., Greenfield, A., Chauvin, K. A., Taylor, R. P., & Sereno, M. E. (2016, August). Percepts from noise patterns: The role of fractal dimension in object pareidolia. In Vision Science Annual Meeting.

[9] Taylor, R. P., Martin, T. P., Montgomery, R. D., Smith, J. H., Micolich, A. P., Boydston, C., ... & Spehar, B. (2017). Seeing shapes in seemingly random spatial patterns: Fractal analysis of Rorschach inkblots. PloS one, 12(2), e0171289.

[10] Bates, D., Mächler, M., Bolker, B., & Walker, S. (2014). Fitting linear mixed-effects models using lme4. arXiv preprint arXiv:1406.5823.

[11] Spehar, B., Clifford, C. W., Newell, B. R., & Taylor, R. P. (2003). Universal aesthetic of fractals. Computers & Graphics, 27(5), 813-820.

Influence of perinatal maternal high fat diet on hedonic responding in adolescent offspring

Harshit Bhasin*, Matthew M. Hurley, Aliasgher Sabir, Shannon C. O'Brien, Timothy H. Moran, Kellie L. K. Tamashiro

Department of Psychiatry & Behavioral Sciences, The Johns Hopkins University School of Medicine, Baltimore, MD USA.
**hbhasin1@jhu.edu*

INTRODUCTION/MOTIVATION

Studies have shown that male offspring of overweight parents are 1.7 times more likely to be overweight than the children of healthy parents (1). Maternal obesity has been shown to have an impact on the fetus and have an increased risk of obesity in the offspring (2-4). Previous studies show lowered dopamine sensitivity in obese individuals (5) which is thought to be, in part, responsible for the development of overeating behaviors. The current experiment was designed to examine the impact of maternal diet on male offspring Sprague-Dawley rat innate reward valuation and the brain reward system. This was done by measuring orofacial responding using the taste reactivity test (TRT) paradigm at two timepoints of the offspring's life. Briefly, the TRT involves analyzing orofacial responses that are conserved across species. Human infants, baby monkeys, and rodents have conserved responses that may be interpreted as "liking" or "disliking" (10,11). This allows us to assess the hedonic state of the animal by quantifying such orofacial responses by watching behavioral videos frame by frame. Previous studies showed that offspring of dams who consumed high fat (HF) diet during gestation and lactation are obese with impaired glucose tolerance and leptin resistance by the time they were weaned compared to standard chow (SC) offspring (6-7). We previously demonstrated that HF rat offspring have a greater preference for palatable food when given a choice. A Brief-Access Taste Test showed no differences between the groups in taste sensitivity (8). However, it is possible that HF offspring have altered 'liking' responding to palatable tastants and this is what drives them to consume more palatable food leading to obesity.

METHODS

Pregnant rats were placed on a Standard Chow ("SC"; n=6) or High-Fat diet ("HF"; n=6) beginning on gestation day (G)2. At weaning on postnatal day (P)21, male offspring (n=11 SC; n=16 HF) were selected from each litter and underwent surgery to implant intraoral catheters which was used to infuse tastants into the animal's mouth. The animals underwent an initial TRT with a 1M sucrose solution at P28-29. Behavior during the test was video recorded for later analysis. At P42, animals underwent a second taste reactivity test with a 1M sucrose solution after which the animals were sacrificed. Videos were scored by 3 scorers blind to the experimental conditions and individual 'liking' and 'disliking' responses were recorded. The scores from all 3 raters were averaged to account for human error.

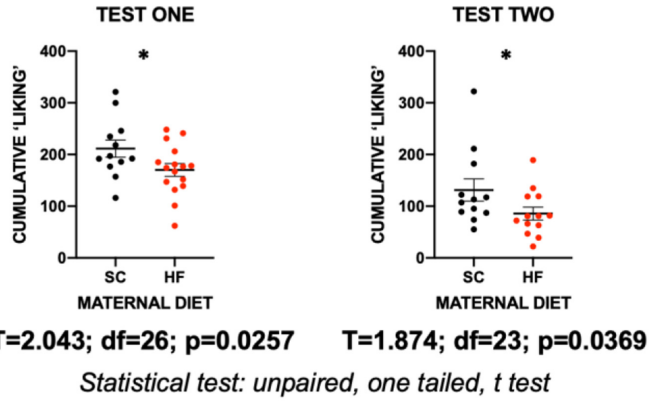

FIGURE 1: Cumulative liking responses from test one and test two.

RESULTS AND DISCUSSION

On P28 offspring were challenged with a 1 molar sucrose TRT. HF offspring displayed significantly fewer cumulative 'liking' responses, compared to the SC offspring (Fig 1 **TEST ONE**). When the animals were tested again on P42, HF offspring again displayed significantly less cumulative 'liking' responses compared to the SC offspring (Fig 1 **TEST TWO**). Both groups showed lower responding at P42 than at P28, in line with previous literature that 'liking' responses reduce with age (12). Taken together, we found that offspring of dams consuming a high fat diet during pregnancy display fewer orofacial responding to a sweet tastant, suggesting blunted hedonic responding. This supports our hypothesis that HF offspring may be driven to consume more palatable food due to an impaired hedonic state leading to obesity.

Keywords: Maternal Diet, Obesity, Taste Reactivity Test, Hedonic Responding

REFERENCES

[1] BAHREYNIAN, M., QORBANI, M., KHANIABADI, B. M., MOTLAGH, M. E., SAFARI, O., ASAYESH, H. & KELISHADI, R. 2017. Association between Obesity and Parental Weight Status in Children and Adolescents. **J Clin Res Pediatr Endocrinol,** 9, 111-117

[2] Yu, Z., et al., Trends in overweight and obesity among children and adolescents in China from 1981 to 2010: a meta-analysis. PLoS One, 2012. 7(12): p. e51949.

[3] Drake, A.J., et al., An unbalanced maternal diet in pregnancy associates with offspring epigenetic changes in genes controlling glucocorticoid action and foetal growth. Clin Endocrinol (Oxf), 2012. 77(6): p. 808-15.

[4] Drake, A.J. and R.M. Reynolds, Impact of maternal obesity on offspring obesity and cardiometabolic disease risk. Reproduction, 2010. 140(3): p. 387-98.

[5] Volkow N. D.; Wang G. J.; Fowler J. S.; Telang F. (2008) Overlapping neuronal circuits in addiction and obesity: Evidence of systems pathology. Philos. Trans. R. Soc., B 363, 3191–3200.

[6] Sun, B., et al., Maternal high-fat diet during gestation or suckling differentially affects offspring leptin sensitivity and obesity. Diabetes, 2012. Jun 29 [Epub ahead of print].

[7] Tamashiro, K.L., et al., Prenatal stress or high-fat diet increases susceptibility to diet-induced obesity in rat offspring. Diabetes, 2009. 58(5): p. 1116-25.

[8] Y. Treesukosol, B. Sun, A.A. Moghadam, N.C. Liang, K.L. Tamashiro, T.H. Moran. Maternal high-fat diet during pregnancy and lactation reduces the appetitive behavioral component in female offspring tested in a brief-access taste procedure Am. J. Physiol. Regul. Integr. Comp. Physiol., 306 (7) (2014), pp. R499-R509

[9] Grill HJ, Norgren R. The taste reactivity test. I. Mimetic responses to gustatory stimuli in neurologically normal rats. Brain Research. 1978;143(2):263-79

[10] Berridge, K.C. "Measuring Hedonic Impact in Animals and Infants: Microstructure of Affective Taste Reactivity Patterns." Neuroscience & Biobehavioral Reviews, Pergamon, 17 Feb. 2000.

[11] Berridge, Kent C., and Morten L. Kringelbach. "Pleasure Systems in the Brain." Neuron, Cell Press, 6 May 2015.

[12] Wilmouth, Carrie E, and Linda P Spear. "Hedonic sensitivity in adolescent and adult rats: taste reactivity and voluntary sucrose consumption." Pharmacology, biochemistry, and behavior vol. 92,4 (2009): 566-73. doi:10.1016/j.pbb.2009.02.009

Deep-sleep-inspired activity induces density-based-clustering on memories and entropic, energetic and classification gains

Chiara De Luca[1,2]*, Cristiano Capone[1], Pier Stanislao Paolucci[1]

[1]Instituto Nazionale di Fisica Nucleare (INFN), Sezione di Roma, Rome, Italy
[2]Ph.D. Program in Behavioural Neuroscience, Sapienza University of Rome, Rome, Italy
**Chiara.DeLuca@infn.roma1.it*

INTRODUCTION/MOTIVATION

Sleep is known to be essential for awake performance[1][2], but the mechanisms underlying its cognitive functions are still to be clarified: here we aim to investigate the effect of deep-sleep like activity over internal memories representation. Relying on very minimal assumptions, which are the thalamo-cortical structure and the presence of cortically generated cortico-thalamic slow oscillations we formally find out that sleep might naturally perform a "density-based clustering" in the thalamo-cortical connections. We demonstrate this process improves the performances of visual classification tasks (e.g. MNIST) in both a rate and spiking networks. Finally, we measure the entropic and energetic effects of sleep, that can be applied to experimental data to verify our theoretical predictions.

METHODS

We modelled a thalamo-cortical system with a two-layer network (the thalamus layer where the input is encoded and a cortical layer, reciprocally connected)l and defined a sleep-inspired activity that reshapes the structure of both synapses and stored memories (as depicted in Figures 1A and B). We implemented a rate based model of a network completely disconnected from external stimuli and assume that the populations of neurons are capable of sustaining an Up-state, a short (few hundreds of ms) state with a sustained level of activity, a hallmark of cortical activity during deep sleep. When the Up state occurs, other populations are activated, generating and hebbian association. We performed similar experiments and found similar results for a spike-based model (not shown in this document). We also considered the natural scenario in which training and testing examples are not equally

represented: each example is associated with a mass value that encodes the strength of the expression of that example in the sleeping dynamics. The probability of the Up-state occurring in a population is chosen proportionally to its mass. Coherently with experimental observation, we implemented a homeostatic effect of sleep that progressively lowers the masses of the examples. Our framework was also capable to account for the effect of plasticity on cortico-cortical recurrent connections during sleep-like dynamics. Finally, we made entropy-based measures to the network status at different sleep stages in two different ways: first a microscopic network state analysis and, second, an approximated macroscopic network state analysis to perform measures to be experimentally verified (Figure 2). We applied this analysis to both a 2-class toy dataset and the more complex MNIST dataset in both rate and spiking simulations (as a refinement of network models described in [3] and [4]).

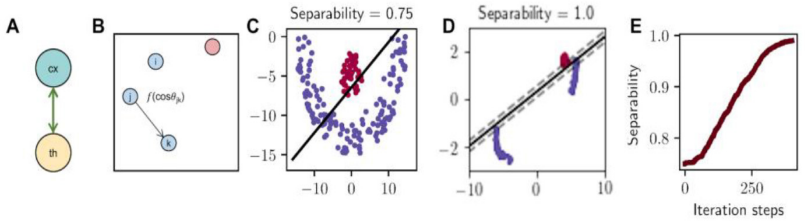

FIGURE 1: Simulated effects of sleep over stored memories with plastic feedforward connections. (**A**) Network diagram: only thalamo-cortical connections are present. They are plastic during the deep-sleep like activity. (**B**) Graphic representation of the internal "Density-based clustering" dynamics generated by sleep. When the population k produces an Up-state the vectors close to each other are attracted more than further ones and tend to create clusters. (**C**) and (**D**) Internal representation of stored memories at the beginning and the end of the sleep phase respectively. Black solid lines depict the optimal separator identified by the classifier. (**E**) Linear separability of the stored memories as a function of sleeping iterations.

RESULTS AND DISCUSSION

In this document, we present results obtained for the rate-based model trainedover a 2-class dataset, the Crescent Full Moon dataset. We found analogous results for the spiking model trained on more complex datasets (i.e. MNIST Dataset, not shown). In this work, we found theoretical and

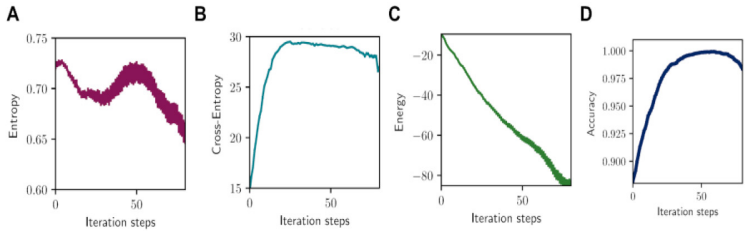

FIGURE 2: Entropy, cross-entropy and energy measures made over the network status during sleep: an increase in performances is associated with a reduction of entropy and energy consumption and an increase in cross-entropy values. (**A**) Entropy of the system at each sleeping step. (**B**) Cross-entropy between the two classes computed at each iteration of sleep to evaluate the separability of memories. (**C**) Synaptic energy consumption of the network at each iteration step. (**D**) Accuracy of the network in classification at each sleeping step of new unseen examples. It is worth noting that after a given amount of sleep iterations, all the internal representations of memories start to collapse in the same representation, with a consequent reduction in classification performances,

experimental evidence that stored memories are reorganized following a density-based clustering: close memories group together (see Figure 1C and D). Specifically, we infer the internal representation of the memories from the synaptic weight distributions: similar synaptic weight patterns, leading also to similar activation patterns in the cortical layer, are associated with closer internal representations. Then, we compute the separability of these memories by a linear separator since we aim to study and model the intrinsic learning capabilities of the network. The huge advantages of such clustering are: not requiring a number of clusters, finding arbitrarily shaped clusters, independence on the number of elements. This improves the linear separability of memories belonging to different classes improving the accuracy during classification tasks (see Figure 1E). We also show that the presence of heterogeneous masses (this can be biologically interpreted as heterogeneity in population recurrent connectivity) speeds up the separability performances for plastic feed-forward connections and improves the separability for plastic recurrent connections. Finally, we propose entropy-based measures that can be applied to experimental data to verify our theoretical predictions (Figure 2). Specifically, to evaluate the quantity of stored information in the network, we measure the entropy associated to the internal representation

of memories (see Figure 2A) through both synaptic weights distribution and output layer activity in retrieval; then, we measure the cross-entropy to evaluate the mutual information of associated to the two classes (see Figure 2B). Finally, we also evaluate the energy used by the network at each sleeping step (see Figure 2C). We show that a reduction in both entropy and energy consumption together with an increase in cross-entropy is associated with an improvement in classification performances (as depicted in Figure 2D).

To sum up, in this work we demonstrate the beneficial effect of association in a deep-sleep like activity over a simple thalamo-cortical network in both rate and spiking simulations.

This opens up for future investigation in expanding this analysis to more complex datasets and other stages of sleep.

Keywords: deep-sleep, synaptic plasticity, learning

REFERENCES

[1] Walker, M. P. & Stickgold, R. Sleep, memory, and plasticity. Annu. Rev. Psychol. 57, 139–166 (2006).

[2] Jadhav, S. P., Kemere, C., German, P. W. & Frank, L. M. Awake hippocampal sharp-wave ripples support spatial memory. Science 336,1454–1458 (2012).

[3] B. Golosio, C. De Luca, C. Capone, E. Pastorelli, G. Stegel, G. Tiddia, G. De Bonis and P.S. Paolucci "Thalamo-cortical spiking model of incremental learning combining perception, context and NREM-sleep-mediated noise-resilience",2020. arXiv.2003.11859

[4] Capone, C., Pastorelli, E., Golosio, B., Paolucci, P.S. Sleep-like slow oscillations improve visual classification through synaptic homeostasis and memory association in a thalamo-cortical model. Sci Rep 9, 8990 (2019). https://doi.org/10.1038/s41598-019-45525-0

Demonstration of altruistic behaviour in rats

Ushnik Das[1]*, Anshu Kumari[2], Shruthi Sharma[2], Laxmi T. Rao[2]

[1] Biology majors, Indian Institute of Science Education and Research, Mohali, India
[2] Neurophysiology, National Institute of Mental Health and Neurosciences, India
**dasushnik@gmail.com*

MOTIVATION

Contrary to the commonly observed trait of reciprocal altruism, a true altruistic behaviour; i.e. to help another while putting itself in distress without any expectation of reward, is very rarely seen in organisms. In rats, Bartal et al.[(1)] demonstrated empathetic responses where they would respond to another rat's distress and help it, but the question of altruism still lingered. The fact that a rat would still help another if it needed to sacrifice its own fitness was still under question.

METHODS

In a 3-chambered apparatus (boxes arranged serially) we placed a free rat in the first chamber and the trapped rat in the third (see Figure 1). The middle chamber was filled with water. Thus, we observed if a trained rat (i.e. a rat who knows how to release the trapped rat) would be willing to get into the water dam (a stressful ambience) to rescue the trapped conspecific or not. The trapped rat was either a cage-mate or a stranger. We further ran anxiety tests (light-dark chamber test) to observe any correlation between the observed behaviour with anxiety.

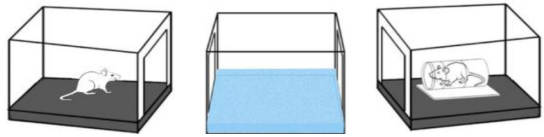

FIGURE 1: The experimental apparatus with the central one having water. Boxes are shown separated for clarity.

RESULTS

Through this experiment we were able to showcase that rats would be willing to put themselves into stressful scenarios to help another conspecific out of distress. The free rats had a similar latency to cross the well and release the trapped rat irrespective of the kinship and their individual anxiety levels. We thus demonstrate true altruistic behaviour in a laboratory setup through rodents and observe it for the first time in rats.

Keywords: rats, altruism, animal behaviour, empathy, social interaction, rodents

REFERENCES

[1] Ben-Ami Bartal, I., Decety, J., & Mason, P. (2011). Empathy and pro-social behavior in rats. Science (New York, N.Y.), 334(6061), 1427–1430. https://doi.org/10.1126/science.1210789

Source monitoring: Effect of language and false information

Aleksandra Dolgoarshinnaia[1]*, Beatriz Martín-Luengo[1]

[1]Centre for Cognition and Decision making, Institute for Cognitive Neuroscience, HSE University, Russian Federation
**adolgoarshinnaya@hse.ru*

INTRODUCTION/MOTIVATION

Human memory does not record everything we experience. Memory is a reconstructive process from which we encode new information assimilating it to the schemata we have about different actions and situations [1]. Because of the reconstructive process we sometimes include information which was not presented at the original event but that it was later suggested [8]. This effect of incorporating false information into our memories is the so-called misinformation effect [5]. In a series of experiments it was shown that not only the suggested post event information was susceptible of being incorporated to the memory, but also the wording used (e.g., smash, touch) can alter the estimation of other variables as the speed of the car passing by [5]. The information suggested can come from different types of sources affecting its credibility and endorsement [4], being one of those types the language used.

In the globalized world we are living there is an increase of bilingualism accompanied with the access to information offered in different languages. Yet, scarce research has focused on investigating the effect of bilingualism in the misinformation effect [3]. One related topic linked with the use of different languages is the convergent evidence of an enhanced executive functioning by bilinguals, specifically, inhibitory control, in different processes such as decision-making, attention, and memory [6]. In turn, executive functioning is related to source monitoring, which is considered important for misinformation endorsement [7]. Furthermore, bilinguals could rely on more reasonable and deliberate System-2 related to analytic processing as opposed to use of heuristics from System-1 [2]. These studies suggest that bilinguals can be more analytical when processing information in the second language, consequently, exhibiting stronger inhibition of irrelevant or erroneous information. Thus, it can be expected a higher acceptance of misleading information in the native compared to the second language.

METHODS

To test our hypothesis, we conducted a 2 (Language source: Russian, English) X 2 (Item type: true, misinformation) within-subjects design online experiment on the platform "Gorilla" (https://gorilla.sc). Participants completed the classical three-phased misinformation paradigm. First, participants watched a real video-photage of a car robbery without sound. Second, misleading information was presented in counterbalanced pairs of English and Russian narratives. These two narratives were described as reports by a Russian-native and an English-native eyewitnesses. Finally, participants completed a yes/no recognition task and a source monitoring (EN, RU, none). To ensure that the observed effect was not due to the lack of understanding of presented materials, we recruited only participants with Intermediate and higher levels of English proficiency (according to the Common European Framework of Reference, CEFR). Reported are the results of 41 Russian-native participants (36 females, mean age = 23,8 SD = 4,02) who scored minimum of 16 points (mean = 19.7) on English proficiency test (https://www.cambridgeenglish.org).

RESULTS AND DISCUSSION

Regarding the misinformation effect, we found a main effect of item type reflected in a higher accuracy of the false control information ($M = .79$) than false misleading information ($M = .68$), $p < .0001$, which indicates that the misleading information was endorsed. However, we did not find any interaction of item type and language. We next tested for the differences on the correct attributions by source (Russian, English, None). We found significant differences, $p < .001$, as the correct attributions to None were higher ($M = .72$), than for the other two sources that had similar amount of correct attributions (for Russian ($M = .33$); English ($M = .44$)). Finally, see Figure 1 for statistics, we run a repeated measures ANOVA 3 (Source attribution: Russian, English, None) x 3 (Actual source: Russian, English, None) with the proportion of answers that reported significant differences in the interaction ($p < .001$). To properly describe the results, we split by the actual source. In the univariate ANOVA with the Russian and the None source we found a similar pattern of differences: significantly higher selection of the correct source over the incorrect attributions, and no differences between these incorrect attributions. With the English source, however, the pattern found is slightly different: the proportion of correct selections was still higher than the incorrect ones,

but we found significantly more incorrect EN attributions to the RU source (M = .20) than to None (M = .09), p = .038.

In this study we examined the influence of the foreign language on the acceptance of misinformation and source monitoring. We found the misinformation effect but not the predicted interaction with language, that is, our participants did not accept more false information when presented in their native language. This result contradicts previous results that found higher acceptance of misinformation in the native language [3]. We carefully controlled and fully counterbalanced the content of the narratives and both, misinformation and control items. Thus, it is possible that the absence of effect can be explained in that as people get more proficient in a second language, their interaction with information is not different than in their native language. Analysis on source attributions showed higher correct attribution for all sources. However, while there were no differences on the distribution of misattributions when the actual source was Russian or None, for English source incorrect attributions differed and participants attributed more information to the Russian source than the None. This suggests that participants

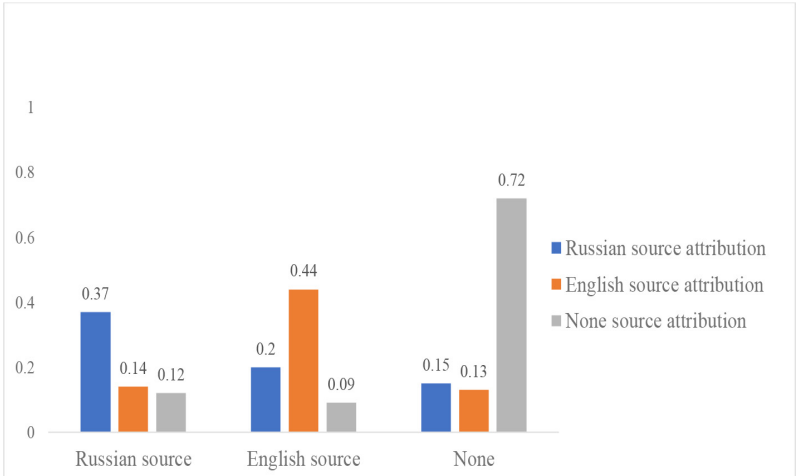

FIGURE 1: Interaction between source attributes and actual sources.

might have used more resources in processing the information in English, which led to a better processing and a consequently better recognition, although wrong attribution. Taking together both results in misinformation and source monitoring, we can conclude that people proficient in a second language might be prone to some memory errors but not all. In future, the persistence of the effect can be tested between different proficiency groups (e.g. Intermediate and Advanced) and in English-Russian bilinguals. Moreover, as all the verbal instructions and the recognition test were always in one language (Russian), we can investigate the influence of the linguistic environment on misinformation acceptance and source monitoring by conducting a mirroring experiment using English as the main language.

ACKNOWLEDGEMENTS

This study was funded by the Russian Science Foundation (RSFU 19-18-00534)

Keywords: misinformation effect, source monitoring, second language

REFERENCES

[1] Bartlett FC, Remembering: a study in experimental and social psychology. Cambridge: Cambridge University Press, 1932.

[2] Caldwell-Harris CL, Emotionality differences between a native and foreign language: Theoretical implications. Front Psychol. 2014; 5: 1055. doi: 10.3389/fpsyg.2014.01055

[3] Calvillo DP, Mills NV, (2018). Bilingual witnesses are more susceptible to misinformation in their less proficient language. Curr Psychol. 2018; 39: 673–680. doi: 10.3389/fpsyg.2014.01055

[4] Johnson MK, Hashtroudi S, Lindsay DS, Source monitoring. Psychol bull. 1993; 114 (1): 3-28. doi: 10.1037//0033-2909.114.1.3

[5] Loftus EF, Palmer JC, Reconstruction of auto-mobile destruction: An example of the interaction between language and memory. J Verbal Learning Verbal Behav. 1974; 13: 585-589.

[6] Roebers CM, Schneider W, The strategic regulation of children's memory performance and suggestibility. J Exp Child Psychol. 2005; 91(1): 24–44. doi: 10.1016/j.jecp.2005.01.001.

[7] Ruffman T, Rustin C, Garnham W, Parkin AJ, Source monitoring and false memories in children: Relation to certainty and executive functioning. J Exp Child Psychol. 2001; 80: 95–111. doi: 10.1006/jecp.2001.2632

[8] Schacter DL, The seven sins of memory: Insights from psychology and cognitive neuroscience. Am Psychol. 1999; 54 (3): 182–203. doi: 10.1037//0003-066x.54.3.182

Effect of Avandamet on the behavior of different age rats

Vasyl Gorbachenko*, Elena Lukyanetz

Department of Biophysics of Ion Channels, Bogomoletz Institute of Physiology, NASU, Kyiv, Ukraine
**gva@biph.kiev.ua*

INTRODUCTION/MOTIVATION

It is known that Alzheimer's disease (AD) is an incurable disease in which the death of brain cells and the disruption of neural connections occur. The latter leads to the degradation of brain functions, and the loss of memory. Therefore, drug therapy mitigates the manifestation of symptoms and reduces the rate of negative changes. However, it cannot be cured in patients with AD at present. Recently, the positive effect of drugs used to treat type 2 diabetes mellitus (T2DM) on AD patients has been described [1]. It was also reported that patients with T2DM increase the risk of AD [2]. Comparative efficacy and acceptability of antidiabetic agents for AD and mild cognitive impairment were also studied [3]. These findings indicated a pro-cognitive effect of antidiabetic agents in AD. In several laboratories, the effects of antiglycemic drugs were studied in disease models in rodents. Therefore, our research aimed to study the effect of the antidiabetic drug rosiglitazone in the form of a medicinal product Avandamet (AVD), on memory processes in young and old rats.

METHODS

All experimental procedures were following the European Commission Directive. Experiments were carried out on female Wistar rats aged 3 and 15 months (n=20). We used control groups and treated with AVD for each age. AVD was administered at a dose of 4 mg/kg per os for 1 hour before the experiment. Old rats were used as a model of AD [4]. The automated device and software developed by ourselves [5, 6] were used to register the individual components of sensorimotor reaction (SMR) conditioned food reflex. The behavior registrations based on infrared sensors' operation registered the moving rats' paw in the feeding chamber's hole. In the rats placed in the

main box, the skill, in response to a short sound, was developed to make search movements with a limb in a food feeder, reinforced after 2 seconds by feeding. The experiment's time course and several SMR time indicators were registered (described in the results). They allowed estimating CNS state, including memory working.

RESULTS AND DISCUSSION

During testing the food-getting reflex, we found that success was better in young rats. In the control group, the success of the conditioned reflex's manifestations in young rats was higher (91.6%) than in older ones (84.27%). In the older group, we observed greater variation of this indicator due to age-related difficulties in the extraction of information about conditioning stimuli. The conditioned reflex's success in old rats was increased (to 96,7%) under AVD to values of young group indicators. This parameter achieved 97.28% in young rats after AVD treatment. Thus, AVD substantially improved the success of the conditioned reflex in both age groups. The high success rate of the reflex (over 90%) may be the result of several factors: on the one hand - a reasonably strong link between the representations of the sensory and motor zones in the CNS. On the other - high food motivation. But, as already mentioned, since all animals were in the same conditions of food deprivation, the excitatory process's growth was caused by the action of the AVD.

We determined that while AVD did not affect the number of attempts required to pull food out of the food window (*RN*), the number of approaches to the trough window was significantly increased under this drug in both groups. This value was increased by 68,63% in young and 49,56% in old animals. It should be noted that the value was significantly higher in young rats than in old ones in control conditions. These experiments have shown that AVD enhances the CNS excitatory process, as evidenced by the increase in inter-stimulus reactions in both young and old rats.

Testing the SMR showed that in control experiments in young animals, search movements (rt) in an empty feeder after the conditional sound signal were twice as long as in old ones. The latter can be explained by the higher degree of CNS excitability characteristic of early life, rather than the high degree of food motivation, as rats of both age groups were previously on 24-hour food-deprived. AVD did not affect rt temporal characteristics in two groups

of animals (Fig.1). After treatment with AVD, the time between individual food extraction movements (TRr) and the total time spent on extracting food balls from the feeder (RT) was decreased. Thus, in young rats, the value of TRr decreased by an average of 34.24% and 15.95% ($p<0,05$), respectively. The RT was found to be higher in young rats than in old in control. This can be explained by the fact of the low level of CNS excitation in old rats compared with young promotes a more accurate motor response both in control and under AVD. The time RT decreased in young rats under AVD's influence was 14.7% and 14.4%, respectively.

We determined that while AVD did not affect the number of attempts required to pull food out of the food window (RN), this drug significantly increased the number of approaches to the trough window (RNIS) in both rats' groups. Thus, AVD increased the value RNIS - the number of animal approaches to the food window position between the sound signals during the interstimulus period. RNIS was increased by 68,63% in young and 49,56% in old animals. In old rats, AVD also caused a decrease in RD value (the mean time of the limb staying in the food cell during the single attempt of obtaining the food) by an average of 15.95%, whereas, in young animals, this was changed not significantly (Fig.2).

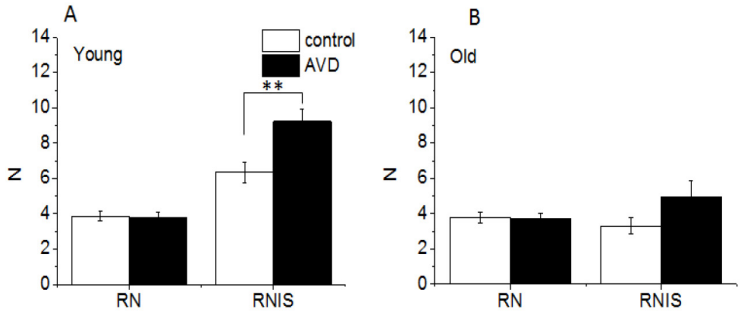

FIGURE 1: The average SMR values were recorded in control and under treatment with AVD in young (A) and old rats (B) are presented. The values are RN- the number of required attempts for getting food and RNIS – the number of approaches to the food window position between the sound signals during the interstimulus period. ** P< 0,01.

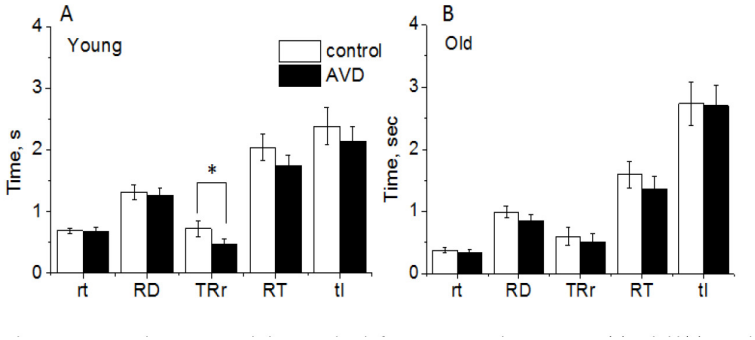

FIGURE 2: The average SMR values were recorded in control and after treatment with AVD in young (A) and old (B) rats. The values are rt - limb staying in the food window before supplying the food, RD - the mean time of the limb staying in the food cell during the single attempt of obtaining the food, TRr - the mean time between the attempts of obtaining the food, RT - total time of getting food from the feeder, tl - latent period, the time before the first the attempt of getting food after the sound stimulus. * P< 0,05.

The latent period of the sensorimotor response (tl) to the conditioned stimulus in control was more prolong in old animals than in young groups. But the speed of processing audio information by young animals was increased in the AVD group by 10.2%. In old rats, tl was not changed under the influence of AVD. Thereby, our data indicate that the antidiabetic drug AVD, which is used to treat T2DM, affects the CNS in young and old rats by increasing their excitability. AVD improved the manifestation of conditioned reflex in old rats (AD model).

ACKNOWLEDGEMENTS

This study was supported by National Academy of Sciences of Ukraine (NASU) SRN 0118U007344 and NASU grant for the development of priority areas of research SRN 0120U001281.

Keywords: Alzheimer's disease, Avandamet, behavior, conditioning reflex

REFERENCES

[1] Akter K, Lanza EA, Martin SA, Myronyuk N, Rua M, Raffa RB. Diabetes mellitus and Alzheimer's disease: shared pathology and treatment? Br J Clin Pharmacol. 2011;71:365-76.

[2] Janson J, Laedtke T, Parisi JE, O'Brien P, Petersen RC, Butler PC. Increased Risk of Type 2 Diabetes in Alzheimer Disease. Diabetes. 2004;53:474.

[3] Cao B, Rosenblat JD, Brietzke E, Park C, Lee Y, Musial N, et al. Comparative efficacy and acceptability of antidiabetic agents for Alzheimer's disease and mild cognitive impairment: A systematic review and network meta-analysis. Diabetes, obesity & metabolism. 2018;20:2467-71.

[4] Shineman DW, Basi GS, Bizon JL, Colton CA, Greenberg BD, Hollister BA, et al. Accelerating drug discovery for Alzheimer's disease: best practices for preclinical animal studies. Alzheimers Res Ther. 2011;3(5):28.

[5] Gorbachenko V, Chereda I, Vrublevsky S, Kruchenko J, Lukyanetz E. Development and testing of the experimental system for registration of food reflex in rats. Bulletin of Taras Shevchenko National University of KyivSeries: Radiophysics and Electronics. 2014;1/2:31-3.

[6] Gorbachenko VA, Kruchenko JO, Chereda IS, Lukyanetz EA. Measurements of the time parameters of conditioned food reflex in rats under memantin treatment with using of automatic registration system. Bulletin of Taras Shevchenko National University of KyivSeries: Radiophysics and Electronics. 2015;1:23-6.

Psychological stress alters cerebellum metabolome

Aikaterini Iliou[1,#], Angeliki-Maria Vlaikou[2,3,#], Markus Nussbaumer[2,3], Dimitra Benaki[1], Emmanuel Mikros[1], Evangelos Gikas[1,4]*, Michaela D. Filiou[2,3]*

[1]Section of Pharmaceutical Chemistry, Department of Pharmacy, School of Health Sciences, National and Kapodistrian University of Athens (NKUA), Athens, Greece
[2]Laboratory of Biochemistry, Department of Biological Applications and Technology, School of Health Sciences, University of Ioannina, Ioannina, Greece
[3]Biomedical Research Division, Institute of Molecular Biology and Biotechnology, Foundation for Research and Technology-Hellas (FORTH), Ioannina, Greece
[4]Section of Analytical Chemistry, Department of Chemistry, School of Science, National and Kapodistrian University of Athens (NKUA), Athens, Greece
**mfiliou@uoi.gr , vgikas@chem.uoa.gr*
[#]equal contribution

INTRODUCTION/MOTIVATION

Psychological stress and stress-related conditions constitute a major health challenge in modern societies. Although the brain circuits involved in emotional processing have been intensively studied (1), the involvement of cerebellum in stress responses and the molecular changes induced by stress exposure in this brain region still need to be elucidated. In the last decade, metabolomics has emerged as a powerful tool to investigate the underlying mechanisms of complex diseases, with a plethora of applications in neuropsychiatric and stress-related disorders (2). While alterations of the brain metabolome induced by stress exposure have been observed in hippocampus and other brain regions, stress effects on the cerebellum metabolome are not extensively investigated. Here, we explored the effects of acute stress exposure to the mouse cerebellum metabolome, after exposing mice to an acute stressor using the forced swim test (FST) paradigm.

METHODS

FST was used as an acute stressor in adult male mice. Each mouse was placed into a 2L glass beaker filled with tap water, so that it was impossible to reach the bottom of the beaker or escape and their behavior (time of struggling,

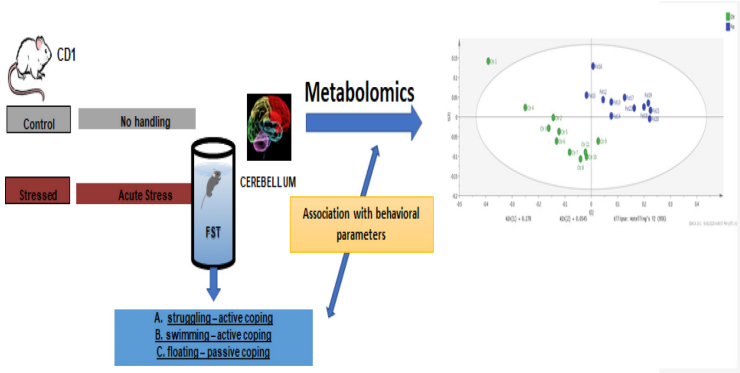

FIGURE 1: Schematic representation of the experimental workflow. Mice were subjected to FST acute stress, while unstressed mice were used as controls. Comparative 1**H** 1D NMR metabolomics analysis was performed in mouse cerebellum. Principal Component (PC) scores plot from PLS-DA model of 1D 1H NMR metabolomics data from the stressed (blue) versus control (green) group showed clear discrimination of the two groups, highlighting a role of cerebellum metabolome in stress response. Altered pathways between the stressed and control groups were identified and selected metabolites were further correlated with FST behavioral parameters.

swimming, floating and latency to the first floating event) was recorded for 6min. A Nuclear Magnetic Resonance (NMR)-based metabolomics approach was utilized to analyze the metabolomic profiles of the cerebellum between stressed and unstressed mice. A spectral bucketing of 0.001 ppm was applied on the 1D ^{1}H NMR data, which were further normalized to total intensity after removal of water region. The sum of normalized signal (bin) intensities corresponding to each annotated peak was used for relative quantitation of the assigned metabolite (3). Both univariate (parametric and non-parametric) and multivariate (Partial least squares regression-Discriminant analysis, PLS-DA) approaches were implemented, while pathway enrichment analysis of the significant metabolites was performed using Over-Representation Analysis (ORA) in order to highlight the affected biochemical pathways. Finally, we correlated acute stress-induced metabolite alterations and behavioral readouts, using the Spearman's test.

RESULTS AND DISCUSSION

PLS-DA analysis of stressed versus unstressed mice, showed a clear separation between the two groups, indicating that the cerebellum plays a still unexplored role in the pathogenesis of stress (Figure 1). In total, 47 known metabolites were annotated in mouse cerebella, 19 of which exhibited significant alterations between stressed and unstressed mice. These include metabolites related to purine/pyrimidine metabolism, amino acids, neurotransmitters and organic acids. Moreover, aspartate metabolism has emerged as the most prominently affected pathway, followed by the urea cycle, the purine metabolism and the glutamate metabolism. Among others, amino acid neurotransmitters exhibited strong association with FST behavioral parameters (swimming and/or floating).

Overall, our study was able to discriminate stressed from unstressed mice based on the cerebellum metabolome and reported alterations in metabolites mainly implicated in neurotransmission and major metabolic pathways, including energy and purine/pyrimidine metabolism. The present study demonstrates the implication of the cerebellum metabolome to stress responses, highlighting its previously unexplored involvement in stress-related disorders.

ACKNOWLEDGEMENTS

We thank Dr. Panagiotis Lekkas and the personnel of the University of Ioannina animal facility for expert animal care. This research is co-financed by Greece and the European Union (European Social Fund- ESF) through the Operational Programme «Human Resources Development, Education and Lifelong Learning 2014- 2020» in the context of the project "How mitochondria regulate stress? Let's ask metabolomics" (MIS 5047652).

Keywords: Forced Swim Test, Cerebellum, Metabolomics, Nuclear Magnetic Resonance, Acute stress, Mouse

REFERENCES

[1] Stressful newborn memories: Pre-conceptual, in utero, and postnatal events. Papadopoulou Z, Vlaikou AM, Theodoridou D, Markopoulos GS, Tsoni K, Agakidou E, Drosou-Agakidou V, Turck CW, Filiou MD, Syrrou M. Front Psychiatry 2019 10:220.

[2] A novel UHPLC-HRMS-based metabolomics strategy enables the discovery of potential neuroactive metabolites in mice plasma, following i.p. administration of the main Crocus sativus L. bioactive component. Karkoula E, Dagla IV, Baira E, Kokras N, Dalla C, Skaltsounis AL, Gikas E, Tsarbopoulos A, J Pharm Biomed Anal 2020 177:112878.

[3] Recommended strategies for spectral processing and post-processing of 1D 1H-NMR data of biofluids with a particular focus on urine. Emwas AH, Saccenti E, Gao X, McKay RT, Dos Santos VAPM, Roy R, Wishart DS, Metabolomics. 2018 14:31.

Facilitating the sharing of data analysis results through in-depth provenance capture

Cristiano A. Köhler[1,2]*, Danylo Ulianych[1], Richard C. Gerkin[3], Andrew P. Davison[4], Sonja Grün[1,2], Michael Denker[1]

[1]Institute of Neuroscience and Medicine (INM-6) and Institute for Advanced Simulation (IAS-6) and JARA Institute Brain Structure-Function Relationships (INM-10), Jülich Research Centre, Jülich, Germany

[2]Theoretical Systems Neurobiology, RWTH Aachen University, Aachen, Germany

[3]School of Life Sciences, Arizona State University, Tempe, AZ, USA

[4]Université Paris-Saclay, CNRS, Institut des neurosciences Paris-Saclay, Gif-sur-Yvette, France

c.koehler@fz-juelich.de

INTRODUCTION/MOTIVATION

Workflows for the analysis of electrophysiology activity data are typically composed of multiple steps. In the simplest case, these comprise several scripts executed in sequence, with several dependencies on data and parameters sets. However, workflows can become increasingly complex during the course of an analysis project: researchers can investigate alternative analysis paths or adjust the workflow components according to new hypotheses or additional experimental data. Considering this complexity and iterative nature, robust tools forming the basis of the workflow are necessary [1] to fully document the workflow and improve the reproducibility of the results. Provenance is the capture and characterization of data manipulations and parameters throughout the workflow [2]. This requires complete and self-explanatory descriptions of the generated data and a method to minimize the need for manually tracking the workflow execution, while maximizing the information content of the provenance trail.

While frameworks to structure the input data and associated metadata exist, a similar representation for the outputs of the analysis part of the workflow is missing. Moreover, workflow management systems capture limited provenance information, as they do not provide details about the functions used inside each analysis script. Finally, the workflow output lacks information pertaining to its generation.

Therefore, to satisfy the requirements of a practically useful provenance trail, existing tools must be improved to implement a data model that captures analysis outputs and their detailed provenance and, ultimately, represents the analysis and its results in accordance with the FAIR principles [3].

METHODS

We focus on two open-source tools for the analysis of electrophysiology data developed in EBRAINS. The Neo (RRID:SCR_000634) framework provides an object model to standardize neural activity data acquired from different sources [4]. Elephant (RRID:SCR_003833) is a Python toolbox for analyses of electrophysiology data [5]. We implemented two synergistic prototype solutions that extend the functionality of these tools with respect to (i) the systematic standardization of analysis results and (ii) the automatical capture of provenance information during the execution of a Python analysis script. Both solutions are under development and being incorporated as new functionality into the Elephant package.

The first solution represents the output of Elephant functions in a data model inspired by Neo. Objects for specific analysis results (e.g., a time histogram) are inherited from a base Python class that supports storage of provenance information such as timestamps and unique identifiers.

The second solution is a provenance tracker implemented as a function decorator. It identifies the objects that are input to and output from the function, creating unique hashes. It also captures timestamps, statement code lines, and additional function parameters. Extended dependencies between objects (such as indexing and attributes) are mapped using the analysis of the abstract syntax tree (AST) obtained from the code.

RESULTS AND DISCUSSION

The solutions presented here capture provenance during the analysis of electrophysiology data with minimal user intervention. The data objects support a hierarchical standardization of the output of Elephant functions (e.g., a time histogram is a specific type of histogram) while encapsulating all the information about the generation of an analysis output. Therefore, these objects can be easily re-used or shared. This will eliminate the need to

manually annotate the output of the analysis with corresponding parameters. The new objects also seamlessly extend the functionality of the Neo classes currently used as output of Elephant functions, and can be integrated into the existing code bases with minimal disruption.

Additionally, we describe how to capture provenance information throughout the Python analysis script using decorators. These track the Elephant and user-defined functions used in the script while mapping the inputs to the outputs. We demonstrate how the captured information can be used to build a graph showing the steps followed in the script, and that can be stored as metadata. The analysis results obtained with or without the use of the two solutions are compared, highlighting the potential benefits for reproducibility and data re-use.

The provenance tracker and the standard data objects capture and manage distinct aspects of the provenance information. In the end, both solutions are complementary. On one hand, the decorator is focused on building the provenance trail and the relationships between the different steps of the analysis within the script. On the other hand, the standard objects focus on the representation of the data, standardizing information that is similar among the outputs of different functions together with the storage of the relevant provenance information as metadata. Ultimately, those two developments aim to increase data interoperability and reusability in accordance with the FAIR principles.

ACKNOWLEDGEMENTS

This work was performed as part of the Helmholtz School for Data Science in Life, Earth and Energy (HDS-LEE) and received funding from the Helmholtz Association of German Research Centres. This project has received funding from the European Union's Horizon 2020 Framework Programme for Research and Innovation under Specific Grant Agreements No. 785907 (Human Brain Project SGA2) and 945539 (Human Brain Project SGA3), and by the Helmholtz Association Initiative and Networking Fund under project number ZT-I-0003. We thank Prof. Stefan Decker for valuable input.

Keywords: provenance, workflows, data analysis, neuroscience, electrophysiology, Python

REFERENCES

[1] Denker, M. and Grün, S. (2016). Designing Workflows for the Reproducible Analysis of Electrophysiological Data. In Brain-Inspired Computing, Amunts, K. et al., eds. (Cham: Springer International Publishing), pp. 58-72.

[2] Ragan, E.D. et al. (2016). Characterizing Provenance in Visualization and Data Analysis: An Organizational Framework of Provenance Types and Purposes. IEEE Transactions on Visualization and Computer Graphics. 22(1):31–40.

[3] Wilkinson, M.D. et al. (2016). The FAIR Guiding Principles for scientific data management and stewardship. Scientific Data 3, 160018.

[4] Garcia, S. et al. (2014) Neo: an object model for handling electrophysiology data in multiple formats. Frontiers in Neuroinformatics 8:10.

[5] http://python-elephant.org

Dynamics of hippocampal activity patterns during spatial learning

Mengmeng Li[1,2], Jiantao Fan[1,2], Shuguan Cheng[1,2], Zhigang Shang[1,2]*, Hong Wan[1,2]*

[1]School of Electrical Engineering, Zhengzhou University, Zhengzhou, China
[2]Henan Key Laboratory of Brain Science and Brain-Computer Interface Technology, Zhengzhou, China
**zhigang_shang@zzu.edu.cn, wanhong@zzu.edu.cn*

INTRODUCTION/MOTIVATION

The hippocampus (Hp) has been proved to be mainly related to spatial learning [1]. Hippocampal neurons are highly adaptive to process and encode the spatial-related information, indicating the crucial role of Hp for spatial learning [2]. Previous studies have shown that the avian Hp is functionally homologous with the mammals [3], which plays an important role in path planning and adjustment of spatial learning process [4][5]. However, the dynamics of hippocampal activity patterns during spatial learning is still unclear. In this study, we explored the neural response patterns of the pigeon recorded from Hp during a goal-directed spatial learning task.

METHODS

In our experiments, the pigeons were trained to carry out a goal-directed spatial learning task in a maze, as shown in Figure 1. At the beginning of the trial, the hamper was opened to provide food at the goal location, and the pigeons were trained to learn a preferred path to the goal. If the pigeon arrived at the goal, this trial was recorded as a correct one. After enjoying the food reward provided in the food hampers, they were trained to go back to the starting position to start the next trial. When a pigeon could reliably perform the trial through a preferred path, in which more than 80% of the total trail numbers were corresponding to the same one path on two consecutive days, it was considered that the pigeon finished the learning task. The infrared detectors distributed on all of the pathlets along the paths were used to define the beginning time and end time for signal segmentation. The behavioral data of the pigeons were recorded by the observation camera placed on the

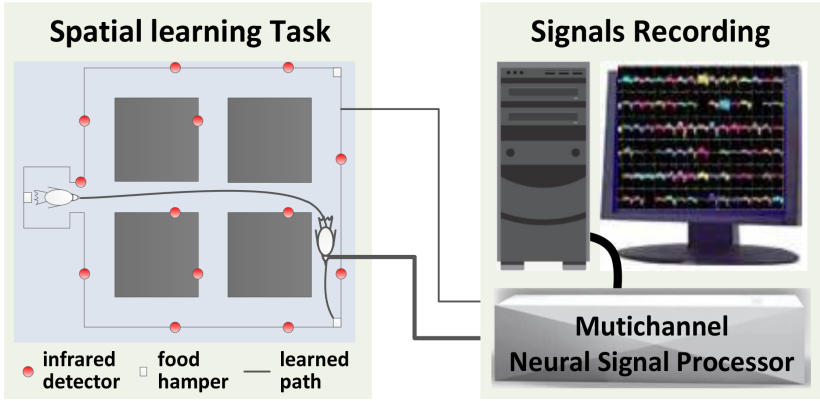

FIGURE 1: Diagram of the maze apparatus for pigeons and experiment procedures.

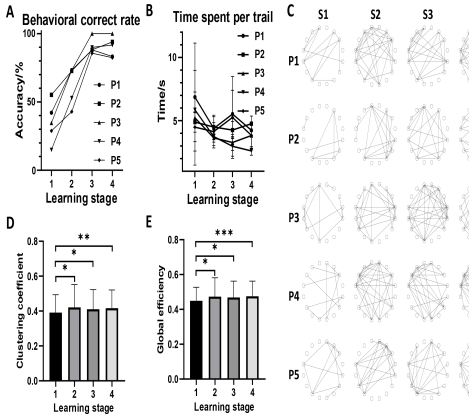

FIGURE 2: Dynamics of behavioral data and hippocampal activity patterns during spatial learning of five pigeons. (**A**) behavioral response accuracy, (**B**) time spent from the starting position to the goal, (**C**) binarized FNs, in which each hollow circle indicates a channel, (**D**) topological characteristic clustering coefficient of FN (mean of all pigeons), (**E**) topological characteristic global efficiency of FN (mean of all pigeons). Statistically significant were indicated by p value as follows:*p < 0.05, **p < 0.01, ***p < 0.001.

ceiling during spatial learning, to calculate the behavioral response accuracy and obtain the time the pigeons spent from the starting position to the goal. Local field potential (LFP) signals in the Hp of the pigeons were acquired and preprocessed. Power spectral density (PSD) analysis, time-frequency (TF) analysis based on wavelet transform, and functional network (FN) analysis based on coherence coefficient were carried out to explore the temporal dynamics of neural patterns during spatial learning.

RESULTS AND DISCUSSION

For all of the sessions from five pigeons, the behavioral correct rate and the average time the pigeons spent from the starting position to the goal under different learning stages were calculated. The results are shown in Figure 2 (A) and (B). The results reveal that the total duration from the starting position to the goal gradually decreases along with the improvement of the behavioral correct rate. To explore the neural activity dynamic patterns during spatial learning further, we calculated the coherence coefficients of the LFPs between all channels in Hp and visualized the corresponding binarized FNs in the theta band during different learning stages, which are shown in Figure 2 (C). It can be seen that the functional connection in Hp becomes denser along with spatial learning. It suggests that the spatial learning process modulates the dynamic network connection pattern in Hp. For further quantitative analysis, the topological characteristics of FN including clustering coefficient and global efficiency are analyzed, and the results are shown in Figure 2 (D) and (E). Both of these two topological characteristic parameters show a rising trend along with the advancement of the learning process.

This current study focuses on the Hp of the pigeon, which is the most concerned target brain region in the study of spatial learning mechanism and explored the dynamics of hippocampal activity patterns during spatial learning. We can conclude that the spatial learning process modulates the dynamic neural pattern of Hp. The dynamic changes of brain network connectivity in Hp during spatial learning may contribute to the understanding of the potential mechanism of spatial cognition. On the other hand, Hp is not the solely responsible region for complex spatial processing independently. Is there any similar or different phenomenon in other spatial-related regions, and the dynamic neural connection patterns between the regions contained in a wider local network remain to be further analyzed and explored.

Keywords: dynamics, hippocampus, spatial learning, pigeon

REFERENCES

[1] Ólafsdóttir HF, Bush D, Barry C (2018). The role of hippocampal replay in memory and planning. Current Biology 28: R37-R50.

[2] O'Keefe J, Nadel LM (1978). The hippocampus as a cognitive map. Clarendon Press, Oxford.

[3] Herold C, Schloemer P, Mafoppa-Fomat I et al. (2019). The hippocampus of birds in a view of evolutionary connectomics. Cortex 118: 165-187.

[4] Kahn MC, Bingman VP (2009). Avian hippocampal role in space and content memory. European Journal of Neuroscience 30: 1900-1908.

[5] Mouritsen H, Heyers D, Güntürkün O (2016). The neural basis of long-distance navigation in birds. Annual Review of Physiology 78: 133-154.

Behavioural characteristics of perceptual inference in a multimodal associative learning paradigm

Zsófia Pálffy[1]*, Kinga Farkas[1,2], Gábor Csukly[2], Bertalan Polner[1]*****

[1]Department of Cognitive Science, Budapest University of Technology and Economics, Budapest, Hungary
[2]Department of Psychiatry and Psychotherapy, Semmelweis University, Budapest, Hungary
**zsofiapalffy@edu.bme.hu*
***farkas.kinga@edu.bme.hu*
****bpolner@cogsci.bme.hu*

INTRODUCTION/MOTIVATION

The Bayesian brain theory states that during perception the brain performs inference when it combines sensory information with prior expectations, all being weighted by their uncertainty [1]. It has been shown that priors influencing perception of ambiguous stimuli can be shaped with associative learning [2]. However, the differential effect of auditory vs. visual associative cues on visual motion perception is still to be investigated. Furthermore, the test-retest reliabilities of variables derived from behavioural tasks are highly variable in the literature [3], and evaluation of these appears especially under-represented in contemporary perceptual inference research.

METHODS

We measured healthy individuals' (N=29; 14 men, mean[SD] age = 26.6[5.5] years) performance on a perceptual inference task twice with a one-week delay (640 trials each). They indicated the perceived direction of illusory motion of dot pairs (see Figure 1A). A visuo-acoustic cue preceded the target stimulus and probabilistically predicted the direction of the motion. In 30% of the trials, motion direction was ambiguous, and in half of these trials, the auditory and the visual dimension of the cue predicted opposing directions (see Figure 1B). Cue-stimulus contingency could change every 40 trials.

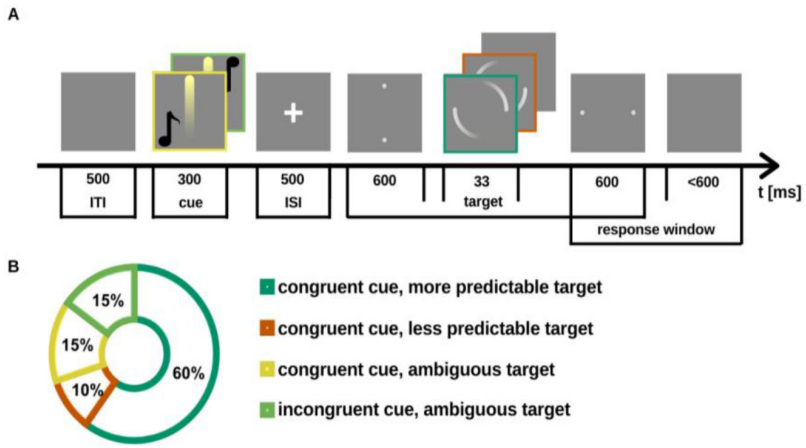

FIGURE 1: Experimental design (**A**) and distribution of conditions in every 40 trials (**B**). Conditions differ in the availability of sensory information, which affects the likelihood: on unambiguous trials a motion illusion sets the likelihood probability of the showed tilt close to 1, whereas on ambiguous trials there is no motion illusion, setting the likelihood probability of each tilt close to 0.5. Since most trials follow a rule, after the cues were presented, the prior probability of the direction it is associated with increases. But unambiguous trials differ in regularity, and it affects the confidence in the learnt priors: more predictable targets are expected from the priors, they increase the precision, whereas less predictable targets are unexpected, they decrease the precision. As their mind unconsciously infers the posterior probability of each direction, they indicate the perceived direction which was the most probable. We hypothesise that reaction time indicates confidence (posterior probability extremely above chance level).

RESULTS AND DISCUSSION

Slower responses to less predictable, relative to more predictable non-ambiguous stimuli and the increased rate of cue-congruent decisions on ambiguous trials showed the impact of associative learning on perceptual decisions. Importantly, on ambiguous trials participants made more decisions congruent with the prediction of the acoustic dimension, when the visual and the auditory dimensions of the cue predicted conflicting directions of motion. Furthermore, all the above effects had substantial inter-individual variability which showed high test-retest reliability (rs > 0.6, see Figure 2).

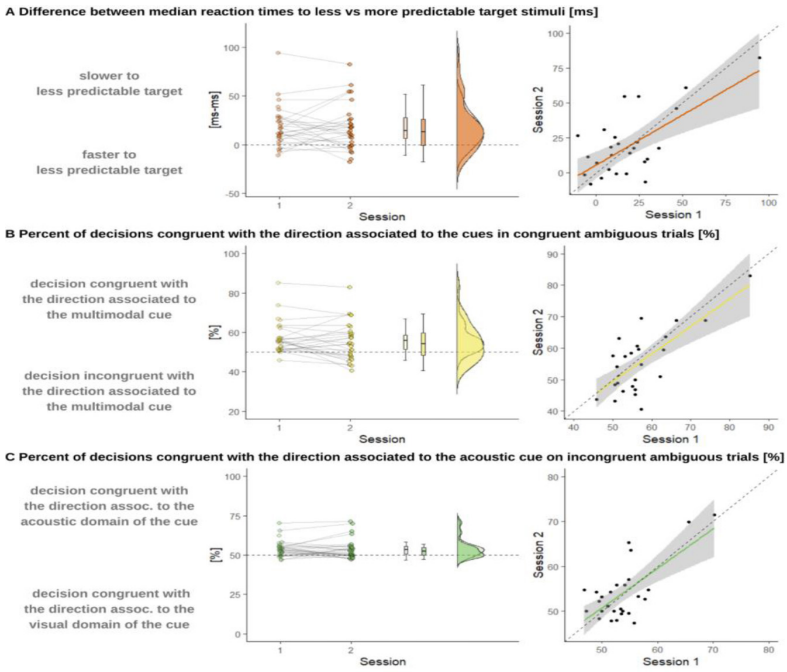

FIGURE 2: Behavioural results. [left] On the left, each dot represents a participant, values from each session connected along the x axis, a boxplot (median, 50% CI) is shown in the middle, and the distribution for each session can be seen on the right. [right] Each dot represents a participant's performance in session 1 and 2 on the x and the y axis, respectively. Trend line shows linear fit with 95% confidence interval and the dashed line indicates the hypothetical perfect correlation. [**A**] Slowing down to unexpected tilts. On the y axis, median reaction times differences are presented when cues were followed by less vs more predictable tilting illusion. If there was no difference between these conditions, dots were mostly around 0 ms (level shown with dashed line). Test-retest stability was high. [**B**] Bias towards direction associated with cue. Along the y axis, we present the percent of decisions congruent with the direction associated with the cues under ambiguity and after congruent cues. Associative learning influenced perceptual inference, as participants made more perceptual decisions consistent with the associative cues (above-chance level [50% shown with dashed line]). [**C**] Bias towards direction associated with tone. Along the y axis, we present the percent of decisions consistent with the direction associated with the acoustic cue in ambiguity after incongruent cues (where the acoustic and visual cues were associated with different directions). Auditory-visual associative learning slightly dominantly influenced perceptual inference, as participants made more perceptual decisions consistent with the auditory cue (above-chance level [50% shown with dashed line]).

Overall, priors based on auditory information seem to have a stronger weight during the perception of illusory visual motion, although the data suggests large differences in perceptual learning and/or decision making. Whether the characteristics of visual vs. auditory processing, attentional processes or encoding the uncertainty of the visual modality caused these behavioural effects, is still up to discussion. Beyond follow-up behavioural experiments, computational modelling combined with neuroimaging could allow testing further hypotheses regarding the potential mechanisms.

ACKNOWLEDGEMENTS

B.Polner's work was funded by BME Biotechnology Project (FIKP-BIO) and NKFI/OTKA K 12859.

Keywords: perceptual inference, Bayesian brain theory, test-retest reliability

REFERENCES

[1] Friston, K. (2010). The free-energy principle: A unified brain theory? *Nature Reviews Neuroscience*, *11*(2), 127–138. https://doi.org/10.1038/nrn2787

[2] Weilnhammer, V. A., Stuke, H., Sterzer, P., & Schmack, K. (2018). The Neural Correlates of Hierarchical Predictions for Perceptual Decisions. Journal of Neuroscience, 38(21), 5008–5021. https://doi.org/10.1523/JNEUROSCI.2901-17.2018

[3] Enkavi, A. Z., Eisenberg, I. W., Bissett, P. G., Mazza, G. L., MacKinnon, D. P., Marsch, L. A., & Poldrack, R. A. (2019). Large-scale analysis of test–retest reliabilities of self-regulation measures. Proceedings of the National Academy of Sciences, 116(12), 5472-5477.

An adaptation aftereffect paradigm to investigate the social impact of built environments: Behavioural and electrophysiological evidences in body judgment tasks in virtual reality

Paolo Presti[1,2], Stefano Lenzi[1], Davide Ruzzon[3,4], Pietro Avanzini[1], Fausto Caruana[1], Giovanni Vecchiato[1*]

[1]Institute of Neuroscience, National Research Council of Italy, Parma, Italy
[2]Department of Medicine and Surgery, University of Parma, Parma, Italy
[3]University IUAV, Venezia, Italy
[4]TUNED, Lombardini22 s.p.a., Milan, Italy
**giovanni.vecchiato@in.cnr.it*

INTRODUCTION

Built environments play a primary role in our life, affecting emotional states and perceptual experience [1]. Evaluating how different architectures shape our ability to perceive the emotional state of other people is fundamental to understand the social role of built environments. Indeed, depending on such perception, we constantly modulate several aspects of our social life such as our tendency to engage interactions, or for example the naturalness with which we talk with other people [2].

The project we are currently working on aims to demonstrate that the experience of different architectures particularly interacts with our capability to judge emotional body expressions, which ultimately affects our tendency to engage social interactions. The hypothesis is that architectures and emotional body expressions share some perceptual mechanisms involving sensorimotor networks [3], thus causing the evaluation of emotional body expressions to be biased by the surrounding architecture. Indeed, as listening to increasing or decreasing notes influences the following perception of dot's vertical movements [4], dynamically experiencing the modulation of architectural features would interact with the following judgment of emotional body expressions. In order to deepen such interaction, we evaluate how the sensorimotor activity elicited during the experience of virtual architectures is related to the adaptation aftereffect on the following judgement of emotional body expressions.

Arousal, valence, and approach-avoidance tendency will be considered as affective dimensions to characterize both the virtual environments and the emotional body expressions as well as the adaptation effect generated by the architecture. We assume that when architectures convey opposite level of arousal, valence, and approach-avoidance tendency compared to the target body expressions, subjects will be facilitated in judging the affect dimension of the body expression [5]sad, anger and fear. Indeed, considering for instance a low arousing adapting stimulus, the following target stimulus will be perceived as more arousing. Thus, in such experimental condition, high arousing body expressions are expected to be recognized easier than low arousing body expression. Behavioural responses and electroencephalographic (EEG) correlates such as event related potential (ERP) and sensorimotor cortical rhythms will reflect the entity of the adaptation effect. Specifically, latency and amplitude of the N170 ERP along with mu rhythm suppression will be investigated to evaluate the perception of emotional body expressions mediated by several adapting architectures [3] [6] [7].

METHODS

A head mounted display (HMD) is used to represent highly immersive scenarios in which participants make the ecological architectural experience. The experimental design is based on two different sets of stimuli, virtual architectures and emotional body expressions (Fig. 1).

Architectural environments were designed to manipulate features such as form (height, width, window) and texture (cold, warm) in a combination of three concatenated rooms. In a validation study, subjects will rate each perceived architecture, after having virtually crossed it, in terms of arousal, valence and approach-avoidance.

In order to create virtual emotional body expressions, the EMILYA database [8] has been exploited. Virtual body postures were created on the basis of kinematic and body features, such as speed of the movement and leaning of the trunk, which are respectively correlated with the dimensions of arousal and valence. These body postures were validated asking subjects to rate them in terms of arousal, valence and approach-avoidance.

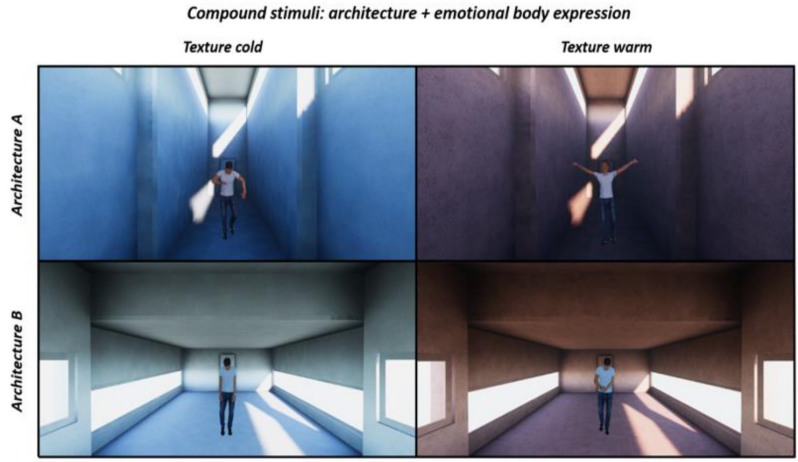

FIGURE 1: Example of four different architechers and emotional body expressions Each virtual enviranment varies in eaither forms (rows) or texture (columns). An avatar conveying different level of arousal through its body posture (high arousal in the upper panels, low arousal in the bottom pannel) is presented within the thired room after the virtual exploration of architechture.

The following behavioural experiment has been designed to test the adaptation aftereffect generated by the architectural experience on the judgement of emotional body expressions. Each trial (Fig. 2) consists in representing firstly the architectural adapting stimulus where the subject experience the environment through a first-person moving camera crossing the first two rooms. As it stops, the avatar appears in front of the subject who will be asked to score its bodily arousal, valence and the approachability by means of visual analogue scales.

The results of the behavioural experiment will set the basis for the electrophysiological study. EEG respons4 behavioural study. We will analyse ERP and cortical rhythms through time-frequency decomposition of the scalp EEG signal across all the experimental conditions.

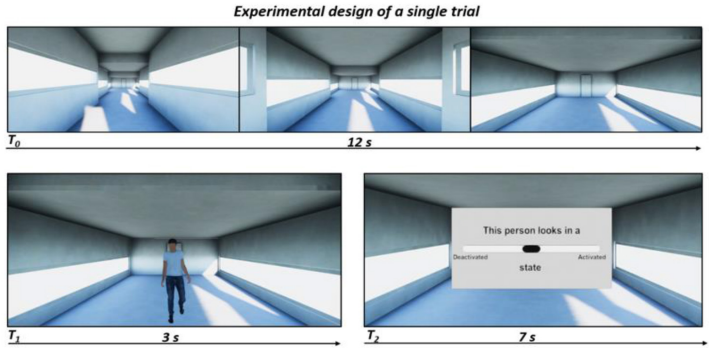

FIGURE 2: scheamitic representation of a single trial. upper panels: architectural adapting stimmulus. from the left right side, each panel represents respectivly the field of view at the start at the middle and at the end of the virtual cross of architehure. The adopting stimulus starts at T_0 and end at T_1 after 12 seconds. Bottom left panel: target stimulus. At time T_1 an emotional body expression assumed by a virtual character is presented for 3 seconds from T_1 to T_2. Bottom right panel: at time T_2 a rating scale is shown with which subjects are asked to judge the arousal scale is shown with which subjects are asked to judge the arousal state of the avator within 7 seconds.

EXPECTED RESULTS

Thanks to the validation studies, both architectures and emotional body expressions will be clustered in groups conveying different levels of arousal, valence and approach-avoidance tendency.

We expect that results from the behavioural experiments will highlight the adaptation effect generated by the architecture on the judgement of the following emotional body expression. Thus, when the architectural adapting stimulus convey a specific level of either arousal, valence or approach-avoidance tendency, the judgment of the following target body stimulus will be biased in the opposite direction, modifying subject's behavioural outcome. In fact, in a first pilot experiment we found out that high arousing architectures led to perceive the following target stimulus as less arousing [7].

Differences in the time-frequency characteristics of the EEG data are expected to arise during the judgement of the emotional body expressions, depending on the adapting architectural experience. Decreased latencies and increased

amplitudes of N170 are expected to arise when the architecture and the emotional body expression convey opposite levels of arousal, valence or approach-avoidance tendency. Moreover, we expect to find an increased sensorimotor mu rhythm suppression in correspondence of those experimental conditions which facilitate subjects in judging the emotional body expressions, such as conditions where the adapting and the target stimulus convey opposite levels concerning the affective dimensions.

DISCUSSION

The resulting behavioural and neural findings will provide a deeper comprehension concerning the perception of architectures and emotional body expressions, thus shedding light on how the architectural experience modulates our perception of the other's emotional state and thus affecting social behaviours. Such findings will allow the creation of spaces where people are facilitated in understanding each other, thus making our everyday social life better, considering the amount of time that we spend within built environments. Possible applications concern the design of places where social activities are encouraged, like schools or recreational buildings. Overall, this knowledge will set the basis for a new approach to design, considering people and their well-being at the core of the process leading to the creation of healthy environments.

Key words: virtual reality, architecture, body expressions, emotions, EEG

REFERENCES

[1] A. Coburn *et al.*, «Psychological and neural responses to architectural interiors», *Cortex*, vol. 126, pagg. 217–241, mag. 2020, doi: 10.1016/j.cortex.2020.01.009.

[2] G. A. Van Kleef, «How Emotions Regulate Social Life: The Emotions as Social Information (EASI) Model», Curr Dir Psychol Sci, vol. 18, n. 3, pagg. 184–188, giu. 2009, doi: 10.1111/j.1467-8721.2009.01633.x.

[3] G. Rizzolatti e C. Sinigaglia, «The mirror mechanism: a basic principle of brain function», Nat Rev Neurosci, vol. 17, n. 12, pagg. 757–765, 2016, doi: 10.1038/nrn.2016.135.

[4] S. C. Hedger, H. C. Nusbaum, O. Lescop, P. Wallisch, e B. Hoeckner, «Music can elicit a visual motion aftereffect», Atten Percept Psychophys, vol. 75, n. 5, pagg. 1039–1047, lug. 2013, doi: 10.3758/s13414-013-0443-z.

[5] S. Halovic, C. Kroos, e C. Stevens, «Adaptation aftereffects influence the perception of specific emotions from walking gait», Acta Psychologica, vol. 204, pag. 103026, mar. 2020, doi: 10.1016/j.actpsy.2020.103026.

[6] B. de Gelder, H. K. M. Meeren, R. Righart, J. van den Stock, W. A. C. van de Riet, e M. Tamietto, «Chapter 3 Beyond the face: exploring rapid influences of context on face processing», in Progress in Brain Research, vol. 155, S. Martinez-Conde, S. L. Macknik, L. M. Martinez, J.-M. Alonso, e P. U. Tse, A c. di Elsevier, 2006, pagg. 37–48.

[7] G. Vecchiato, G. Tieri, A. Jelic, F. De Matteis, A. G. Maglione, e F. Babiloni, «Electroencephalographic Correlates of Sensorimotor Integration and Embodiment during the Appreciation of Virtual Architectural Environments», Front. Psychol., vol. 6, 2015, doi: 10.3389/fpsyg.2015.01944.

[8] N. Fourati e C. Pelachaud, «Perception of Emotions and Body Movement in the Emilya Database», IEEE Transactions on Affective Computing, vol. 9, n. 1, pagg. 90–101, gen. 2018, doi: 10.1109/TAFFC.2016.2591039.

[9] P. Presti, D. Ruzzon, S. Lenzi, F. Caruana, G. Rizzolatti, P. Avanzini, G. Vecchiato. «The relationship between architecture and body expression: a pilot behavioral study in virtual reality». Academy of Neuroscience for Architecture, September 17–19 2020, Salk Institute, San Diego, La Jolla.

Resilience and emotional regulation dynamics during the COVID-19 pandemic in a general population sample

Levente Rónai[1]*, Bertalan Polner[1]

[1] *Department of Cognitive Science, Budapest University of Technology and Economics, Budapest, Hungary*
**lronai@cogsci.bme.hu*

INTRODUCTION AND MOTIVATION

The spread of the COVID-19 pandemic and the associated health, economic, and social adversities have been exerting a significant impact on emotional functioning and may pose a serious threat to mental health. Emotions are complex, dynamic patterns of subjective experiences, physiological and neural responses and behaviour and they are intimately associated with cognition, social functioning and mental health[1]. Yet, little is known about temporal patterns and regulation of emotional states in response to serious global crises such as the COVID-19 pandemic. Previous research has suggested that emotional inertia and instability may indicate maladaptive emotional reactions[2]. First, emotional inertia is said to occur when emotional states remain relatively unchanged for a longer time period and it may reflect the lack of flexible emotion regulation. Emotional inertia can be inferred from the autocorrelation of emotional state time series. Second, emotional instability refers to recurrent, dramatic changes in emotional states and it can be inferred from autocorrelation as well as from indicators of variability of time series (e.g. variance or Mean Square Successive Difference; MSSD). The study of emotional inertia and instability requires intensive time series data that can be collected with Experience Sampling Method (ESM). This methodological approach not only reduces recall biases in self-report but it also offers higher ecological validity since it allows assessment of participants' momentary subjective states across longer periods of time within their natural environments[3].

The goal of this study is to test whether resilience and emotion regulation strategies predict the development of depressive and anxiety symptoms in response to stressors associated with the COVID-19 pandemic. Furthermore,

we expect that such effects are mediated by time series-derived indicators of emotion regulation problems (emotional inertia and instability).

METHODS

Hungarian speaking participants from the general population were recruited through calls posted on social media and in the press. The study started with a cross-sectional assessment of relatively stable characteristics such as trait-level affective functioning[4], cognitive emotion regulation strategies[5], neuroticism[6], resilience[7] and behavioural inhibition/activation[8]. The cross-sectional questionnaires were completed by 304 individuals ($N_{Females}$ = 239, M_{Age} = 37.9, Med_{Age} = 35, SD_{Age} = 13).

Then, participants could enter the ESM phase in which they could take part for a maximum of 28 days. Note that participation was voluntary, and some respondents opted out at this point. Every day, participants were requested to respond to short surveys inquiring about their momentary emotional states and emotion regulation strategies (notifications were emailed every second hour between 8 AM and 10 PM). Every third day, participants were asked to complete surveys measuring symptoms of depression and anxiety[9]. In addition, exposure to stressors and availability of support during the previous 3 days were assessed with a checklist (which included relatively objective descriptions of financial, social and health-related events e.g. loss/growth of income, pastime with significant others, workplace conflict, unpaid bills, significant deterioration in own/significant other's health). After the cross-sectional assessment, a large, dominantly female but otherwise demographically heterogeneous sample of individuals (N = 275, $N_{Females}$ = 220, M_{Age} = 39.21, Med_{Age} = 38, SD_{Age} = 13.57) decided to take part in the ESM phase. On average, participants responded to the ESM surveys for 16.78 days (Med = 19, SD = 16.78) and on average, they returned 38.2% (Med = 37.5 SD = 20.32, $Total_{Returned}$ / $Total_{Sent}$ = 43%, $N_{Returned}$ = 15 823) of the surveys they received before their participation ended. Data collection took place between 2020-05-18 and 2020-07-28.

RESULTS AND DISCUSSION

During the ESM phase, participants reported varying exposure to stressors (*M* = 1.1, *SD* = 1.23, *Min* = 0, *Max* = 7) and availability of support (*M* = 0.98, SD = 0.92, *Min* = 0, *Max* = 4), allowing the investigation of their effects on emotional dynamics and mental health. Furthermore, participants reported varying levels of depression (*M* = 15.46, *SD* = 12.68, *Min* = 0, *Max* = 49, theoretical range: 0-52) and anxiety (*M* = 3.61, SD = 3.944, *Min* = 0, *Max* = 19, theoretical range: 0-20).

The study may shed light on factors influencing how humans react to extremely unpredictable and threatening changes in the environment (i.e. the pandemic and its consequences in daily life). Moreover, using ESM data to estimate indirect parameters of temporal patterns in emotional reactions can provide valuable insights for neuroscience as well. Our findings based on intensive self-reported data may facilitate generating hypotheses regarding how cognitive control mechanisms moderate the effect of intensive external stressors on emotions and mental health under real-life circumstances. As neurocognitive and self-reported measurements of emotional functioning take place on different levels of scientific examination, future studies should clarify how between- and within-person differences of objectively vs. subjectively assessed emotion regulation are mapped to each other.

ONGOING PLANNED WORK

In this unique and rich dataset, we use multilevel models to test our hypotheses (analyses are in progress at the time of submission). We predict that emotional inertia and emotional instability will strengthen in response to stressors, will precede changes in mental health, and will be related to trait resilience, neuroticism and behavioural avoidance. Furthermore, we will evaluate age and gender differences.

ACKNOWLEDGEMENTS

BP was supported by BME Biotechnology Project (FIKP-BIO) and NKFI/OTKA K 12859.

Keywords: COVID-19, emotion regulation, emotional instability, emotional inertia, individual differences, longitudinal study, ESM

REFERENCES

[1] Russell, J. A. (2003). Core affect and the psychological construction of emotion. Psychological Review, 110(1), 145–172. https://doi.org/10.1037/0033-295X.110.1.145

[2] Trull, T. J., Lane, S. P., Koval, P., & Ebner-Priemer, U. W. (2015). Affective Dynamics in Psychopathology. Emotion Review : Journal of the International Society for Research on Emotion, 7(4), 355–361. https://doi.org/10.1177/1754073915590617

[3] Myin-Germeys, I., Oorschot, M., Collip, D., Lataster, J., Delespaul, P., & van Os, J. (2009). Experience sampling research in psychopathology: Opening the black box of daily life. Psychological Medicine, 39(9), 1533–1547. https://doi.org/10.1017/S0033291708004947

[4] Watson, D., Clark, L. A., & Tellegen, A. (1988). Development and validation of brief measures of positive and negative affect: The PANAS scales. Journal of Personality and Social Psychology, 54(6), 1063–1070. https://doi.org/10.1037/0022-3514.54.6.1063

[5] Garnefski, N., Kraaij, V., & Spinhoven, P. (2001). Negative life events, cognitive emotion regulation and emotional problems. Personality and Individual Differences, 30(8), 1311–1327. https://doi.org/10.1016/S0191-8869(00)00113-6

[6] John, O. P., Robins, R. W., & Pervin, L. A. (2008). Handbook of Personality, Third Edition: Theory and Research. Guilford Press.

[7] Connor, K. M., & Davidson, J. R. T. (2003). Development of a new resilience scale: The Connor-Davidson Resilience Scale (CD-RISC). Depression and Anxiety, 18(2), 76–82. https://doi.org/10.1002/da.10113

[8] Carver, C. S., & White, T. L. (1994). Behavioral inhibition, behavioral activation, and affective responses to impending reward and punishment: The BIS/BAS Scales. Journal of Personality and Social Psychology, 67(2), 319–333. https://doi.org/10.1037/0022-3514.67.2.319

[9] Derogatis, L. R., & Cleary, P. A. (1977). Confirmation of the dimensional structure of the scl-90: A study in construct validation. Journal of Clinical Psychology, 33(4), 981–989. https://doi.org/10.1002/1097-4679(197710)33:4<981::AID-JCLP2270330412>3.0.CO;2-0

Effects of memantine on behavioral indices of rats in the open field

Yu. M. Tyshchenko*, E. A. Lukyanetz

Bogomoletz Institute of Physiology, NASU, Kyiv, Ukraine
**u.tishenko@biph.ua*

INTRODUCTION

Examination of the mechanism of action of pharmacological agents necessarily includes estimation of the effects of these drugs on the behavior of animals in model experiments. The open field test is one of the most extensively used methods for the evaluation of behavioral characteristics. Long-lasting observations in the open field allow researchers to estimate the dynamics of phenomena related to stress and anxiety and interaction of these manifestations with the processes of adaptation/habituation [1, 2]. Memantine is a drug extensively used at present in the therapy of diseases related to dementias of one genesis or another (including Alzheimer's disease). This drug is widely used in clinics; its effects have been tested on very extensive samplings of patients and control subjects. At the same time, information on the effects of memantine on the behavior of animals in model experiments is clearly insufficient. Our earlier studies of changes in the motor behavior of rats induced by memantine demonstrated that the respective effects can be rather significant [3–5].

METHODS

Experiments were carried out on ten three-month-old female Wistar rats (body mass 155 to 220 g). Rats were kept under standard vivarium conditions Animals were divided into control and experimental groups (n = 5 in each). For 5 days, control rats received perorally an aqueous sucrose solution each day, while experimental animals were treated with an aqueous solution of memantine hydrochloride (20 mg/kg; officinal form Akatinol Memantine). Rats were tested in the open field 1 hour after introduction of the drug. The intensity of horizontal motor activity (HA, number of crossed squares), that of

vertical motor activity (VA, number of rearings with support on the arena wall or without such support), index of general motor activity (sum of the HA and VA indices), number of goings of the animal in the central squares, number of grooming episodes (short- and long-lasting), and number of defecation acts were evaluated.

All experimental procedures on animals were performed in accordance with the Council of Europe Convention, November 24, 1986 (86/609/EEC), as well as were in compliance with the Law of Ukraine "On Protection of Animals from Inhumane Treatment," February 21, (2006).

RESULTS AND DISCUSSION

In the control group, the HA (number of crossed squares) intensity during the 2nd and 3rd days decreased significantly (more than two times on the 3rd day). During the 4th and 5th days, this index demonstrated a trend toward recovery but did not reach the initial value. The VA (number of rearings) intensity in the control group demonstrated the dynamics similar to those of HA. On the 3rd day, the VA intensity in control rats decreased by more than 60%. The index of general motor activity in the control group was significantly smaller than the initial one within the last days of the testing period (on the 3rd day, it showed practically a twofold drop). The number of goings of animals in the central squares was the index showing the clearest intergroup differences. In the control group, this index during days 2 to 5 demonstrated a clear decrease (on the 3rd day, this drop was more than tenfold compared to the value on the 1st day). Short grooming episodes during days 2 to 5 were much rarer than those on day 1. At the same time, the frequency of episodes of long-lasting grooming was maintained in control rats on a relatively high and nearly stable level. The total number of episodes of grooming behavior in the control group was significantly smaller during days 2 to 5 than that on day 1. The number of defecation acts in the control group was clearly greater than the analogous index in the experimental group. In the control group, the respective range was from 1.0 to 3.0 (mean 2.04). The HA intensity in this group during days 2 to 5 was significantly lower than that on the 1st day. The numbers of rearings during days 2 to 5 were much smaller than on the 1st day. It seems probable that control rats demonstrated certain suppression of this behavioral component induced by stress, on the one hand, and by the habituation process, on the other hand.

Introduction of memantine into animals of the experimental group on the 1st testing day exerted no significant effects on the HA and VA intensities. On the 2nd day VA intensity increased noticeably and exceeded the initial values. Within the 3rd to 5th days, experimental rats demonstrated significantly greater values of general motor activity; on the 3rd day, its value was more than two times greater than that in control rats. In the experimental group treated with memantine, the number of central squares goings was several times greater than the analogous values in control animals (on the 3rd day, more than 30 times). In experimental animals the initial frequency of short-lasting groomings (observed on the 1st day) was significantly lower than in control rats. During days 3 to 5, this index, however, demonstrated a rather stable trend toward increase and exceeded the respective values in the control group. The total number of grooming episodes in experimental rats increased significantly during days 2 to 5 and nearly reached the level observed in the control. The mean number of defecation acts in experimental group within the observation period varied from 0.1 to 0.8 (0.50, on average). The number of squares of the open field visited within the observation period (the HA index) characterizes the intensity of locomotor activity under testing conditions. The dynamics of this index demonstrated significant specificities in the control and experimental groups. Rats treated with memantine maintained rather high HA indices within the entire testing period. The number of rearings (VA) is interpreted as an index characterizing the intensity of orientational/research activity of the animal. This index in the experimental group (as compared with the control one) demonstrated more significant specificity than the HA index. In memantine-treated animals, this index increased noticeably within a late part of the testing period (days 4 and 5). The interest of experimental rats in the novel surrounding was maintained on a somewhat increased level within the entire testing period. As was mentioned above, the most significant difference between control and experimental animals was found with respect to the number of goings of rats to the central squares. In rats treated with memantine, this index was many times greater than that in control animals. This fact, together with the maintenance of orientational/research activity, is probably indicative of a much lower level of anxiety in the experimental group. Results of observation of grooming behavior agree, in general, with the above conclusion. The frequency of grooming episodes is interpreted as one of the indices characterizing the state of the emotional sphere; this index, however, is not in some simple (linear) dependence on the levels of anxiety, stressing, and other indices of emotionality. Changes in the number of grooming episodes and defecation acts within the observation period show that memantine exerts rather considerable effects on the activity of

central emotiogenic structures. Observations of animals in the open field do not provide experimenters with direct information on changes in the level of anxiety; such information can be obtained with the use of other behavioral tests (elevated labyrinth, in particular). At the same time, the maintenance of a relatively high frequency of orientational/research behavioral phenomena and the absence of suppression of visits to the central squares are indicative of a rather low anxiety in rats treated with memantine. Significant modifications of the dynamics of behavioral indices of rats within the 5-day-long testing period were another clear result of the memantine treatment. In fact, the dynamics of all examined indices in animals of the experimental and control groups differed significantly from each other. Probably, it should also be noted that our results provoke doubts with respect to the existing statement that the memantine effects are not cumulative. At present, it is difficult to answer the following question: are changes in the examined parameters during the testing period related to adaptation (in the broad sense of the term) or do they result from accumulation of the sequential doses of memantine. Thus, we can conclude that the toxicity of the drug used is rather low; this agent augments significantly the motivation level, intensifies orientational/research activity of the animals, and decreases the level of anxiety and fear. In general, the effects of memantine can be characterized as adaptational/stimulating ones.

Keywords: open field, memantine, behavioral/emotional indices, dementia, rats

REFERENCES

[1] Kh. Yu. Ismailova, T. M. Agayev, and T. P. Semenova, Individual Peculiarities of Behavior (Monoaminergic Mechanisms), Nurlan, Baku (2007).

[2] V. I. Rodina, N. A. Krupina, G. N. Kryzhanovskii, and N. B. Oknina, "A novel technique of estimation of the anxiety/phobic states in rats," Zh. Vyssh. Nerv. Deyat., 43, No. 5, 1006–1017 (1993).

[3] Z. A. Kruchenko, V. A. Gorbachenko, I. S. Chereda, et al., "Effect of memantine on motor behavioral phenomena in rats of different ages," Neurophysiology,46, 448–451 (2014).

[4] V. Gorbachenko, I. Chereda, S. Vrublevsky, et al., "Development and testing of the experimental system for registration of food reflex in rats," Bull. Taras Shevchenko Natl. Univ. Kyiv Ser. Radiophys. Electron.,1/2, 31-33 (2014).

[5] V. A. Gorbachenko, J. O. Kruchenko, I. S. Chereda, et al., "Measurements of the time parameters of condi-tioned food reflex in rats under memantine treatment using the automatic registration system," Bull. Taras Shevchenko Natl. Univ. Kyiv. Ser. Radiophys. Electron.,1, 23-26 (2015).

Robustness versus reliability of inter-individual behavioural variance in reinforcement learning

Stefano Vrizzi[1]*, Mael Lebreton[2], Anis Najar[1], Stefano Palminteri[1]*

[1]Département d'études cognitives, Laboratoire de Neurosciences Cognitives Computationnelles, École normale supérieure, PSL, Paris, France
[2]Swiss Center for Affective Science, University of Geneva, Geneva, Switzerland
**stefano.vrizzi@ens.psl.eu, stefano.palminteri@ens.psl.eu*

INTRODUCTION

Computational cognitive science pursues two complementary goals: profiling the decision patterns of the average and understanding the behavioural traits of the individual. These aspects are important to develop both theory and potential applications, including diagnostic tools for psychiatric disorders [1], economic interventions [2] and educational resources [3].

A suitable computational framework in cognitive science comes from the concept of prediction error in reinforcement learning (RL) [4]. RL is a fundamental adaptive learning process where the individual learns the expected value of a given choice by trial-and-error. One key measure in RL tasks is correct choice rate (or accuracy), namely the fraction of total trials in which the subject chooses the most advantageous (or less disadvantageous) option. By leveraging on the sensitivity to reward-seeking versus punishment-avoidant behaviour, different learning contexts can be designed to analyse both average and individual behavioural patterns.

In our study, we aim to go beyond the average behaviour to explore the structure of inter-individual behavioural variance. More specifically, we investigate: (i) if average behavioural variance is a stable population construct (robustness) and (ii) if accuracy per learning context is a stable individual construct (reliability).

METHODS

Our study capitalised on a dataset collected from a cohort of subjects (N=200) performing the RL task from Palminteri et al. [5] (Fig. 1). We analysed the

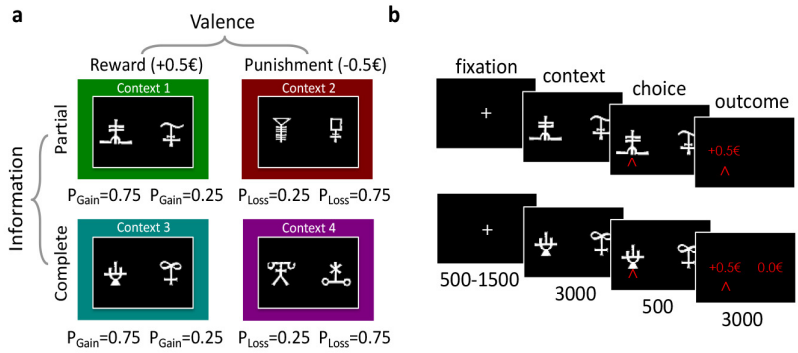

FIGURE 1: Reinforcement learning task with valence and information manipulations. (a) Learning task with four different learning contexts: RP, PP, RC, PC. P_{Gain} = probability of winning 0.5€; P_{Loss} = probability of losing 0.5€. Each context corresponded to a different pair of symbols. Coloured frames are shown only for illustrative purposes. (b) Successive screens of typical trials in RP (top) and RC (bottom) learning contexts. Durations are given in milliseconds. The experiment comprised two sessions, each session was composed by the four learning contexts as a block design, with 20 trials for each context, totalling 160 trials. Adapted from Palminteri et al. [5].

dataset (test) and ran a follow-up (re-test) experiment on the same subjects after six months. Both the test and retest experiments were performed online, employing the Prolific platform [6]. This methodology enabled us to gather data efficiently for test-retest analysis from a large number of participants. It is designed for incentive-compatible participation and it ensures higher safety standards for participants. The experiment conformed with the ethical requirements of the designated ethics committee; informed consent was obtained from the participants and their data was anonymised.

The learning task was based on two manipulations: valence (positive versus negative) and feedback information (partial versus complete). When valence was set as positive, the subject could receive either a set reward or none; when valence was negative, a set punishment or none. In the case of partial feedback information, the subject was provided only with their choice outcome; if complete, also the counterfactual outcome was shown. Valence manipulation aimed to test the reward-seeking versus punishment avoidance behaviour; feedback information manipulation assessed the role of regret

and relief. The 2×2 factorial design defined four different learning contexts (Fig. 1a): reward-partial (RP), punishment-partial (PP), reward-complete (RC), and punishment-complete (PC).

We looked at accuracy for each learning context, within each experiment (test and retest). We tested for robustness and reliability between the two experiments. In the case of robustness, we compared test and retest average values by Wilcoxon signed-rank test, a non-parametric version of the paired t-test, as Saphiro-Wilk tests revealed that the normality assumption was violated in all learning contexts ($p<.05$). Additionally, we tested the effect of valence and information on accuracy within each experiment by Wilcoxon signed-rank tests with Bonferroni correction. To test for reliability, we computed Pearson's correlation between test and retest across participants.

Furthermore, within each experiment, for each subject, we fitted a GLM model to predict their accuracy from valence and feedback information as dummy variables (-1 and +1), their interaction and a baseline. We performed the procedure mentioned above to check test-retest robustness and reliability on the values from each of the four regressors.

Finally, we compared our results with test-retest correlation from standard psychological questionnaires [7]. We collected personality measures using the BIS/BAS (behavioural activation system/behavioural inhibition system) scale, in line with our focus on the reward-seeking versus punishment avoidance behaviour.

The statistical analysis was performed in Python 3.7.3. The code is openly available upon request.

RESULTS AND DISCUSSION

Average accuracy did not differ between test and retest in any learning context (RP, $p=0.78$; PP, $p=0.99$; RC, $p=0.57$; PC, $p=0.47$) (Fig. 2a), implying that the structure of behavioural variance was stable at population level. Valence had no significant effect ($p>0.0125$) on accuracy in either the test or retest, while information did in both experiments. Individual accuracy correlations between test and retest were significant in all learning contexts ($p<0.0025$), but very weak, except for PP, where the correlation was weak (Fig. 2b-e).

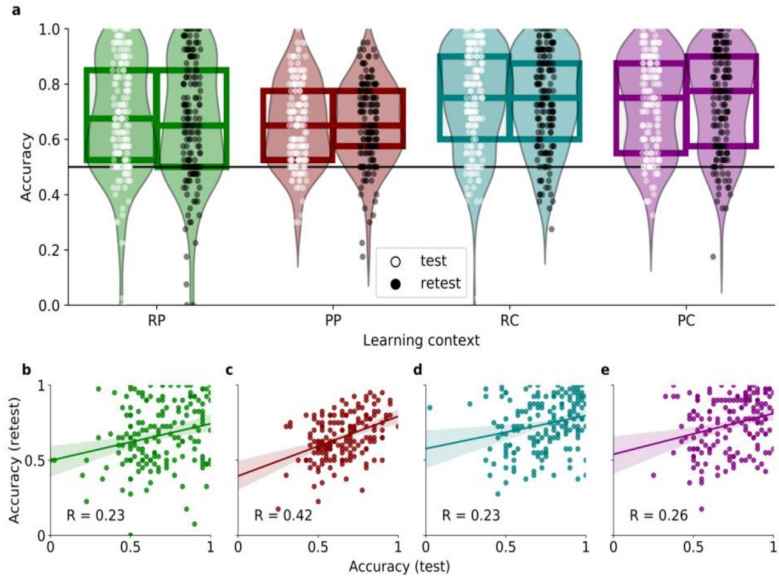

FIGURE.2: Test-retest robustness reliability assessment on accuracy per learning context. (a) Box plots showing the quartiles of accuracy in either the test or retest experiment for each learning context, overlaid by the respective underlying distributions and their kernel density estimations. (b-e) Accuracy correlation between test and retest across individuals. R represents the Pearson's correlation value. Colour-coding reflects learning contexts in Fig. 1a.

The gap between population- and individual-level replicated also for the fitted values of the GLM regressors (not shown). Only the baseline displayed a weak correlation ($R=0.43$, $p<0.001$) and valence a very weak correlation ($R=0.19$, $p<0.02$).

On the contrary, test-retest correlations for both BIS and BAS scales were strong ($R_{BIS}=0.81$, $R_{BAS}=0.74$, $p<0.001$).

Further analysis will involve Principal Component Analysis (PCA) to study loadings and variance explained.

In summary, our results suggest both robustness and very low reliability in the inter-individual behavioural variance structure of the RL task examined. This

avenue of research highlights the importance of investigating inter-individual differences on large samples in a fundamental adaptive learning process.

Keywords: decision-making, reinforcement learning, test-retest reliability, inter-individual variability

REFERENCES

[1] Huys, Q. J., Maia, T. V., & Frank, M. J. (2016). Computational psychiatry as a bridge from neuroscience to clinical applications. *Nature neuroscience*, **19**(3), 404.

[2] Haushofer & Fehr (2014). On the psychology of poverty. *Science*, **344**(6186), 862-867.

[3] Goswami, U. (2006). Neuroscience and education: from research to practice? Nature reviews neuroscience, 7(5), 406-413.

[4] Sutton & Barto. (1998). Reinforcement learning: an introduction. IEEE

[5] Palminteri et al. (2015). Contextual modulation of value signals in reward and punishment learning. Nat Commun 6, 8096. https://doi.org/10.1038/ncomms9096

[6] Palan & Schitter (2018). Prolific. ac—A subject pool for online experiments. Journal of Behavioral and Experimental Finance, 17, 22-27.

[7] Enkavi et *al.* (2019). Large-scale analysis of test–retest reliabilities of self-regulation measures. *Proceedings of the National Academy of Sciences*, **116**(12), 5472-5477.

Advantages of publishing in Frontiers

OPEN ACCESS
Articles are free to read for greatest visibility and readership

FAST PUBLICATION
Around 90 days from submission to decision

HIGH QUALITY PEER-REVIEW
Rigorous, collaborative, and constructive peer-review

TRANSPARENT PEER-REVIEW
Editors and reviewers acknowledged by name on published articles

Frontiers
Avenue du Tribunal-Fédéral 34
1005 Lausanne | Switzerland

Visit us: www.frontiersin.org
Contact us: info@frontiersin.org | +41 21 510 17 00

REPRODUCIBILITY OF RESEARCH
Support open data and methods to enhance research reproducibility

DIGITAL PUBLISHING
Articles designed for optimal readership across devices

FOLLOW US
@frontiersin

IMPACT METRICS
Advanced article metrics track visibility across digital media

EXTENSIVE PROMOTION
Marketing and promotion of impactful research

LOOP RESEARCH NETWORK
Our network increases your article's readership